The role of cell and virus-encoded ion channels in the replication cycle of Human respiratory syncytial virus

by

Hussah A S A Taqi

Submitted in accordance with the requirements

for the degree of Doctor of Philosophy

The University of Leeds

Faculty of Biological Sciences

School of Molecular & Cellular Biology

July 2016

The candidate confirms that the work submitted is his own and that appropriate credit has been given where reference has been made to the work of others.

The contribution of the candidate and the other authors to this work has been explicitly indicated below. The candidate confirms that appropriate credit has been given within the thesis where reference has been made to the work of others.

The Chapter 3 of this thesis was based on the work from jointly-authored publication:

Hover S, King B, Hall B, Loundras EA, Taqi H, Daly J, Dallas M, Peers C, Schnettler E, McKimmie C, Kohl A, Barr JN, Mankouri J*. Modulation of potassium channels inhibits bunyavirus infection. J Biol Chem. 2015. J Biol Chem. 2016, 291(7):3411-22.

To my husband, Abdulwahab', who took care of my children in Kuwait while I was in UK, for his patient, care and endless support. Thank you for your sacrifices during the completion of this thesis. Also, to my little sons, Mohammad and Ali, who are my source of happiness. To my parents for their unwavering support.

Acknowledgement

First and foremost I would like to offer my honest gratitude to my supervisors, John Barr and Jamel Mankouri for their endless support and encouragement during my PhD research. Your advice on my research has been priceless. One simply could not wish for better or friendlier supervisors.

I also owe my deepest thanks to my colleagues and all lab members for their help and support in the laboratory during the experimental work. Special thank to Gareth Howall for his advice about FACS and Brian Jackson for his advice about confocal microscopy. Moreover, I would like to thank Dr. Stuart Armstrong from university of Liverpool for carrying my mass spectrometry analysis in Chapter 4 and 5. Also, special thanks to Julian Hiscox and his student Waleed Aljaber for sharing experiences, knowledge and advice.

I would also like to thank the Ministry of Health and Kuwait National Government for their financial support throughout my study.

Finally, I would like to express my love and appreciation to my family in Kuwait for their infinite love and support. To my beloved dad and mum for their continuous encouragement. Furthermore, I would like to express my special thanks for my beloved husband, Abdulwahab Alnaqi, and my lovely sons, Mohammad and Ali, for sharing good and hard times during my PhD.

Abstract

Infection with human respiratory syncytial virus (HRSV) causes both acute and chronic respiratory problems in children and the immunosuppressed. There is currently no HRSV vaccine, although prophylactic immunotherapy offers protection to at-risk individuals. However, this treatment is expensive and incompletely protective.

Ion channels are pore-forming proteins that regulate ion homeostasis across membranes in cells, acting as signaling proteins that regulate many aspects of cell physiology from cell cycle progression to apoptosis and gene transcription. Since ion channels play a key role in many aspects of lung cell physiology, I have investigated their involvement during HRSV infection in cultured respiratory cells.

Using ion channel modulating drugs I have investigated the role of host cell ion channels in promoting HRSV replication, in which an important role for specific potassium channels were identified during both early and late stages of the virus life cycle. I also examined the role of the HRSV small hydrophobic protein (SH), which is a known viroporin, in perturbing the cellular proteome in continuous (A549) and primary cell cultures (HBEpC) by quantitative proteomics using mass spectrometry.

This study is the first to demonstrate a dynamic role of specific ion channel families in the HRSV lifecycle. This may pave the way for future studies highlighting ion channels as druggable targets for a repertoire of lung-associated virus infections.

List of Contents

List of Abbreviations

ASL	airway surface liquid
K_{ATP} channels	ATP-sensitive K^+ channels
AQP5	aquaporin 5
BAP31	B-cell receptor-associated protein 31
BSA	bovine serum albumin
BUNV	Bunyamwera virus
BVDV	bovine viral diarrhoea virus
K_{Ca}	Ca^{2+}-activated K^+ channels
Cdc42	cell division control protein 42 homolog
CPZ	chlorpromazine
CSFV	classical swine fever virus
CME	clathrin-mediated endocytosis
CCHFV	Crimean-Congo hemorrhagic fever virus
CNG	cyclic nucleotide-gated
TLC	cytotoxic T lymphocytes
DMSO	dimethyl sulphoxide
DMEM	Dulbecco's modified Eagle's medium
EM	electron microscopy
EGF	epidermal growth factor
ENaCs	epithelial sodium channels
ER	endoplasmic reticulum
EV71	enterovirus 71
FBS	fetal bovine serum
Fis1	fission 1 membrane protein
FACS	fluorescence activated cell sorting
FIRSV	formalin-inactivated respiratory syncytial virus
GE	gene end
GS	gene start
GJ	gene junction
GAGs	glycosaminoglycans
GCU	Green calibration unit/ cell
HBSS	Hanks' balanced salt solution
HAZV	Hazara virus
HPA	Health Protection Agency
HPACC	Health Protection Agency Culture Collections
HA	hemagglutinin

HCV	hepatitis C virus
HMA	hexamethylene amiloride
HPI	hour post infection
HIV-1	human immunodeficiency virus type 1
HEp-2	human larynx carcinoma cell
A549	human lung alveolar basal epithelial cell
HPV-16	human papillomavirus type 16
HRSV	human respiratory syncytial virus
HTLV-1	human T-lymphotropic virus type 1
IF	immunofluorescence
IFN	interferon
IBV	infectious bronchitis virus
IAV	influenza A virus
IPA	ingenuity pathway analysis
IRF-3	interferon regulatory factor 3
IL-8	interleukin 8
Kir	inward-rectifying K^+ channels
JPV	J paramyxovirus
JC	John Cunningham polyomavirus
LDH	lactate dehydrogenase
LRTI	lower respiratory tract infection
MS	mass spectrometry
M	matrix protein
MPV	metapneumovirus
MQAE	6-methoxy-quinolyl acetoethyl ester
Mon	monensin
MOI	multiplicity of infection
MuV	mumps virus
MHV	murine hepatitis virus
N	nucleoprotein
NOD	nucleotide-binding oligomerization domain
NLR	NOD like receptor
ORFs	open reading frames
PIV5	parainfluenza virus 5
PAMPs	pathogen associated molecular patterns
PCL	periciliary liquid
P	phosphoprotein
PVDF	poly-vinylidine fluoride
RANTES	Regulated on Activation, Normal T-cell Expressed and Secreted
RSV	respiratory syncytial virus
RBV	ribavirin

RNP	ribonucleoprotein
RdRp	RNA-dependent RNA polymerase
PAK1	serine/threonine-protein kinase
SFM	serum free media
SARS-CoV	severe acute respiratory distress syndrome-associated
STAT	signal transducer and activator of transcription
SIV	simian immunodeficiency virus
SV40	simian virus 40
-ssRNA	single-strand negative-sense RNA
SH	small hydrophobic
SDS-PAGE	sodium dodecyl sulphate polyacrylamide gel
sG	soluble G protein
SOCS3	suppression of cytokine signaling 3
TLR	toll-like receptor
TNF-α	tumor necrosis factor alpha
K2P	two-pore domain K^+ channels
URTI	upper respiratory tract infection
vDED	variant of death effector domain
vRNA	virus ribonucleic acid
Kv	voltage-dependent K^+ channels

List of Figures

List of Tables

Chapter 1: Introduction

Introduction

1.1 Virus Classification and natural history

Respiratory syncytial virus (RSV) is one of the major causes of severe lower respiratory tract infection in humans, causing severe bronchiolitis and pneumonia in infants, young children, elderly and the immunosuppressed (Arnott et al., 2011). In 1956, the virus was firstly isolated from a chimpanzee and named as “chimpanzee coryza agent” (Morris et al., 1956). In 1957, the same virus was isolated from two children suffering from respiratory illness, and since then it has been known as human respiratory syncytial virus (HRSV) due to its ability to induce the formation of syncytia in cultured cells. HRSV has several close genetic relatives that can infect and cause disease in a variety of animals (Chanock et al., 1957) including cows (Bovine RSV; BRSV), goats (caprine RSV; CRSV), sheep (ovine RSV; ORSV) and mice (pneumonia virus of mice; PVM).

The modern virus taxonomic system developed by the International Committee on Taxonomy of Viruses (ICTV; Table 1.1) has classified HRSV and its various animal-infecting relatives as members of the *Paramyxoviridae* family, order *Mononegavirales*. Within this family these viruses are further classified within the *Pneumovirinae* sub-family and *Pneumovirus* genus. HRSV has a negative-sense, non-segmented single-stranded RNA genome typically comprising approximately 15,220 nucleotides (Sullender, 2000), and isolates can be classified into two distinct subtypes, A and B (Arnott et al., 2011), which can be distinguished both genetically and serologically. The *Paramyxovirinae* sub-family also contains the genus *Metapneumovirus*, which includes avian metapneumovirus (AMPV) and human metapneumovirus (HMPV), both of which bear some important similarities to HRSV and also contribute towards the burden of respiratory diseases in their associated human and animal hosts. All the viruses within the *Mononegavirales* order can also be classified within Group V of the Baltimore classification system, which categorizes viruses based

on their strategies of gene expression and viral mRNA production. It is known that this order includes many viruses that cause severe and serious disease in humans, and many of these are shown in table 1.1.

Family	Subfamily	Genus	Prototype
Bornaviridae		*Bornavirus*	Borna disease virus
Filoviridae		*Ebolavirus*	Zaire ebolavirus
		Marburgvirus	Lake Victoria marburgvirus
Paramyxoviridae	*Paramyxovirinae*	*Avulavirus*	Newcastle disease virus
		Henipavirus	Hendra virus
		Morbillivirus	Measles virus
		Respirovirus	Sendai virus
		Rubulavirus	Mumps virus
	Pneumovirinae	*Pneumovirus*	HRSV
		Metapneumovirus	Avian metapneumovirus
Rhabdoviridae		*Cytorhabdovirus*	Lettuce necrotic yellows virus
		Ephemerovirus	Bovine ephemeral fever virus
		Lyssavirus	Rabies virus
		Novirhabdovirus	infectious hematopoietic necrosis virus
		Nucleorhabdovirus	Potato yellow dwarf
		Vesiculovirus	Vesicular stomatitis virus

Table 1. 1. Classification of the order *Mononegavirales* and the families and sub-families that make up this large group of viruses. This classification follows the ICTV virus taxonomy released in 2009, and updated in 2014 (www.ictvdb.org).

1.2 Clinical infection and disease

HRSV infects only ciliated epithelial cells of the respiratory tract with no clear indication of cytopathology (Prince et al., 1986) The disease caused by HRSV typically starts with an upper respiratory tract infection (URTI), which includes symptoms such as rhinitis, fever, croup, sneezing, nasal congestion and rhinorrhea, followed by a moderate possibility of developing lower respiratory tract infection (LRTI), which includes symptoms such as coughing, harsh wheezing, pneumonia, bronchiolitis and a decrease in lung function and hypoxia (Welliver, 2003; Toms, 1987). In large animal models, such as adult male specimens of southern muriqui (a species of woolly spider monkey, *Brachyteles arachnoides*), HRSV can cause severe pneumonia leading to pulmonary lesions as well playing an important role in the development of microthrombosis in other organs such as the liver, kidney, and heart (Santos et al., 2012). However, similar symptoms to these have yet to be discovered in humans infected with HRSV. HRSV can cause re-current infections throughout adult life due, in part, to the high genetic variability of the virus that mostly gives rise to changes in the amino acid sequences of the surface glycoproteins, and result in immune evasion.

Neonates and young children are more susceptible to HRSV infection due to their naïve immune system. The immune response is poorly protective and so successive infections are common throughout adulthood (Toms, 1987). Moreover, HRSV infection can cause long-term effects following severe acute LRTI, leading to chronic abnormalities of pulmonary function including asthma and allergy (Hall et al., 1984; Sigurs et al., 2000). A high risk of asthma can occur in adult life as a consequence of recurrent infection with HRSV in early life, particularly during childhood. Recent evidence suggests that T cell function may become impaired and affect the immunoregulatory mechanisms that lead to the increase in allergic disease as a life-long effect (Krishnamoorthy et al., 2012).

In the same way, HRSV infection not only causes serious problems for infants and young children, but can also lead to severe illness in high-risk adults and the elderly (Falsey et al., 2005). In the 1970s, HRSV infection was recognized

as a serious problem in mature and elderly adults in long-term care facilities (Vikerfors, T., M. Grandien, 1987; Hart, 1984). In most countries, HRSV infection is considered a seasonal disease and at such times is responsible for 65% of hospitalized cases of respiratory illness. Generally the peak number of HRSV cases occurs during the cold season in mild temperate climates, during the rainfall season in tropical countries, and during the wet season in Mediterranean climates (Stensballe et al., 2003; Weber et al., 1998).

One of the main advantages of having a successful vaccine for infectious HRSV would be to reduce the chances of severe cases of HRSV in early childhood, thus reducing or preventing the possibility of developing frequent childhood asthma and airway hypersensitivity (Graham et al., 2015).

1.2.1 Burden of disease

In the United States, it has been estimated that over 150,000 children under the age of 1 are admitted to hospital as a result of HRSV infection. Moreover, 18% of all emergency department visits in children under 5 years of age were also attributed to HRSV infection (Mazur et al., 2015; Shay et al., 1999; Hall et al., 2009). Beyond the substantial disease burden during severe infection, bronchiolitis caused by HRSV infection is thought to play a major role in developing recurrent wheeze symptoms that are linked to asthma development (Shay et al., 1999; Beigelman and Bacharier, 2013). There is evidence to suggest that recurrent lower respiratory infection with HRSV causes recurrent wheeze (Régnier and Huels, 2013; Stein et al., 1999) specifically during the adult years when asthma has a permanent impact (Dnb et al., 2010). However, the long-term pathogenic effects and morbidity of HRSV still remain unclear. Some biological mechanisms linking the recurrent wheeze and the epithelial damage caused by HRSV infection to the development of asthma include continuing bronchial hyper-responsiveness at the late stage of HRSV infection. This impairs the T-regulatory function that activates the innate immune response, triggering T-helper-2 cells (Th2) that causes airway remodeling and increases the chances of allergy because of the barrier function of the airway tract epithelium (Feldman et al., 2015).

Most HRSV cases in child patients require hospital admission rather than treatment in outpatient clinics resulting in disproportionate health care and financial burden for children under five years old (Escobar et al., 2013; Ducharme et al., 2014); 99% of the mortality rate related to HRSV disease are in low-income countries where most fatal cases are associated with LRTI, which is also closely related to HRSV infection (Draft et al., 2015; Nair et al., 2010).

Two different estimates of mortality resulting from HRSV infections have been reported, based on two different modeling approaches. One report based on a systematic review of epidemiology data revealed that the incidence of LRTI from HRSV infection was 33.8 million cases in children under 5 years old globally in 2005, with 3.5 million (10%) being admitted to hospital resulting in an estimated 66,000-199,000 fatalities (see Figure 1.1). This report also suggested that HRSV causes insignificant mortality rates in children over two years of age. The second study, based on the Institute for Health Metrics and Evaluation's Global Burden of Disease data, showed that 2013 estimates for deaths from pneumonia caused by HRSV infection of mortality in children under 5 years old was 41,100 (Draft et al., 2015; Mazur et al., 2015). Individuals at high risk of contracting HRSV infection are HIV-infected children or those with other immunocompromised status, premature infants and infants with very low birth weight (Mazur et al., 2015; Moyes et al., 2013; Holman et al., 2003). However, most children that were admitted to hospital with HRSV LRTI were previously healthy. The accuracy of statistical estimates regarding HRSV burden of disease are limited by the quality of monitoring methods, absence of a universal definition, paucity of monitoring outside the hospital setting, and the rarity of a definite HRSV diagnosis amongst a variety of other potential viral respiratory pathogens (Mazur et al., 2015).

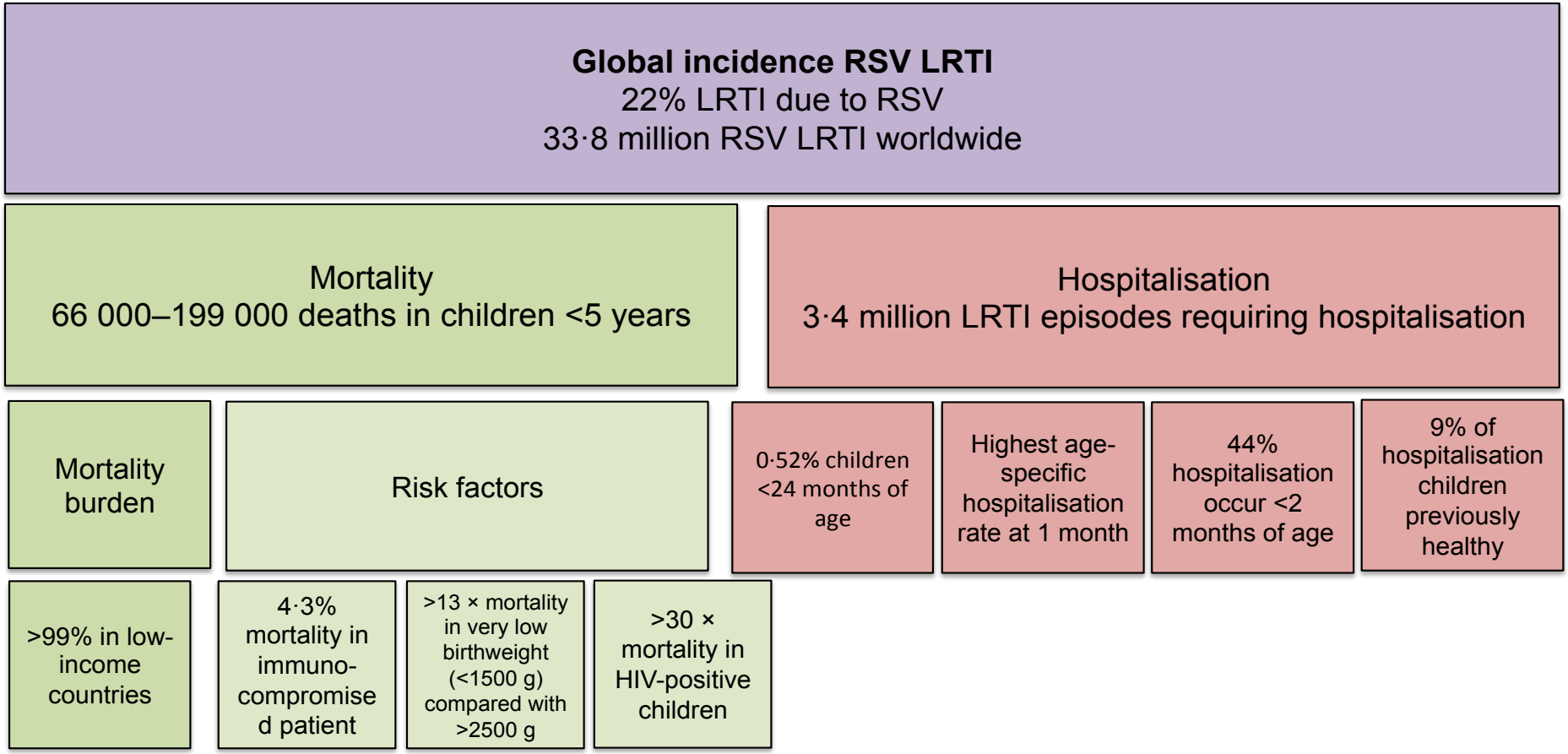

Figure 1. 1. HRSV burden of disease: Key facts.

Estimated percentage of hospitalized patients and deaths due to global incidence of lower respiratory tract infection (LRTI) caused by HRSV. Statistics obtained from (Mazur, 2015)

1.3 Virus structure and genome

HRSV is an enveloped virus that can be described as being pleiomorphic, consisting of both spherical and filamentous forms, as well as particles bearing a combination of both these morphological characteristics. The negative-sense RNA genome is around 15.2 kb in length and the genes are arranged in a linear order from the 3' to the 5' RNA end (Collins, 2007) (Figure 1.2B). From the 3' end of the negative stranded genome (vRNA) the initial 44 nucleotides (nt) comprise the leader (Le) region that contains *cis*-acting sequences that have been shown to promote and direct viral RNA synthesis. The roles that individual nucleotides within this leader region play in building up the promoters for mRNA transcription and RNA replication have been thoroughly dissected (Collins, 2007).

Following the Le region, and moving further towards the vRNA 5' end, the HRSV genome contains 10 genes that are separated by sequences known as gene junctions (see section 1.5.2). These gene junction sequences direct the viral polymerase to transcribe a single mRNA from each of the 10 genes. Each mRNA encodes for a single protein, with the exception of the M2 mRNA, which encodes M2-1 and M2-2 from overlapping open reading frames (ORFs). The viral proteins involved in gene expression include the nucleoprotein (N), phosphoprotein (P), matrix protein (M), M2-1, possibly M2-2 and polymerase (L) (Huang et al., 1985; Tawar et al., 2009; Arnott et al., 2011). An additional three viral proteins are located in the virus envelope, namely the attachment glycoprotein (G), fusion (F) protein and small hydrophobic (SH) protein (Sullender, 2000; Arnott et al., 2011). Figure 1.2A shows a schematic representation of the HRSV virion, showing the location of each structural protein. The remaining two HRSV proteins, namely NS1 and NS2, are considered to be non-structural proteins, and thus are not present within the virion. Figure 1.2B illustrates the map of the RNA genome of HRSV, which conforms to the basic genetic structure that is shared by all the viruses within the subfamily *Pneumovirinae*.

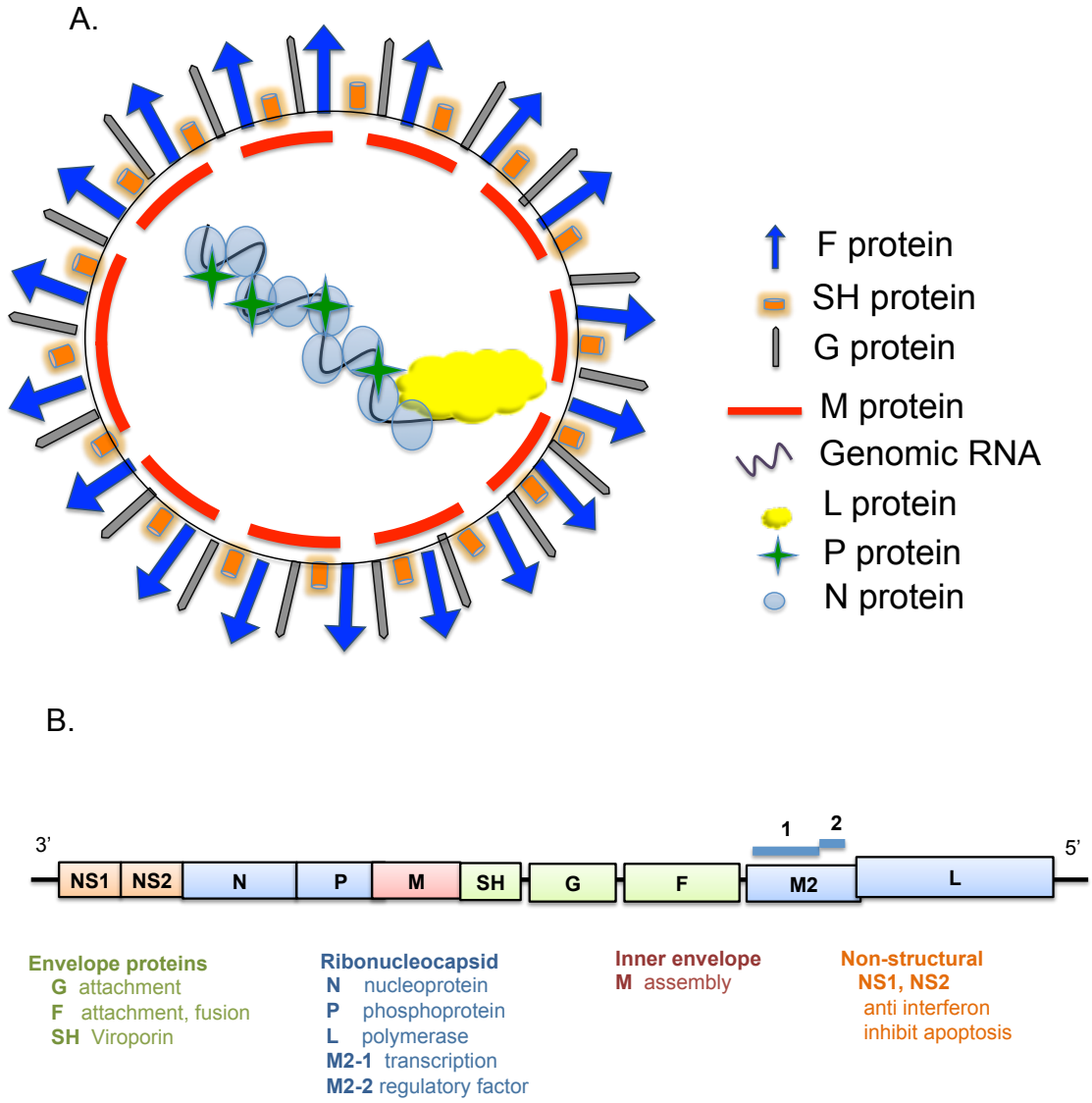

Figure 1. 2. Schematic representation of the HRSV virion and genome.

A. Schematic representation of the HRSV virion and the location of viral proteins. **B.** Schematic representation of the HRSV RNA genome, which is a single-stranded negative-sense RNA molecule that is transcribed into 10 mono-cistronic mRNAs from a 3' end promoter. The M2 gene encodes two proteins (M2-1 and M2-2) from overlapping ORFs.

1.4 The HRSV proteins

1.4.1 Envelope proteins

1.4.1.1 HRSV G protein

The G protein is a type II trans-membrane glycoprotein and consists of between 282 to 319 amino acids depending on the strain. Its main function lies in cell surface attachment, shown by the fact that antibodies that are specific to G protein are able to prevent the binding of the virus to some cultured cells. The G protein can be a dimer or heavily glycosylated monomer with a hydrophobic amino-terminal transmembrane domain encompassing residues 38 to 66 (Johnson et al., 1987; Jason S. McLellan et al., 2013), and this region is flanked by the ecto- and endo-domains. Within the central region of the ecto-domain there is a short segment (amino acids 164-167) and four cysteines (residues 173, 176, 182 and 186) that are conserved in all HRSV isolates, and these have been proposed to form the possible receptor-binding site (Johnson et al., 1987; Collins and Melero, 2011). The ectodomain is believed to form a relatively extended and unfolded mucin-like structure that may serve to facilitate movement of the virus through mucus-covered respiratory surfaces found in the respiratory tract (Collins and Graham, 2008). G is heavily modified by post-translational glycosylation, with addition of both N-linked and O-linked carbohydrates, raising the molecular weight of the protein backbone from the native 32 kDa to around 90 kDa.

A second function has been demonstrated for the G glycoprotein, namely, its expression in a secreted form, which arises from translation initiation at the second AUG in the ORF (at amino acid 48) such that the resulting polypeptide does not contain the entire trans-membrane anchor (Pellet and Roizmann, 2007). The resulting soluble G protein (sG) is thought to serve as an antigen decoy by reducing the productivity of HRSV antibody-mediated neutralization and has an important role in inhibiting the antibody-mediated antiviral response by affecting the Fc receptor-bearing leukocytes. Moreover, expression of sG has been shown to restrict HRSV replication in animal models such as mice (Bukreyev et al., 2012).

The G protein plays a major role in the host immune response to HRSV infection. It induces pulmonary inflammation and eosinophilia by activating Th2-biased memory response (Bembridge et al., 1998). It also inhibits toll-like receptor (TLR) 3 or TLR4 induction of interferon beta (IFN-β) (Shingai et al., 2008). Moreover, G protein has been shown to enhance proinflammatory responses in respiratory epithelial cells, as well as in multiple innate immune responses in monocytes, dendritic cells and macrophages. It also boosts the cytotoxic T cell response and suppresses the suppression of cytokine signaling 3 (SOCS3) protein expression that leads to a decrease in the production of type I IFN (Chirkova et al., 2013).

The G protein is thought to mediate HRSV cell attachment via glycosaminoglycans (GAGs) including chondroitin sulfate B and heparin sulfate B. However, HRSV lacking G protein expression through deletion of the G gene from the genome can still infect cells *in vitro* (Sun et al., 2013). A previous study (Tripp et al., 2001) showed that CX3CL1 (chemokine) competes with G protein to bind to the host receptor as they have a similar motif at the binding side and both attract host neutrophils. Moreover, a recent study showed that CX3CR1 is used as a receptor to HRSV to bind at the human airway epithelial (HAE) cells (Johnson et al., 2015).

1.4.1.2 HRSV F protein

The fusion (F) protein is a glycoprotein that is responsible for HRSV binding to the host cell plasma membrane, and in addition for the fusion of viral and cellular membranes to permit uncoating of the viral genome leading to its release into the cytosol. The F protein is a type I transmembrane surface protein (Collins, 2007), and is initially synthesized with a N-terminal signal peptide that is subsequently cleaved off, and possesses a C-terminal membrane anchor that mediates insertion into the virus envelope (Mufson et al., 1985). F assembles into trimeric homo-multimers that form spikes that are visible using electron microscopy (EM) on the surface of HRSV virions.

In addition, F protein has been shown to activate TLR4 on human leukocytes to initiate immune response in host cell (Collins and Melero, 2011). F protein has

been shown to be responsible for binding to permissive host cells through its interaction with the cellular protein nucleolin in both cultured cells and in a mouse model (Collins and Melero, 2011).

Different groups have proposed that the process of F protein-mediated virus fusion occurs at either the plasma membrane or within endosomes (Krzyzaniak et al., 2013; Kolokoltsov et al., 2007b; Srinivasakumar et al., 1991). In either case, the stages of membrane fusion that are thought to occur are similar, and require double cleavage of an initially expressed F0 to yield F1 and F2 polypeptides that are disulphide linked, with the release of a polypeptide fragment known as p27. The bulk of F1 forms a stalk and neck region, whereas F2 forms the head region that interacts with the proposed cellular receptors. The F0 cleavage is thought to occur via the cellular protease furin, which exposes a hydrophobic peptide at the extreme N terminus of F1, known as the fusion peptide. Conformational changes in the cleaved F1-F2 heterodimer result in the insertion of the fusion peptide into the target host membrane, and further conformational changes bringing together heptad repeats (HR-A and HR-B) that allows the formation of a highly stable six-helix bundle, which then allows the viral and cellular membranes to fuse. Once host and viral membranes have mixed, the viral genome can enter the cell and initiate gene expression.

The formation of the six-helix bundle within the F1 stalk is a critical stage in the HRSV infection process, being required for virus entry, and consequently many anti-viral compounds have been designed to disrupt its formation. A solution of the crystal structure of the F-protein trimer in the pre-fusion (pre-triggered) conformation allowed a better understanding of this important target (McLellan et al., 2013).

The F protein is also the target for the only clinically approved anti-HRSV therapy that has proved to be effective, namely palivizumab, which is further described in section 1.7. Palivizumab is a humanized monoclonal antibody that targets a neutralizing epitope within the F protein ectodomain comprising amino acids 254-277. When palivizumab binds to this region, the conformational changes required to mediate membrane fusion are prevented, and thus the infectious cycle is blocked. Therefore, developing entry inhibitors of HRSV by

targeting the F protein with small molecules, peptides or antibodies is a proven efficacious approach (Sun et al., 2013).

1.4.1.3 HRSV SH protein

The small hydrophobic (SH) protein is the smallest trans-membrane glycoprotein encoded for by HRSV (Murphy et al., 1986; Collins and Mottet, 1993) and mainly accumulates within the Golgi complex, endoplasmic reticulum membrane and plasma membrane of infected host cells. SH is also incorporated into the envelope of infectious HRSV particles, although with considerably less abundance than either F or G proteins.

In contrast to the HRSV G and F glycoproteins, the functional role of the SH protein within the virus replication cycle is poorly understood (Gan et al., 2008). When the gene encoding the SH protein is deleted from the HRSV genome (HRSV ΔSH) and then used to infect cells in culture, the virus is still able to complete its entire replication cycle as well as being able to form syncytia. In addition, the titre of HRSV ΔSH generated in cell culture systems is comparable to a parental recombinant wild-type RSV (rRSV). However, HRSV ΔSH replicates to 10-fold lower titres *in vivo,* particularly within the upper respiratory tract of the mouse model (Bukreyev et al., 1997). In terms of the pathogenicity of HRSV ΔSH, infection of chimpanzees resulted in fewer disease symptoms such as reduced rhinorrhea in comparison with the rRSV wild type. Moreover, the deletion of the SH gene in HRSV leads to an attenuated disease phenotype in baby rats (Karron et al., 1997; Jin et al., 2000). Taken together, these findings suggest that the SH protein is an important virulence factor in HRSV pathogenesis (Gan et al., 2012). HRSV ΔSH has been proposed as a live vaccine candidate in humans, as well as a similarly SH gene-deleted BRSV for use in calves (Karron et al., 1997; Taylor et al., 2014).

It has been suggested that the SH protein delays or inhibits apoptosis in infected cells (Sandra Fuentes et al., 2007). A similar effect been also been detected in other members of the *Paramyxoviridae* family possessing an SH protein such as the mumps virus (MuV), parainfluenza virus 5 (PIV5), J paramyxovirus (JPV) (Jack et al., 2005; Li et al., 2011). In all these viruses, it

was shown that their respective SH proteins act as anti-apoptotic factors by blocking the tumor necrosis factor alpha (TNF-α) pathway (Sandra Fuentes et al., 2007; Ren et al., 2011; Douglas et al., 2003; Wilson et al., 2006). When the PIV5 SH protein was replaced with HRSV SH protein, the result was that apoptosis was prevented via the inhibition of TNF-α-mediated NF-κB pathway, suggesting that the HRSV SH protein acts through a similar pathway to the other *Paramyxoviridae* family members. However the underlying mechanisms through which SH mediates this apoptosis block is still unknown. The anti-apoptotic effect induced by HRSV SH protein could prevent apoptosis to enable prolonged virus replication in host cells (Torres et al., 2015).

Wild-type HRSV is known to activate the cellular inflammasome, which is a multi-protein cytosolic complex that is involved in the induction of a pro-inflammatory cytokine response through the detection of invading viral components by cytoplasmic sensors. In the case of HRSV, it is thought that inflammasome activation contributes to the lung pathology and disease exacerbation characteristic of HRSV infection (Triantafilou and Triantafilou, 2014). A variety of nucleotide-binding oligomerisation domain (NOD) receptors (NLRs) are associated with inflammasomes, and their activation following detection of HRSV pathogen associated molecular patterns (PAMPs) leads to recruitment of caspase-1 to the inflammasome complex, which consequently leads to activation of an inflammatory response characterized by induction of IL-1β. HRSV has been shown to specifically activate inflammasomes associated with NLRP3 (Triantafilou et al., 2013b). Interestingly, HRSV ΔSH has recently been shown to be unable to activate the NLRP3 inflammasome and thus the subsequent secretion of IL-1β is blocked (Triantafilou and Triantafilou, 2014). This indicates SH may play a role in inflammasome activation with direct consequences for infection outcome and pathology. It has been proposed that the underlying mechanism behind SH-mediated inflammasome activation lies in changes of ion homeostasis between cellular organelles such as the Golgi system and the endoplasmic reticulum (ER), and the cytosol mediated by the viroporin activity of SH. This concept was derived from the finding that the M2 protein of influenza A virus (IAV) triggers NLRP3 activation through its ability to mediate H^+ or ion flux between the Golgi compartment and the cytosol

(Ichinohe et al., 2010). A similar effect was observed with poliovirus and enterovirus 71, both of which have been shown to activate NLRP3 through the imbalance of Ca^{2+} homeostasis (Ito et al., 2012), mediated by the 2B protein, which is a known viroporin. To test involvement of HRSV SH in perturbing cellular ion balance, HRSV infected cells were treated with a viral ion channel inhibitor (Pyronin B, SH blocker) that led to suppression of inflammasome activation (Triantafilou et al., 2013a). Moreover, when SH protein accumulates in lipid raft structures this can lead to monovalent cation (K^+ and Na^+) activity that might be related to the NLRP3 activation (Triantafilou and Triantafilou, 2014) . Another recent study showed the SH protein possessed weak cationic selectivity at neutral pH, and anionic selectivity at acidic pH (Li et al., 2014). However this link between cellular ion conductance and SH protein channel activity has not yet been confirmed.

1.4.1.3.1 RSV SH protein structure

The SH protein is 64 amino acids long in subtype A HRSV strains and 65 in subtype B strains (Collins et al., 1990). It contains a single transmembrane (TM) domain (Gan et al., 2008; Teng and Collins, 1998). While the C-terminus of SH is oriented on the outside of the viral envelope, the N terminus of SH faces the inside of the virus particle (Gan et al., 2008; Teng and Collins, 1998), or the lumen of intracellular compartments in which it is inserted. The TM domain encompasses a major part of the total protein sequence, and is thought to extend between amino acid residues 20-42 (Krogh et al., 2001). Another study in which SH oligomers were reconstituted in a lipid bilayer model proposed that the TM domain of SH extended between residues 18-43, and forms a stable α-helical structure (Gan et al., 2012; Gan et al., 2008). The first direct visualization of SH by EM (electron microscope) suggested that it formed ring-like structures with a central pore, consistent with its proposed role as a viroporin (Carter et al., 2010). The rings were SH multimers, predominantly comprising five or six SH monomers, with a central pore of either 1.9 nm (pentamers) or 2.6 nm (hexamers). *In silico* modeling suggested that the helical TM regions would cluster together through hydrophobic charges to form an extremely stable multimeric complex when membrane bound.

The high-resolution structure of the SH protein was determined using NMR spectroscopy, with the SH multimer formed in lipid bilayers and in detergent micelles. The results largely confirmed the previous EM analysis, and showed that SH protein has a single α-helical TM domain within a homo-pentameric structure, which was able to form in several detergents (Gan et al., 2012). Figure 1.3 shows a model representation of the SH pentamer. It was also found that the TM domain of SH protein is surrounded N-terminally by α-helices forming a ring-like structure around the lumen of the pore, and the C-terminus forms an extended β-turn. This study also showed that the protein has pH-dependent (acid-activity) channel activity in the plasma membrane region of the transfected HEK293 cells (Gan et al., 2008).

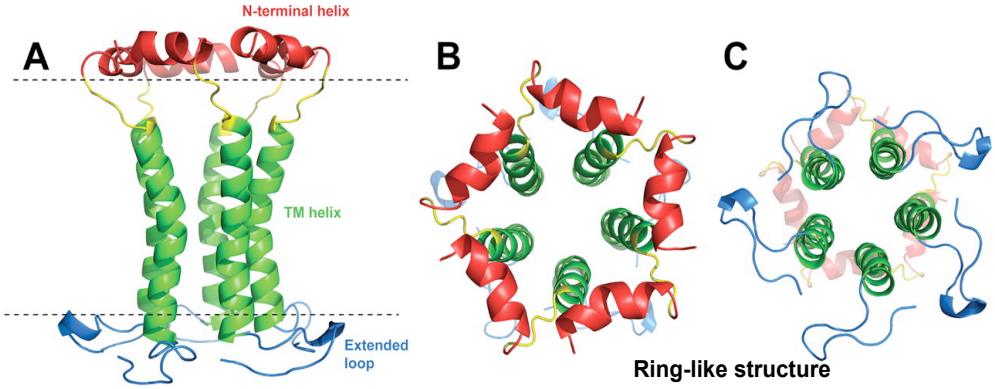

Figure 1. 3. Schematic representation of the structural model of the HRSV SH protein pentamer, determined using NMR.

(**A)** Side, (**B)** top and **(C)** bottom views of the SH oligomer. Adapted from (Gan et al., 2012).

SH protein can be present in several forms depending on its glycosylation status (Olmsted and Collins, 1989); two forms are non-glycosylated and include a truncated 4.5 kDa species (SHt) and a full-length 7.5 kDa form (SH0). SH_g on the other hand is glycosylated by N-linkages, while SHp is polylactosaminoglycan-modified. All these forms exist at the surface of host cells, excluding the truncated SHt, whilst SH0 is the most abundant of these forms (Gan et al., 2008; Teng and Collins, 1998). In addition, the SH protein is phosphorylated at specific tyrosine residues during infection, a process that affects its subcellular distribution (Rixon et al., 2005).

1.4.1.3.2 Protein-protein interaction involving HRSV SH protein

To identify potential SH protein-binding partners, a membrane-based yeast two-hybrid system (MbY2H) was used in combination with the human lung cDNA library, revealing an interaction between SH and the B-cell receptor-associated protein 31 (BAP31) (Li et al., 2015). BAP31 plays an important role in sorting newly synthesized membrane proteins and is located in the endoplasmic reticulum (ER) membrane (B. Wang et al., 2008). BAP31 has two coils at the C-terminus; one of them holding a variant of death effector domain (vDED) (Nizet et al., 1997) bordered by two cleavage sites specific for caspase-8. The cleavage of BAP31 depends on caspase-8 activation (Breckenridge et al., 2003; Breckenridge et al., 2002) resulting in the release of a p20 fragment that functions as a proapoptotic factor (Breckenridge et al., 2003; Rosati et al., 2010). This domain (BAP31) can develop a complex with mitochondrial fission 1 membrane protein (Fis1) (Iwasawa et al., 2011) that crosses the ER and the mitochondria to act as a platform for caspase-8 activation. However, details concerning the interaction between BAP31 and SH protein are not yet clear. The interaction between SH protein and BAP31 is dependent on caspase-8 activation; thus, for example, SH protein could bind with the vDED site and prevent the cleavage of BAP31 to p20 by inhibiting the caspase-8 activation leading to a delay in host apoptosis induction (Figure 1.4).

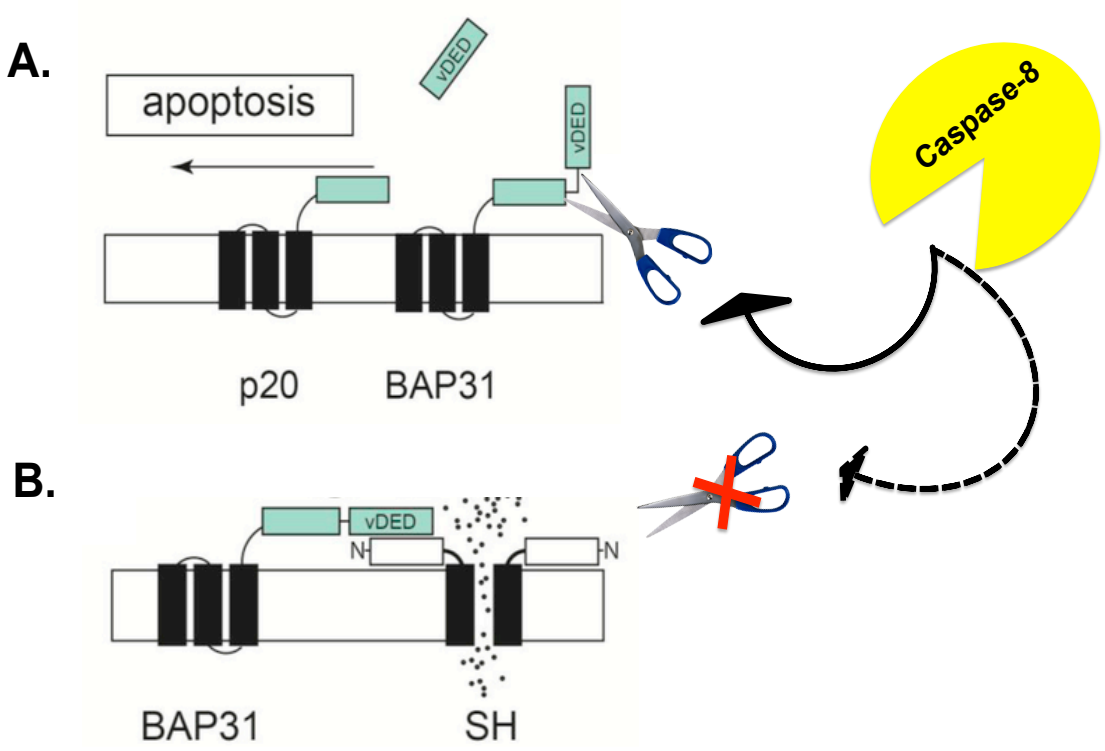

Figure 1. 4. A schematic representation of the hypothetical model of the role of SH protein in delaying apoptosis through its interaction with BAP31.

A. The activation of caspase-8 upon TNF-α or other stimulators leads to cleavage of the cytoplasmic vDED domain to form the p20 fragment that is a pro-apoptotic effector. **B**. SH protein contributes to inhibiting the BAP31 cleavage via blocking caspase-8. Figure adapted from (Torres et al., 2015).

1.4.2 Matrix protein

The HRSV matrix (M) protein is the major structural component of the virus particle. By analogy with M proteins of other related viruses, it is thought to possess a major role in viral assembly. This role was recently confirmed by tomographic images of HRSV particles in which M protein was shown to form a layer that bridges the viral N protein covered RNA genome with the cytoplasmic tails of the envelope glycoproteins (Liljeroos et al., 2013). Consistent with this critical role in virus assembly, removal of the M gene from the HRSV genome prevents the rescue of infectious virus. In addition, the use of gene expression ablation techniques such as siRNA to silence M protein expression during HRSV infection causes reduction in virus production and disturbs the development of virus-like filaments at the host cell membrane, which impedes the production of infectious virus (Kipper et al., 2015).

At later stages of the virus replication cycle, M protein accumulates at the inner surface of the plasma membrane, along with other structural proteins. At the point of virus release whilst the formation of virus particles is in progress the M protein assembles in a planar layer resulting from M-M dimer interactions, to eventually form an extended oligomer. The crystal structure of HRSV M has been determined and reveals a large hydrophobic surface (Money et al., 2009). It has been proposed that this interacts with membrane surfaces, as well as several charged clefts that are believed to interact with its other virus-encoded interaction partners. Residues that are thought to be involved in dimer formation have been shown to be critical for formation of infectious virus particles, suggesting formation of the M-M dimer is a critical event in the virus assembly process (Förster et al., 2015). M is thought to interact with both F and G envelope proteins, as well as components of the nucleocapsid, and in addition M2-1 (Henderson et al., 2002; Teng and Collins, 1998).

M protein has been observed in the nucleus at the early stage of infection and is thought to be involved in the shutdown of host cell transcription (Ghildyal et al., 2003). In addition, cellular interaction partners of the M protein have been characterized using a microfluidics screen and include components of the receptor mediated endocytosis pathway, ZNF502, and actin-binding protein cofilin 1 (Kipper et al., 2015).

1.4.3 Ribonucleocapsid proteins: L, N, P and the M2 proteins

Five viral proteins (N, P, L, M2-1 and M2-2) comprise the viral ribonucleoprotein (RNP) complex which is responsible for all RNA synthesis activities of the viral RNA genome (Bermingham and Collins, 1999). The L protein possesses the catalytic activity of the RNA-dependent RNA polymerase (RdRp) that is responsible for all replicase and transcriptase enzyme activities (Collins, 2007). As part of this process, the L protein also contains active sites that perform 5’ mRNA capping and 3’ polyadenylation, which results in the formation of a mRNA that resembles a functional and mature cellular mRNA complete with 5’ methylated cap structure and the addition of a 100-120 nt long poly (A) tail (Liuzzi et al., 2005). In contrast to these mRNAs, the viral RNA replication products do not possess 5’ cap and 3’ poly (A) tail features; thus the

stability of these RNA products is thought to be mediated by their tight encapsidation with the nucleocapsid (N) protein, in order to prevent degradation from cellular nuclease activities.

At all stages of the life cycle of the virus, the N protein binds tightly to the viral RNA to form a nuclease-resistant helical RNP complex. The N protein also binds the RNA anti-genome that is the positive sense replicative intermediate. N protein contains 391 amino acids meaning it is relatively smaller than other *Paramyxovirinae* subfamily counterparts that mostly lie within the range of 489-553 amino acids. The crystal structure of the HRSV N protein takes the form of a decameric annular ring, and modeling of high-resolution N protein monomers using cryo EM images of purified RNPs allowed a high-resolution model of an intact RNP to be derived (Tawar et al., 2009). This showed details of N-N interactions, as well as interactions between each monomer and the RNA strand which is tightly sequestered into a positively charged groove that lies between N- and C-terminal N protein lobes. This provided an explanation of the high degree of nuclease resistance offered by N protein encapsidation.

The P protein is a component of the viral RdRp, along with the catalytic component L. P comprises 241 amino acids and is thus considerably smaller than its *Paramyxovirinae* subfamily counterparts that are typically in the range of 391-602 amino acids. The phosphoprotein (P) as its name suggests is phosphorylated by host cell kinases at multiple sites, and these modifications have functional consequences in terms of RNA synthesis (Collins, 2007). P binds the N protein and acts as a chaperone, ensuring it does not associate with cellular RNA prior to delivering N to the RNA genome during encapsidation (Tawar et al., 2009; Collins and Graham, 2008). The functional form of P is thought to be a tetramer, and it is involved in further interactions with the M2-1 protein, in which P tetramers interact with M2-1 tetramers (Castagné et al., 2004; Rodríguez et al., 2004).

While N, P and L proteins are necessary to guide the viral RNA replication to generate full-length replication products, transcription to yield mRNAs requires in addition the M2-1 protein. When M2-1 is absent, the RdRp prematurely terminates mRNA transcription (Collins et al., 1996) and for this reason it was

proposed that M2-1 acts as a polymerase processivity factor. Later, M2-1 was also shown to influence transcription termination at the end of genes, and hence was also described as having transcription anti-termination activities. These two activities are likely related, and so taken together, M2-1 is considered to be an essential transcriptional factor (Bermingham and Collins, 1999; Fearns and Collins, 1999) required for the synthesis of discrete full length mRNAs.

As described above, the M2-1 protein is known to associate with P protein with both interacting partners in the tetramer form, and this interaction is thought to deliver M2-1 to the RNA template (Tran et al*.,* 2009). Moreover, the association of M protein with an inclusion-like structure formed by N and P proteins is related to the presence of M2-1 (Li et al., 2008; Ghildyal et al., 2002). The recent identification of M2-1 within extracellular virus particles suggests that it may also perform a role in virus assembly. It has been suggested that M2-1 forms a layer bridging the RNP and M protein layers (Kiss et al., 2014), although this is not consistent with the recently determined crystal structure of M2-1, which suggests its only possible conformation is that of a ring-like tetramer in which all available oligomerization domains are occupied (Tanner et al., 2014).

The last component of the RNP is the M2-2 protein, which has been shown to participate as a regulatory protein, controlling the switch in polymerase activity from transcription to RNA replication (Bermingham and Collins, 1999). Preventing M2-2 expression through gene deletion does not prevent virus viability, however the resulting recombinant viruses do exhibit reduced growth, and M2-2 deleted viruses are being considered as live vaccine candidates.

1.4.4 Non-structural proteins

The viral proteins NS1 and NS2 are considered to be non-structural proteins, as they are not present to any great degree in the virion, whereas upon infection the non-structural proteins are abundantly expressed in the host cell cytosol. The NS1 and NS2 mRNAs are expressed in high abundance relative to all other viral mRNAs due to their 3’ proximal position on the genome,

and consequently NS1 and NS2 production is also likely to highly abundant (see section 1.5.2). Both NS1 and NS2 are involved in suppressing the activation of the cellular innate immune response to HRSV infection that is induced following expression of type 1 interferon. Several mechanisms have been proposed to account for how these two proteins mediate innate immune blockade, including preventing nuclear translocation of the interferon regulatory factor 3 (IRF-3) and inhibition of type I interferon signaling by degrading signal transducer and activator of transcription (STAT2), with Elongin-Cullin E3 ligase (Moore et al., 2008).

HRSV with NS1 or/and NS2 genes deleted showed reduced induction of tumor necrosis factor alpha (TNF-α), interleukin 8 (IL-8) and RANTES (Regulated on Activation, Normal T-cell Expressed and Secreted) compared with wild type recombinant virus which supported the use as attenuated vaccine candidates (Spann et al., 2005).

1.5 The HRSV life cycle

In its natural environment, HRSV infects ciliated epithelial cells of the upper and lower respiratory tract (Zhang et al., 2002). In the laboratory, HRSV can infect a broad range of epithelial cell types including HEp-2 (human larynx carcinoma cell), A549 (human lung alveolar basal epithelial cell) cell lines and Vero cells (African green monkey kidney epithelial cell) that vary in their ability to support viral propagation and efficiency of infection.

1.5.1 Binding and entry

The virus binds cells via an interaction between GAGs (glycosaminoglycans) on the host cell surface such as heparin (Hallak et al., 2000) and the viral surface glycoproteins F and G (Hallak et al., 2000). Following this initial binding process, a higher affinity interaction occurs between the virus and host cell, which involves the specific cellular receptors nucleolin and the chemokine fractalkine (Santini, 2015; Haynes et al., 2001). The following events that result in the entry and uncoating of the virus within infected cells are still unclear. It has been suggested that the virus enters cells by fusion

of its envelope with the plasma membrane via clathrin-mediated endocytosis (also known as receptor-mediated endocytosis), which transports the virions into the cytoplasm (Kolokoltsov et al., 2007a) (Figure 1.5). However, it has also been suggested that HRSV entry to the host cell is mediated by the activation of a signaling cascade involving the epidermal growth factor (EGF) receptor, cell division control protein 42 homolog (Cdc42) and the serine/threonine-protein kinase PAK1, as well as other downstream effectors. These effectors cause cellular actin rearrangement, cell rounding and the formation of blebs that increase fluid uptake, all characteristics of macropinocytosis. Following internalization, the virus was found within Rab5 positive macropinosomes, from which it subsequently escaped an average of approximately 50 minutes after internalization (Krzyzaniak et al., 2013).

1.5.2 Transcription and replication of the viral genome

According to the Baltimore system HRSV is classified under Group V as a consequence of its single-strand negative-sense RNA (-ssRNA) genome, which must be copied by an RdRp to yield positive-sense mRNAs that can then be translated by cellular ribosomes. The -ssRNA genome is transcribed by the RdRp to give predominantly mono-cistronic positive-sense mRNAs and this process occurs in the host cytoplasm. This cytoplasmic replication cycle is typical for the majority of mononegavirales members, but there are some exceptions that involve the nucleus at critical stages of the life cycle. These examples include influenza A virus that performs mRNA transcription and RNA replication in the nucleus of the infected cell (Krug et al., 1987).

Some four hours post-infection, mRNA transcription and translation is initiated and proceeds for 12 to 18 hours (Collins, 2007). Transcription occurs by the viral RdRp attaching to a single entry site at the 3’ genome terminus and moving in the 3’ to 5’ direction, transcribing mRNAs from each of the 10 HRSV genes in a sequential stop-start manner. During this movement, the progression of the RdRp is controlled by conserved signals at both the beginning and end of each gene, which are called gene start (GS) and gene end (GE) signals, respectively. Adjacent GS and GE sequences are separated by a variable sequence called an intergenic region (IGR) and together these three elements

form the gene junction (GJ). All evidence suggests that the RdRp may not enter the genome at internal locations or GJs within the genome. The result is a total of 10 subgenomic positive-sense mRNAs (Figure 1.6), each of which is 5' capped and 3' polyadenylated, having been formed by repetitive copying of the U residues at the polyadenylation site within the GE (Kuo et al., 1997). Importantly, the abundance of these mRNAs is not consistent. Instead, the abundance of mRNAs decreases in approximate accordance with the position of each gene on the linear HRSV genome. Those genes located nearer to 3' are expressed with greater abundance than those positioned towards the 5' end.

The explanation for this is that a proportion of the RdRps that load on the 3' genome end, disengage from the template as the GJ is reached. This level of RdRp disengagement (or fall-off) is thought to be approximately 30% thus genes located near the genome 5' end are transcribed in extremely low abundance in relative terms. Thus, mRNA expression of any particular gene is dependent on its distance from the 3' end of the RNA genome, or in other words, on the gene order (Barik, 1992; Dickens et al., 1984). This mechanism of viral gene expression appears to be conserved across all mononegavirales members (Cordey and Roux, 2007; Kolakofsky et al., 1998).

The RdRp also acts as a replicase to synthesize a complete complementary copy of the initial vRNA, to give a full-length positive strand RNA known as an antigenome or cRNA. A major difference between mRNA transcription and RNA replication is that in replication, the RdRp must fail to respond to the GJ signals and enter a read-through mode resulting in synthesis of an entire complementary RNA strand of identical length as the initial RNA template. Once the antigenomic cRNA is made, it can then be further copied by the RdRp to form further vRNAs, again of precisely equal length to the original template. The abundance of genomic vRNAs in infected cells is significantly higher than the antigenomic cRNAs (Collins, 2007).

As yet, there is no precise understanding of how the virus switches between transcription and replication activities. However, it is thought that related viruses can control the balance between transcription and replication through

expression of their proteins. As an example, the V protein of Sendai virus has the ability to inhibit the RNA replication via interaction with N protein (Andrejeva et al., 2004). In the case of HRSV, it has been shown that expression of M2-2 can control virus transcription and replication (Bermingham and Collins, 1999) and as evidence of this control, the over expression of M2-2 has been shown to significantly suppress HRSV replication in the host cell (Cheng et al., 2005).

1.5.3 Assembly and budding

Approximately 10 to 12 hours post-infection the first mature virions are released, with the peak of virus release being reached within approximately 24-48 hours. At later time points, between 48 to 72 hours post-infection, the infected cells lyse (Collins, 2007). During assembly and budding of HRSV particles the RNP complexes and envelope proteins as well as M are transported to the plasma membrane where they assemble (Marty et al., 2003). The assembly sites where viral envelope glycoproteins associate with the already formed RNP complex are enriched with lipid-raft ganglioside GM1 or caveolin-1 (Brown et al., 2002) on the apical surface of polarized epithelial cells (Brock et al., 2003) (Figure 1.5).

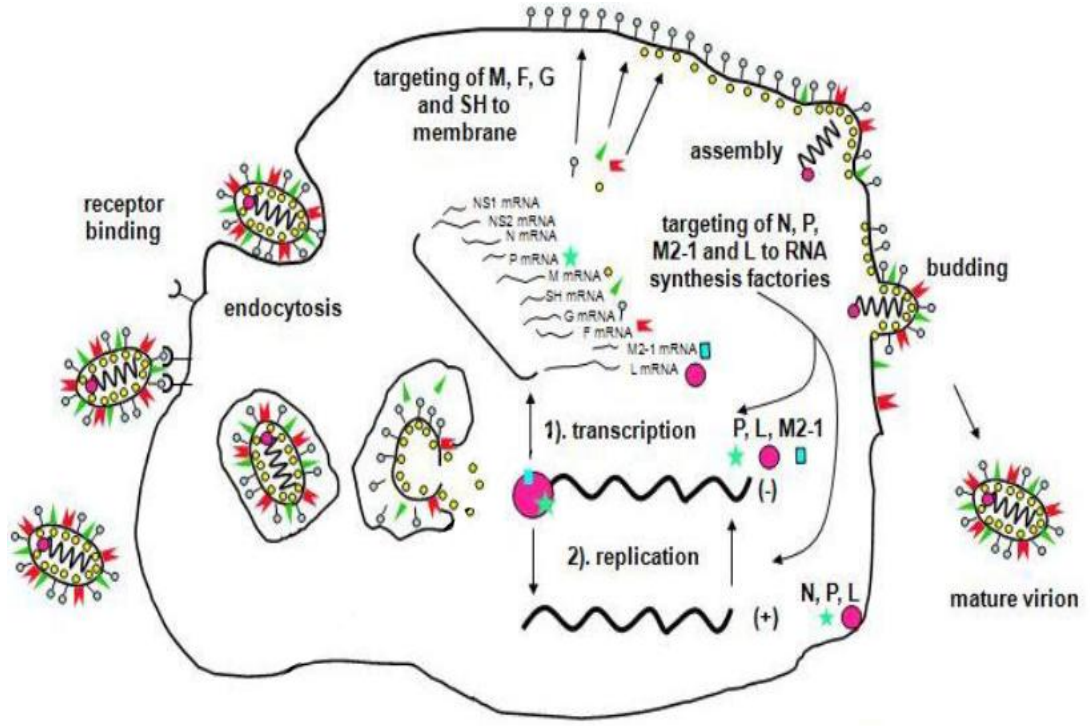

Figure 1. 5. Schematic representation of the HRSV life cycle.

The HRSV replication cycle starts with its binding at the host cell surface mediated through F and G proteins. Virions may enter the plasma membrane through clathrin-mediated endocytosis or macropinocytosis. The input negative stranded RNA genome is first transcribed to yield 10 individual mRNAs that are then translated into virus proteins by host cell ribosomes. Some of these proteins subsequently allow replication of the input genome to yield an antigenomic RNA that serves as a replication intermediate. Other viral proteins block innate immune responses of the host cell, while others are trafficked to the plasma membrane for virion assembly. Further replication of the antigenome provides more negative stranded genomes for either further transcription or for packaging into virus particles. Virus proteins accumulate and assemble on the intracellular surface of the host cell, from which viruses assemble and bud. (Figure adapted from Dr. John Barr).

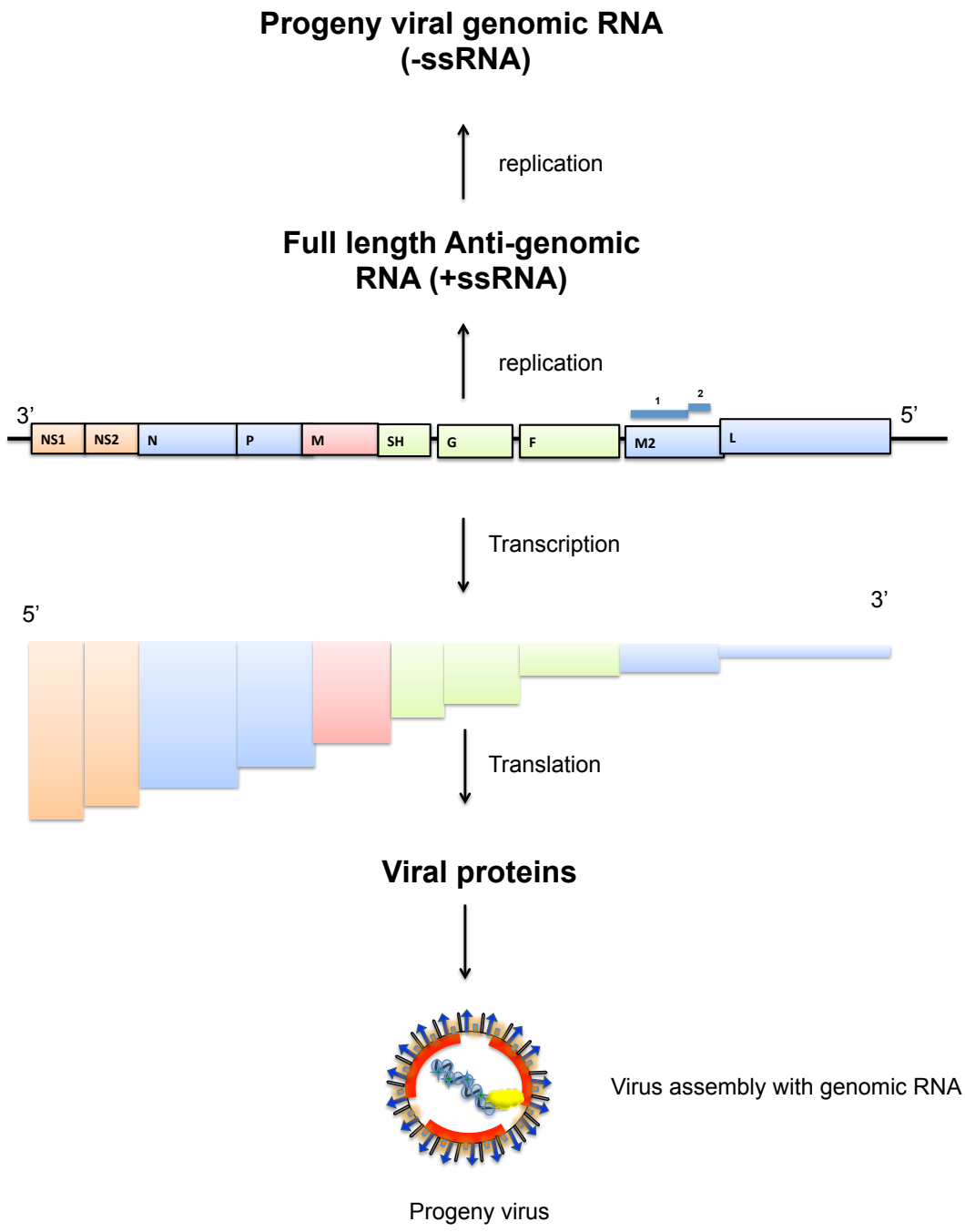

Figure 1. 6. Schematic representation of the HRSV transcription and translation strategy.

The HRSV RNA genome is transcribed to 10 individual mRNAs, which are readable by host cell ribosomes. The abundance of each mRNA forms a gradient, where mRNA abundance decreases with increasing distance from the 3' end promoter. Each mRNA encodes a single viral protein (monocistronic) except M2, which encodes two proteins M2-1 and M2-2 though different ORFs. The negative stranded input genome is

replicated to form an antigenome that can be further replicated to form additional negative sense genomes ready for either further transcription, or for packaging into progeny virus.

1.6 HRSV pathogenesis

It is known that HRSV infects epithelial cells in the upper and lower respiratory tract specifically the bronchial epithelium and alveolar cells type I, also known as pneumocytes. When HRSV succeeds in infecting the human pneumocytes it leads to ~20% of children having hypoxemia (oxygen deficiency in the blood), even when there have been no previous or current significant symptoms. Autopsy studies show that fatal HRSV infection can be caused by an obstruction in small airways with sloughed epithelia and inflammatory cells mixed with fibrin and mucus (Johnson et al., 2007). In addition, it results in the signs of wheezing characteristic of young children with acute disease. This virus is one of the main pathogens encountered in premature neonates or young infants, although the impact of HRSV infection on the developing lung and airway is still not clear.

There are some pathogenic features that are determined by HRSV in the host cell that gives the virus its virulence characteristics. One of the most important factors in determining characteristic HRSV pathogenicity is its tissue tropism for which it has a high degree of specificity for ciliated cells of the upper and lower respiratory tract, described above, which are the primary and characteristic sites of disease. In addition, the virus has the ability to cause reinfection throughout life without significant antigenic change (Prince et al., 1987; Siber et al., 1994) and the reasons for this are not entirely clear. Genetic variation likely plays an important role in reinfection, with a noticeable lack of neutralizing antibodies present on subsequent encounters with the virus also significant. HRSV exhibits a high degree of infectivity and ease of transmission, and it is one of the most contagious human pathogens that cause childhood hospitalization due to bronchiolitis or pneumonia (Abdallah et al., 2003). In addition another specific factor in determining HRSV pathogenicity is that HRSV encodes the NS1 and NS2 proteins that are highly efficient in blocking innate immune pathways, and thus ensure virus survival (Bitko et al., 2007).

A significant characteristic of HRSV is its ability to infect humans in the early stages of life and evade the passive immunity conferred by maternal antibodies. Virus replication is a serious problem for young infants that have small and narrow airways that lower the ability of the infant to tolerate severe HRSV infection and resulting inflammation through induction of the immune response. As an example a study has observed that infants infected with HRSV that are less than three months old show an induced Th2-biased response in comparison with older infants (Kristjansson et al., 2005). Hence, HRSV can play an important role in shaping host immunity, including the exaggeration of the cytotoxic T lymphocytes (TLC) response in certain age groups. Therefore, the host immune response varies according to the overall effectiveness of the immune response that is associated with the age and the health of infected human (Collins and Graham, 2008).

Overall, HRSV pathogenesis is associated with the high infectivity, tissue tropism, immune host response and its ability to cause early life infection and reinfection. Understanding and defining viral pathogenesis in all age groups will be important in order to design a HRSV vaccine or an anti-viral agent.

1.7 Virus encoded ion channel proteins (viroporins)

Viruses encode encoded ion channels, and these play an important role in virulence and pathogenicity. The ion channels encoded by viruses are mainly categorized under the name of viroporins, which are a group of small and hydrophobic virus proteins that can oligomerize and form pores in lipid membranes, which can include those of both the virus or the host cell (Gonzalez and Carrasco, 2003). They act by modifying the normal ionic homeostasis present within the cell or a cellular compartment, and have been shown to mediate many diverse functions including virus entry into the cell, enabling virus replication or leading to conformational changes in the membrane and thus altering cell permeability (Ciampor, 2003). Viroporins are typically small proteins consisting of between 60-120 amino acids with one or two alpha (α) helical TM regions, and that allow ion exchange or the passage of small molecules across lipid bilayers present either within the cell or virion (Gan et al., 2008). Viroporins can act as virulence factors that support the replication

of the viral pathogen during infection. When viroporins function as ion channels, the subsequent disruption of normal cellular ion homeostasis may cause dissipation of the membrane potential resulting in a diverse range of effects (Ciampor, 2003). To date, at least 27 viroporins have been recognized and the M2 proton channel of IAV is one of the best-studied examples (Stouffer et al., 2008; Schnell and Chou, 2008). Table 1.2 shows all identified viroporins.

Generally, based on *in vivo* and structural electrophysiological studies, viroporins are very hard to observe due to the difficulty of expression and purification of these hydrophobic membrane proteins. Despite this, structures of the HIV-1 Vpu protein (Sharpe et al., 2006), HCV p7 protein (Cook and Opella, 2010), and SARS-CoV E protein (Pervushin et al., 2009) have been determined by NMR methods. These proteins have had their channel activity confirmed by using *in vitro* reconstitution assays such as black lipid membranes (BLM) and these assays can also be used to identify channel blocking compounds, such as hexamethylene amiloride (HMA) (Premkumar et al., 2004). In contrast, the coronavirus envelope (E) protein shows a very mild susceptibility to amiloride when observed by NMR, but it supports channel activity in a mammalian whole cell patch clamp set-up (Pervushin et al., 2009).

Classification	Family	Virus	Name	A.A	TMDs	Ion specificity	Role of channel function
ssRNA (−)	*Paramyxoviridae*	HRSV	SH	64	1	K^+/Na^+	TNF antagonist Pathogenesis
	Orthomyxoviridae	Influenza A virus	M2	97	1	H^+	Entry, Viral production (some)
		Influenza B virus	BM2	115	1	H^+	Entry
		–	NB	100	1	H^+	–
		Influenza C virus	CM2	115	1	H^+	Entry
ssRNA (+)	*Picornaviridae*	Poliovirus	2B	97	2	Ca^{2+}	Viral production, cell lysis
			VP4	68	1	–	Entry
		Coxsackievirus B3	2B	99	2	Ca^{2+}	Viral production, cell lysis
		EV71	2B	99	2	Cl^-	Virus spread

		Human rhinovirus	VP4	68	1	–	Entry
	Flaviviridae	Hepatitis C virus	p7	63	2	H^+	Particle production, entry?
		BVDV	p7	63	2	H^+	Viral production
		CSFV	p7	63	2	Ca^2	Viral production
		Dengue virus	M	75	2	K^+/Na^+	Viral production
	Togaviridae	Semliki Forest virus	6K	60	2	K^+/Na^+	Viral production
		Sindbis virus	6K	55	1	K^+/Na^+	Viral production
		Ross River virus	6K	62	1	K^+/Na^+	Viral production
	Coronaviridae	SARS-CoV	E	76	1	K^+/Na^+	Viral morphogenesis and assembly
			3a	274	3	K^+	Virus release

			8a	39	1	K^+/Na^+	–
		MHV	E	83	1	K^+/Na^+	Viral production
dsRNA	*Reoviridae*	Rotavirus	NSP4	175	1/3	Ca^{2+}	Viral production, endotoxin
Reverse transcription (RNA)	*Retroviridae*	HIV-1	Vpu	81	1	K^+/Na^+	Viral production
		HTLV-1	P13ii	87	2	K^+	Mitochondrial permeability
dsDNA	*Polyomaviridae*	SV40	VP4	125	1	Ca^{2+}	Viral production
		JC	Agno	71	1	Ca^{2+}	Viral production
	Papillomaviridae	HPV-16	E5	83	3	H+	Oncogene signalling/trafficki

Table 1. 1. Summary of viruses with known viroporins: The table illustrates the viroporin size in kDa, length in amino acids (AA), ion specificity and number of transmembrane domains (TMDs). Table information obtained from Scott (2015).

Abbreviations: HRSV (human respiratory syncytial virus) EV71 (enterovirus 71); HCV (hepatitis C virus); BVDV (bovine viral diarrhorea virus) SARS-CoV (severe acute respiratory distress syndrome-associated coronavirus); CSFV (classical swine fever virus); MHV (murine hepatitis virus); HIV-1 (human immunodeficiency virus type 1); SV40 (simian virus 40); JC (John Cunningham polyomavirus); HPV-16 (human papillomavirus type 16); HTLV-1 (human T-lymphotropic virus type 1).

1.8 Therapeutic approaches

Since there is no licensed HRSV vaccine, passive antibody immunization has been developed to lessen HRSV morbidity. Infants, including those that suffer from congenital heart disease or bronchopulmonary dysplasia, are targeted for treatment (McLellan et al., 2010). Palivizumab (commercial name - Synagis) is the only humanized anti-infective monoclonal antibody that is approved by the US Food and Drug Administration (FDA) for HRSV treatment and prevention (McLellan et al., 2010). Palivizumab was humanized from an initially characterized anti-F protein monoclonal antibody (1129) that originated from mice. This antibody binds at a linear 24-residue epitope that forms a helix-loop-helix on the globular domain of the F protein, and binding prevents the conformational changes of the F protein, and thus impinges on the fusion event between the viral envelope and the host cell that is required for virus infectivity. Palivizumab is administered at a dose of 15mg/kg when needed to prevent infants from severe virus infection. It reduces HRSV-related hospitalization by 55%, and while its efficacy is proven, it is a highly expensive treatment that is out of the reach of the most vulnerable patients in economically poor regions.

Motavizumab is a derivative of Palivizumab, engineered by systematically substituting all alternative amino acids at each of the 59 positions within the antigen-binding site. The outcome was a new antibody that was ten-fold more potent than its predecessor, and which has demonstrated high efficacy in clinical trials (O'Brien et al., 2015). Furthermore, it has the ability to recognize F glycoprotein in different configurations. However, motavizumab has failed to achieve FDA approval, and is no longer in development (Rodriguez and Ramilo, 2014; Shah et al., 2010).

Another current FDA-approved HRSV treatment, ribavirin (RBV), is a synthetic nucleoside analog that consists of an incomplete purine (guanosine) ring (Mazur et al., 2015; Shah et al., 2010). It is also known as virazole, rebetol, and ribasphere depending on the country of sale. It can be introduced orally by either tablet delivery or as an aerosol (inhaled ribavirin). RBV is a broad-spectrum antiviral that is approved for use against many DNA and RNA viruses *in vivo*, and furthermore is used to treat several highly pathogenic viral

infections as a last resort in non-FDA approved situations. Originally, RBV was approved to treat children infected with HRSV, but now it also forms part of a successful regime for treating patients with hepatitis C virus (HCV) in combination with pegylated interferon (Shah et al., 2010).

Several cases of treatment failure of RBV on patients infected with HRSV have been recorded, and as a consequence it is no longer recommended by the American Academy of Pediatrics (AAP). The possible reasons for this are difficult to understand due to insufficient evidence of effectiveness. The mode of action of RBV against HRSV infection is still unclear, and several mechanisms have been proposed. One of these is that RBV increases the error rate of the viral polymerase while copying or transcribing the HRSV RNA genome. When the error rate increases above a certain point, the virus becomes non-viable as too many nucleotide changes are incorporated with lethal consequences. Mutation of the viral RNA polymerase is a possible reason for the treatment failure; as a single mutation in the polymerase may lead to the virus gaining resistance to RBV. Hence, the failure of some RBV treatments could be explained by drug resistance via viral mutation (Shah et al., 2010).

Overall, there is no effective, economical treatment for HRSV. The oxygen inhaler still remains as the only economically feasible and supportive measure to reduce the symptoms of severe lower respiratory tract disease that are caused by HRSV (Schickli et al., 2009).

1.8.1 HRSV vaccine development

There is an unmet need to develop an HRSV vaccine that must be effective both in stimulating an immune response and also in demonstrating a low pathology among infants, due to their immunologic immaturity. In the 1960s, a formalin-inactivated respiratory syncytial virus (FIRSV) vaccine was tested in human infants and was unable to protect against subsequent wild-type virus mediated disease, and led to a severe exacerbated disease with 80% of the vaccinated children being hospitalized following subsequent exposure to HRSV, resulting in 2 fatalities (Empey et al., 2010). Retrospective investigation of the underlying cause for exacerbated disease outcome suggested that the

chemically inactivated virus induced the generation of antibodies that were non-neutralizing, thus offering poor protection. The non-neutralizing antibodies also formed immune complexes with their intended viral antigen targets, and deposition of these in the lungs caused complement activation during subsequent HRSV infections (Polack et al., 2002) and this was a major contributing factor to increased viral pathogenesis.

1.8.1.1 Goals of Vaccination

The primary aim of vaccine development is to prevent LRTI in young infants who are susceptible to HRSV infection, and who are particularly at risk from acquiring HRSV infection from school-age siblings (Graham, 2016) or any family member who could carry the pathogen from an outside environment. Endpoints would include the prevention of hospitalization or medically attended LRTI. The other goals of developing a useable vaccine are: (1) to prevent medically attended LRTI in young children; (2) to prevent morbidity and hospitalization of the elderly and, (3) to reduce childhood wheezing and all morbidity related to HRSV infection in children and adults (Figure 1.7). Moreover, five other populations have been prioritized as needing protection from HRSV infection, namely; pregnant women, infants under six months, infants between six months and two years, toddlers and school-age children (two- to five-year olds) and those over 60 years of age (Graham, 2016).

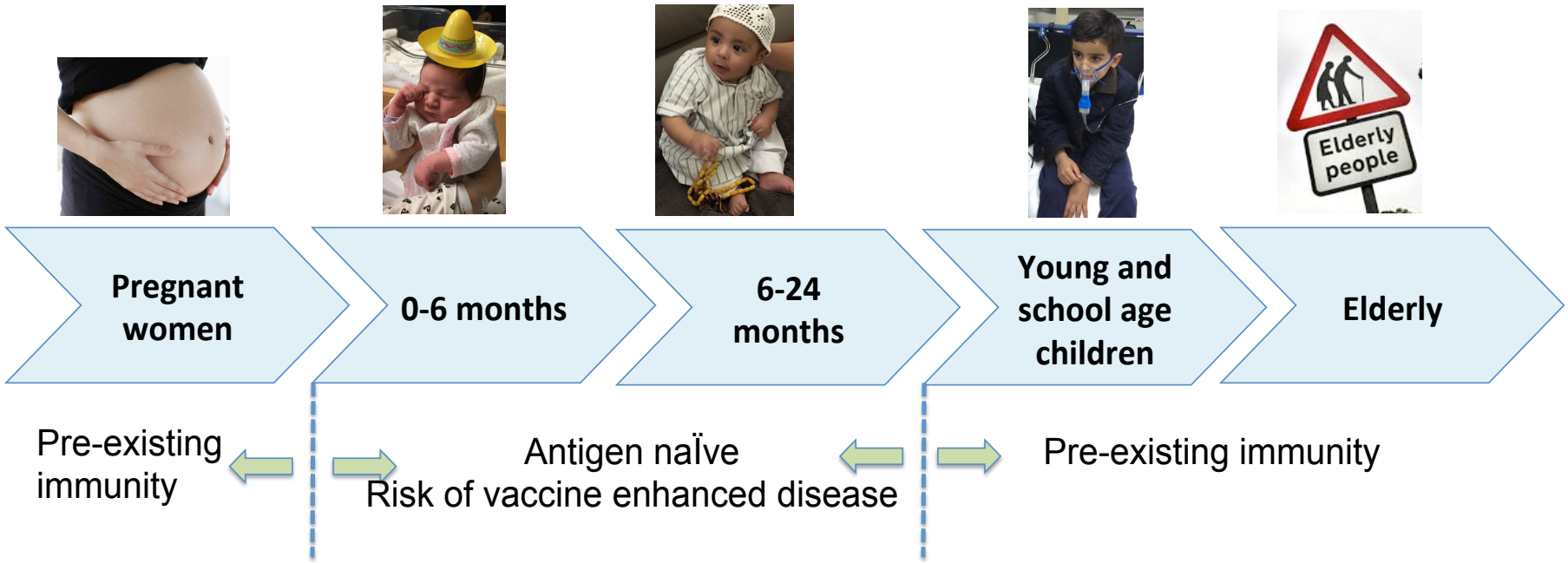

Figure 1. 1. Potential target populations for a HRSV vaccine.

1. Pregnant women, 2. Infants less than six months old 3. Infants and toddlers aged six months to two years. 4. School-aged children (two to five year olds) 5. Those over 60 years of age. Children aged 0 to 24 months would be most directly affected if an effective vaccine was developed. School-age children would be protected from recurrent HRSV infection and wheezing that could develop into asthma later in life. For the over-60s and pregnant women this would boost pre-existing immunity. Figure adapted from Graham (2016).

1.8.1.2 Live-attenuated vaccines

Live vaccines are one of the approaches being implemented for the generation of an HRSV vaccine, by using an attenuated strain of the virus for intranasal administration. This strategy fulfills several aims: it induces both systemic and local mucosal immunity; the intranasal administration fights the suppressive effects of maternal serum antibodies, and it provides complete protection and is more immunogenic compared with inactivated vaccines. Finally, it is less likely to be associated with the enhanced disease caused by the previous FIRSV inactivated vaccine, described above.

A common strategy used to select attenuated live viruses as vaccine candidates is to pass viruses in cell culture at a low temperature of approximately 33°C (cold passage), and also to combine this with the use of chemical mutagenesis to increase the rate of mutation accumulation (Empey et al., 2010). The resulting viruses adapt to growing and replicating at a relatively low temperature that is consistent with the upper respiratory tract of a human host, rather than at the slightly higher temperatures found in the lower respiratory tract. The negative consequences of this attenuation method are that the resulting virus may exhibit growth that is either over- or under-attenuated. The under-attenuated viruses pose the risk of causing disease when individuals are then exposed to the vaccine, whereas viruses that are over-attenuated may elicit only a poor immune response that fails to protect.

Thus, another strategy for generating live attenuated vaccines has been developed, using reverse genetics by producing a complete infectious virus in cell culture from cloned complementary DNA (Collins et al., 1995). This approach allows specific sequence changes to be engineered into the HRSV genome, to get a more precise level of growth attenuation combined with sufficient immunogenicity. Using this method, a recombinant HRSV A2 was engineered with the name cp248/404/1030/ΔSH (MEDI-559; MedImmune and National Institute of Allergy and Infectious Diseases). This virus includes multiple point mutations previously identified as being attenuating from cold-passage studies, including mutations in NS2, M2-2 and L genes (Mazur et al., 2015) but in addition the SH gene was deleted by manipulating a recombinant

cDNA representing the HRSV genome. This was the first candidate virus that was sufficiently attenuated to be suitable for administration to neonates between one and two months of age. Other vaccine candidates include recombinant HRSV A2 cpts530/1009ΔNS2 and recombinant HRSV A2 cpts248/404/ΔNS2, both of which carry NS2 gene deletions along with cold-passage acquired mutations, and these are under development. Despite their high levels of immunogenicity in animal models, there are still concerns regarding their genetic stability and evaluation in humans is ongoing (Empey et al., 2010).

1.8.1.3 Subunit vaccines

Non-replicating subunit vaccines provide a safe vaccination option compared to a live-attenuated vaccine candidate, as they offer no possibility of reversion to a pathogenic wild type strain. The basic idea behind a subunit vaccine is to immunize an individual with purified HRSV structural proteins that are targets for anti-HRSV neutralizing antibodies, such as M, G and F proteins. These antigens subsequently elicit the generation of protective antibodies. Examples of these subunit vaccines are: a combined subunit vaccine containing F, G, and M proteins (in development by Sanofi Pasteur); BBG2Na, a G peptide conjugated to streptococcal protein G; and a combined subunit vaccine containing F, G, and M proteins (also in development by Sanofi Pasteur). However, these vaccines are likely to be very weakly immunogenic in very young children and neonates due to their poorly developed immune systems. HRSV N protein and F envelope protein are important antigens for subunit vaccines especially for pregnant women (Johnson et al., 1987) since this type of vaccine does not cause a serious risk to the baby in pregnant woman (Mazur et al., 2015).

1.8.1.4 Vector vaccines

The overall aims of this method are to generate a vaccine that provides a high level of immunogenicity, no possibility of disease, and a high degree of genetic stability. To achieve these aims, HRSV proteins are expressed using a

heterologous and non-pathogenic virus that are specifically engineered using recombinant techniques (Empey et al., 2010).

1.8.1.5 Bivalent vaccines

Another strategy that has been used to elicit a protective immune response using a live attenuated vaccine is to express the HRSV F protein using a backbone that represents a bovine/human chimeric parainfluenza type 3 genome (PIV3)/RSV F2 (MEDI-534), in the hope of protecting recipients from future infections of either HRSV or PIV3. Studies in animal models (monkeys) suggest this vaccine candidate is highly protective against HRSV wild type (Empey et al., 2010). Serological analysis shows immunization stimulates high titers of HRSV and human PIV3-neutralizing antibodies. Nevertheless, further study is needed to examine the immunogenicity and safety in children.

1.8.2 Antiviral therapies

The discovery of antiviral drugs would be an important development that could be used to treat or protect young children with low immune responses from HRSV infection and disease. Poor immune responses in infants may be due to underdevelopment of adaptive or innate immune systems, or due to genetic abnormalities. To date, some 11 antivirals for HRSV are under study in various clinical trials. These can be classified into four main therapeutic classes: (1) siRNAs post-transcriptional gene silencing, (2) passive immunoglobulin therapies, (3) small molecules and (4) fusion protein inhibitors. These strategies target five HRSV proteins out of a total of 11, namely, G (viral attachment), F (fusion) and P, N and L (RNP components).

1.8.2.1 Virus encoded ion channels as drug targets

Virus-encoded ion channels may also serve as suitable antiviral targets that block virus growth and thus virus-mediated disease. One of the most widely studied antiviral inhibitors, namely amantadine, was developed for influenza A virus (IAV) and was subsequently shown to inhibit the activity of the M2 proton channel. This drug has been used clinically since 1966 following its approval for human usage by the FDA (Oxford and Galbraith, 1980). However, in 1985 a

study found that IAV could develop resistance to amantadine (Hay et al., 1986), and the mechanism behind this resistance was shown to be genetic mutation of M2, which strongly suggested that the antiviral activity mode of amantadine was to target M2. In the following years, an increasing number of amantadine-resistant viruses were isolated from all regions of the globe, with all circulating strains being resistant by 2008/2009. The use of amantadine as an antiviral agent has now been discontinued (Pielak and Chou, 2010).

Another reported ion channel drug (an amiloride derivative) was reported to block ion channel activity of coronavirus E protein and HIV-1 Vpu protein (Wilson et al., 2006; Ewart et al., 2002). Drugs including amantadine, long-alkyl-chain iminosugar derivatives and hexamethylene amiloride (HMA) also demonstrated an inhibitory effect on the hepatitis C virus (HCV) p7 ion channel protein, which may represent a promising anti-viral target (Wilson et al., 2006; Ewart et al., 2002; Premkumar et al., 2004). HCV p7 protein showed different responses to these drug treatments (Griffin et al., 2008). Moreover, this paper described the use of a liposome-based screening system *in vitro* to investigate the ion channel activity of the responsible virus protein that could lead to a suitable method of screening for future anti-viral drugs.

1.9 Ion channel activity and virus-host interaction

1.9.1 Virus production

Generally, viroporins do not play a role in viral genome replication or gene expression. However they contribute towards processes relevant for viral production during the viral life cycle such as entry, assembly, protein trafficking and virus release (Nieva et al., 2012; Steinmann and Pietschmann, 2010). As evidence of these important roles in the replication cycle, blocking the activity of viroporins using specific antiviral compounds or through preventing viroporin expression by gene deletion or RNA interference techniques can significantly reduce yield of virus particles, such as HCV lacking p7, or alternatively SARS-CoV in which the E gene is deleted results in approximately 100-fold decreased virus titres (DeDiego et al., 2007; Kuo and Masters, 2003). On the other hand, some viruses are more tolerant when viroporin encoding genes are deleted,

such as HIV-1 deleted Vpu and IAV lacking M2 in cell culture (Dubyak, 2004; Steinmann and Pietschmann, 2010; Minor et al., 1998). Moreover, in some other cases, the deletion of a viroporin gene from the viral genome will only show an effect during the infection of primary cells rather than cells derived from cancer-derived continuous cultures. As an example, HRSV with the SH gene deleted showed equivalent growth in cell culture as the wild type, but in contrast showed limited virus production in nasal turbinates of infected chimpanzees and mice (Bukreyev et al., 1997; Whitehead et al., 1999). However, the role that ion conductivity plays in boosting virus production remains unclear and further investigation is needed to understand the mechanisms behind these observations. Pharmacological inhibition studies help our understanding of viroporin ion channel conductance and the role of ion channel activity in virus propagation.

A list of ion channel inhibitors showing their effect on inhibiting the ion conductance of the virus viroporin and its ion channel activity is shown in Table 1.3. These are ion channel inhibitory compounds that supressed the viral viroporin that affect viral growth and pathogenicity. The known cellular pathways influenced by viroporin-mediated changes in ion conductivity are summarized in Figure 1.8.

Class	Compound	Target	Reference
Adamantane	Amantadine: 1-adamantylamine	IAV M2 HCV p7 Dengue M	(Hay et al., 1986; Griffin et al., 2003; Premkumar et al., 2004)
	Rimantadine: 1-(1-adamantyl)ethanamine	IAV M2	(Hay et al., 1986; Griffin et al., 2008)
	“H”: 5-(1-adamantyl)-2-methyl-1H-imidazole	HCV p7	(Foster et al., 2011)
	Spiro[piperidine-2,2′-adamantane] 3	IAV M2	(Kolocouris et al.,2008)
	Spiroadamantane	IAV M2	(Wang et al., 2011)
	M2WJ332: (3S,5S,7S)-N-{[5-(thiophen-2-yl)-1,2-oxazol-3-yl]methyl}tricyclo[3.3.1.1～3,7～]decan-1-aminium	IAV M2	(Wang et al., 2013)

Spirane-amine	BL-1743: (2-[3-azaspiro (5,5)undecanol]-2-imidazoline)	IAV M2	(Kurtz et al., 1995)
Alkyl imino-sugar	NN-DNJ: N-nonyl deoxynojirimycin	HCV p7	(Pavlovic et al., 2003)
Amiloride	HMA: 5-(N,N-hexamethylene)amiloride	HCV p7 Dengue M HIV Vpu	(Premkumar et al., 2004; Premkumar et al., 2005; Wilson et al., 2006; Ewart et al., 2002)
	BIT225: N-[5-(1-methyl-1H-pyrazol-4-yl)-naphthalene-2-carbonyl]-guanidine	HIV Vpu HCV p7	(Luscombe et al., 2010)
Other	CD: 1,3-dibenzyl-5(2H-1,2,3,4-tetraazol-5-yl) hexahydropyrimidine	HCV p7	(Foster et al., 2011)
	LDS25: N-(1-phenylethyl)-2-[4-(phenylsulfonyl)-1-piperazinyl]-4-quinazolinamine	HCV p7	(Foster et al., 2014)

	Emodin: 6-methyl-1,3,8-trihydroxyanthraquinone	SARS-CoV 3a	(Schwarz et al., 2011)
	Verapamil	CSFV p7	(Gladue et al., 2012)
	DIDS: 4,4′-diisothiocyano-2,2′-stilbenedisulfonic acid	EV71 2B	(Xie et al., 2011)
	MV006	HPV-16 E5	(Wetherill et al., 2012)
	Pyronin B	HRSV SH	(Li et al., 2014)

Table 1. 1. Viroporin modulating drugs. Summary of lists of viroporin inhibitors (drugs) that were used to target the viral ion channels and attenuate the virus replication.

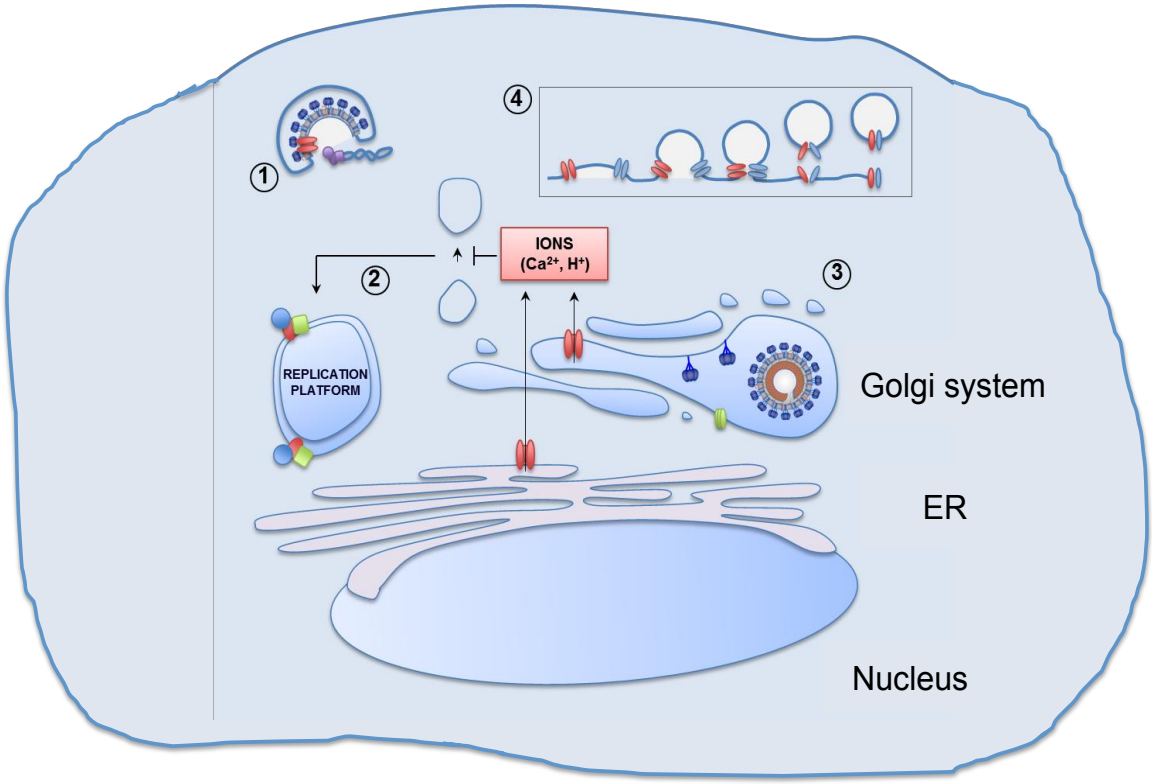

Figure 1. 8. Illustrated summary of possible modes of action of viroporins that influence ion channel conductance to benefit virus production.

(1) Embedded viroporins (red ellipses) in the envelope of viruses enter the host cell through endocytosis. Here the viroporin can mediate structural changes in the fusion and matrix proteins allowing uncoating of the virus ribonucleoproteins. (2) A Viroporin is transported to the Golgi system or ER and causes ionic leakage into the cytosol to block vesicle transport, and provide sites for viral factories. Blue, red and green structures show viral replication, the process whereby membranes accumulate to serve as a platform for viral morphogenesis and replication. (3) Viral envelope proteins (green ellipses and blue structures) mainly located in the Golgi system are protected from the acidic lysosomes (4) Viroporins (blue and red ellipses) are located in the budding virus envelope where they oligomerise, rearranging the formation of a new channel that facilitates virion scission. Figure adapted from (Nieto-Torres et al., 2015).

1.9.1.1 Viral entry

Viroporins can facilitate viral entry by mediating changes in ion channel conductivity. A viroporin located in the viral envelope is in the appropriate location to be involved in viral entry, the classic example being IAV M2 protein, which is required for virion disassembly and RNP release following internalization via the endocytosis process (Stauffer et al., 2014). Shortly

following infection and IAV attachment at the plasma membrane, the virion is internalized within endosomes that fuse with the acidic organelles such as lysosomes to form endolysosomes. The endolysosomes pump the H^+ through the H^+ ATPase inside their lumen to lower the pH level and create a highly acidic environment, with a pH below 5 (Stauffer et al., 2014). The acidic condition of the endosomes causes a dramatic conformation change in the viral hemagglutinin (HA) protein that leads to fusion peptide exposure followed by fusion of the viral envelope with the endosomal membrane (Wharton et al., 1994; Bullough et al., 1994). At the same time the M2 protein within the viral envelope causes an influx of protons that leads to further acidification of the virion interior. The consequence of this is conformational changes to the matrix protein layer surrounding the ribonucleoproteins, which leads to virion disassembly (Stauffer et al., 2014) and release of the ribonucleoproteins into the host cell cytosol. This is one example showing how a viroporin is used to facilitate viral entry; however in the case of other viroporins, their mode of action is less well characterized and further study is necessary to establish their precise roles.

1.9.1.2 Remodeling of the cell organelles

Modification of ionic balance in cellular organelles by viroporins can cause changes in organelle function and thus may facilitate specific stages of the virus replication cycle (Nieto-Torres et al., 2015). As an example, specific viroporins have been shown to play an important role in modifying both the Golgi apparatus and also endosomes, resulting in changes to cellular protein trafficking and signaling pathways that may abrogate virus multiplication (Nakamura et al., 2005). In the case of infectious bronchitis virus (IBV), it encodes a small hydrophobic protein known as the E protein, which is required for efficient virus assembly (Hsieh et al., 2005) and also is known to exhibit ion conductance activity *in vitro* (Wilson et al., 2006). In infected cells, the E protein is thought to affect protein transport and trafficking by influencing the secretory pathway (Ortego et al., 2007). When E protein expression is prevented through gene deletion, or when critical residues that block E protein ion channel conductance are mutated (Ruch and Machamer, 2012; Ruch and Machamer, 2011), mature virus particles accumulate within the secretory pathway

suggesting that they may be incorrectly sorted preventing egress (Ruch and Machamer, 2012). Furthermore, E protein expression correlates with Golgi morphological changes, and taken together it is now thought that E protein acts as an ion channel in specific compartments within the secretory pathway, which drives rearrangement of secretory organelles to favor the efficient assembly and budding of virions. Interestingly, a recent report has suggested that the E protein expressed by SARS-CoV also plays a role in the activation of the NLRP3 inflammasome (Nieto-Torres et al., 2015), an activity that is shared by the HRSV SH protein, described above (Triantafilou et al., 2013c) as well as later in this thesis.

In addition, the 3a protein of SARS-CoV has been proposed to act as a calcium pump, most likely altering the concentration of Ca^{2+} ions within membraneous cellular compartments (Minakshi et al., 2014). The SARS-CoV 3a protein has been shown to play an important role in promoting Golgi fragmentation and accumulation of intracellular vesicles that may be required for virus formation or non-lytic virus release (Dnb et al., 2010; Freundt et al., 2010). The exact mechanism governing the link between unbalanced ion homeostasis and delayed protein transport remains to be established. It has been speculated that the ion channel modification could delay the cellular trafficking and accumulate the membranous content that acts as a platform to facilitate virus replication and budding (de Jong et al., 2008).

1.9.1.3 Protection of viral progeny

Viroporins can also play a critical role in protecting viral progeny by maintaining the low pH in the lumen of the Golgi apparatus and the secretory pathway in order to protect the virus, or virus components, from degradation, as the forming virions are acid sensitive (Wozniak et al., 2010). IAV M2 ion channel activity is thought to maintain the relatively high pH of the Golgi apparatus and associated vesicles in order to prevent premature activation via conformational changes of the hemagglutinin (HA) protein that may result in non-infectious virus. Blocking the function of the M2 protein using amantadine stimulated irreversible activation of HA (Takeuchi and Lamb, 1994). Another example is for the p7 protein of HCV that causes H^+ leakage into intracellular

organelles such as Golgi apparatus to create alkaline pH, required for the formation of infectious viruses (Wozniak et al., 2010). Mutant HCV that was p7 deficient was not rescued, also the wild type virus that was treated with amantadine that blocks the p7 protein was greatly reduced in the yield of infectious virions (Wozniak et al., 2010).

1.9.1.4 Virus release

In many instances, over expression of viroporins in host cells results in cell lysis, which is one mechanism that favours the release of non-enveloped viruses (Nieva et al., 2012). In addition, it has been suggested that the imbalance of the cellular ion gradient in the cytosol may activate membrane fusion that is important for terminating the budding and release of enveloped virus particles (Nieva et al., 2012). This could also lead to oligomerization that forms an ion channel to facilitate budding termination and virus release (Nieto-Torres et al., 2015). IAV M2 protein is thought to be involved in mediating one of the final stages of virus release, with the M2 protein being localized to the neck of the budding virion (Rossman et al., 2010) and playing a critical role in membrane scission.

In addition, the HIV-1 Vpu protein is involved in enhancing the release of progeny HIV virions by inhibiting a cellular acid-sensitive K^+ channel TASK-1, which leads to a chain-like budding structure (Strebel, 2004).

1.9.2 The role of viroporins in pathogenesis

Viroporins are not only involved in virus propagation in cell culture systems but they also act as virulence factors in intact infection model systems, and deletion of viroporin expression or function has been shown to attenuate viral pathogenicity phenotypes. HRSV lacking the SH protein showed minor growth attenuation in viral-infected chimpanzee and mice, although SH deletion was associated with significantly milder disease outcomes (Whitehead et al., 1999; Åkerström et al., 2007). Thus, expression of the viroporin may stimulate cellular signaling pathways, and while these effects may have little influence on virus replication and thus released viral titres, they may play important roles in

determining pathogenicity resulting from enhanced immunopathology. Another example where expression of a viroporin stimulates immunopathology is for the SARS-CoV E protein. When E expression is prevented by gene deletion of recombinant virus, the resulting viruses show reduced mortality in animals in comparison with the wild-type virus (Nieto-Torres et al., 2014). Most noticeably, infection of the mouse animal model with the 3a gene deleted virus showed less excess water accumulation in the lung airway (edema) in comparison with mice infected with the wild-type virus. This effect was also noted in human patients suffering with acute respiratory distress syndrome (ARDS), which is associated with high accumulation of edema in the lungs as one of its symptoms (Matthay and Zemans, 2011). Excessive fluid uptake in the lungs abrogates the gas interchange in the alveoli, leading to hypoxemia and eventually death. There is a good correlation between the accumulation of edema in the lungs and the disjunction between airway epithelia, as both are connected to the ion balance and water reabsorption in the lungs. Moreover, edema accumulation is also related to increased proinflammatory response in the lung airway (Matthay and Zemans, 2011). The expression levels of specific cytokines (IL-1, TNF and IL-6) are decreased in the 3a gene deleted mutant virus of infected lung parenchyma in comparison with the wild type. IL-1 belongs to the cytokine family that is resistant to that virus in infected cells and stimulates the inflammatory response; however overstimulation of this cytokine can lead to harmful effects in the host. As an example, over production of IL-1 causes asthma, gout, diabetes and ARDS (Pugin et al., 1996; Strowig et al., 2012).

It is becoming clear that several viruses that express their own ion channels are capable of stimulating the inflammatory response through activation of inflammasomes, which are activated by a variety of stimuli including pathogen recognition when PAMPs or intact pathogens are encountered, or when a disturbance occurs in the cellular milieu. Such a disturbance may include an imbalance to ion homeostasis (Murakami et al., 2012; Muñoz-Planillo et al., 2013).

The NLRP3 inflammasome is the best characterized of all inflammasome complexes, and is activated by HRSV (Ichinohe et al., 2010), which results from early stages of viral invasion when HRSV genes are initially being expressed.

The second signal occurs when the component of the inflammasome assembly results in caspase-1 activation. Caspase-1 processes pro-IL-1 to become active IL-1 that is secreted extracellularly to promote proinflammation (Ichinohe et al., 2010). The virus ion channel activity associated with the second signal induces the mainly K^+, Ca^{2+} or and H^+ efflux from the cellular compartment to the cytoplasm in order to enable this inflammasome activation to trigger IL-1 (Figure 1.9) (Nieto-Torres et al., 2015). This pathway was first noticed as a result of IAV M2 viroporin proton conductance and NLRP3 activation (Ichinohe et al., 2010). In the case of HRSV, NLRP3 inflammasome activation has been shown to be mediated via the SH viroporin (Triantafilou et al., 2013a) leading to increased immunopathology (Triantafilou et al., 2013a). However, the molecular basis for SH-mediated inflammasome activation is still unclear.

Overall, the wide range of modes of action connected to viroporins, such as viral propagation, ion channel activity and pathogenic effects suggest they will likely represent a promising therapeutic target in the near future.

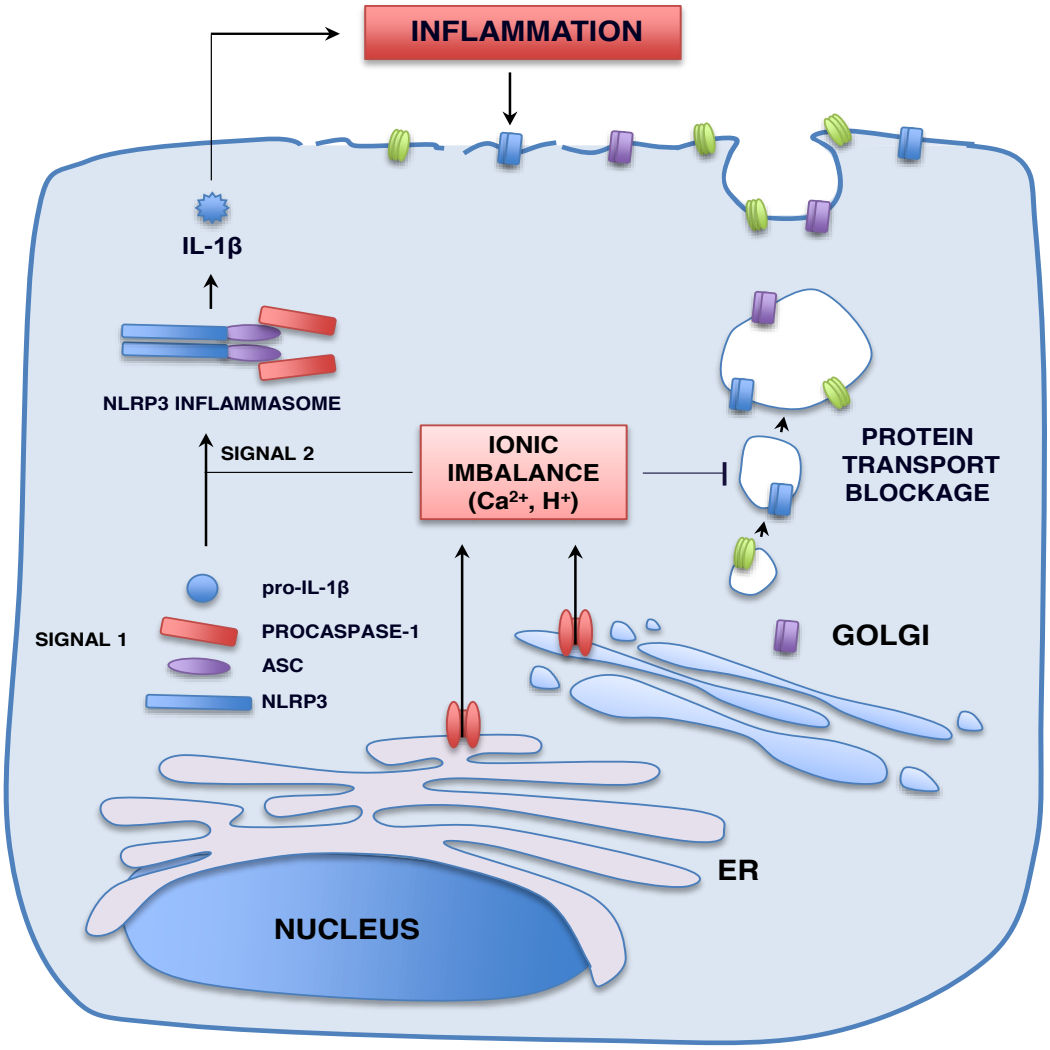

Figure 1. 9. Schematic representation of mechanisms of viroporin mediated cellular pathogenesis.

The host cell is infected with a pathogen expressing a viroporin, which primes the inflammasome for activation (signal 1) by multimerisation of NLRP3 via its LRR (Leucine-Rich Repeats), as well as NACHT domains. The PYD domain within this oligomer then interacts with the ASC (Associated Speck-Like Protein Containing CARD), which in turn recruits pro-caspase-1 through its CARD domain to form the active NLRP3 inflammasome. An imbalance to ion homeostasis caused by the viroporin stimulates the activation of caspase-1, which then activates the inactive pro-IL-1 creating active pro-inflammatory cytokine IL-1 that is eventually secreted and causes local inflammation. This also leads to a decrease in the level of MHC-1 (class I molecules; shown as blue rectangles) at the plasma membrane, which prevents the infected host cell from being recognized by the immune system. This also leads to protein transport inhibition reducing the activity level of the surface ion channel and transporters that may lead to edema accumulation, such as epithelial sodium channels (ENaC) (green rectangles) and Na+/K+ ATPase (purple rectangles).

1.10 Cellular ion channels in the respiratory system

Cellular ion channels are cell-encoded membrane anchored protein complexes located in the plasma membrane and intracellular organelles that regulate ion movement through the membrane depending on the electrochemical gradient. Cellular ion channels play an important role in cell physiology and are involved in many critical cellular processes such as cell volume control, cell proliferation and cell death. For example, an increase in cell volume is the preparatory step for cell proliferation, and this is mediated by specific Cl^- and K^+ ion channels. Cl^- and K^+ ion channel activity can facilitate the osmolyte flux and lead to an increase in cell volume. At the same time, HCO_3- exits across the membrane and the acidity level in the cytosol is increased, leading to an inhibition of cell proliferation (Lang et al., 2005).

Blocking any of these ion channels can affect cellular mechanisms including ion channel transport depending on cell type, cultivation time and culture condition (Lang et al., 2007). Each cell type expresses a specific compliment of ion channels according to their function. In this thesis, we are particularly interested in pulmonary epithelial ion channels as HRSV infects only respiratory epithelial cells.

In respiratory epithelial cells, ion channels serve epithelial cell physiology, as described the next section. Some studies showed that ion channel dysfunction caused by environmental allergens, infections by microorganisms and exposure of the airway tissue to various toxins (Holgate et al., 2009) are associated with serious diseases of the respiratory system (Valverde et al., 2011; RamaKrishnan and Sankaranarayanan, 2016; López-Barneo et al., 2004; Sheikh et al., 2015; Weir et al., 2010). The respiratory diseases that are related to cellular ion channel dysfunction are asthma, hypoxia, and chronic obstructive pulmonary disease (COPD) (Weir et al., 2010; Valverde et al., 2011; Sheikh et al., 2015).

As mentioned before, HRSV infection has an indirect relationship to recurrent asthma throughout life (Knudson and Varga, 2015). HRSV stimulates a Th-2 response that induces interleukins such as IL-4, IL-5 and IL-13 (Dakhama et al.,

2005; Barends et al., 2004) that are also associated with allergic airway inflammation, which is linked with asthmatic patients (Siegle et al., 2010; Howard et al., 2002; Schwarze et al., 1999). Asthma was also linked with Ca^{2+} homeostasis in the endoplasmic reticulum (ER) (Cantero-Recasens et al., 2009). Ca^{2+} cytosolic signal has been involved with cytokine production and T cell proliferation (Vig and Kinet, 2009).

COPD is common respiratory disease that typically causes over-production of mucus and dysregulation in water and ion balance. Imbalance of Cl^- and Na^+ secretion and adsorption in the epithelial lung epithelium are mainly associated with this disease (Sheikh et al., 2015). Moreover, specific K^+ channel function is associated with oxygen sensing in the human lung (Kemp and Peers, 2007) that when in case of any deficiency in the oxygen level in the lung can lead to hypoxia (Wenger and Gassmann, 1997).

Linking respiratory disease that is related to defects in epithelial cellular ion channel functions and HRSV infection symptoms could lead to new therapeutic approach to prevent HRSV infection and/or the serious affects of HRSV infection by the development of pharmaceutical ion channel modulating drugs.

1.10.1 Airway epithelium ion channels

There are two types of epithelial cells in human bronchioles: the airway epithelia and the alveolar epithelia (Hollenhorst et al., 2011). The airway epithelia, including the nose, trachea and the bronchi, are mainly responsible for the passage of oxygen to the lung where gas exchange can occur. Figure 1.10 illustrates the distribution of epithelial cells within the respiratory system. Epithelial lung cell types consist of ciliated cells, Clara cells, goblet cells and undifferentiated basal cells (Hollenhorst et al., 2011).

Ciliated cells express a set of ion channels involved in mucociliary clearance and airway surface liquid (ASL) regulation, which contain periciliary liquid (PCL) and mucus (Hollenhorst et al., 2011). Ion absorption and secretion enables the cell to control the water levels of the PCL that help to optimize the ciliary beat

(Hollenhorst et al., 2011). Figure. 1.11 illustrates the ion channels expressed in ciliated airway epithelial cells.

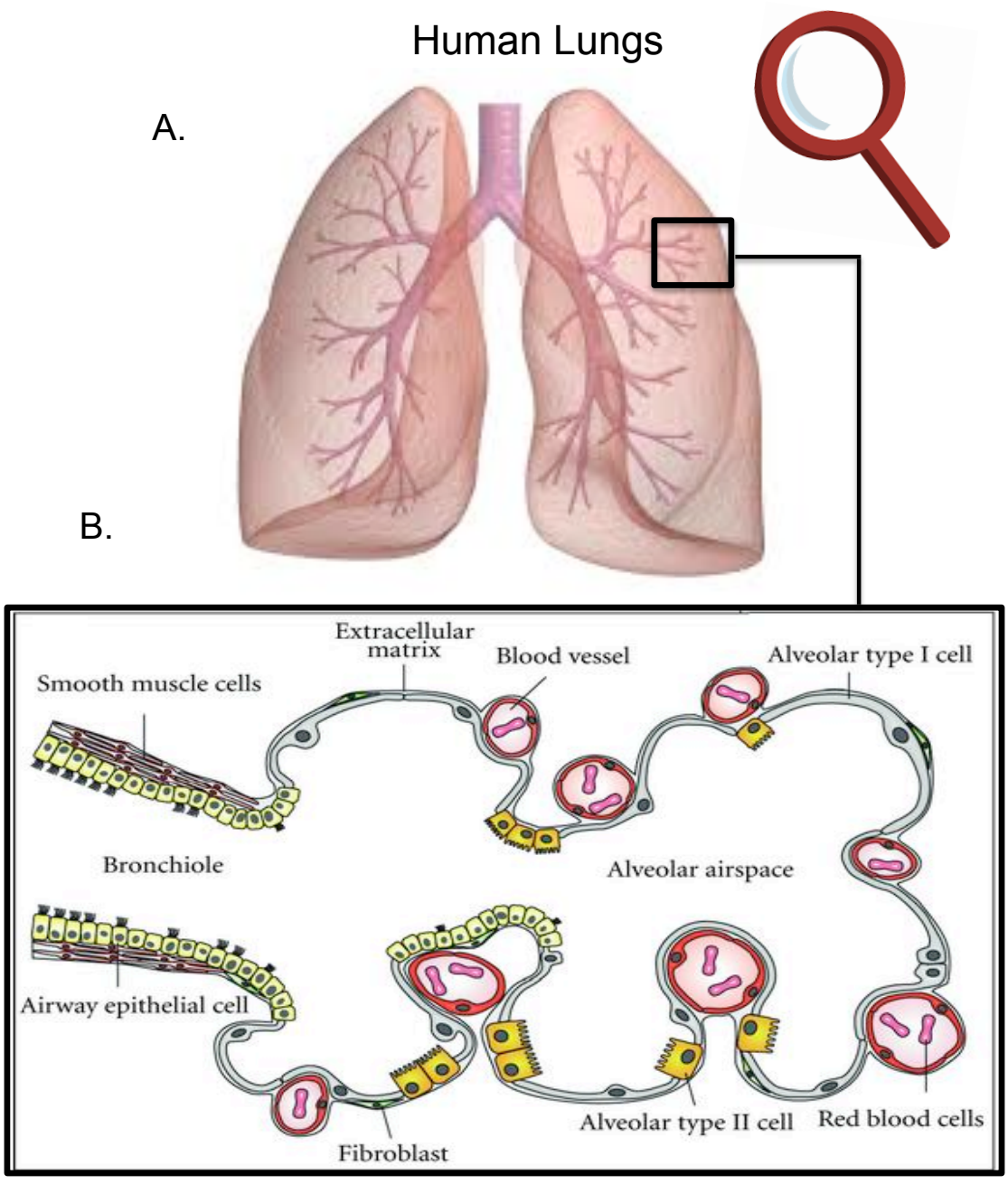

Figure 1. 10. Schematic representation of epithelial cells that are distributed along the human respiratory system.

(A) An overview of the human respiratory organs. **(B)** Schematic representation of alveolar cells within the lung. (Figure adapted from (Hollenhorst et al., 2011).

Mucociliary clearance is essential to maintain lung health as part of the immune system. It is involved in cleaning the lungs from inhaled particles and pathogens and consists of two main elements: ciliary beating and ion balance. Both these

factors can control the airway epithelial cells by controlling the water flow in the lungs to regulate the PCL composition through the ciliary beat (Song et al., 2009; Boucher, 2002). When this area is infected by pathogenic microorganisms, ciliary beating is impaired. This defect may be due to a reduction in water content of the ASL in the airway due to unbalanced ionic distribution resulting from modified ion channel activity. Several ion channels in the ciliated airway epithelial regulate ASL by ion transport processes including Na^+, Ca^+, K^+ and Cl^- ions (Hollenhorst et al., 2011).

1.10.1.1 Sodium ion channels

Epithelial Na^+ ion channels (ENaCs) are ligand-gated Na^+ channels (Horisberger and Chraïbi, 2004) that control Na^+ ion influx, a process which is amiloride sensitive (Mall et al., 1998). Cyclic nucleotide-gated CNG cation channels also control Na^+ reabsorption. Cl^- ion secretion helps to maintain passive trans-epithelial water flow, which leads to optimum ASL levels in conjunction with Na^+ absorption (Shah et al., 2009). Na^+ is secreted at the basolateral side via Na^+/K^+ ATPase pumps that are ubiquitously expressed in the airway epithelia and give the driving force for apical Na^+ reabsorption (Crump et al., 1995; Dodrill and Fedan, 2010).

1.10.1.2 Chloride ion channels

Several ion channels contribute to the control of Cl^- secretion including the basolateral outward rectifying channel (BORC); the basolateral inward rectifying channels (BIRC); and the basolateral cystic fibrosis transmembrane-like channel (BCFTR). Additionally, apically-located ion channels include the CFTR conductance regulator and Ca^+ dependent Cl^- channels (CaCC)(Hollenhorst et al., 2011). A transmembrane protein TMEM16, also known as anoctamin 1 (ANO1), is a calcium-activated chloride channel (CaCC) in the airway. The CFTR has been shown to affect ENaC regulation since cystic fibrosis patients with deficient CFTR often show Na^+ hyper-absorption (Mall et al., 1998; Burch et al., 1995). BORC is also voltage dependent activation upon swelling and DIDS (broad spectrum Cl^- inhibitor drug) sensitive (Fischer et al., 2007). In airway epithelia $Na^+/K^+/Cl^-$ contraporters (NKCC) are identified and

support Cl^- secretion in the apical side and maintain Cl^- cellular supply (Tessier et al., 1990).

1.10.1.3 Potassium ion channels

Potassium ion channels are expressed in a wide variety of airway cells. The various cellular potassium channels are classified into different subgroups depending on their activation mechanisms, conductance properties and transmembrane domain. K^+ ion channels are important in regulating apical Cl^- secretion by maintaining the electrochemical gradient and membrane potential. Several K^+ channels have been identified on the basolateral sides of epithelial cells, most of which are voltage sensitive (Bernard et al., 2003). Channels such as Kv7.1, $K_{Ca}3.1$ (SK4), whereas BK_{Ca} and $K_{Ca}3.1$ located on the apical surfaces of epithelial cells (Hollenhorst et al., 2011). Kv7.1 has been found to play an important role in maintaining cAMP-dependent Cl^- secretion (Mall et al., 2000). Moreover, SK4 has been shown to play a role in Ca^{2+} dependent secretion of Cl^- (Bernard et al., 2003). BK_{Ca} channels are also important in regulating the ASL volume in human bronchial epithelium (Manzanares et al., 2011).

1.10.2 Alveolar epithelium ion channels

The alveolar surface area of the lung is specialized to allow efficient gas exchange with the blood. The alveoli consist of a layer of alveolar epithelium (AE) that is close to the vascular endothelium. At the surface of the AE, alveolar lining fluid (ALF) covers the AE and separates the epithelium from the air (O'Grady and Lee, 2003). The role of AE is to control ALF volume and regulate the electrolyte composition. Also, AE allows the limited diffusion of solutes to maintain the alveoli from dryness. Figure 1.12 shows an overview of the ion channels expressed in alveolar cells.

1.10.2.1 Chloride channels

For chloride transport, CFTR Cl^- channels balance the ALF through Cl^- absorption (Fang et al., 2006; Jiang et al., 1998), and secretion (Brochiero et al., 2004; Sommer et al., 2007). Other chloride ion channels including CLC2 and CLC5 are voltage gated (Johnson et al., 2009). Additionally, ionotropic γ-aminobutyric acid type A ($GABA_A$) Cl^- channels have been detected in alveolar epithelium (Jin et al., 2006). Generally, Cl^- channels exist in the apical membrane of the pulmonary epithelial cell; however, research has also indicated that the Cl^- channels is also localized in the basolateral membrane of the AE cells (Berger et al., 2011). However, the precise role of Cl^- channels in AE cells is still not completely understood (Hollenhorst et al., 2011).

The important components for trans-epithelial Cl^- transport include NKCC and KCC (K^+ and Cl^- transporters). Moreover HCO_3/Cl^- exchangers have been found in AE (Berger et al., 2011). The previously mentioned contraporters and exchangers facilitate Cl^- uptake against the electrochemical gradient. This uptake is crucial to enable the Cl^- passive diffusion along its electrochemical gradient (Hollenhorst et al., 2011).

1.10.2.2 Sodium Channels

Generally, in the upper airways, the major driving force of fluid reabsorption is provided by the amiloride-sensitive epithelial Na^+ channels or the epithelial sodium channels (ENaCs) in addition to the amiloride-insensitive nonselective cyclic nucleotide-gated (CNG) cation channels, which are responsible for the passive apical sodium ion uptake by fluid reabsorption in AE (Johnson et al., 2002; Wilkinson et al., 2011). The basolateral ouabain-selective Na^+/K^+ ATPase maintains the electrochemical gradient thus facilitating the osmotic gradient to remove water out of the alveoli into the interstitium (Hollenhorst et al., 2011). ATI cells are associated with the process of trans-epithelial ion transport as well as mediating water permeability due to the expression of aquaporin 5 (AQP5) (Hummler et al., 1996).

1.10.2.3 Potassium Channels

One of the main functions of K^+ channels is to control the membrane potential, which regulates the electrochemical gradient that is needed for fluid and ion transport. Moreover, these channels are also involved in sensing oxygen levels as part of the lung physiology (Bardou et al., 2009a). K^+ channels are classified into 3 main groups: 4 TMD K^+ channels subgroups of two-pore domain K^+ channels (K2P); 6 TMD K^+ channels consisting of Ca^{2+}-activated K^+ channels (K_{Ca}) and voltage-dependent K^+ channels (Kv); and 2 domain K^+ channels, also known as inward-rectifying K^+ channels (Kir). A number of subtypes of Kv have been detected, namely, Kv1.1, Kv1.3, Kv1.4, Kv2.2 Kv4.1, Kv4.2, Kv4.3 and Kv9.3 that were reported in AE type II (Bardou et al., 2009b; O'Grady and Lee, 2003; Leroy et al., 2006). BK_{Ca} channels are thought to be involved in oxygen sensing as the opening time of these channels is shortened in response to low oxygen levels (Jovanović et al., 2003). Another potassium channels in the Kir family (inward rectifier family) is Kir2.1 (IRK1), detected from isolated fetal guinea pig lungs (Monaghan et al., 1996). However further investigation is needed to fully understand the function of this channel. Other Kir family members have been detected in adult alveolar cells such as Kir6.1, which has the ability to assemble the ATP-sensitive K^+ channels (K_{ATP} channels). K_{ATP} channels act as metabolic sensors as their function depends on the concentration of intracellular ATP. When the cellular metabolic state changes, the ATP intracellular level is affected, which in turn influences the channel activity that subsequently affects membrane potential (Zhang et al., 2010; Nichols, 2006). It has been shown that blocking K_{ATP} reduces cell migration, wound healing and proliferation in cultured ATII primary cells of rat (Trinh et al., 2007).

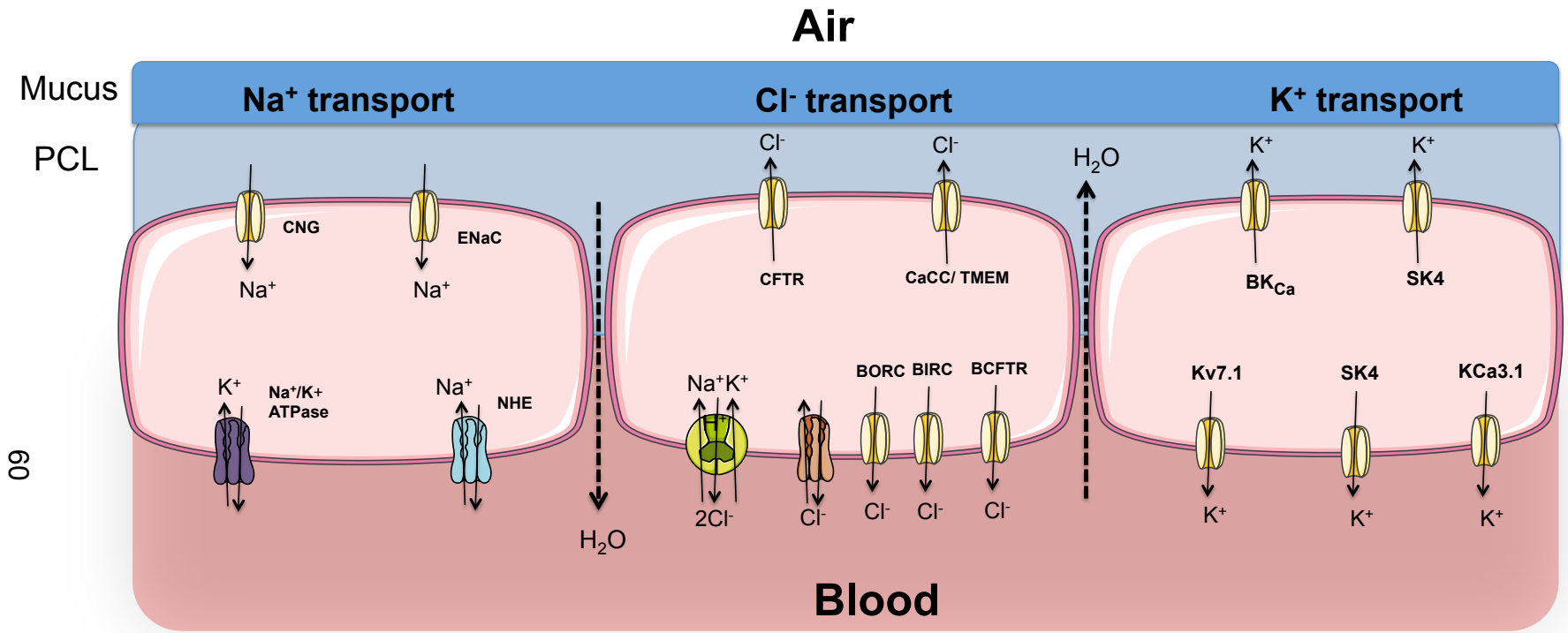

Figure 1. 1. Schematic representation of ciliated airway epithelial cells with Na^+, Cl^-, and K^+ channels and transporters.

On the apical side, Na^+, K^+ and Cl^- ions are regulated by specific ion channels. The PCL that cover the cilia are mainly regulated by ion channels either by reabsorption of Na^+ or secretion of K^+ and Cl^- ions. Basolateral side Cl- ion channels and K+ ion channels have been identified and are characterized as playing a role in ion secretion.

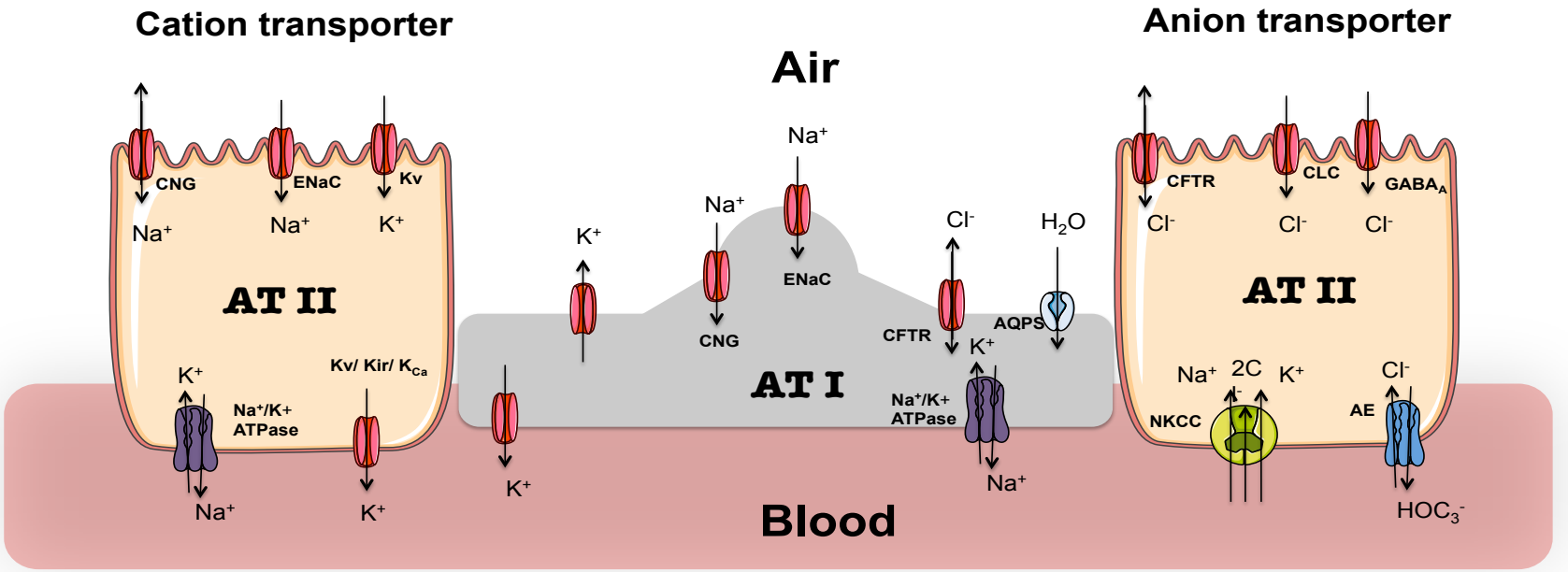

Figure 1. 2. Schematic drawing of Alveolar type 1 (ATI) and alveolar type Ii cells (ATII) including anion transport and cation transport.

Ions including Na^+, K^+ and Cl^- are regulated by specific ion channels. On the apical side, Na^+ and Cl^- are operated by reabsorption and K^+ in secretion. Those on the basolateral side are mainly regulated by protein transporters. The K^+ ion channels in airway cells have not yet been specified.

1.11 AIMS AND OBJECTIVES

This literature review shows that HRSV disease has a serious heath impact in infants, elderly and immunocompromised people. There is neither a completely safe and reliable treatment for HRSV infections, nor an effective vaccine for the prevention of HRSV mediated disease. For this reason, alternative approaches to blocking HRSV multiplication and disease need to be evaluated. One approach is to target host cell and viral components that represent pathogenicity or virulence factors by virtue of their ability to enhance various stages of the virus replication cycle.

This PhD thesis describes experiments that investigate the role played by both cellular and virus encoded pore forming proteins in the HRSV replication cycle.

The project has the following objectives:

1) To investigate the role of host cell ion channels in promoting HRSV replication.

2) To understand the role of the SH viroporin within the HRSV replication cycle in continuous and primary cell cultures by quantitative proteomics using mass spectrometry.

Chapter 2: Materials and Methods

Chapter 2: Materials and Methods

2.1 Materials

2.1.1 Human cells line

A549 cells are adenocarcinomic human alveolar basal epithelial cells (D J Giard et al., 1973). HEp2 cells are derived from HeLa cells, originally obtained from cancer cells of human cervical epithelia (Toolan, 1954). HBEpC are human bronchial epithelial primary cells. All three cells were obtained from the Health Protection Agency (HPA) Culture Collections (HPACC, UK).

2.1.2 HRSV strains

HRSV wild type (WT) subgroup A2 was obtained from Dr. Patricia Cane and Dr. Brian Dove (HPA, UK). HRSV rA2, HRSV rA2 ΔSH and HRSV rA2 ΔSH were kindly provided from Michael N. Teng (University of South Florida Morsani College of Medicine).

2.2 Methods

2.2.1 Cell culture methods

2.2.1.1 Continuous cell culture

HEp2 cells were used exclusively for HRSV production whilst A549 cells were used for subsequent experiments. Both types of cells were grown in Dulbecco's modified Eagle's medium (DMEM; Sigma) supplemented with 10% (v/v) fetal bovine serum (FBS) and 1% (v/v) of penicillin-streptomycin. Cells were grown as an adherent monolayer in 25, 75 or 175 cm^2 flasks and incubated for 24-48 hours until reaching 60%-70% confluency. Cells were passaged every two to three days and maintained at 37°C with 5% CO_2 in a humidified incubator.

2.2.1.2 Primary cell culture

HBEpC cells were used for the experiments conducted in Chapter Five. They were grown in specialized bronchial/tracheal epithelial cell growth media (ECACC, 511-500) as an adherent monolayer in 75 (T-75) or 175 cm^2 (T-175) flasks and incubated until reaching 60%-80% confluency. During this time media was replaced every other day. Cells were passaged when cells were fully confluent and maintained at 37°C with 5% CO_2 in a humidified incubator. The media volume was doubled when the culture was over 45% confluent, or if cells were left over the weekend. A specialized subculture reagent kit (ECACC, 090K) was used to passage primary cells.

2.2.1.3 Continuous cell line storage

A549 and HEp2 cells were prepared for long-term storage in liquid nitrogen as follows: Cells were grown in four T-175 flasks after which media was aspirated then cells were washed three times with previously prepared ice cold PBS. After trypsinizing and neutralization, cells were counted and were then centrifuged at 500 rpm for 5 minutes. Supernatant was discarded and pellets were washed with ice-cold PBS and centrifuged again. Pellets were re-suspended with an appropriate volume of 10% (v/v) DMSO (Dimethyl Sulphoxide; Sigma) in FBS to give approximately 10^6 cells per vial. The cell suspension was aliquoted into labeled cryovials. Primary cells were frozen at -80°C overnight then transferred into liquid N_2. Some 9 ml of FBS with 1 ml of 10% (v/v) DMSO (Sigma-Aldrich) was mixed then aliquoted with cell pellets for distribution, 1 ml per cryovial.

2.2.1.4 Primary cell line storage

HBEpCs were stored as follows: Cells were trypsinized with trypsin/EDTA (ECACC, 090K) then mixed with a specialized neutralizing agent. Growth media was added and centrifuged at 400 rpm for five minutes. The cell pellet was washed by re-suspension in HBSS, after which the suspension was centrifuged again. The cell pellet was mixed with previously prepared mixture containing 8 ml of growth media, 1 ml of FBS and 1 ml of DMSO, which was filtered using a sterile 0.2 µm filter and kept at 4°C for use. After re-suspending

cells, 1 ml was aliquoted per cryovial and frozen overnight for short-term use. For long-term storage aliquoted cryovials were then transferred to the liquid N_2 tank. Cell performance cannot be guaranteed after cryopreservation as this may compromise cell quality.

2.2.2 Virological techniques

2.2.2.1 Infection assay

Cells were seeded as shown in Table 2.1 at a confluency of 60-70%. Virus titers were calculated according to the following equation:

$$Multiplicity\,of\ \inf ection\,(MOI) = \frac{number\,of\ cells\,(seeding\,density)}{(the\,virus\,titer\ pfu/ml)}$$

Virus stocks were diluted in serum-free DMEM (or HBEpC growth medium) and added to the vessel. Cells were then incubated for 2-4 hours with manual shaking every 10-20 minutes to facilitate virus distribution. Some 2-4 hours following infection, virus supernatants were removed and replaced with fresh complete media for a further 24 hours.

To study the HRSV infection cycle, infected cells were incubated for 24 hours and for virus propagation and increased viral titration, infected cells were incubated for five days or until cells were lysed.

Cell Culture Vessels	Seeding Density	Diluted virus in Serum-Free Media (ml)	Growth Medium (ml)
Dishes			
60 mm	$8x10^5$	1-1.5	3
Cluster Plates			
6-well	$2X10^5$	.5-1	2
12-well	$2X10^5$	.5-1	1-2
24-well	$2X10^5$	.5	1
96-well	$1X10^4$	.05	0. 2
Flasks			
T-25	$5.2X10^6$	2.5	5
T-75	$1.5X10^6$	4-5	10
T-175	$3X10^6$	5-7	25

Table 2. 1. Seeding density of A549 cells and HEp-2 cells. The table shows the quantity of cells required to reach the stated seeding density in all culture plastic ware used in the study, as well as the dilution volumes used.

2.2.2.2 HRSV production

HRSV was infected at an MOI of 0.1 and propagated in HEp-2 cells in four T-175 flasks. HRSV was harvested five days after infection or when

infected HEp-2 cells began to detach from the flasks. Infected cells were disrupted by agitation with autoclaved glass beads to increase virus release. The cell suspension was centrifuged at 320xg for 10 minutes to clarify virus supernatants from cell debris. Virus supernatant was collected and snap-frozen using ethanol/dry ice, and stored at -80°C or purified (as below).

2.2.2.3 HRSV purification

HRSV supernatants were purified by sucrose density gradient centrifugation. Virus was first precipitated using a solution comprising 50% (w/v) polyethylene glycol (PEG)-6000 dissolved in NT buffer [(50 mM, Tris-HCl (pH 7.5) 150 mM NaCl, 1 mM EDTA, 100 mM $MgSO_4$)] and HRSV supernatants were added to reach 10% of final concentration. The HRSV/PEG mixture was incubated for 90 minutes at 4°C with moderate stirring to allow virus precipitation. The mixture was then centrifuged at 3200xg for 10 minutes at 4°C. The virus pellet was isolated and re-suspended in 2.5 ml of cold NT buffer. Discontinuous sucrose gradient was prepared from 60%, 45% and 30% (w/v) sucrose dissolved in NT buffer and 2.5 ml of each concentration was added to a 14x89 mm centrifuge tube. The virus suspension was added to the top of the discontinuous sucrose gradient. The tube was centrifuged at 35,000 rpm for 90 minutes at 4°C in a TH-641 swinging rotor. An opalescent band was observed in the discontinuous sucrose gradient, specifically between the 30-45% layers. The band was collected using a 25-gauge needle and 5ml syringe and diluted in 2 ml of cold NT buffer.

Diluted virus was added on top of the continuous sucrose gradient made from 60% and 30% of sucrose and 3 ml of each concentration was added to 14x89 mm centrifuge tubes. The continuous sucrose gradient was prepared one day prior to centrifugation in a TH-641 swinging rotor at 35,000 rpm for 90 minutes at 4°C to allow diffusion between layers. The opalescent band was observed at ~45% sucrose density and collected as per the previous step. Purified virus was aliquoted and snap-frozen in dry ice and stored at -80°C.

2.2.2.4 HRSV titer determination

This technique was adapted from previous studies using methylcellulose plaque assays (McKimm-Breschkin, 2004). HEp-2 cells were seeded at $2x10^5$ in a 24-well plate prior to infection. A 50 µl volume of HRSV stock was diluted in 450 µl of serum-free DMEM and then serially diluted by a factors of 10^{-1} to 10^{-8}. Each infection was performed in duplicate, and a volume of 400 µl of serum-free DMEM was added as a mock-infected control. The 24-well plate was incubated for two hours to allow virus adsorption, after which each well was washed once with sterile PBS to remove unbound virus. Then 1.6% high viscosity carboxymethyl-cellulose (Sigma) was mixed 1:1 with DMEM and added to each well. Cells were incubated at 37°C for 3-5 days or until syncytia were evident. The mixture was aspirated, and cells were washed four times with PBS. The infected monolayer was fixed with 80% (v/v) cold methanol for one hour. Cells were washed three times with PBS-0.1% Tween (PBS-T; 150 mM NaCl, 2.5 mM KCl, 10 mM Na_2HPO_4, 1 mM KH_2PO_4, pH 7.4, 0.5% Tween-20). Following this, 5% (w/v) dried skimmed milk in PBS was applied as a blocking solution for one hour at room temperature with rocking and incubated overnight at 4°C. Goat-anti HRSV primary antibodies (Abcam; 20745) diluted 1:200 in blocking solution were applied to each well overnight at 4°C with rocking. Secondary horseradish peroxidase (HRP) conjugated anti-goat (Abcam; ab6741) antibodies were then added in blocking medium for one hour at room temperature. 4-chloro-1-naphthol (4-CN) (Pierce [Thermo Scientific; 34010) was prepared in advance and diluted with ethanol or methanol 1/10 in 10 ml of PBS. The diluted 4-CN was mixed with 30% hydrogen peroxide (H_2O_2) immediately before application to the wells. The 24-well plate was incubated for 10 minutes on a rocker at room temperature until purple plaques appeared in the wells. Only duplicated wells that contained between 10 to 100 purple plaques were counted and calculated using the following formula:

$$\text{irus titre (pfu per mL)} = \frac{\text{(number of plaques)}}{\text{((dilution factor x volume (mL))}}$$

2.2.3 Protein analysis

2.2.3.1 Preparation of whole cell lysate

Cell monolayers were washed once with cold PBS and lysed in RIPA buffer containing 50 mM Tris-HCl (7.5), 150 mM NaCl, 1% (v/v) NP-40, 0.5% (w/v) sodium deoxycholate, 0.1% (w/v) sodium dodecyl sulphate (SDS) supplemented with EDTA-free protease inhibitor cocktail (Roche Applied Science). Cells were lysed in 200µl of RIPA buffer in a 6-well plate for 30 minutes at 4°C followed by sonication for 30 seconds. Lysates were centrifuged at 13,0000xg for 20 minutes at 4°C and supernatants stored at -80°C. This method is required for SDS-PAGE with Coomassie staining or immunoblot analysis.

2.2.3.2 Determination of protein concentration by BCA assay

The protein concentration of whole lysates was determined using the micro bicinchoninic acid (BCA) protein assay system (Pierce). Bovine serum albumin (BSA) standards were used to calibrate a standard curve. The protein containing cell lysate solution was diluted 1/25 in PBS and the whole procedure was performed according to the manufacturer's 96-well plate protocol. The samples were tested in a Dynex microplate reader to measure absorbance at 570 nm.

2.2.3.3 Sodium-Dodecyl Sulphate Polyacrylamide Gel (SDS-PAGE)

Protein samples were separated by 12% SDS-PAGE gels according to established protocols (Sambrook and Russell, 2006). Table 2.2 shows the SDS-PAGE gel recipes used in the current study. Protein samples were prepared using 4x lithium dodecyl sulfate (LDS) sample buffer (Invitrogen) supplemented with 50 mM reducing agent and heated at 70°C for 10 minutes to enable protein denaturation. Then 5-10 µg of protein sample was loaded and referenced using ColorPlus pre-stained protein marker, broad range 7-175kDa (BioLab, P7709S). The resulting SDS-PAGE gel was run at 15V/cm in SDS-PAGE running buffer (0.25mM Tris, 1.92 mM glycine, 2 ml glycerol, 0.5% (w/v) SDS) for 45 minutes

or until it resulted in the optimum separation of the protein marker. At this stage, the gel was either stained with Coomassie or analyzed by Western blot.

<table>
<tr><th colspan="2">12% Resolving gel (10 ml)</th><th colspan="2">5% Stacking gel (5ml)</th></tr>
<tr><td>Concentration</td><td>12%</td><td>Concentration</td><td>5%</td></tr>
<tr><td>30% acrylamide</td><td>4 ml</td><td rowspan="2">30% acrylamide</td><td rowspan="2">0.83 ml</td></tr>
<tr><td rowspan="2">1.5 Tris-HCl
pH 8.8
Tris-Base (Fisher chemical)</td><td rowspan="2">2.5 ml</td></tr>
<tr><td rowspan="3">1.5 Tris-HCl
pH 6.8</td><td rowspan="3">0.63 ml</td></tr>
<tr><td rowspan="3">ddH_2O</td><td rowspan="3">3.3 ml</td></tr>
<tr><td>ddH_2O</td><td>3.4 ml</td></tr>
<tr><td>10% (w/v) SDS</td><td>50 µl</td></tr>
<tr><td rowspan="2">10% (w/v) SDS</td><td rowspan="2">100 µl</td><td>10% (w/v) APS</td><td>50 µl</td></tr>
<tr><td rowspan="3">TEMED</td><td rowspan="3">5 µl</td></tr>
<tr><td>10% (w/v) ammonium persulphate (APS)</td><td>100 µl</td></tr>
<tr><td>N,N,N,N-tetramethylethylenediamine (TEMED)</td><td>10 µl</td></tr>
</table>

Table 2. 2. Table of SDS-PAGE resolving and stacking gel recipes.

2.2.3.4 Protein visualization by Coomassie stain

Proteins resolved by SDS-PAGE were directly visualized by soaking the SDS gel in Coomassie stain (0.25% (w/v) Coomassie R-250, 50% (v/v) methanol, 10% (v/v) glacial acetic acid) at room temperature with rocking for one hour then de-stained for two hours in same the conditions (de-staining solution: 40% (v/v) methanol, 10% (v/v) glacial acetic acid), then soaked in water for rehydration prior to imaging.

2.2.3.5 Western blot analysis

Traditional Western blotting with blot exposure to x-ray film was done as follows: Proteins were transferred onto poly-vinylidine fluoride (PVDF) membranes (Millipore) activated with methanol and equilibrated in Towbin transfer buffer (25 mM Tris, 92 mM glycine, 20% (v/v) methanol) at 15V for one hour using the trans-blot SD semi-dry transfer cell (Bio-Rad). Membranes were then blocked with 10% (w/v) skimmed milk powder (Sigma) dissolved in Tris-buffered saline containing 0.5% Tween-20 (TBS-T; 50 mM Tris-HCl, 150 mM NaCl, pH 7.6, 1% Tween-20) for one hour at room temperature or overnight at 4°C. Membranes were washed with TBS-T and probed with polyclonal goat-anti RSV (Abcam; 20745) 1:1000 in 5% milk in TBS-T 5 ml as total volume for one hour or overnight at 4°C. Membranes were then washed in TBS-T and labeled with secondary anti-goat HRP-conjugated (Abcam; ab6741) antibodies (1:2500) in a 5 ml volume of blocking solution for one hour at room temperature. Membranes were washed in TBS-T and proteins detected using 1:1 concentration of a electrochemiluminescence (ECL) substrate made in-house (ECL Luminol: 250 mM 3-aminophthalydrazide (Sigma), DMSO 0.44g/10 ml) and ECL p-coumaric acid: 90 mM p-coumaric acid (Sigma), DMSO 0.15g/10 ml). The target proteins were visualized on CL-Xposure film (Thermo Scientific) using a Konica SR0101 processor.

All other Western blots were done as followed: Proteins in SDS PAGE gels were transferred onto fluorescence-compatible PVDF membrane (FL-PVDF) (Immobilon-FL Transfer membranes; Millipore) using a Trans-Blot semi-dry cell (Bio-Rad) in Towbin buffer (25 mM Tris, 192 mM glycine, 20% (v/v) methanol)

for one hour at 15 V. FL-PVDF was then blocked for one hour at room temperature or overnight at 4°C using 1:1 (v/v) Odyssey blocking buffer (LiCor) and TBS (50 mM Tris-HCl pH 7.5, 150 mM NaCl). The membrane was then washed once with TBS and replaced with primary antibody diluted in blocking buffer (1:1 LiCor blocking buffer and TBS) then incubated overnight in a rocker incubator at 4°C. A full list of primary antibodies used to detect immobilised proteins is provided in Table 2.3. FL-PVDF membranes were washed three times with TBS (five minutes per wash) and replaced with fluorescent secondary antibody and incubated for one hour with rocking at room temperature avoiding light exposure. The secondary antibody list is provided in Table 2.4. FL-PVDF membranes were washed three times with TBS then rinsed with water. FL-PVDF was left to dry then visualised using Odyssey Sa Infrared imaging system (Li-Cor).

2.2.4 Immunofluorescence (IF)

Cells were grown at 1.5-2x10^5 in 6-well or 12-well plates containing glass coverslips until 60%-70% confluent. Cells were fixed in 4% (w/v) paraformaldehyde, washed again with PBS, and then permeabilised with 0.1% (v/v) Triton X-100 in PBS for 10 minutes at room temperature. They were then blocked in 1% BSA in PBS for a further 10 minutes at room temperature. Cells were then washed in PBS and labeled with primary antibody (Table 2.3) for one hour at room temperature. After extensively washing the cells, secondary antibody was applied (listed in table 2.4) for one hour. Cells were then washed using PBS-T and following this, a drop of Prolong Gold® anti-fade mounting media with DAPI (Invitrogen) was applied on the coverslip containing the cell monolayer and placed on a glass microscope slide. The mounted coverslip was kept overnight in a dark area to allow adhering. The coverslip was sealed using nail varnish and stored at 4°C in darkness to protect from light for long-time storage.

Confocal images were captured on either an LSM700 META inverted microscope (Carl Zeiss Ltd) or an upright LSM510 META Axioplan microscope (Carl Zeiss Ltd). The excitation and emission wavelengths of the lasers used are as follows: for detecting FITC and Alexa Fluor 488 conjugated antibody

excitation wavelength was 488 nm and emission wavelength 518 nm. For DAPI the excitation wavelength was 405 nm and for emission 450 nm. All pinholes were set to allow an optical section of 1-2 µm to be captured. All confocal microscopes were equipped with 40x and 63x oil-immersion lenses.

2.2.5 Flow Cytometry

Cells were seeded in 60 mm dishes until there were 60-70% confluent, representing approximately $8x10^5$ cells in total. For FACS analysis cells were washed with PBS 24 hours post-infection, and detached using accutase (Sigma). Detached cells were centrifuged at 400 rpm for 5 minutes to form pellets, then washed with PBS and fixed in 4% (w/v) paraformaldehyde (PFA-AlfaAesar), 4% (w/v) of PFA dissolved in boiled 1x PBS at pH 7.4, for 10 minutes and washed with PBS. Cells were permeabilised with 0.5% (v/v) Triton X-100 in PBS for 10 minutes at room temperature and blocked in 1% BSA in PBS for 10 minutes at room temperature. Cells were washed in PBS and labeled with primary antibody or FITC conjugated antibody (those labeled with FITC conjugated did not need a secondary antibody) in 2% FBS in PBS for one hour at room temperature. Cells were washed three times with PBS then stained with secondary antibody and re-washed with PBS and re-suspended with FACS buffer (1 mM EDTA [Promega] in PBS, 1% FBS, 1M HEPES [Gibco]) and directly assessed by FACS analysis. HRSV infected cells were examined and analysed using the LSR Fortessa cell analyzer (BD Biosciences).

2.2.6 Toxicity Test

2.2.6.1 MTT assays

MTT assays were performed on all ion channel modulating drugs using a total of 1x10 cells seeded into 96-well plates. Different concentrations of each ion channel modulator were diluted in growth medium (Table 2.5), and 24 hours post seeding, 100 µm of the diluted ion channel drug was added into each well. Cell viability and cytotoxicity was assessed using CellTiter 96® AQ_{ueous} One Solution Cell Proliferation Assay (Promega), which contains a novel tetrazolium compound [3-(4,5-dimethylthiazol-2-yl)-5-(3-carboxymethoxyphenyl)-2-(4-

sulfophenyl)-2H-tetrazolium, inner salt; MTS] and an electron-coupling reagent (phenazine ethosulfate; PES). Some 20 µl of CellTiter 96® AQ_{ueous} One Solution Reagent was mixed with 100 µl of DMEM and added into each well. The cells were incubated at 37°C for 1-4 hours in the dark, and the % live cells assessed by measuring the absorbance at 490 nm on a 96-well plate reader (Dynex).

2.2.6.2 LDH cytotoxicity Assay

LDH cytotoxicity was measured using the Pierce LDH Cytotoxicity Assay Kit (ThermoFisher [88953]) according to the manufacturer's instructions. Briefly, HBEpC cells in 96-well plates were infected at an MOI of 1 and incubated for 48 hours, after which 50 µl of infected supernatant was added to a fresh 96-well plate. A volume of 20 µl of lactate dehydrogenase (LDH) reaction solution was added to the supernatant. Treated infected cells were incubated for 30 minutes at room temperature then assessed by measuring the absorbance at 490 nm on a 96-well plate reader (Dynex). The mock control consisted of un-infected treated cells. The reaction mixture catalyzes the conversion of lactate to pyruvate via NAD+ reduction to NADH. Diaphorase then uses NADH to reduce a tetrazolium salt (INT) to formazon (red colour) that can be measured at 490 nm.

2.2.7 Measuring intracellular chloride concentration by MQAE

Intracellular chloride ion concentrations were measured using $2x10^5$ cells seeded in 12-well plates and treated with 5 mM 6-methoxy-quinolyl acetoethyl ester (MQAE) (BioLegend) in DMEM for one hour at 37°C. Then cells were washed three times using PBS then infected with HRSV at an MOI of 1 diluted in DMEM phenol-red free media and placed directly onto the IncuCyte Zoom Live-cell imager. The average fluorescence mean/well was measured at hourly intervals until six hours post-infection.

2.2.8 Statistical analysis

Statistical analysis was carried out to compare the difference in HRSV growth between cells infected and treated with ion channel drugs, and cells infected with HRSV but untreated, using a one-way ANOVA. The test was

performed using the StatPlus program in Excel and values were deemed to be significant when they were less than or equal to a p value of 0.05.

2.2.9 Mass spectrometry

2.2.9.1 Sample preparation for LC-MS/MS

Infected cells were trypsinized, neutralized with media and centrifuged as normal at 400 rpm. Cell pellets were washed three times with cold PBS. The sample was suspended in 0.1% RapiGest (Walter) diluted in 25 mM ammonium bicarbonate. Three cycles at intervals of freeze-thaw were carried out (using liquid N_2) with five minutes vortex after each cycle. This was followed by two 15-minute cycles of sonication in an ice water bath. The sample was heat-inactivated at 80°C for 10 minutes in an Eppendorf tube and a protein assay was carried out to determine protein concentration. The insoluble fraction of the samples was then removed by centrifugation for 20 minutes At 12,000 rpm. The protein concentrations of the whole lysate were measured by BCA and a sample containing a total mass of 100µg was dispensed for further sample processing. The following steps were carried out by Dr. Stuart Armstrong at The University of Liverpool, as described below. DTT was added to a final concentration of 3 mM, then the sample was incubated at 60°C for 10 minutes. The sample was cooled to room temperature then IAA was added to a final concentration of 9 mM and then incubated for 30 minutes at room temperature in the dark. Trypsin was added 50:1 or 100:1 protein: trypsin ratio and then incubated at 37°C with shaking overnight. Trifluoroacetic acid (TFA) was added at a final concentration of 0.5% (v/v) and incubated at 37°C for one hour. The sample was centrifuged at 14,000 rpm at 4°C for 30 minutes and then the supernatant was removed to a fresh Eppendorf tube. Digestion efficiency was then tested using SDS PAGE analysis. Internal standards of known fmol quantities were mixed with the sample digest and analyzed on Orbitrap Velos (ThermoFisher).

2.2.9.2 Proteomics data analysis

Data analysis to determine protein abundance changes was performed manually based on the fold-change that was calculated from the normalised protein abundancy of each sample given data in excel sheet. The normalised protein abundancy from proteomics given data were averaged (N=3) and normalised with mock control (normalised protein abundancy of un-infected cells, N=3) and calculated as Log_2 value of fold change in excel. Significance p-values (ANOVA) were also calculated in excel to $-Log_{10}$(p-value). The $–Log_{10}$(p-value) results showed the significant protein that are represented above the value of 1.3 ($– Log_{10}$ [p-value]), which is equivalent to 0.05. The significant fold change considered as greater than Log_2 fold change = 1.

2.2.9.3 Ingenuity Pathway Analysis (IPA)

Network pathways were obtained from the IPA software by providing the averaged normalised fold change and ANOVA p-value for each sample. The software programme analyzed the data provided and linked the pathways based on the proteomics data.

2.3 List of primary antibodies

Target	Vendor	Catalogue number	WB	IF	FACS
RSV	Abcam	Ab20745	1:1000	1:100	-
RSV	Abcam	Ab20391	N/A	1:100	1:100
GAPDH	Abcam	Ab8245	1:5000	-	
Calmodulin	Abcam	Ab45689	1:1000	-	1:50
CHERP	Santa Cruz	SC-100650	1:50	N/A	N/A

	Abcam	Ab15951			
Caspase-1	Cell Signalling	2225S	1:1000	-	-
STAT-1	Abcam	Ab92506	N/A	-	1:50
STAT-3	Cell Signalling	9139S	1:1000	-	-
EGF complex	ThermoFisher	E13345	-	1:500	-

Table 2. 3. List of primary antibodies

2.4 List of secondary antibodies

Target primary cell	Conjugation	Vendor	Catalogue number	WB	IF	FACS
Goat	horseradish peroxidase (HRP)	Abcam	Ab6741	1:2500	N/A	N/A
Mouse	HRP	Sigma	A4116	1:10,000	N/A	N/A
Rabbit	Alexa Fluor 647	Invitrogen	A21245	N/A	-	1:2500
Mouse	IRDye 680RD	Li-Cor	926-68072	1:500-1:10,000	N/A	N/A
Rabbit	IRDye 800CW	Li-Cor	926-32213	1:500	N/A	N/A
Sheep	IRDye 800CW	Li-Cor	926-32214	1:2500	N/A	N/A

Table 2. 4. List of secondary antibodies.

2.5 List of ion channel modulators

Drug	Abbreviation	Vendor	Catalogue number
Barium chloride	**$BaCl_2$**	**Sigma**	**202738-5G**
Pinacidil	**Pin**	**Sigma**	P154
Glibenclamide	**Glib**	**Sigma**	**G0325000**
Tolbutamide	**Tol**	**Sigma**	T1700000
Halothane	**Hal**	**Sigma**	**H0150000**
Ruthenium red	**RR**	**Sigma**	R2751
Arachidonylethanolamide	**AEN**	**Sigma**	**A0580**
Haloperidol	**Halo**	**Sigma**	H0100000
4-Aminopyridine	**4-AP**	**Sigma**	**275875**
Chromanol 293B	**Chrom**	**Sigma**	**C2615**
Ergtoxin	**Erg**	**Sigma**	**E9904**
Sotalol	**Sot**	**Sigma**	39863
Tram-34	**Tram**	**Sigma**	T6700

Apamin	**Apa**	**Sigma**	A1289
Tetraethylammonium	**TEA**	**Sigma**	86608
Quinine	**Q**	**Sigma**	**69311**
Quinidine	**Q-HCl**	**Sigma**	**Q0750**
Potassium Chloride	**KCl**	**Sigma**	**P5405**
Tetrodotoxin	**TTX**	**Tocris**	1078
Lidocaine *N*-ethyl bromide	**L-HCL or L**	**Sigma**	L5783
α-Pompilidotoxin	**α-Pom**	**Sigma**	**P6237**
Disopyramide phosphate salt	**Dp**	**Sigma**	D6035
Amiloride HCL	**Am**	**Sigma**	G1006627
R(-) Me5 Hydriodide	**Me5**	**Sigma**	**M0814**
Procainamide hydrochloride	**Pro**	**Sigma**	**P3050000**
Nifedipine	**Nif**	**Sigma**	**N0750000**
Nitrendipine	**Nit**	**Sigma**	**N0905000**
Nimodipine	**Nim**	**Sigma**	**N0850000**

Verapamil	**Ver**	**Sigma**	**V0100000**
Bay K8644	**BayK**	**Sigma**	**B133**
Niguldipine	**Nig**	**Sigma**	**N162**
2-Aminoethoxydiphenyl borane	**2APB**	**Sigma**	**D9754**
R(+)IAA-94	**RIAA**	**Sigma**	**I117**
5-Nitro-2-(3-phenylpropylamino)benzoic acid	**NPPB**	**Sigma**	**N4779**
4,4'-diisothiocyanatostilbene-2,2'-disulfonic acid disodium salt hydrate	**DIDS**	**Sigma**	D3514
Ribavirin **(Used as positive control compared with ion channel drugs)**	**RBV**	**Sigma**	**R9644**

Table 2. 5. List of ion channel modulator drugs.

Chapter 3: the role of host ion channel during HRSV infection

Chapter 3: The role of host cell ion channel function during HRSV infection

3.1 Introduction

Whilst it is known that the HRSV-SH protein acts as a viroporin (Gan et al., 2012), the contribution of cellular ion channel function during the HRSV lifecycle has remained undefined. Recent studies have demonstrated that modulating cellular ion channels with specific ion channel drugs can be detrimental to RNA virus infection, implicating the control of cellular ion channel functionality as a critical host cell interaction during virus multiplication (Piccini et al., 2015; Hover et al., 2015; Kunzelmann et al., 2007; Igloi et al., 2015). Cellular ion channels play a key role in many aspects of lung cell physiology (Hollenhorst et al., 2011), indeed many symptoms of HRSV infection can linked to altered ion channel function including mucus discharge, the cough reflex and bronchiolitis (Boucher, 2004). In this chapter, the role of cellular ion channel activity during HRSV infection was investigated in adenocarcinomic human alveolar basal epithelial cells (A549), the cell line of choice for the majority of published HRSV studies (Krzyzaniak et al., 2013). HRSV virus was used effectively thorough infection assays and performed in the presence of broad-spectrum ion channel modulators for the four major channel types (K^+, Na^+, Cl^- and Ca^{2+}). The optimal concentration of each channel modulator was assessed by MTT assays. HRSV infection was assessed through detecting the expression of HRSV proteins, known to correlate with virus production. In this chapter, a role of specific ion channel families was identified during the HRSV lifecycle. This may pave the way for future studies highlighting ion channel modulators as a new avenue of much needed anti-HRSV therapies.

3.2 Optimisation of HRSV replication in A549 cells

3.2.1 HRSV Purification and titration.

Ion channel function can be modified by growth factors and cytokines (Feske et al., 2015) that are secreted during HRSV-infection in culture. For this reason, purified HRSV stocks free of such molecules were used for all HRSV assays. Sucrose gradients are the most popular method to purify HRSV, and can increase virus yields by up to 60% (Mbiguino and Menezes, 1991). The production of high titre HRSV stocks additionally allows the infection of cells with a high multiplicity of infection (MOI), which represents an approximation of the number of virions added per cell. This allows HRSV supernatants to be concentrated by ultracentrifugation, following PEG-6000 precipitation as described in Materials and Methods (Chapter 2, section 2.2.2.3). The first ultracentrifugation step used a discontinuous sucrose density gradient. A second centrifugation step was implemented using a continuous sucrose density gradient that ensured that all virus particles were separated from host cell debris. In both steps, an opaque band appears between 30% and 45% sucrose fractions, representing purified virus (Figure 3.1A). A second lower opaque band was also visible, which represented cellular debris. The second centrifugation step was bypassed when the debris bands of the continuous gradient were faint.

To determine the MOI of the purified virus, plaque assayed was performed as described in Materials and Methods (Chapter 2, section 2.2.2.4.). Purified HRSV typically displayed titres ranging of ~ 1×10^7 to 2×10^7 PFU/ml compared to titres of ~ 1×10^5 PFU/ml from the original supernatant (Figure 3.1B).

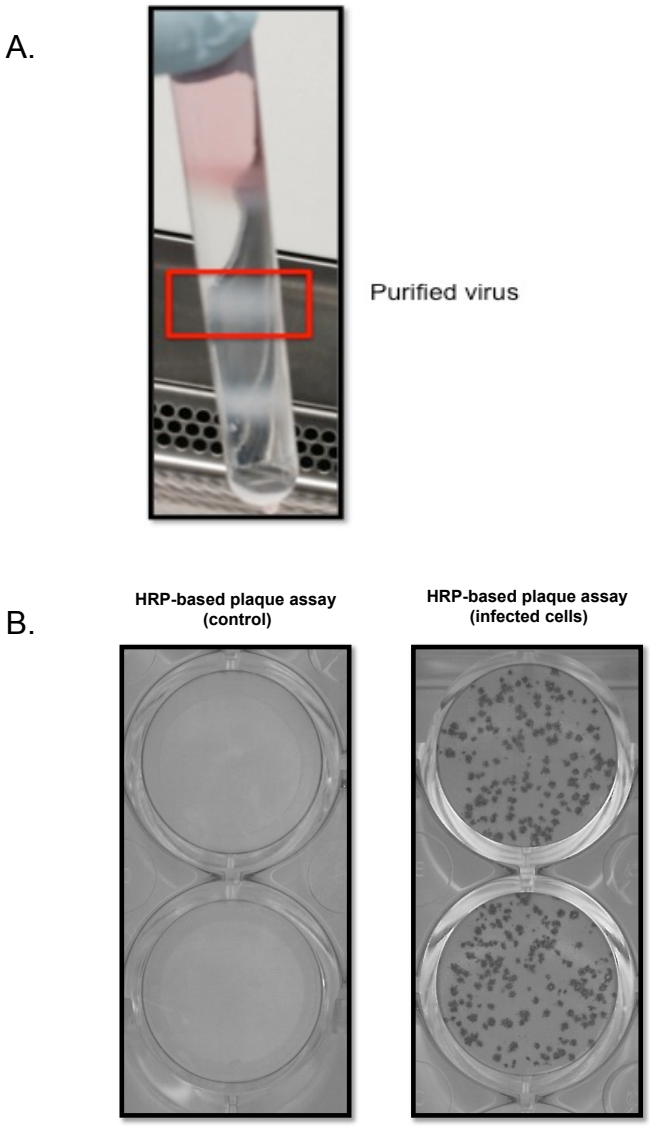

Figure 3. 1. HRSV purification and titration.

A. Discontinuous sucrose gradient. The top white opaque band represents concentrated HRSV particles that appear between 30% and 45% of the sucrose density gradient. The bottom white band represents host cell debris that were separated from purified HRSV particles. B. Plaque assay of the 20-40% fractions containing HRSV. Infected cells are represented by purple colonies due to HRSV staining. Plaques were counted from duplicate wells to ensure accurate estimates of virus titres.

3.2.2 HRSV A2 WT growth curves in A549 host cells

To identify a suitable MOI to assay virus growth in A549 cells, cells were infected at a range of MOIs (3, 1.0 or 0.1). Infected cells were harvested 24 hours post infection (hpi), and HRSV protein expression assessed by western blot analysis using well characterized commercially produced anti-HRSV polyclonal antibodies. Western blots were analysed to establish an MOI that allowed consistent and detectable HRSV protein expression (Figure 3.2). To ensure specific labelling of HRSV proteins, infected cells were treated with the known HRSV inhibitor ribavirin (RBV) during virus infection.

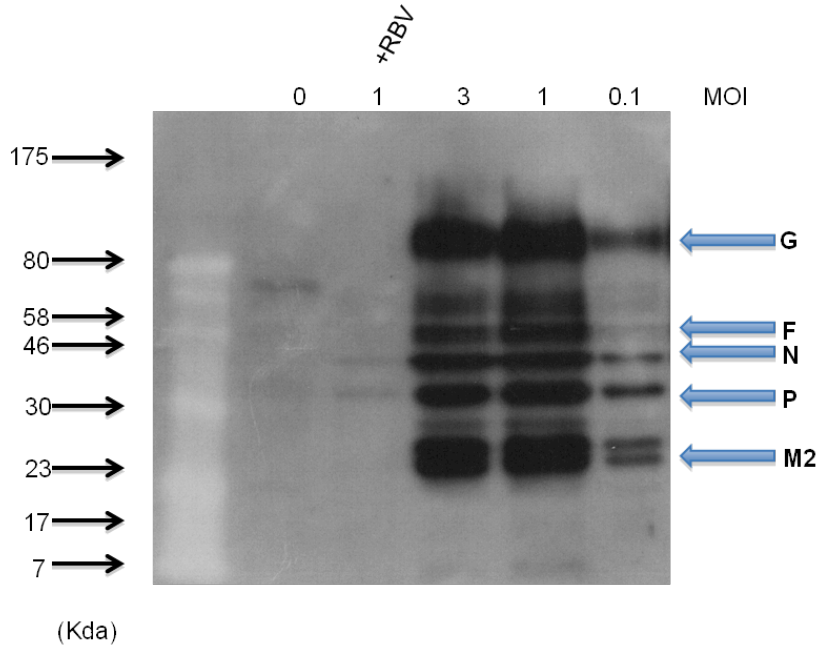

Figure 3. 2. Western Blot analysis of HSRV protein expression in A549 cells infected with the indicated MOIs for 24 hours.

Mock-infected cells were treated with complete media alone. For RBV treatment, cells infected with an MOI of 1.0 were treated with 500 μM RBV for 24 hours. The HRSV proteins detected and their respective sizes are as follows G protein (~ 90 kDa), F protein (~ 55 kDa), N protein (~ 42-46 kDa), M2 (~22-28 kDa) and P (~35 kDa).

Figure 3.2 shows that increased HRSV G, F, N, P and M2 protein expression was evident at an MOI of 1.0 and 3.0, compared to an MOI of 0.1. Comparatively, an MOI of 1.0 or 3.0 produced similar virus protein expression levels. As expected, treatment with RBV dramatically reduced virus expression

confirming these bands to be representative of HRSV proteins (Figure 3.2, lane 3). From these data, it was decided that cells would be infected with an MOI of 1.0 for further HRSV infection assays.

The time points at which HRSV proteins could be detected were next investigated to obtain an optimal time point for addition of the ion channel inhibitory compounds. Both growth curve and immunofluorescence analysis (IF) were performed to assess virus gene expression and cell health at various hpi. Infectious HRSV WT was diluted to an MOI of 1.0 in serum free media for these infection assays. For IF analysis, cells were infected for 2, 3, 4, 6, 12, 24, 48 and 72 hours. These represent the times for which cells were incubated with HRSV. Cells were fixed, permeabilised and HRSV was detected using commercial FITC conjugated goat anti-HRSV antibodies. Cell nuclei were stained with DAPI to assess cell viability. Representative confocal images of infected A549 cells are shown in Figure 3.3.

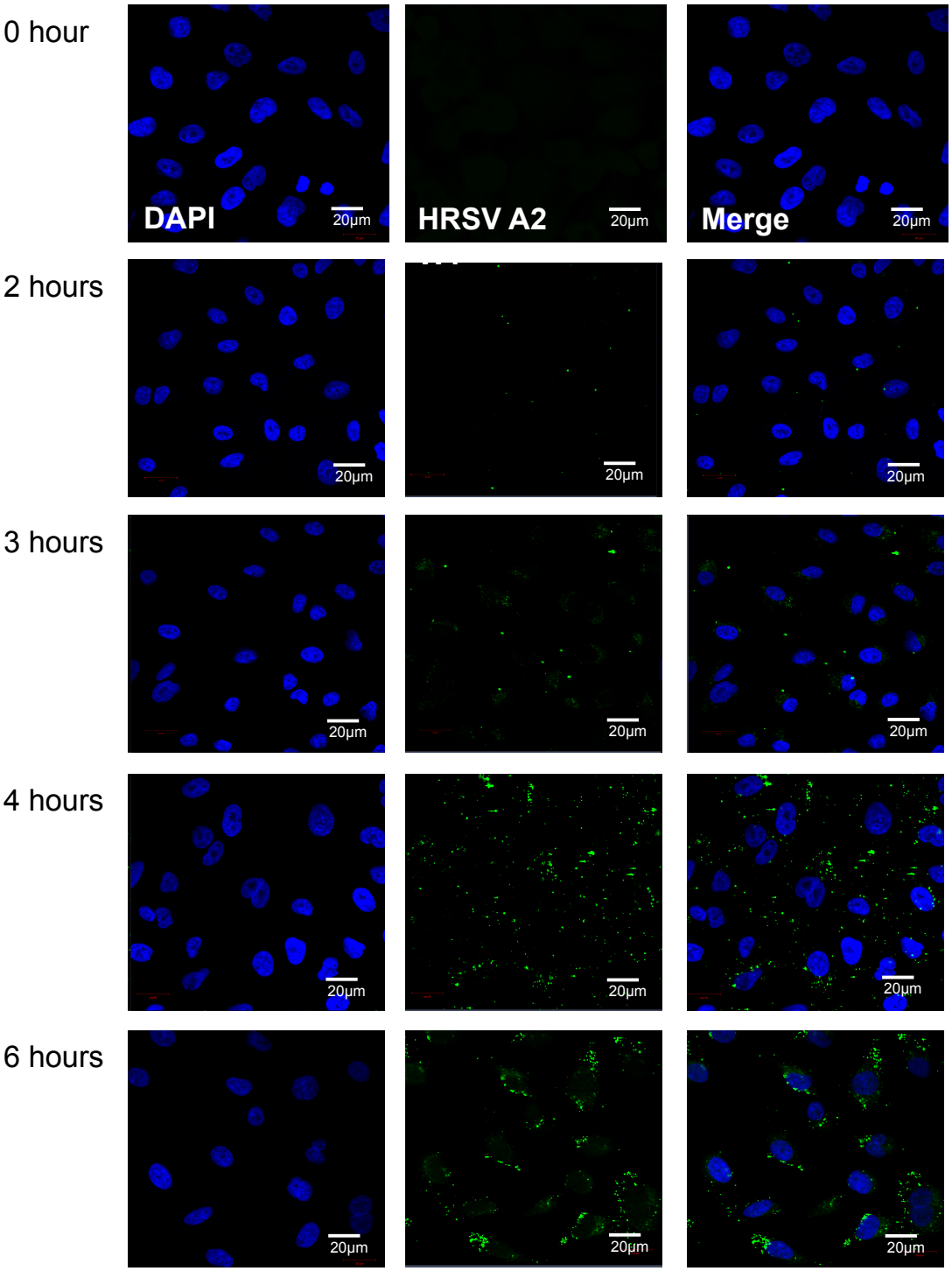
0 hour
DAPI
20μm
HRSV A2
20μm
Merge
20μm
2 hours
20μm
20μm
20μm
3 hours
20μm
20μm
20μm
4 hours
20μm
20μm
20μm
6 hours
20μm
20μm
20μm

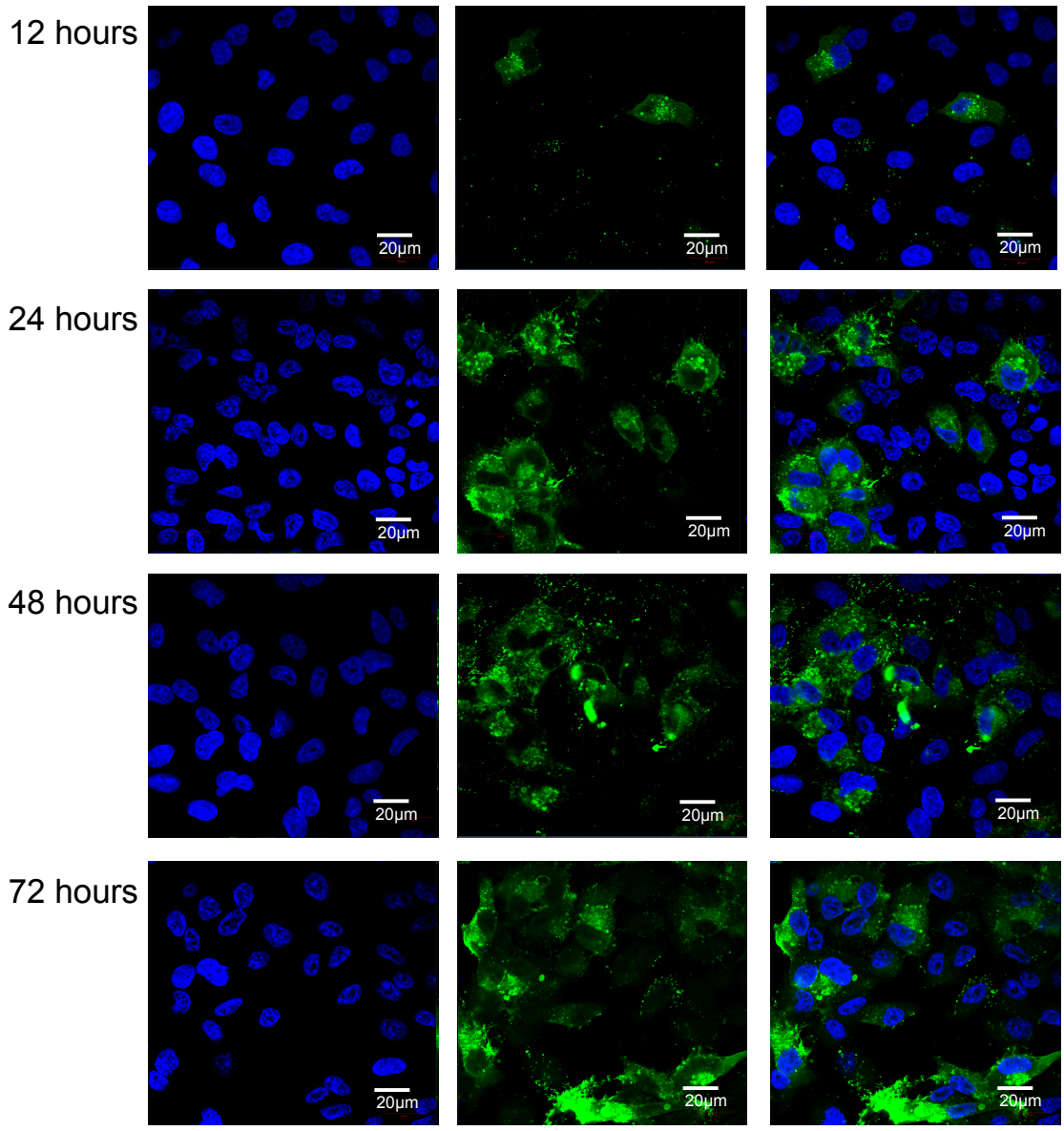

Figure 3. 3. Timecourse of HRSV infection in A549 cells.

Cells were infected for 2, 3, 4, 6, 12, 24, 48 and 72 hours at an MOI = 1.0. Cells were labelled with FITC conjugated anti-HRSV antibodies (green) and the nuclei stained with DAPI. Images were taken using upright LSM 510 META Axioplan microscope. Representative images for each time point are shown. Scale bar = 20 µm

Figure 3.3 demonstrates that at 2 hpi, infectious HRSV A2 particles were detectable at the cell surface, which may illustrate virus attachment to the cell membrane. From 3 to 4 hours, the staining of viral particles increased in abundance, particularly around the cell periphery. At 6 to 12 hpi, the intensity of HRSV protein staining increased, most likely due to virus replication and translation of new virus proteins. The highest levels of viral protein expression as assessed by the increased intensity of fluorescent staining were observed

between 24 and 48 hpi. Comparatively, HRSV protein expression increased from 24-48 hours suggesting virus replication and protein synthesis occur predominantly during this period. The majority of cells also appeared healthy 48 hpi as minimal nuclear fragmentation was detected, as assessed by DAPI staining. By 72 hpi, cells began to reduce in number indicating cell lysis, which is consistent with the stages reported for HRSV assembly and release to occur (Collins, 2007).

To assess HRSV growth over time and generate a growth curve, a monolayer of A549 cells was infected with HRSV in 12-well plates at an MOI of 1.0. After 3 hours of incubation, unattached viruses were washed off and replaced with complete media. Cells were harvested by scraping into the culture media after 4, 6, 12, 24, 48 and 72 hpi. Total cell lysates were collected and quantified by plaque assay (Figure 3.4).

According to the growth curve in Figure 3.4, the amount of infectious HRSV progeny steadily increased between 24 ($9.7x10^5$ PFU/ml) and 48 ($2.8x10^7$ PFU/ml) hours indicating this as the timeframe at which the peak of virus production occurs. Following 48 hours, a sharp drop in viral production occurred, up to 72 hours ($6.2x10^5$ PFU/ml). The time points represented on the growth curve show virus production after the adsorption phase that is assumed to occur in the first 4 hours. From 4 to 12 hours, virus levels steadily increased from $2.2x10^4$ PFU/ml to $6.1x10^5$ PFU/ml, which may illustrate virus entry and early replication events. Overall, the growth curve confirmed the optimal conditions for peak HRSV protein detection, and cells were infected with an MOI of 1.0 for a time period of 24 hours for all subsequent assays.

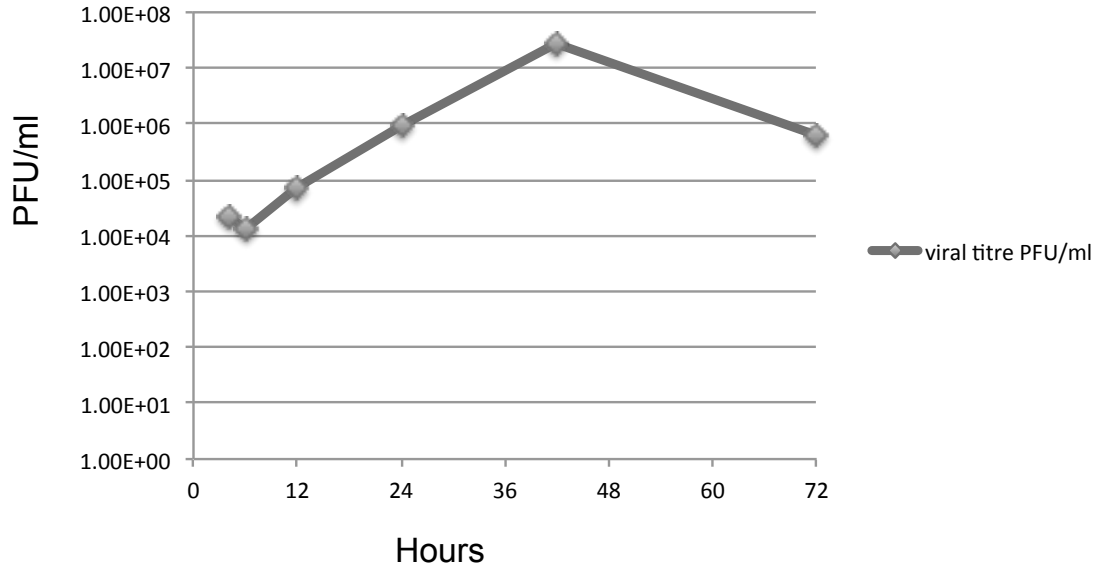

Figure 3. 4. Growth curve of HRSV A2 WT.

Growth curves were assessed in A549 cells infected at an MOI 1.0. Samples for analysis were collected at 4, 6, 12, 24, 48 and 72 hours post infection. The total infectivity of each sample was determined by HRP-based plaque assay.

3.3 Analysis of A549 cell viability in response to cellular ion channel modulating drugs

A549 cells express a range of diverse ion channel families. However, how these ion channels contribute to the normal A549 cell physiology is unknown. Before assessing the effects of the ion channel modulating compounds on HRSV infection, non-toxic concentrations of each ion channel modulator had to be selected. Cell viability was monitored by MTT assays (described in Methodology section 2.2.6.1). A549 cells were treated with a range of concentrations of each channel modulator for 24 hours at concentrations previously characterized to modulate specific ion channel families (Hover et al., 2015; Igloi et al., 2015; Sakurai et al., 2015b; Irvine et al., 2007; Hsu et al., 2004).

Studies were initiated using potassium (K^+) ion channel modulating compounds as these represent the largest family of cellular ion channels. Over 70 genes encode K^+ channel subunits in the human genome, which are divided into subfamilies of (i) 6 trans-membrane domain (6TMD) voltage-gated K^+ channels (Kv) or calcium-activated K^+ channels (K_{Ca}), **(ii)** 2TMD inwardly rectifying K^+ channels (Kir) and **(iii)** 4TMD two-pore K^+ channels (K2P) channels. Table 3.1 shows the drugs that were tested and the K^+ channel family member affected by each modulator.

Type	Subtype	Activators	Blockers
Inward Rectifier (Kir)	Kir 1.1 (ROMK;KCNJ1) Kir 2.1-2.4 (IRK;KCNJ 2, 12, 4, 14) Kir 3.1-3.4 (GIRK1-4;KCNJ 3, 6, 9, 5) Kir 4.1-4.2 (KCNJ 10, 15) Kir 5.1 (KCNJ 16) Kir 7.1 (KCNJ 13	-	Barium chloride ($BaCl_2$) Spermine (Sper)
ATP-Sensitive (K_{ATP})	Kir 6.1-2 (KCNJ 8, 11)	Pinacidil (Pin)	Glibenclamide (Glib) Tolbutamide (Tol)

2-P Domain (K_{2P})	KCNK1 (TWIK-1) KCNK2 (TREK-1) KCNK3 (TASK-1) KCNK4 (TRAAK) KCNK5 (TASK-2) KCNK6 (TWIK-2) KCNK7 KCNK9 (TASK-3) KCNK10 (TREK-2) KCNK12 (TALK-1) KCNK13 (TALK-2) KCNK15 (TASK-5) KCNK16 (THIK-2) KCNK17 (THIK-1)	Halothane (Hal)	Ruthenium red (RR), Anandamide, AEN, Haloperidol (Halo)
Voltage-Gated (Kv)	Kv1.1-1.8 (KCNA1-8) Kv2.1-2.2 (KCNB1-2) Kv3.1-3.4 (KCNC1-4) Kv4.1-4.3 (KCND1-3) Kv5.1 (KCNF1) Kv6.1-6.3 (KCNG1-3)		4-Aminopyridine (4-AP) Chromanol 293B (Chrom) Ergtoxin (Erg), Sotalol (Sot),

	Kv8.1 (KCNB3) Kv9.1-9.3(KCNS1-3) KCNQ1-5 (Kv7.1-7.5) KCNH1-8 (HERG, EAG, ELK)		Haloperidol (Halo)
Calcium-Activated (K_{Ca})	Large Conductance BK (Slo1/Maxi-K) Slack/Slo2. Intermediate Conductance IK (KCNN4). Small conductance SK1-3 (KCNN1-3)	-	Tram-34 Apamin (Apa)
Broad spectrum	Non selective K^+ channel	-	Tetraethylammonium (TEA), Potassium chloride (KCl), Quinine (Q) Quinidine (Q-HCl)

Table 3. 1. K^+ channel types expressed in cells and the ion channel modulating drugs that target these channels.

Each drug was selected and MTT tests performed to ensure no effects on cell viability. Non-toxic concentrations of each compound were taken forward for future HRSV assays.

Figure 3.5 shows that the majority of channel modulating compounds were non-toxic at the stated concentrations following 24 hours of treatment. When toxicity was observed, for example with KCl (50 mM) and AEN (100 μM), a broad spectrum inhibitor of K^+ channel activity through collapsing the K^+ gradients

required for channel activity, and a K_{2P} specific channel inhibitor respectively, a lower non-toxic concentration of each channel modulator was taken forward for future assays. MTT assays were also performed for modulators of the other major channel families namely sodium (Na^+), calcium (Ca^{2+}) and chloride (Cl^-) channels (Figures 3.6). Table 3.2 shows the ion channel drugs assessed and their respective ion channel targets. The cytotoxicity of RBV in A549 cells was also assessed to ensure its validity as a positive control in subsequent experiments (Figure 3.7). Cells that were treated with 500 μM RBV displayed no loss of viability, indicating that at this concentration it is non-toxic inhibitor of HRSV infection.

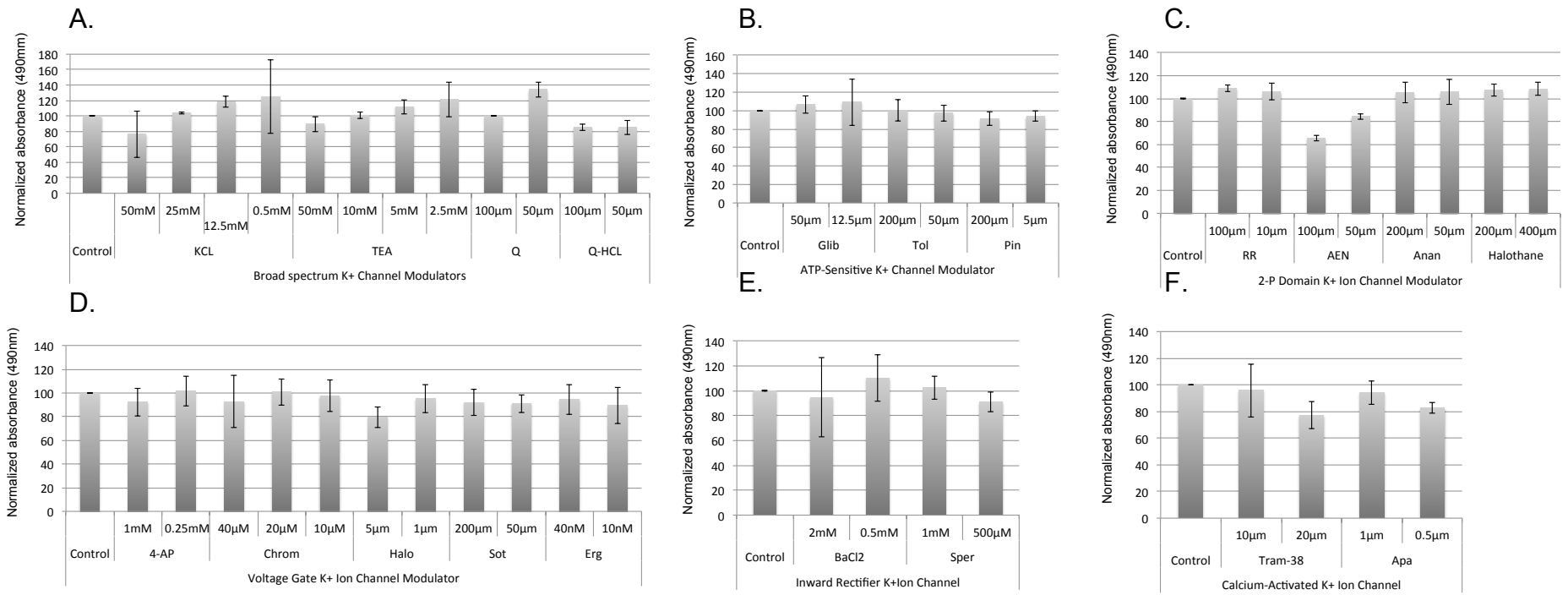

Figure 3. 1. Cellular toxicity of K^+ channel modulators in A549 cells.

A549 cells were treated with the indicated concentrations of K^+ ion channel modulators for 24 hours and cell viability assessed by MTT assay. **A.** Broad spectrum voltage gated K^+ ion channel drugs. **B.** ATP-sensitive K^+ channel modulators. **C.** K_{2P} channel drugs. **D.** Voltage gated K^+ ion channel drugs. **E.** Kir drugs. **F.** Calcium sensitive K^+ ion channel drugs. Each drug concentration was assessed in triplicate (n=3). Data are expressed as mean ± SE (n=3).

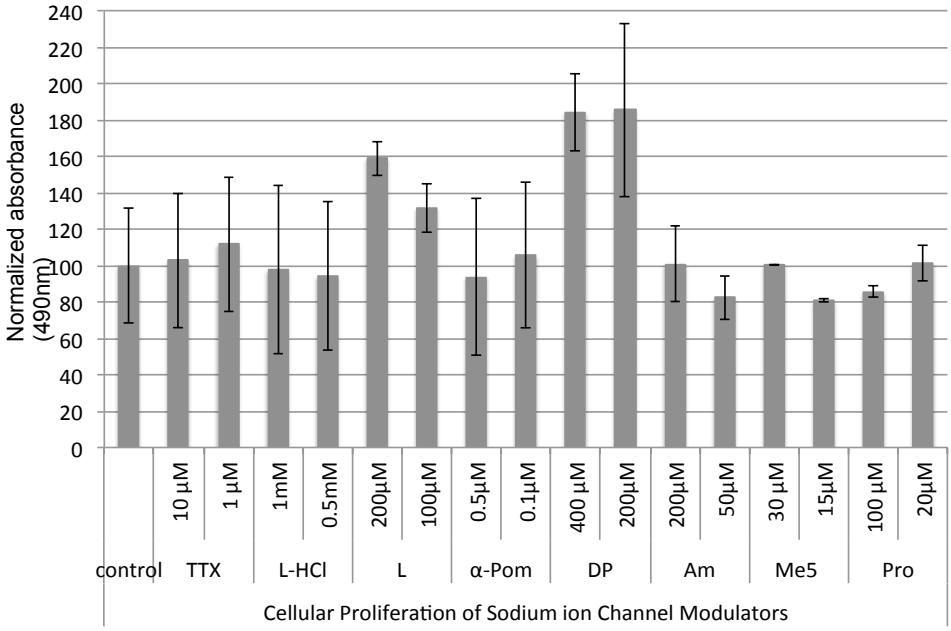
Normalized absorbance (490nm)
240
220
200
180
160
140
120
100
80
60
40
20
0
10 µM
1 µM
1mM
0.5mM
200µM
100µM
0.5µM
0.1µM
400 µM
200µM
200µM
50µM
30 µM
15µM
100 µM
20µM
control
TTX
L-HCl
L
α-Pom
DP
Am
Me5
Pro
Cellular Proliferation of Sodium ion Channel Modulators

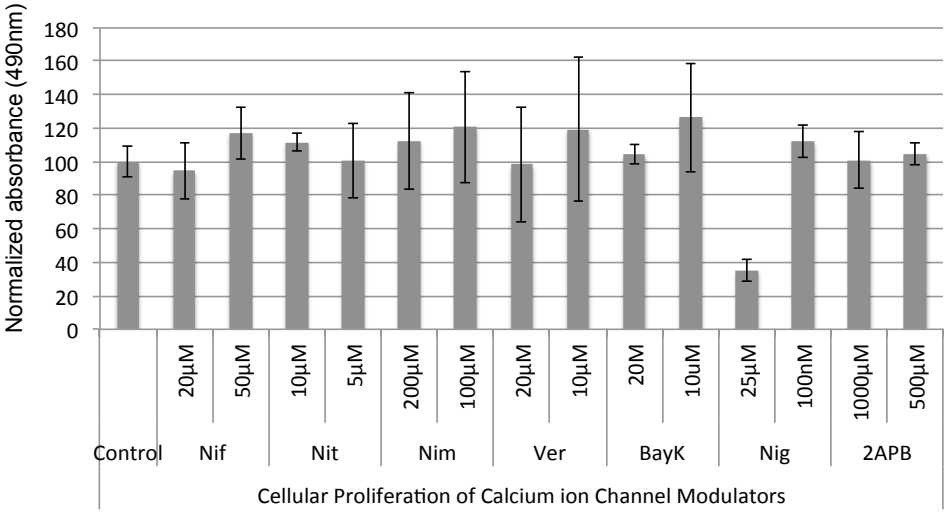
Normalized absorbance (490nm)
180
160
140
120
100
80
60
40
20
0
20µM
50µM
10µM
5µM
200µM
100µM
20µM
10µM
20M
10uM
25µM
100nM
1000µM
500µM
Control
Nif
Nit
Nim
Ver
BayK
Nig
2APB
Cellular Proliferation of Calcium ion Channel Modulators

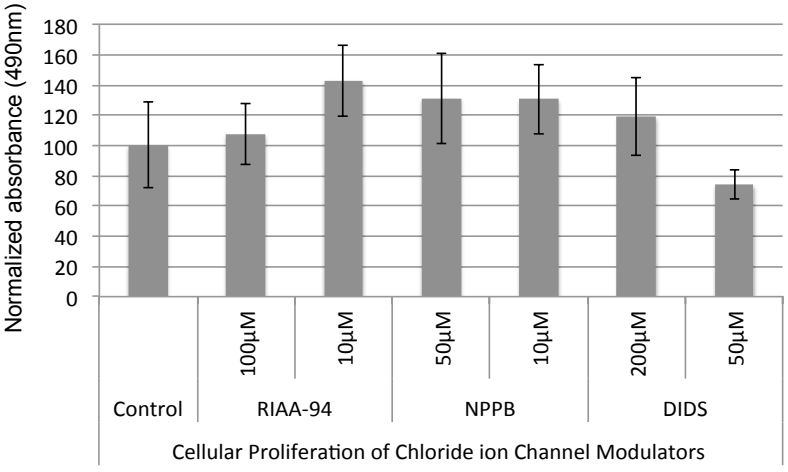
Normalized absorbance (490nm)
180
160
140
120
100
80
60
40
20
0
100µM
10µM
50µM
10µM
200µM
50µM
Control
RIAA-94
NPPB
DIDS
Cellular Proliferation of Chloride ion Channel Modulators

Figure 3. 6. Assessment of cell viability in response to Cl^-, Na^+ and Ca^{2+} channel modulation in A549 cells.

A549 cells were treated with the indicated concentrations of ion channel modulating drugs targeting **A.** Na^+ channels. **B.** Ca^{2+} channels **C.** Cl^- channels, all for for 24 hours and with cell viability assessed by MTT assay. Each drug concentration was assessed in triplicate (n=3).

Compound	Label	Ion channel family	Target ion channel type
Tetrodotoxin	TTX	Na^+	Broad spectrum voltage gated Na^+ channel pore blocker
Lidocaine *N*-ethyl bromide	L L-HCL	Na^+	Blocks fast voltage gated Na^+ channels and inactivating Na^+ channel conductance.
α-Pompilidotoxin	α-Pom	Na^+	Voltage-gated Na^+-channel activator
Disopyramide phosphate salt	Dp	Na^+	Na^+-channel blocker

Amiloride HCL	Am	Na^+	Epithelial sodium channel (ENaC) inhibitor
R(-) Me5 Hydriodide	Me5	Na^+	Na^+ channel blocker
Procainamide hydrochloride	Pro	Na^+	Na^+ channel blocker
Nifedipine	Nif	Ca^{2+}	L-type Ca^{2+} channel inhibitor
Nitrendipine	Nit	Ca^{2+}	L-type Ca^{2+} channel inhibitor
Nimodipine	Nim	Ca^{2+}	Inhibits slowly inactivating Ca^{2+} channels
Verapamil	Ver	Ca^{2+}	Inhibits T-type (transient) and L- (long-lasting) Ca^{2+} channels
Bay K8644	BayK	Ca^{2+}	L-type Ca^{2+} channel activator
			L-type Ca^{2+} channel

Niguldipine	Nig	Ca^{2+}	blocker
2-Aminoethoxydiphenylborane	2APB	Ca^{2+}	Inhibits intracellular TRP channels. Inhibits Ca^{2+} influx
R(+)IAA-94	RIAA	Cl^-	Blocks medium-conductance, voltage-sensitive Cl^{--} channels such as CLC-2 and CLC-3
5-Nitro-2-(3-phenylpropylamino) **benzoic acid**	NPPB	Cl^-	Broad spectrum anion (particularly large-conductance Cl^- channel) blocker
4,4'-diisothiocyanatostilbene-2,2'-disulfonic acid disodium salt hydrate	DIDS	Cl^-	Broad spectrum anion channel blocker.

Table 3. 2. Modulators of Na^+, Ca^{2+} and Cl^- channels investigated in the study.

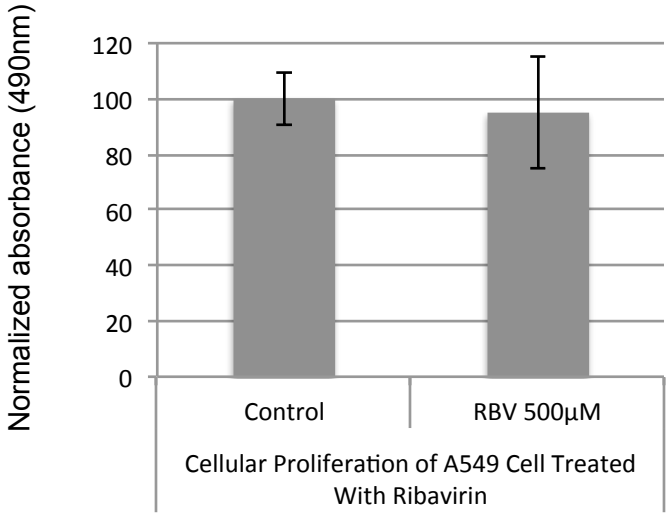

Figure 3. 7. Assessment of cell viability in response to RBV in A549 cells.

Cells were treated with 500 μM RBV for 24 hours and cell viability assessed by MTT assay (n=3).

3.4 Assessment of the effects of ion channel modulation on HRSV growth in A549 cells post-virus attachment/entry

To determine if the activity of cellular ion channels are required for HRSV growth, HRSV infectivity was assessed in the presence of each individual ion channel compound. FACS based assays were used to assess the percentage of HRSV infected cells following each drug treatment as illustrated in Figure 3.8. For these assays, A549 cells were infected with HRSV (MOI = 1.0), and the channel inhibitors added 3 hpi. Infected cells were then harvested 24 hpi, and HRSV gene expression was assessed by FACS analysis through staining fixed cells with FITC conjugated anti-HRSV antibodies. Each assay contained cells that were mock infected (example FACS plot in Figure 3.9A), HRSV infected (example FACS plot in Figure 3.9B) or HRSV infected and treated with RBV (example FACS plot in Figure 3.9C). Figure 3.9B shows that following infection, approximately 20% of the cell population were positive for HRSV proteins, whilst mock-infected cells showed no HRSV staining. Importantly, the number of HRSV positive cells was drastically reduced in RBV treated cells, confirming the sensitivity of the assay to detect a reduction in HRSV infection. In these

samples, 20000 single cells were counted and all values were normalised to HRSV infected no-drug controls.

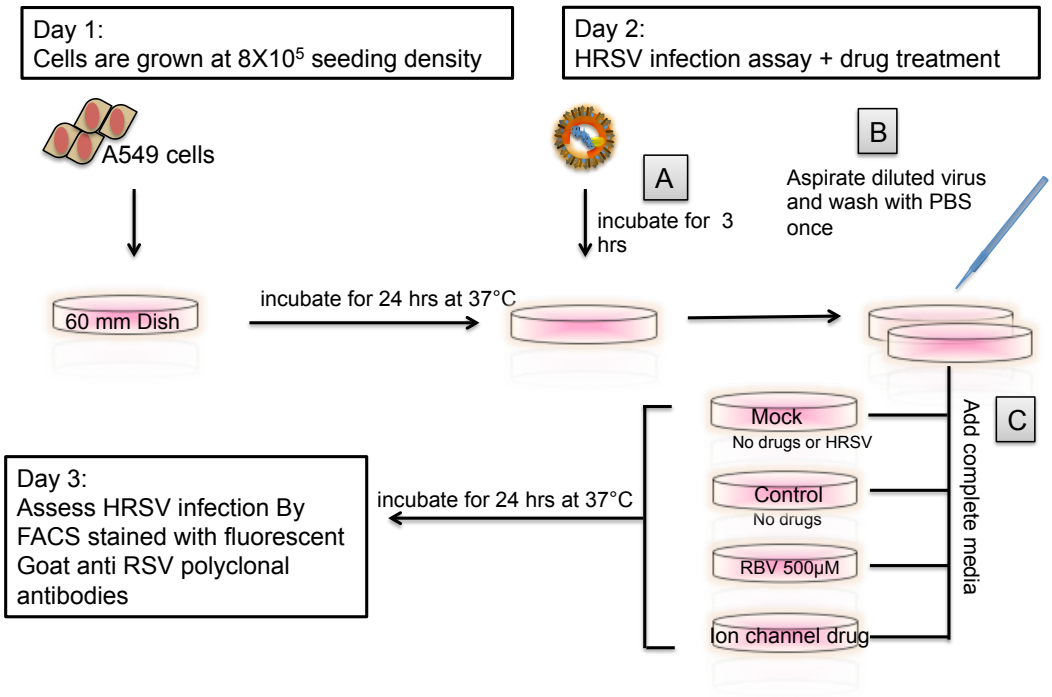

Figure 3. 8. Schematic demonstrating the FACS based assay for assessment of the effects of ion channel modulation on HRSV infection.

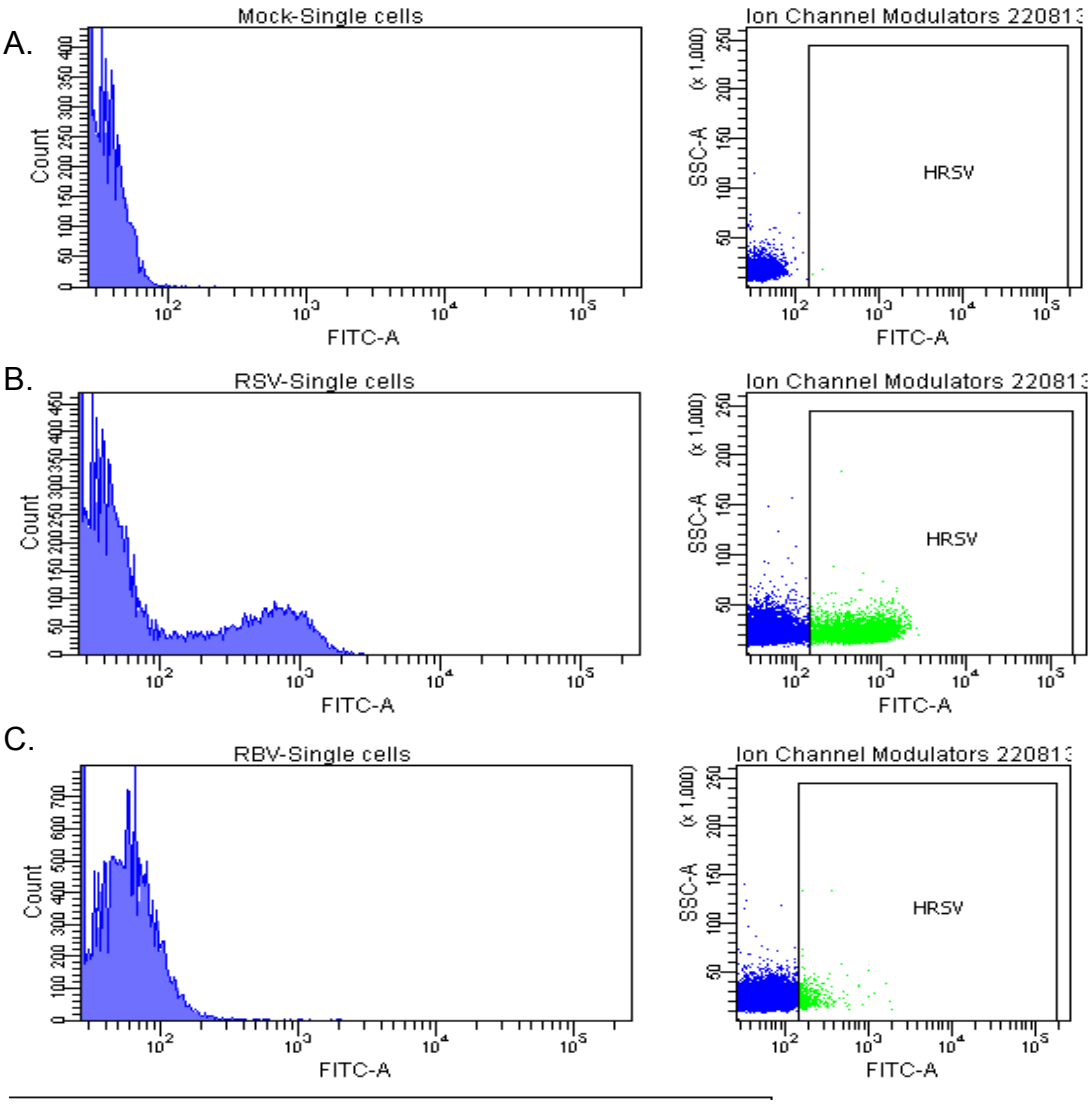

Figure 3. 9. Quantification of HRSV infection in A549 cells by FACS analysis.

Representative FACS plots from HRSV infected cells. A**.** Left panel represents the number of cells (y-axis) vs. FITC fluorescent intensity (x-axis). Right panel, shows a dot plot each representing single cell counts. Infected cells are represented by green dots indicating fluorescently labelled cells. Blue dots represent unlabelled cells. **B**. Charts of untreated HRSV infected cells. **C**. Charts of HRSV infected cells treated with 500 μM RBV.

3.4.1 K^+ channels and HRSV

Using the FACS based assay, cells were treated with each K^+ channel modulator after virus had been adsorbed onto cells in order to investigate their effects on HRSV processes that occurred post-virus attachment. When HRSV infection was performed in the presence of broad K^+ channel modulators including TEA, KCl, quinine, quinidine and $BaCl_2$, only TEA at high

concentrations (50 mM) reduced HRSV infectivity (Figure 3.10A, 68% reduction ± 32 p≤ 0.05) with minimal to no effects of the other K^+ channel modulators evident. When more specific K^+ channel modulators of individual channel families were investigated, no inhibition of HRSV infection occurred in comparison to no-drug controls (Figure 3.10). The values of infected cells treated with each K^+ channel drug were as follows, for the broad-spectrum K^+ channel modulators (Figure 3.10A); KCl = 86.6% ± 13.3, Quinine = 120.9% ± 20.9%, Quinidine = 104.6% ± 4.6%. For K_{ATP} channel modulators (Figure 3.10B); Glibenclamide = 111.8% ± 11.8, tolbutamide = 121% ± 21%, pinacidil = 139.8% ± 39.8%. For Kv channels (Figure 3.10C), 4-Aminopyridine (4-AP) = 82.8% ± 17.2%, chromanol 293B = 101.3% ± 1.3%, sotalol = 92.4% ± 7.6, Ergtoxin = 111% ± 11%, haloperidol = 76.7% ± 23.3%. For the K_{2P} channel modulators (Figure 3.10D): ruthenium red = 109.2% ± 9.2%, AEN = 84.6% ± 15.4%, anandamide = 106.8% ± 6.8%, haloperidol = 87.5% ± 12.5%. For the Ca^{2+}-activated K^+ channel modulators (Figure 3.10E): Tram-34 = 76.9% ± 23.1%, apamin = 112.9% ± 12.9. For Kir channel modulators (Figure 3.10F): $BaCl_2$ = 82.9% ± 17.1%, spermine = 70.8% ± 29.2%.

To authenticate the results of the inhibitor screen, the expression of HRSV proteins in the presence of TEA was assessed by western blot analysis (Figure 3.11A.). TEA at 50 mM was observed to reduce HRSV protein expression consistent with the FACS results (Figure 3.10A). However, at decreasing TEA concentrations of 5-10 mM, no effects on HRSV growth occurred with comparable HRSV protein expression to control cells observed (Figure 3.11 A and B). The lack of effects of TEA at these concentrations were confirmed by FACS analysis (Fig 3.11.B) with identical numbers of HRSV infected cells being recorded in the presence and absence of 5, 10 mM TEA. TEA is a non-selective K^+ channel blocker that generally inhibits K^+ channels at concentrations ranging from 2 mM-20 mM. Given the fact that these lower more K^+ channel specific concentrations of TEA did not influence HRSV infection coupled to the lack of effects of other K^+ channel modulators at concentrations that inhibit K^+ channel functionality, these data suggest that the effects of 50 mM TEA was most likely due to its off-target effects that include the inhibition of Cl^- channels and/or $Na^{+/}K^+$ exchangers (Siegl et al., 1984). Given this data, it was suggested that

the modulation of cellular K^+ channels does not influence HRSV growth under these conditions. Other cellular ion channel families were therefore investigated.

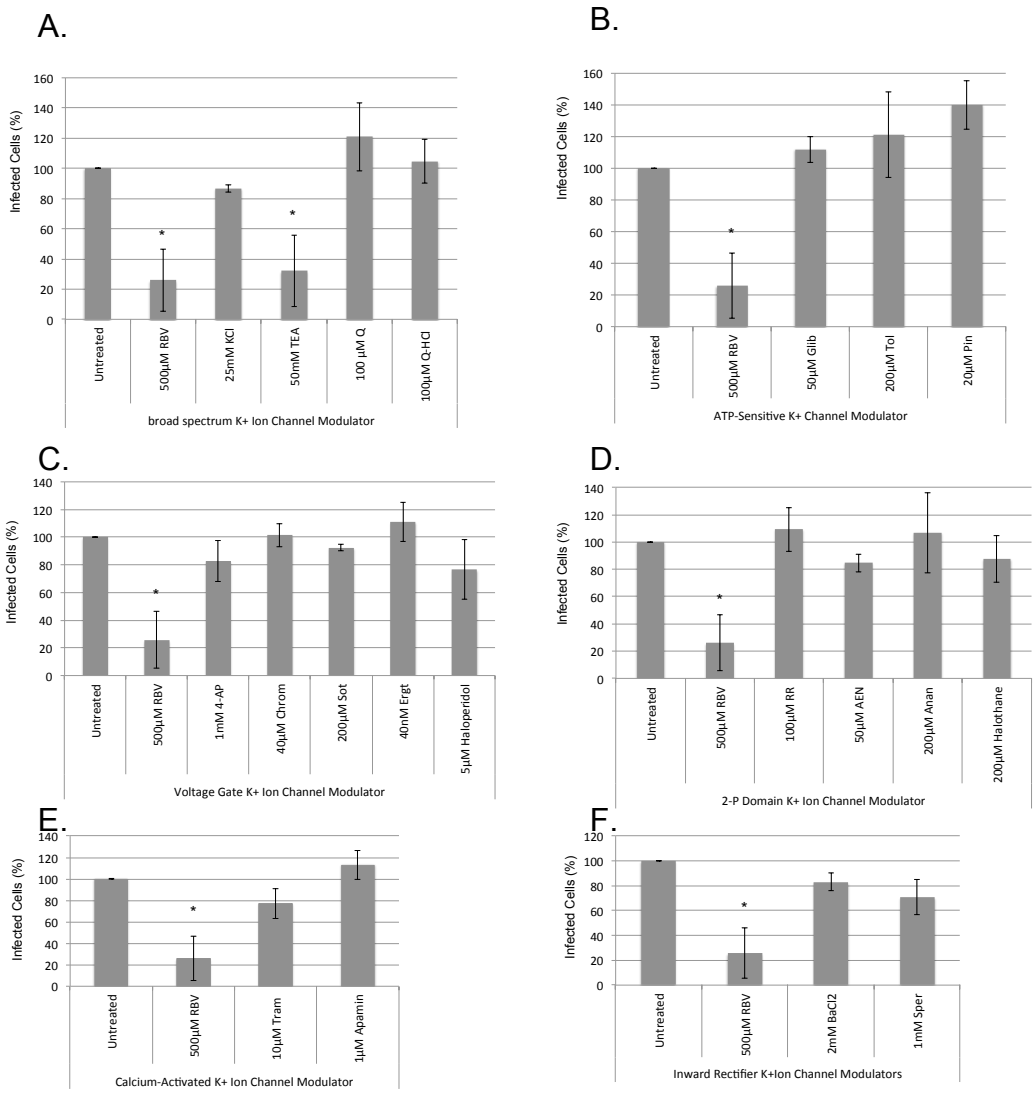

Figure 3. 10. Effects of K^+ channel modulation on HRSV A2 in A549 cells post-virus attachment/entry.

Cells were infected with HRSV MOI 1.0 and treated with the indicated K^+ channel modulators. Cells were fixed, permeabilised with 0.5% (v/v) Triton X-100 and labelled with goat anti-HRSV FITC conjugated antibodies. Percentages of infected cells were assessed by FACS analysis and normalized to no-drug infected controls. Cells were treated with 0.5 mM (v/v) RBV for assay validation. The K^+ channel families targeted included **A**. Broad spectrum. **B.** ATP-sensitive K^+ channels (K_{ATP}) modulators. **C**. Voltage gated (Kv) modulators. **D**. 2-P domain K^+ channels (K_{2P}) modulators. **E**. HRSV replication in A549 cells treated with Ca^{2+} activated K^+ ion channel modulators. **F**.

Inward rectifier K^+ channel (Kir) modulators. Data are expressed as mean ± SE (n=3). *Significant differences from untreated value p<0.05 level.

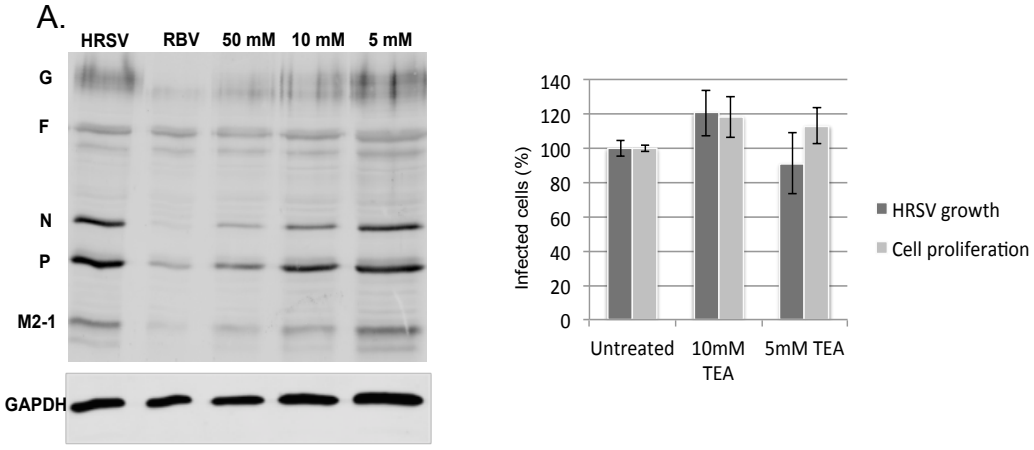

Figure 3. 11. TEA does not inhibit HRSV at concentrations that inhibit K^+ channel function.

A. Representative Western blot analysis of A549 cells infected with HRSV in the presence of TEA (at 50, 10 and 5 mM concentrations), and Ribavirin (RBV) 0.5 mM (v/v). Expression of GAPDH was examined as a loading control. Each lane was loaded with 5µg of cell lysate. **B.** The effect of TEA at 10 mM and 5 mM concentrations on HRSV A2 WT replication was examined by FACS analysis. In addition, an MTT assay was performed to determine cell viability when cells were treated with TEA at 10 mM and 5 mM concentrations. Data are expressed as mean ± SE (n=3). *Significant differences from untreated control p<0.05 level.

3.4.2 Na^+ channels and HRSV

In alveolar cells, a variety of Na^+ channels types are expressed. A panel of Na^+ channel modulating drugs were therefore assessed for their effects on HRSV infection (Figure 3.12). Interestingly, inhibitors of voltage gated Na^+ channels (NaV) enhanced HRSV growth as evidenced by 158% ± 58% increase in HRSV infection levels in the presence of tetrodotoxin (TTX), a broad spectrum NaV channel pore blocker, and Me5, a potent broad-spectrum Na^+ channel antagonist (150.9% ± 50.9% increase p≤ 0.05). These effects were confirmed by Western blot analysis were enhanced HRSV protein expression was observed in the presence of both TTX and Me5, suggesting that NaV channel inhibition by these compounds acted to promote HRSV activities. Amiloride, an inhibitor of numerous alveolar sodium channels including ENaC (epithelial Na^+ channels) did not recapitulate the effects of TTX or Me5 (Figure 3.12, Am = 87.2% ± 12.8) despite the fact that Na^+ diffuses passively into

alveolar cells primarily through amiloride-sensitive cation channels. In addition, lidocaine, which is an anaesthetic drug that blocks fast NaV channels had no significant effects on HRSV (Figure 3.12, Lidocaine = 125.3% ± 25.3%). Procainamide, another known NaV blocker (Figure 3.12, Pro = 122.3% ± 22.3) and α-pompilidotoxin, an activator of NaV channels also did not significantly affect HRSV infection (α-Pom = 98.8% ± 1.2%). Taken together these findings suggest that specific NaV members that are sensitive to TTX and Me5 modulation may promote HRSV infection when their activity is inhibited.

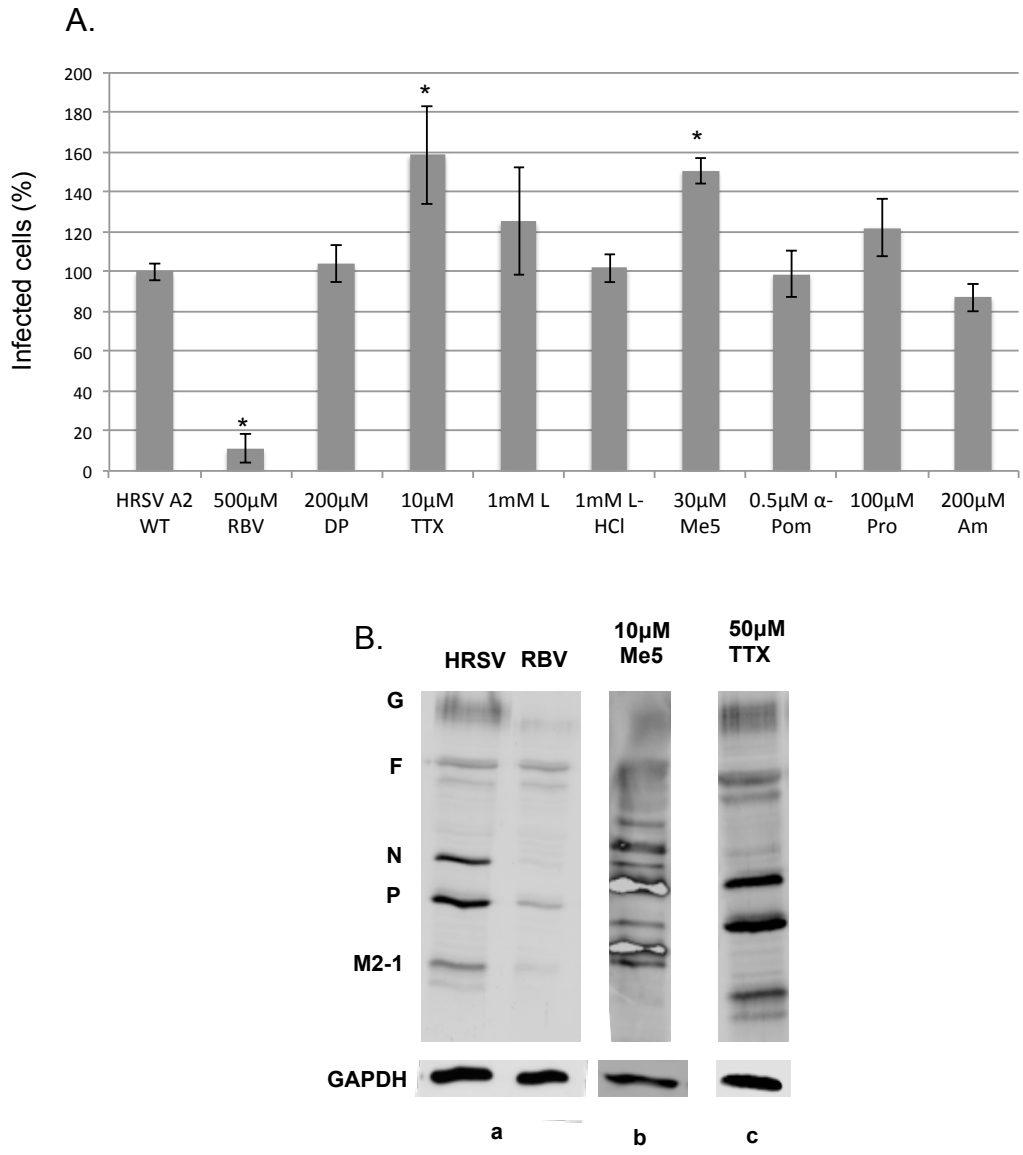

Figure 3. 12. Assessment of the effects of Na^+ channel modulation during the post-entry stages of HRSV A2 WT infection.

A. Effects of Na^+ channel modulators on HRSV in A549 cells assessed by FACS analysis. **B**. Representative Western blot analysis of cells infected with HRSV in the presence Na^+ channel modulators and RBV. Each lane was loaded with 5 µg of cell lysate and probed for GAPDH as a loading control (all WB bands are obtained from one gel). FACS data are expressed as mean ± SE (n=3). *Significant differences from untreated controls $p<0.05$ level.

3.4.3 Ca^{2+} channels and HRSV

Cell surface and intracellular Ca^{2+} channels regulate Ca^{2+} influx and thus play a critical role in many cellular Ca^{2+} dependent processes. Cytosolic Ca^{2+} is

regulated by many viruses including HIV, HCV, HBV and rotavirus (Choi et al., 2003; Hayashi et al., 2002; Michelangeli et al., 1995; Li et al., 2007) to adapt and create their own tailored cellular environment (Zhou et al., 2009). Upon assessment of the effects of Ca^{2+} channel modulation on HRSV infection, Nitrendipine reduced HRSV growth (Figure 3.13.A, 62.6% ± 37.4%). Nitrendipine is a dihydropyridine Ca^{2+} channel inhibitor, with specificity for long-lasting (L-type) channels. These data were confirmed by western blot analysis that demonstrated Nitrendipine reduced HRSV protein expression when compared to no-drug infected controls (Figure 3.13B). To confirm a reliance on L-type Ca^{2+} channels during HRSV infection, Nimodipine was assessed as an independent L-type Ca^{2+} blocker but did not decrease HRSV infection. This compound thus failed to recapitulate the HRSV inhibition observed during Nitrendipine treatment suggesting that L-type channel modulation does not contribute to HRSV growth and the anti-HRSV effects observed were Nitrendipine specific. These data were further confirmed using Bay 8644K (BayK); an L-type Ca^{2+} activator that did not influence HRSV infection (Figure 3.13B, 98.2% ± 1.8). Other voltage gated L and T (transient) type inhibitors namely verapamil, and niguldipine also did not influence HRSV growth with comparable levels of infected cells (Figure 3.13B, Verapamil = 129.3% ± 29.3%; Niguldipine = 91.5% ± 8.5%) to the no-drug controls observed. In addition, 2-Aminoethoxydiphenylborane (2APB), an inhibitor of intracellular TRP channels (Transient receptor potential channels that regulate Ca^{2+} and Mg^{2+} transport across intracellular membranes) also did not influence HRSV growth (Figure 3.13B, 2APB = 102.3% ± 2.3). Taken together these data suggest that, whilst nitrendipine displays anti-HRSV activity, voltage gated Ca^{2+} channels are not required during HRSV infection.

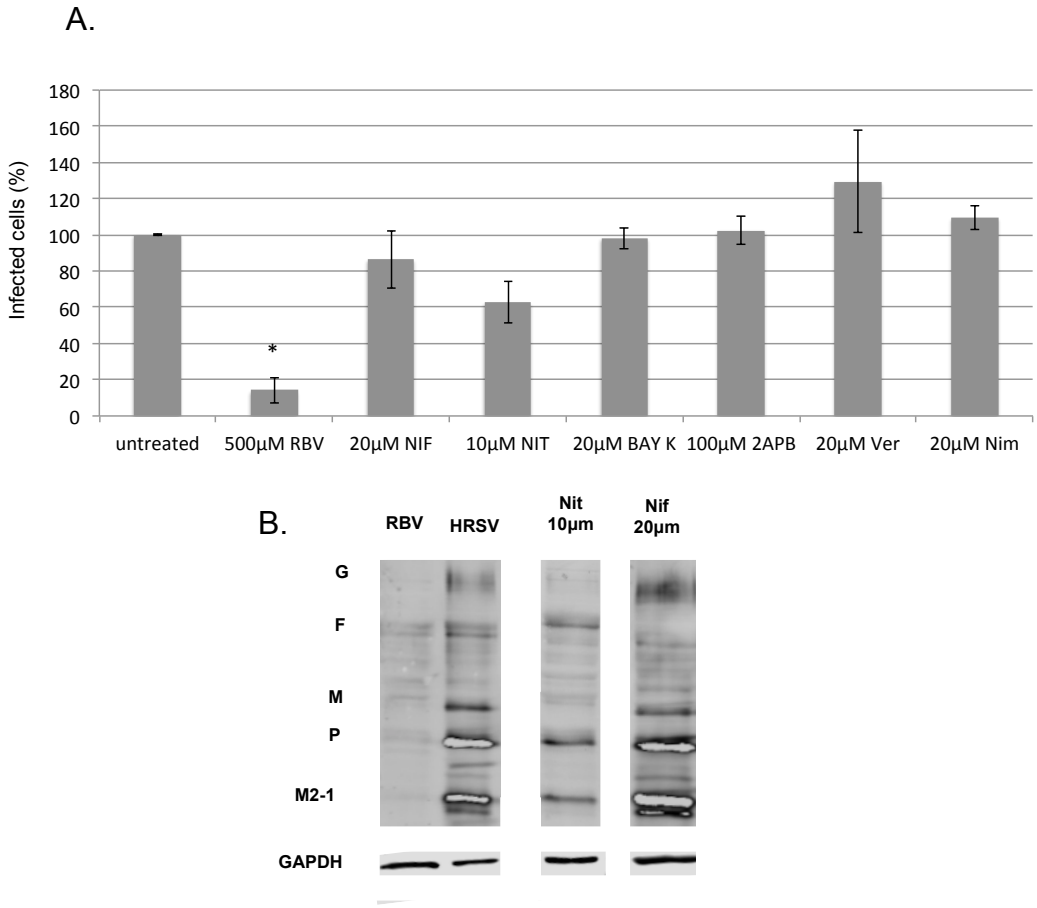

Figure 3. 13. Assessment of the effects of Ca^{2+} channel modulation during the post-entry stages of HRSV A2 WT infection.

A. The effect of Ca^{2+} channel drugs on HRSV replication in A549 cells by FACS analysis. **B**. Representative Western blot analysis of cells infected with HRSV in the presence of the indicated Ca^{2+} channel modulators. HRSV protein expression is reduced in RBV treated cells at a concentration of 0.5 mM (v/v). Each lane was loaded with 5 µg of cell lysates, and GAPDH was re-probed as a loading control (all WB bands are obtained from one gel). FACS data is expressed as mean ± SE (n=3). *Significant differences from untreated value $p<0.05$ level.

3.4.4 Cl^- channels and HRSV

Cl^- channels are absolutely required for cell volume control and apoptosis regulation (Okada and Maeno, 2001). Intracellularly, Cl^- transport across organelle membranes is involved in endosomal, lysosomal, and organelle function (Diciccio and Steinberg, 2011). Indeed, previous studies (Igloi et al., 2015) have shown that Cl^- channel inhibition can suppress HCV replication when added at late stages of the virus lifecycle. When the well-

characterized Cl^- channel blockers, 5-nitro-2-3-phenylpropylamino benzoic acid (NPPB), indyanyloxyacetic acid 94 (IAA-94), and diisothiocyanostilbene-2,20-disulfonic acid (DIDS) were assessed for their effects on HRSV infection, no significant differences from no-drug controls were observed (Figure 3.14, 87.3% ± 12.7; 95.6% ± 4.4%; 84.3% ± 15.7, p≤ 0.05, respectively). This data suggested that the post-entry modulation of Cl^- influx does not influence the HRSV life cycle in A549 cells.

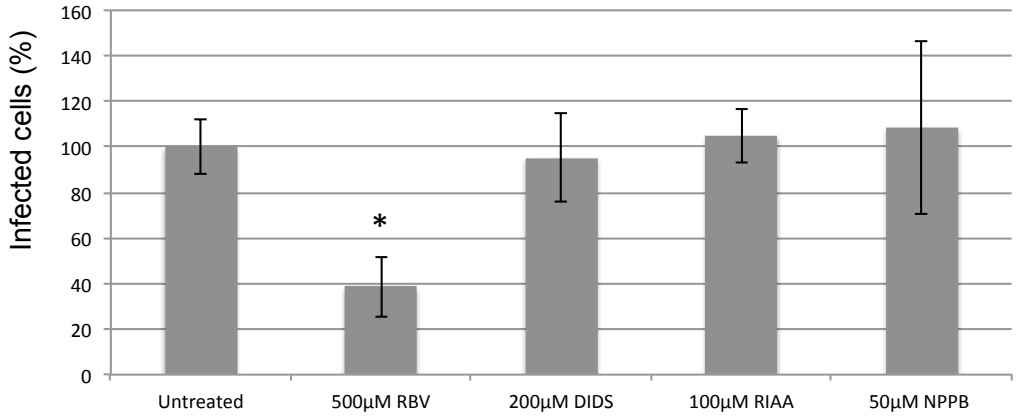

Figure 3. 14. Assessment of the effects of Cl^- channel modulation during the post-entry stages of HRSV A2 WT infection.

Effects of Cl^- drugs on HRSV in A549 cells by FACS analysis. FACS data is expressed as mean ± SE (n=3). *Significant differences from untreated values p<0.05 level.

3.5 Assessment of the effects of ion channel modulation on the early stages of the HRSV lifecycle

The results of the previous sections showed that modulation of the major ion channel families failed to identify key channel family members that influence the post entry stages of HRSV infection. It was reasoned that ion channel functionality may therefore be required for earlier virus events including membrane attachment, entry and trafficking of internalised virions through the vesicular transport network. To assess this possibility, A549 cells were directly infected with HRSV in the presence of each ion channel modulator, and virus production assessed by FACS analysis as outlined in Figure 3.15.

Figure 3.16 shows that the number of virus positive cells was lower in TEA treated cells at concentrations that would inhibit K^+ channel activity (5 mM and 10 mM), and the decreases were statistically significant compared to no-drug controls (at 5 mM, 53% cells infected; at 10 mM, 60% cells infected). Similarly, treatment with KCl showed that only 56.9% of cells were infected compared to no drug controls. Taken together, these findings suggest that these broad-spectrum K^+ channel drugs can influence the early stages of the HRSV replication cycle, such as events that include entry into host cells, rather than post entry stages. Interestingly, $BaCl_2$ an inhibitor of Kir channels also reduced the number of HRSV infected cells by 39.4% compared to no drug controls, ($p \leq 0.05$) suggesting that a $BaCl_2$ sensitive channel influences early events in the virus replication cycle but is not required for post entry events. Other drugs that did not show any significant changes on HRSV included the K_{ATP} channel modulators (Figure 3.16; Tol = 88.3 ± 11.7%; Glib = 75.7% ± 24.3%), the K_{2P} channel modulators (Figure 3.16, RR = 74.2% ± 25.8%, Hal = 63.9% ± 36.1), Kv channel modulators (Figure 3.16, 4-AP = 73.9 ± 26.1%; Chrom = 70.8% ± 29.2%; Sot = 87.6% ±12.4%) and Ca^{2+}-activated K^+ channel modulators (Figure 3.16, Apamin = 68.3% ± 31.7%).

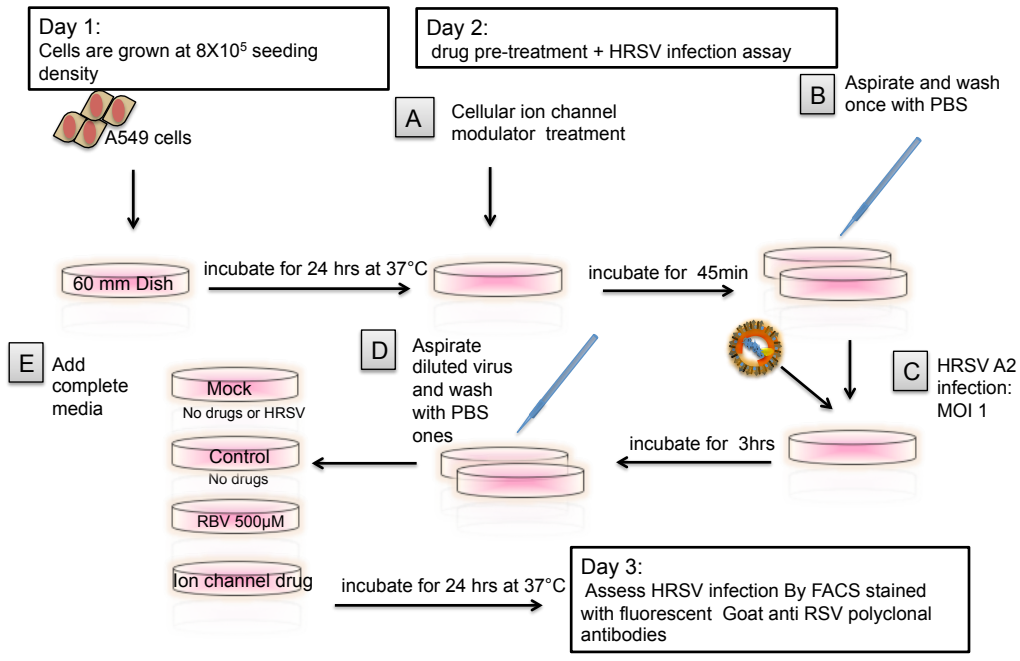

Figure 3. 15. Schematic representing how ion channel modulation was assessed at the early stages of HRSV infection.

Ion channel drugs were included prior to and during HRSV infection. HRSV infection levels were assessed by FACS analysis as described above.

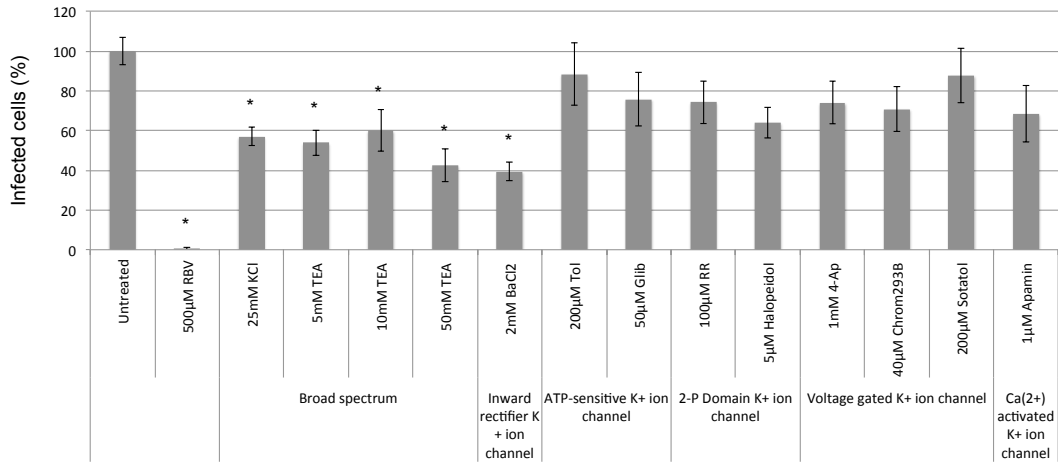

Figure 3. 16. Effects of K^+ channel modulation during the early HRSV stages.

Percentages of infected cells were assessed by FACS assay and normalized to untreated controls. Cells were also treated with 0.5mM (v/v) RBV. Data are expressed as mean ± SE (n=3). *Significant differences from untreated value ($p<0.05$).

When cells were pre-treated with the Na^+ ion channel modulators (TTX and lidocaine) during HRSV infection, similar percentages of infected cells to no-drug controls were observed (Figure 3.17A, lidocaine = 85.6% ± 14.4%; TTX = 124% ± 24%). Similarly, Ca^{2+} channel modulators (Figure 3.17B, Nifedipine = 104.1% ± 4.1%; verapamil = 138.1% ± 38.1%, and BayK = 74.2% ± 25.8%) did not significantly influence HRSV infection. This data suggested that Na^+ and Ca^{2+} channel modulation does not influence the early stages of the HRSV lifecycle.

When Cl^- channel modulators were assessed, NPPB displayed no discernable effects on HRSV infection (Figure 3.17C, NPPB = 101.5% ± 1.5% increase, $p \leq 0.05$), but the broad spectrum anion channel inhibitor DIDS significantly reduced the number of HRSV infected cells (Figure 3.17C, 6.5% ± 93.5% reduction, $p \leq 0.05$). These data were strongly suggestive of a requirement for DIDS sensitive Cl^- channels during HRSV attachment/early viral processes,

since treatment with DIDS during the later stages of virus replication did not influence HRSV infection (Figure 3.14). To further confirm the effects of DIDS when added during the early stages of HRSV infection, viral protein expression in the cells was assessed by Western blot analysis (figure 3.18). KCl and $BaCl_2$ were also included in these assays since both showed an inhibitory effect during the early stages of the HRSV lifecycle, although to a lesser extent than for DIDS. When lysates were assessed, all three inhibitors resulted in reduced HRSV protein expression, consistent with reduced virus entry. The relative reduction in protein expression correlated with the reduced number of cells infected, as shown in Figure 3.16, with DIDS showing the greatest reduction in protein expression, and KCl showing the least (Figure 3.18). These data confirmed that KCl, $BaCl_2$ and DIDS act during the early stages of HRSV infection to inhibit HRSV activities.

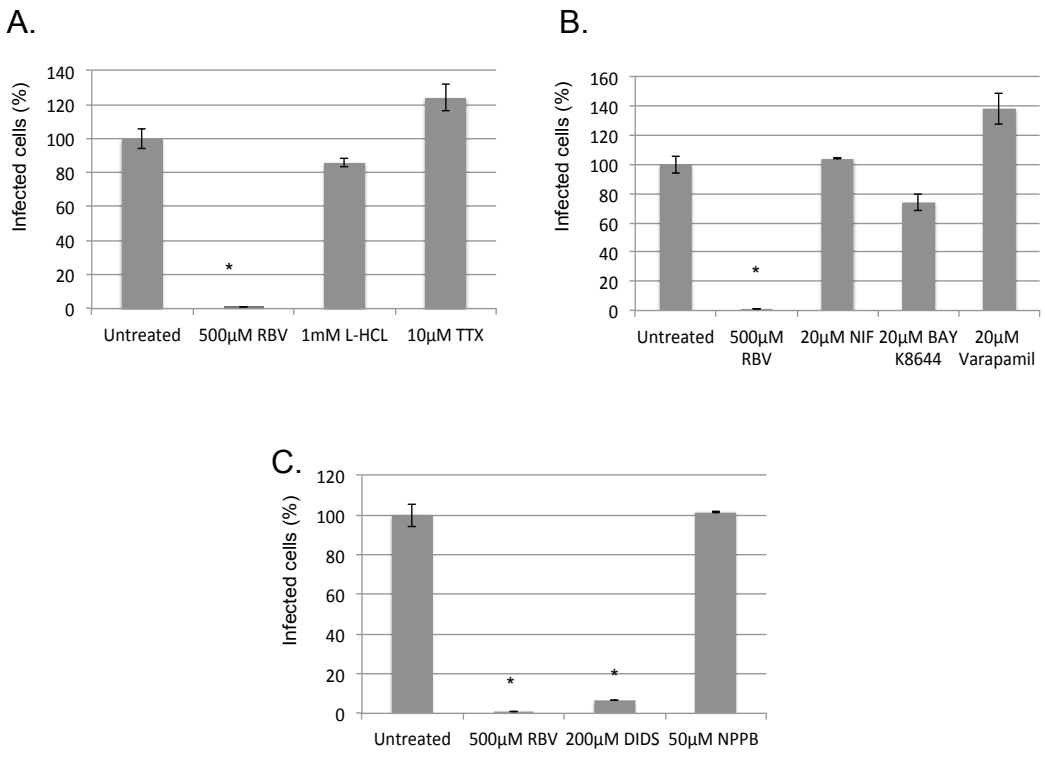

Figure 3. 17. Assessment of the effects of ion channel modulation during the entry stages of HRSV A2 WT infection.

The effect of various classes of ion channel modulating drugs when added early during the HRSV lifecycle **A**. Shows the effects of Na^+ channel specific drugs, **B**. Ca^{2+} channel specific drugs. **C.** Cl^- channel specific drugs. Data are expressed as mean ± SE (n=3). *Significant differences from untreated controls $p<0.05$ level.

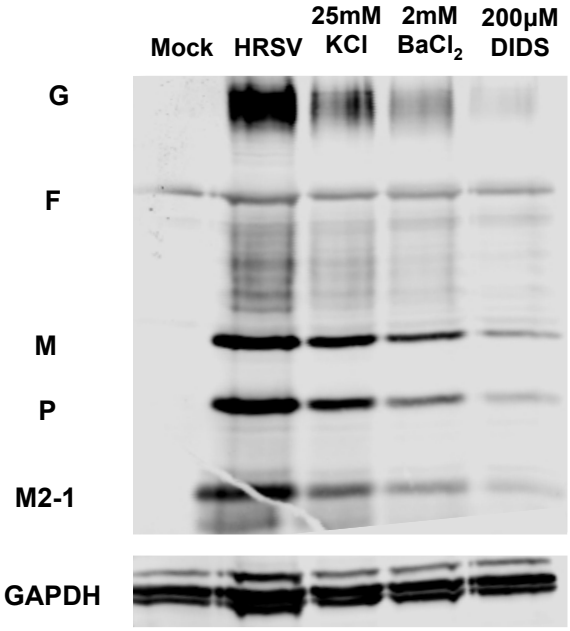

Figure 3. 18. Comparative assessment of Cl^- channel modulators at the early stages of HRSV A2 WT infection in A549 cells.

Representative Western blot analysis of cells infected with HRSV A2 WT in the presence KCl, $BaCl_2$ and DIDS. HRSV protein expression was detected using HRSV polyclonal serum. GAPDH was re-probed as loading control. Each lane was loaded with 5 µg of lysate. Lane 1 (Mock), neither drug-treated nor infected. Lane 2, (HRSV) infected with HRSV, but no-drug added. Lane 3 (KCl) infected cells were treated with KCl, Lane 4 ($BaCl_2$) infected cells treated with 2 mM $BaCl_2$, Lane 5 (DIDS) infected cells treated with 200 µM DIDS.

3.5.1 DIDS and $BaCl_2$ inhibit HRSV entry

To further validate the effects of both $BaCl_2$ and DIDS on HRSV growth, HRSV attachment/entry was assessed in the presence of these compounds. HRSV can enter host cells either by endocytosis (including macropinocytosis and clathrin-mediated endocytosis) or by fusing of the viral envelope directly to the plasma membrane (Krzyzaniak et al., 2013). To assess HRSV entry, DIDS and $BaCl_2$ were added only during the initial 3 hours of HRSV attachment/entry. Cells were then washed, surface attached viruses were removed via the addition of 0.5% trypsin in the wash buffer, and infection allowed to proceed in the absence of these compounds for 24 hours. If entry were blocked, upon removal of the virus/drug an inhibition of later virus processes 24 hours post-infection would be observed as assessed by both western blot and

immunofluorescence analysis of infected cells. To further validate the assays, we included monensin and chlorpromazine (CPZ); inhibitors of clathrin mediated endocytosis, and amiloride, known to abrogate the Na^+/H^+ exchangers required for macropinocytosis.

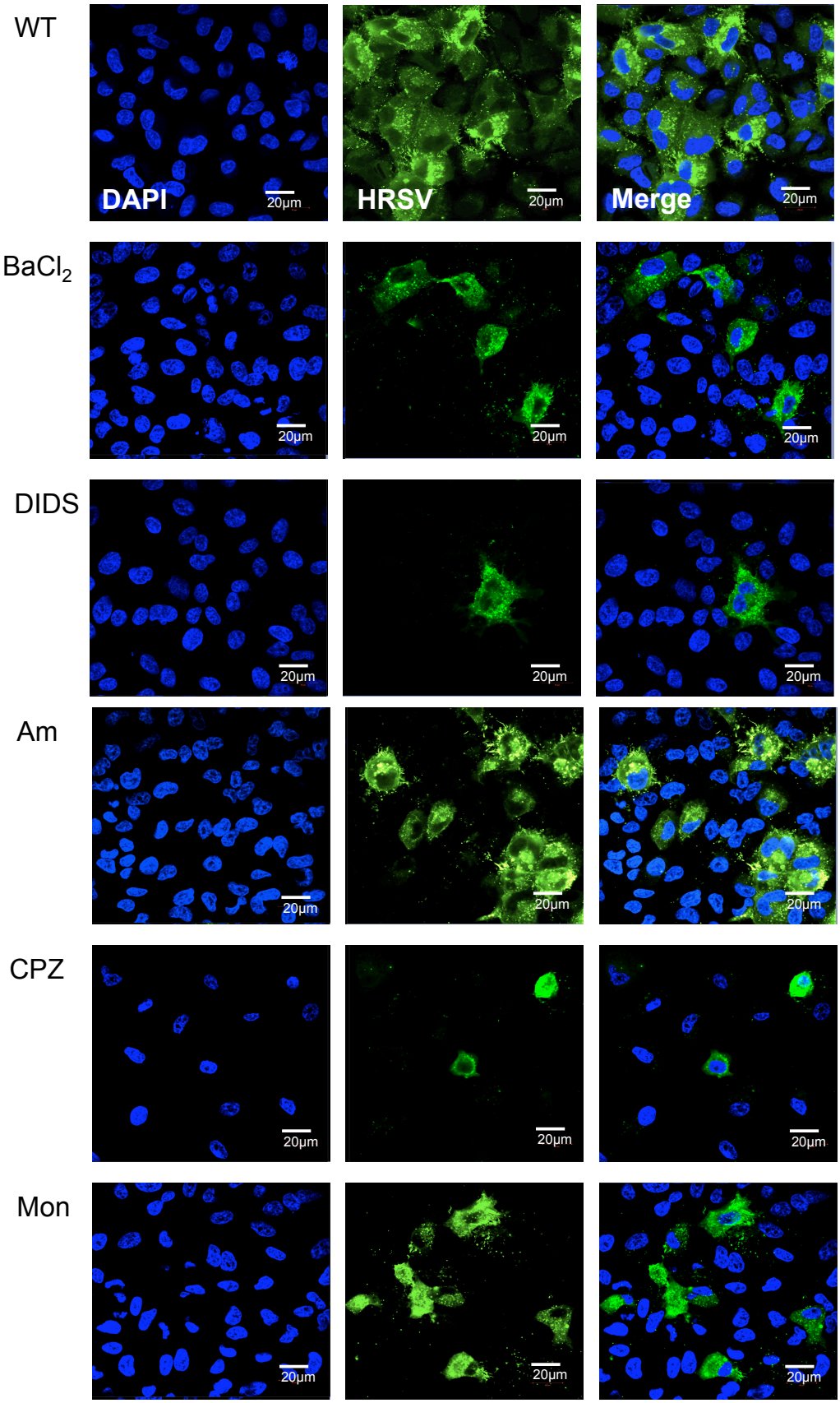

Figure 3. 19. Representative immunofluorescence images from HRSV entry assays in A549 cells.

Cells were pre-treated with the indicated drugs and infected with HRSV at an MOI of 1.0. Cells were labelled with FITC conjugated anti-HRSV antibodies (green) and the nucleus stained with DAPI. Drug concentrations were as follows; $BaCl_2$ 2 mM; DIDS 200 µM; Am 200 µM; CPZ 30 µM; and Monensin 20 µM. Images were taken using an upright LSM 510 META Axioplan microscope. Scale bar = 20µm.

As illustrated in Figure 3.19, the number of infected cells when treated with $BaCl_2$ during the entry chase were significantly lower than no-drug HRSV infected cells, as observed by both reduced HRSV fluorescence and the number of infected cells. These effects were more apparent when DIDS was assessed, with the number of infected cells almost completely abolished compared to untreated controls. Surprisingly, only a very modest reduction was observed following the addition of amiloride in the entry chase. Amiloride is a known inhibitor of macropinocytosis (Kolokoltsov et al., 2007a) previously identified as the major route of HRSV entry in HeLa and A549 cells (Kolokoltsov et al., 2007a). Treatment with CPZ, known to inhibit the assembly of clathrin lattices leading to an inhibition of clathrin mediated endocytosis (CME), led to drastically reduced numbers of HRSV-positive cells in comparison to untreated controls (Figure 3.19). Monensin also led to a small but moderate decrease in the percentage of HRSV positive cells further suggesting that HRSV uses CME to enter A549 cells. Western blot analysis (Figure 3.20) confirmed these findings; DIDS/$BaCl_2$ treatment reduced HRSV protein expression following their inclusion during virus entry, confirming that Kir and Cl^- channel activity is required. Lysates from cells pre-treated with either CPZ or Monensin also correlated with the IF data, as both compounds caused a reduction in HRSV band intensity when compared to untreated controls. Figure 3.20 also shows that amiloride caused a minimal reduction in HRSV protein expression when included during virus entry, confirming this compound to have a minimal influence on HRSV attachment/entry.

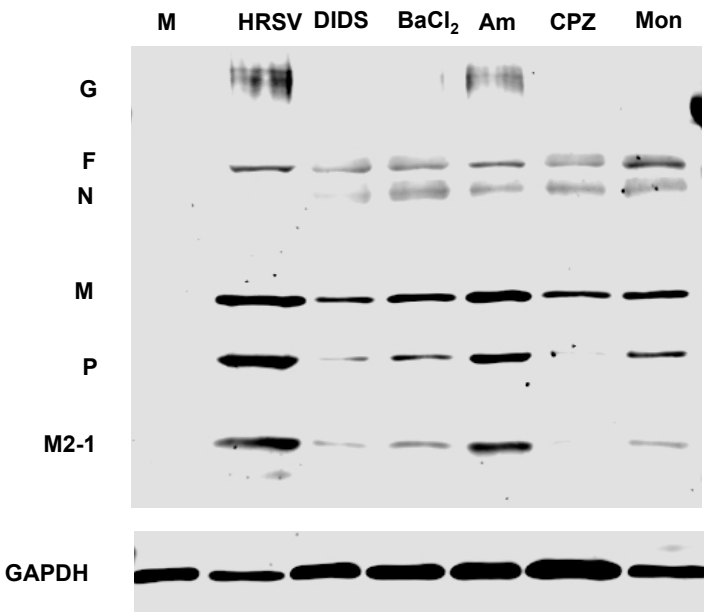

Figure 3. 20. **Representative western blot showing the expression of HRSV proteins following the addition of Cl^- channel blocking compounds and inhibitors of cellular entry pathways**.

Infected cell lysates were assessed by western blot analysis using an anti-HRSV polyclonal sera. Each lane was loaded with 5µg of protein content, with GAPDH detected by re-probing the blot as a loading control. Lane loadings were as follows: Lane 1, (M) mock-infected cells that were untreated; Lane 2 (HRSV) infected cells that were drug-untreated. Lane 3, (DIDS) HRSV infected cells treated with 200 µM of DIDS. Lane 5, ($BaCl_2$) HRSV infected cells treated with 2 mM of $BaCl_2$. Lane 5, (Am) HRSV infected cells treated with 200 µM Am, macropinocytosis blocker. Lane 6, (CPZ) HRSV infected cells treated with 30 µM of CPZ, an inhibitor to CME. Lane 7, (Mon) HRSV infected cells treated with 20 µM of Mon, also an inhibitor CME.

3.5.2 DIDS is not a global inhibitor of endocytosis in A549 cells

Given the potent effects of DIDS on HRSV entry, we sought to confirm it was an HRSV specific effect, and not due to a global inhibition of cellular endocytic processes. The signalling output from the epidermal growth factor (EGF) receptor controls many important biological processes including cell differentiation, migration, proliferation and survival. EGFR signalling is known to be intrinsically controlled by EGFR endocytosis, the routes of which have been dissected in great detail in numerous biological studies (Vieira et al., 1996; Burke et al., 2001). When added to cells, EGF binds EGFR at the cell surface. EGFR then dimerises and is internalised by CME, delivered to early endosomes and then late endosomal compartments, and subsequently degraded in the lysosomes (Dikic, 2003). As such, EGF internalisation is now the gold standard for the analysis of any cellular or viral proteins that may co-opt this route during

endocytosis. Labelled-EGF was pulsed into live cells for 30 minutes in the presence and absence of DIDS. Cells were then fixed and assessed by confocal microscopy. The appearance of internalised puncta in cells is indicative of their ability to internalise labelled EGF ligand suggesting CME to be active and unaffected by drug treatment. It was observed that DIDS treated cells did not inhibit CME processes since clear internalized EGF positive vesicles were present in EGF treated cells. However, EGF appeared to display an altered intracellular distribution; whilst untreated cells displayed small and dispersed puncta, DIDS treatment resulted in the accumulation of larger and accumulated intracellular puncta. Whilst the reasons for this are unclear, these data are suggestive that DIDS may influence the post-entry trafficking of EGFR in A549 cells. However since EGF was still internalized into DIDS treated cells, a global inhibition of endocytic uptake could not explain the DIDS effects observed on HRSV, suggesting that DIDS acts to specifically inhibit an HRSV dependent entry process during infection.

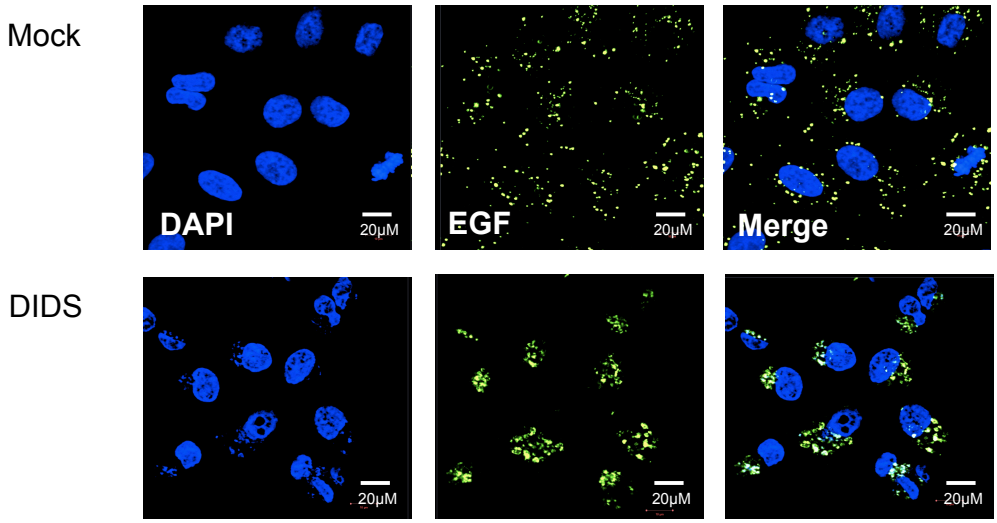

Figure 3. 21. Assessment of the effects of DIDS on cellular endocytic trafficking.

A549 cells were treated with DIDS (200μM) and the endocytosis of EGF was assessed through pulsing fluorescently labeled EGF-488 into cells for 30 mins at 37°C (shown in green), after which cells were fixed and cell nuclei were stained with DAPI. Images were taken using an LSM700 Zeiss META inverted microscope. Scale bar = 20μm.

3.5.3 HRSV alters Cl^- transport during the early stages of virus infection

Given the ability of DIDS to inhibit HRSV entry, it was reasoned that HRSV might alter Cl^- channel function during the early (DIDS sensitive) stages of infection. Cellular Cl^- influx/efflux can be measured using ethoxycarbonylmethyl-6-methoxy-quinolinium bromide (MQAE), a Cl^-indicator that is quenched by enhanced Cl^- concentrations. Thus, a decrease in MQAE fluorescence indicates that intracellular Cl^- concentrations are increased.

Cl^- homeostasis was measured in A549 cells infected with HRSV at an MOI of 1.0 and MQAE fluorescence measured using the IncuCyte apparatus at 1-hour intervals for up to six hours. The cellular concentration of Cl^- is proportional to the mean intensity of green fluorescence GCU (Green Calibration Unit/cell). Live images were taken from several wide field images. Figure 3.22 shows that HRSV infection led to a time-dependent reduction in fluorescence intensity indicating that the intracellular concentration of Cl^- is enhanced during early HRSV processes. This suggests that HRSV quenched Cl^- influx consistent with the previous finding that DIDS displays anti-HRSV activity, possibly through block blocking this event. Taken together, these data suggest that Cl^- influx is a crucial pre-requisite required for early HRSV processes. similar experiment suggested to be repeated with DIDS modulator to observe the effect of DIDS of Cl^- consumution during HRSV infection.

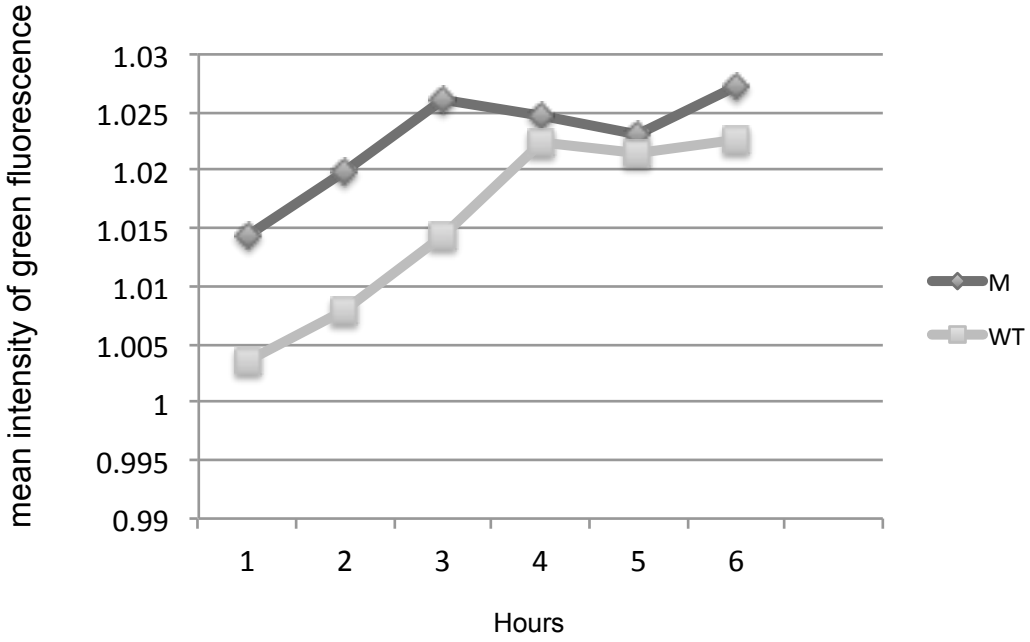

Figure 3. 22. Assessment of Cl^- channel activity during the early stages of HRSV infection.

A549 were treated with 5 mM of MQAE for 1 hr and infected with HRSV (MOI 1.0 of HRSV A2 WT) for the indicated time points. Mock represents the resting A549 intracellular [Cl^-]. MQAE intensity was measured through the assessment of the green fluorescent intensity (average of GCU/well) measured using IncuCyte ZOOM live cell imaging. Values represent 6 hours post infection time points (n=3).

3.6 Discussion and summary

In this chapter, HRSV infection assays were performed in the presence of a variety of ion channel modulators, used at pharmacologically relevant concentrations. The data presented in this chapter showed that cellular ion channel blockers specific for K^+ channels did not affect HRSV growth or viral protein expression when added 3 hpi suggesting K^+ activity is not required during the later stages of the HRSV infection cycle (Figure 3.10). TEA a non-selective K^+ channel inhibitor inhibited HRSV growth at concentrations ≥ 50 mM, but not at concentrations ranging from 5-10 mM (Figure 3.11). Although 50 mM leads to non-K^+ channel selective effects of TEA, it was non-toxic to A549 cells. When the effects of K^+ channel modulation were assessed when the K^+ channel compounds were added during HRSV attachment/entry, TEA, KCl and $BaCl_2$ displayed small but inhibitory effects on HRSV infection (Figure 3.16). KCl collapses K^+ gradients and suppresses K^+ channel activity, while $BaCl_2$ is a

specific inhibitor of Kir channels. These data were suggestive that HRSV is influenced by the function of Kir channel activity during the early stages of the virus life cycle in A549 cells. This is consistent with other negative sense RNA viruses including Bunyamwera virus (BUNV) that has been shown to require K^+ channel activity during early post-entry stages of infection(Hover et al., 2015). TEA almost completely inhibited BUNV at a concentrations ≥ 2 mM, which represent significantly lower concentrations than those inhibitory to HRSV (TEA used at 50mM, 10 mM and 5 mM). In addition, BUNV was insensitive to the early addition of $BaCl_2$ whilst this compound inhibited HRSV. The ability of BUNV to multiply in the presence of TEA drug was tested in different cell lines (derived from insects and other mammalian hosts) and all gave similar effects that suggested the requirement of K^+ channels during BUNV infection was not restricted to a specific cell line. Similar effects were observed for cells treated with KCl at concentrations of 30 mM and above (Hover et al., 2015). Similarly, Hazara virus (HAZV), a member of the *Nairovirus* genus that is closely related to the lethal pathogenic virus Crimean-Congo hemorrhagic fever virus (CCHFV) (Dowall et al., 2012) was inhibited by TEA concentrations ≥ 2 mM (Hover et al., 2015). On the other hand, hepatitis C virus (HCV) entry or replication were not affected by either TEA or KCl (Igloi et al., 2015). The findings here suggested that Kir channels are the K^+ channel family mediating the effects on HRSV since Kir channels are sensitive to modulation by KCl, TEA, and $BaCl_2$ (Figure 3.16). $BaCl_2$ represents the most specific inhibitor of Kir channels of these three compounds.

The inhibition of voltage gated Na^+ channels with TTX at the post entry stages of virus infection enhanced HRSV levels, suggesting Na^+ channel inhibition acted to promote HRSV activities (Figure 3.12). Blocking Na^+ channels prior to infection however, did not influence HRSV infection. This fact could be connected to a previous study that found HRSV inhibited Na^+ absorption of the apical membrane and at the tracheal epithelium of mice (Kunzelmann et al., 2007). Thus the inhibition of Na^+ transport may help HRSV to adapt and replicate in host cells.

Host cell Ca^{2+} homeostasis has been shown to be interrupted by some viruses such as HIV-1 and rotavirus (RV) (Zhou et al., 2009). However, in the case of

HRSV, inhibiting or activating Ca^{2+} channels did not affect HRSV either during the initial stages of infection, or when added 3 hpi during the later stages of the virus life cycle. This is in contrast with Ebola virus (another negative sense RNA virus), that requires two pore domain Ca^{2+} channels (TPCs) to be released from endosomal vesicles during virus entry (Sakurai et al., 2015b). Of the Ca^{2+} channel modulators assessed in this study, nitrendipine showed an inhibitory effect on HRSV. However since the other panel of Ca^{2+} channel modulators assessed did not recapitulate the nitrendipine effect, it was deemed to be drug specific and not mediated through the modulation of L or T-type Ca^{2+} channels.

Finally, when modulators of Cl^- channels were assessed for their effects on HRSV, DIDS was found to be inhibitory when added early during virus infection (Figure 3.17C). It was further shown that DIDS did not influence HRSV when added 3 hpi suggesting its inhibitory effects are restricted to HRSV entry processes (Figure 3.14). This was confirmed when HRSV entry was specifically assessed in the presence of DIDS, the ability of HRSV to infect cells was impaired when DIDS was included only during the attachment/entry phase, then removed (Figure 3.19 and 3.20). This assay also suggested that CME was the primary route of HRSV entry in A549 cells as it was blocked by the CME inhibitors Monensin and CPZ. Importantly DIDS, whilst effecting EGF distribution during cell entry, did not block EGFR endocytosis (Figure 3.21) suggesting that DIDS does not cause a global block to cellular uptake and its effects on HRSV are likely to be virus specific. An interesting finding was that these effects were not recapitulated by a second Cl^- blocker NPPB suggesting two possible scenarios (1) the effects were DIDS specific and not mediated through Cl^- channels, (2) HRSV entry requires Cl^- channels that are sensitive to DIDS but insensitive to NPPB, many of which have been described. The latter scenario was deemed likely since HRSV was found to enhance Cl^- influx most likely through Cl^- channel activation (Figure 3.22), during virus attachment and entry (0-6 hpi). Interestingly this differs from BUNV that did not influence cell surface Cl^- influx during virus infection in A549 cells (Hover et al., 2015) again suggesting differences in ion channel modulator sensitivity between these two viruses.

In summary, it was found that blocking cellular Na^+ channels during the post entry stages of the HRSV life cycle can enhance HRSV infection most likely through enhancing virus replication. It was further shown that blocking DIDS sensitive Cl^- channels or Kir channels impedes HRSV entry. HRSV was also found to enhance Cl^- influx into cells consistent with its dependence on Cl^- channel function during its entry stages. This is the first to demonstration of a role of specific ion channel families in the HRSV lifecycle and highlights ion channel modulation as a potential future drug target in the design of much needed HRSV therapies. Many of these drugs are used clinically used to human such as; glibenclamide (ant-diabetic drug), haloperidol (hyperactive medication), sotalol (cardiac arrhythimias), tetraethylammonium (hypertension), amiloride (hypertension), lidocaine (treat ventricular tachycardia), nifedipine and verapamil (high blood pressure).

Chapter 4:

Investigating the role of the viroporin SH during HRSV infection

Chapter 4: Investigating the role of the viroporin SH during HRSV infection.

4.1 Introduction

Ion channels are multi component structures that allow passage of ions across cellular membranes, including the plasma membrane and intracellular organelles. Through controlling ion movement, ion channels are responsible for many essential cellular processes such as the transmission of nerve impulses, muscle contraction and the control of mucus and fluids level in the respiratory system (Hollenhorst et al., 2011). Many viruses including hepatitis C virus (HCV), influenza A virus (IAV) and HRSV (SH) encode small hydrophobic proteins termed viroporins that display ion channel activity. Whilst in most cases, viroporins are not fundamental for virus replication, their presence is known to promote viral growth and spread. Viroporins interact with different host-membranes and can self-assemble forming pore like structures that conduct cellular ions across those membranes. They function in many cellular processes that are important for enhancing virus replication via adapting the host cell to the requirements of the virus. As such they act as virulence factors that often enhance the pathogenicity of a particular virus through enabling a critical virus activity such as virus assembly and release as in the case for both the HCV P7 and M2 IAV proteins (Nieto-Torres et al., 2015). HRSV-SH is a viroporin that has non selective catatonic activity (Gan et al., 2012) and is thought to be primarily distributed within the Golgi complex and endoplasmic reticulum in infected cells (Rixon et al., 2004). Through its viroporin activity, HRSV-SH is thought to play a role in delaying apoptosis of infected host cells, through dampening inflammatory responses including caspase-8 (Li et al., 2015; Fung et al., 2015). However, the role of HRSV-SH during virus infection has not been fully defined. This chapter describes experiments that investigate the role of HRSV-SH during virus infection. The chapter attempts to examine

the relationship between cellular ion homeostasis and HRSV-SH by screening ion channel modulators in cells infected with either wild type (WT) or mutant HRSV viruses in which the SH gene has been deleted (HRSV ΔSH and HRSV ΔSH eGFP), and analysing their effects on the virus lifecycle. This study aimed to reveal if the presence of the HRSV-SH protein dictates HRSV sensitivity to cellular ion channel modulation. The functional effects of HRSV-SH are further investigated through comparison of the global cellular proteomic changes in A549 cells infected with WT and HRSV ΔSH viruses.

4.2 Optimisation of HRSV (rA2, ΔSH and ΔSH eGFP) infection in A549 cells

4.2.1 Recombinant HRSV growth curve

HRSV rA2 was generated in 1998 as a recombinant infectious strain of HRSV synthesised from cDNA (Jin et al., 1998). It resembles the commonly used laboratory A2 strain of HRSV, but also contains silent (non-coding) genetic markers that distinguish it from the non-recombinant HRSV A2. The HRSV ΔSH strain was produced by deleting the SH gene and the associated control sequences (HRSV rA2 ΔSH; Bukreyev et al., 1997). A second ΔSH virus was also generated in which the SH ORF was replaced with the ORF for eGFP (HRSV rA2 ΔSH eGFP). All viruses are depicted in Figure 4.1.

Recombinant HRSV (HRSV rA2, HRSV ΔSH and HRSV ΔSH eGFP) viruses were originally grown in Vero cells and passaged 3 times in HEp-2 cells prior to virus purification. These steps were necessary as HRSV growth in Vero cells leads to virus attenuation and poor yields due to truncation of the HRSV-G protein (Kwilas et al., 2009). Recombinant viruses were infected at an MOI of 0.1 for 5 days and virus supernatants collected for sucrose gradient purification as described in Materials and Methods Section 2.2.3.

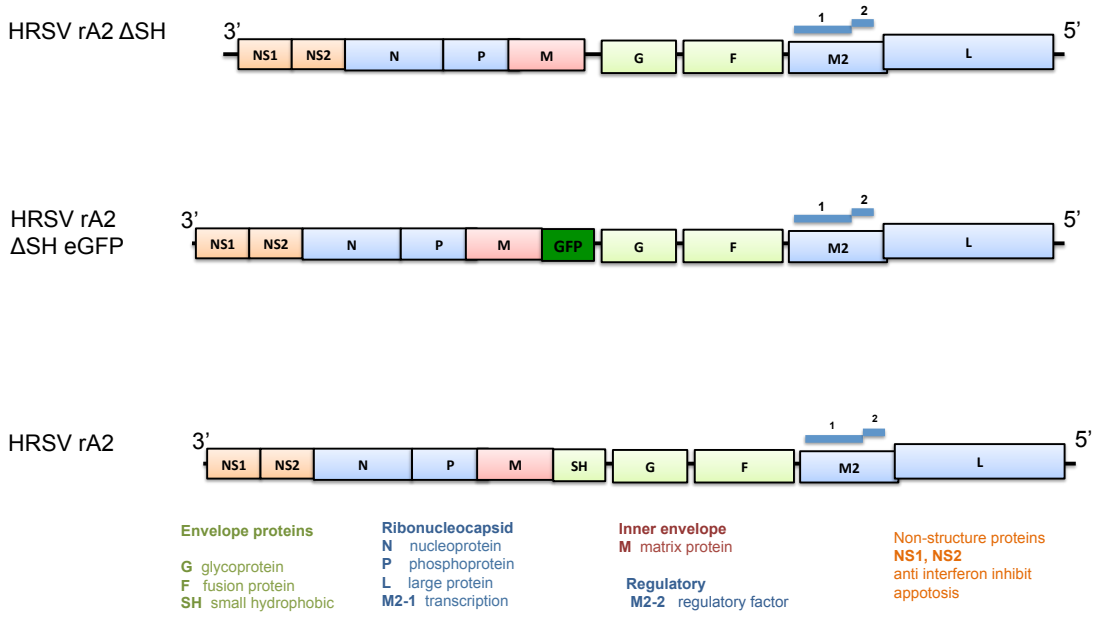

Figure 4. 1. Genome maps of the recombinant HRSV A2 strains used to investigate the role of HRSV-SH during the study.

To assess the ability of the engineered viruses to replicate in cell culture, multistep growth curves were generated in A549 cells, infected with each purified recombinant virus at an MOI of 1.0 for the indicated time points. Cells were then fixed and stained with polyclonal anti-HRSV proteins by indirect immunofluorescence analysis (as described in Chapter 2, section 2.2.4) and supernatants purified for the assessment of virus titres using plaque assays as described in Chapter 2, section 2.2.2.4.

Figure 4.2 shows IF images of A549 cells infected with HRSV rA2 at an MOI of 1.0 and incubated at different time points, namely 2, 3, 4, 6, 12, 24, 48 and 72 hpi. Punctate HRSV staining was evident as early as 2 hpi, which increased in intensity at 6 hpi (Figure 4.2). The HRSV staining pattern was punctate as these time points most likely representing captured virions that were cell surface bound, as well as some internalised HRSV virions during the early stages of virus infection. When HRSV staining was assessed 12 hpi, a more intense and diffuse staining pattern was evident most likely as a result of virus gene expression and the translation of new viral proteins. By 24 hpi, all stained cells displayed this staining pattern and by 48 hpi the peak infection levels had been reached and the majority of cells were infected. To confirm these observations,

growth curves following HRSV rA2 infection were performed and virus titres at the indicated time points assessed by plaque assay. Figure 4.3 shows that HRSV rA2 production was detectable at 4 hpi ($1x10^4$ PFU/ml) and increased up to 72 hpi ($2.5x10^6$ PFU/ml). A modest increase of viral titre was observed between 4-6 hpi ($2x10^4$ PFU/ml) followed by a small reduction 6-12 hpi ($1.7x10^4$ PFU/ml). A significant increase in HRSV rA2 titre was observed ≥12 hpi with peak virus production achieved at 48 hpi ($9x10^7$ PFU/ml). HRSV rA2 titres then decreased from 48-72 hpi ($2.5x10^6$ PFU/ml) most likely due to the cytopathogenesis of the prototypic HRSV A2 strain previously reported at these later time points (Collins, 2007).

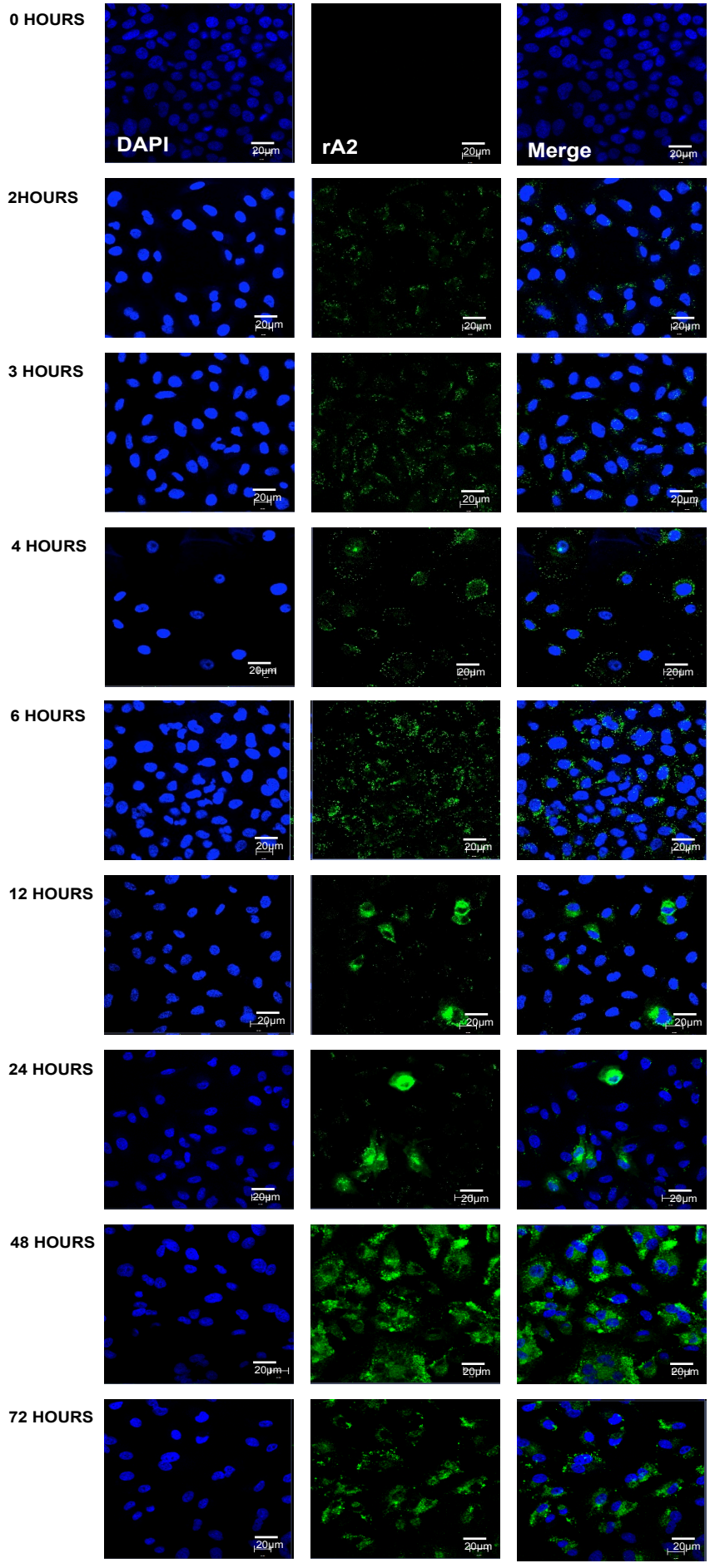
0 HOURS
DAPI
rA2
Merge
2HOURS
3 HOURS
4 HOURS
6 HOURS
12 HOURS
24 HOURS
48 HOURS
72 HOURS
20µm

Figure 4. 2. Representative immunofluorescence images of HRSV rA2 infected A549 cells.

A549 cells (2×10^5 cells/well) cells were infected at an MOI 1.0, and incubated for time periods of 2, 3, 4, 6, 12, 24, 48 and 72 h. Cells were fixed then labelled with FITC conjugated anti-HRSV antibodies (green) and the nucleus stained with DAPI (blue). Images were taken using an upright LSM 510 META Axioplan microscope. Representative images for each time point are shown. Scale bar = 20 µm.

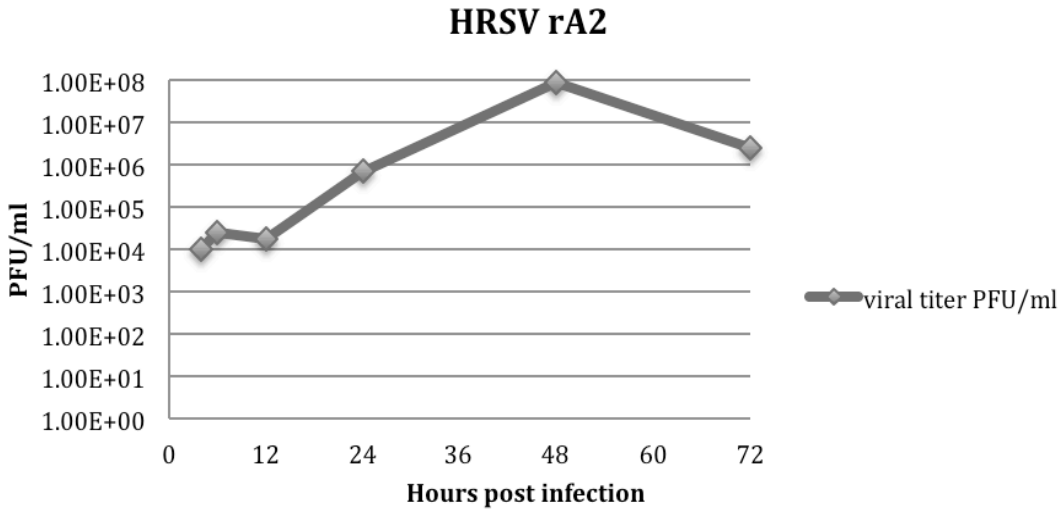

Figure 4. 3. Assessment of WT HRSV rA2 replication and virus production.

A549 cells were infected with HRSV rA2 (MOI = 1.0) and virus titres were estimated by HRP-based plaque assays from virus supernatants at 4, 6, 12, 24, 48 and 72 hpi. Total infectivity (PFU/ml = plaque forming units per ml) of each sample was determined.

Whilst the precise function of HRSV-SH remains to be determined, it has been reported to be completely dispensable for HRSV growth in tissue culture (Biacchesi et al., 2004). To address the relative growth kinetics of each of the viruses used in this study HRSV ΔSH and HRSV ΔSH eGFP were assessed by both IF and plaque assay, and their infection kinetics were compared to the parental HRSV rA2. Figure 4.4.A shows that when assessed by IF analysis, the growth of both HRSV ΔSH and GFP HRSV ΔSH were comparable to HRSV rA2 in A549 cells, namely, the presence of punctate HRSV staining ≤ 6 hpi, more diffuse and intense HRSV expression ≥12 hpi and peak HRSV expression ≥48

hpi. Most cells were positive for HRSV proteins by 72 hpi, indicating extensive infection and efficient virus propagation.

For the comparison of virus growth using multistep growth curves**,** samples were harvested at several time points post-infection, beginning at 2 h. Consistent with previous findings, HRSV ΔSH and HRSV ΔSH eGFP (Figure 4.4) reached comparable titres to the parental isolate following infection. The average HRSV rA2 titres peaked at $9x10^7$ PFU/ml (Figure 4.3) for an MOI of 1.0 at 48 hpi, whilst the peak average titres for HRSV ΔSH and HRSV ΔSH eGFP after infection were $1x10^7$ PFU/ml and $1.5x10^7$ PFU/ml at MOI = 1.0, respectively at 48 hpi. These relatively high titres were expected and consistent with the observed cytopathic effect (CPE) and infectivity data previously reported for each of these viruses. One finding of note was that both HRSV ΔSH and HRSV ΔSH eGFP achieved higher levels of virus production at 24 hpi (Figure 4.4, HRSV ΔSH = $6x10^6$ PFU/ml vs HRSV ΔSH eGFP = $6x10^6$ PFU/ml compared to Figure 4.3, $7x10^5$ PFU/ml for WT HRSV rA2) and displayed a more gradual increase to the peak virus titres obtained at 48 hpi, compared to the parental strain. Previous findings have reported that absence of SH has only a marginal effect on replication of HRSV in HEp-2 cells whilst in Vero cells, the onset of HRSV ΔSH progeny virus production was reported as accelerated compared to that of HRSV WT (Oomens et al., 2003). Overall, despite the differences in the content of proteins between the viruses, relative replication levels between all viruses were similar in the A549 cells tested. This confirmed previous findings that HRSV-SH does not impart a growth advantage to HRSV replicative processes in the cultured A549 cell line.

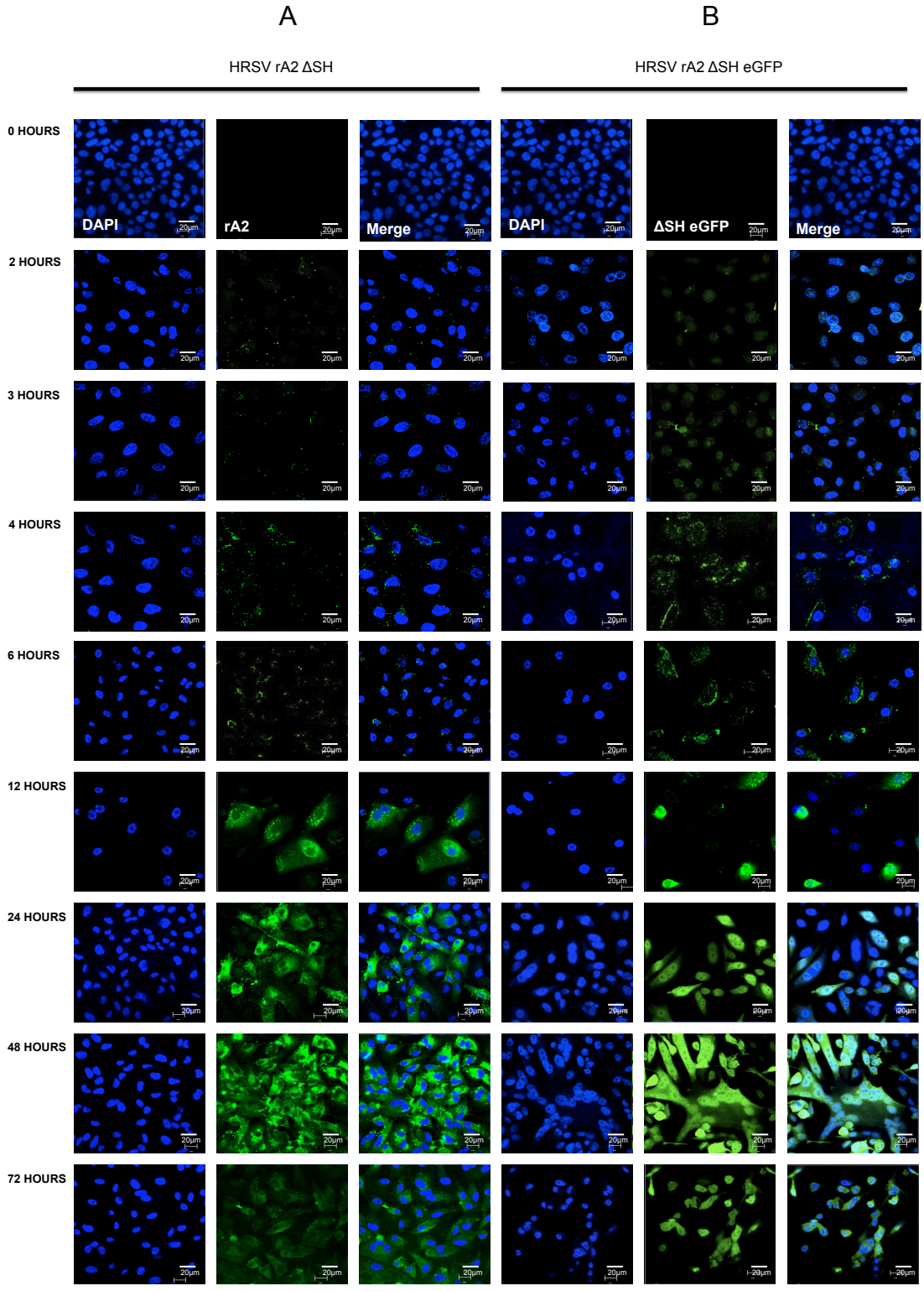

Figure 4. 4. Representative immunofluorescence images of A549 cells infected with HRSV ΔSH recombinant viruses.

A549 cells (2×10^5 cells/well) were infected with (A) HRSV rA2 ΔSH or (B) HRSV rA2 ΔSH eGFP at an MOI 1.0, and incubated for 2, 3, 4, 6, 12, 24, 48 and 72 hpi. Cells were fixed and labelled with FITC conjugated anti-HRSV antibodies (green) and the nuclei stained with DAPI (blue). Images were taken using upright LSM 510 META

Axioplan microscope. Representative images for each time point are shown. Scale bar = 20 µm.

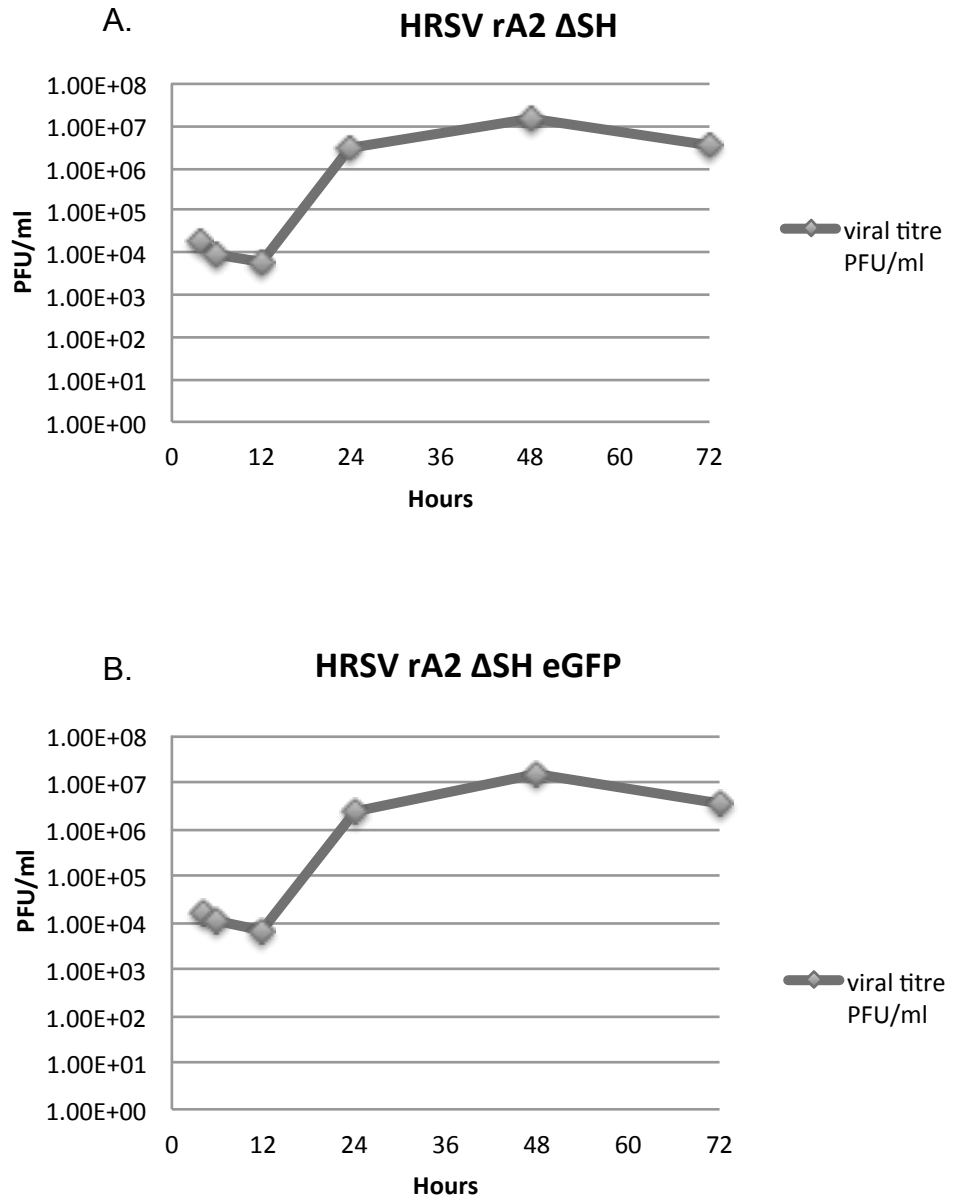

Figure 4. 5. Assessment of HRSV rA2 ΔSH production.

A549 cells were infected with either HRSV rA2 ΔSH (A) or HRSV rA2 ΔSH eGFP (B) (MOI =1.0) and virus titres estimated by HRP-based plaque assays from virus supernatants at 4, 6, 12, 24, 48 and 72 hpi. Total infectivity (PFU/ml = plaque forming units per ml) of each sample was determined by plaque assay.

4.3 Assessment of the effects of cellular ion channel modulation on HRSV rA2 ΔSH viruses in A549 cells

HRSV-SH has been classified as a viroporin, known to alter membrane permeability and display properties of a cation-selective ion channel. HRSV-SH is not essential for viral replication *in vitro* displaying similar replication kinetics and virus production to HRSV WT. However, and of note, it has been reported that the deletion of the SH gene leads to growth attenuation in mouse and chimpanzee animal models, suggesting an important role for SH in HRSV infectivity and pathogenicity *in vivo.* Having established that specific cellular ion channel modulators can influence the WT HRSV lifecycle in Chapter 3, the effects of altering cellular ion channel functionality was reassessed in cells infected with the mutant HRSV in which the SH gene had been deleted, namely, HRSV ΔSH virus. This would reveal if the SH mediated control of ion permeability conferred protection, and/or sensitivity to specific cellular ion channel families, elucidating further mechanisms by which SH contributes to HRSV pathogenesis.

To investigate the effects of cellular ion channel modulators on the early stages of the HRSV ΔSH life cycle, identical time of addition assays to those employed in Chapter 3, Section 3.4.2 were performed. Briefly, A549 cells were pre-treated with ion channel modulators that target the major Na^+, K^+, Ca^{2+} and Cl^- families at the non-toxic concentrations identified in Chapter 3 and cells were infected with HRSV ΔSH (MOI = 1) for 3 hours. The cells were then washed, and treated with each ion channel modulator for 24 hours. Cells were then fixed, stained for HRSV protein expression, and the percentage of HRSV ΔSH infected cells assessed by FACS analysis. To assess the effects of each ion channel modulator on late stage HRSV ΔSH processes, including HRSV ΔSH replication, the ion channel modulators were omitted from the initial three hours of HRSV ΔSH infection, and added 3 hpi after HRSV ΔSH adsorption and entry. Cells were fixed 24 hpi and HRSV ΔSH protein expression assessed by FACS analysis.

4.3.1 Effects of K^+ channel modulation during HRSV ΔSH infection

Figure 4.6 shows the effects of modulating the major cellular K^+ channel families on HRSV lacking the SH protein. The effects of K^+ channel modulator addition prior to virus entry were initially assessed. When the broad spectrum K^+ channel blocker TEA was added during the attachment stage of HRSV ΔSH infection, an inhibition of HRSV ΔSH production was observed only at non-K^+ channel selective concentrations (50 mM - 45.7% inhibition), with minimal effects on HRSV ΔSH observed at more K^+ channel specific concentrations of 10-20 mM. This was similar to the data reported for HRSV WT (Figure 3.10A) and confirmed that TEA does not significantly influence HRSV growth either in the presence or absence of SH. When HRSV ΔSH infection was performed in the presence of other K^+ channel modulators including KCl, the ATP sensitive K^+ channel modulators (Figure 3.10B); glibenclamide (Glib) and tolbutamide (Tol), the voltage-gated K^+ channel modulators 4-AP, chromanol 293B and sotalol, and the Ca^{2+}-activated K^+ channel modulator apamin (Apa), no effects on HRSV ΔSH infection were observed and the levels of virus infection were comparable to no-drug HRSV ΔSH controls (Figure 4.6A). In agreement with the findings for HRSV WT, the modulation of inward rectifier K^+ channels using $BaCl_2$ significantly reduced the number of HRSV ΔSH infected cells by 44.7% (Figure 4.6A) compared to no drug controls, ($p \leq 0.05$) suggesting that a $BaCl_2$ sensitive Kir channel is also required during HRSV ΔSH replication. However, some differences to the parental HRSV WT strain were observed for HRSV ΔSH, as in the presence of the K_{2P} channel modulators ruthenium red (RR) and Haloperidol (Halo), a respective 75% and 47.1% decrease (Figure 4.6A) in HRSV ΔSH infectivity was observed. This data suggested that the deletion of SH confers sensitivity of HRSV ΔSH viruses to K_{2P} channel modulation.

The effects of these compounds were next investigated when added 3 hpi, which represents a time point after HRSV adsorption/entry has occurred. When assessed, $BaCl_2$ displayed similar levels of HRSV ΔSH inhibition when added 3 hpi compared to when added during attachment, 62.8% inhibition (Figure 4.6B), suggesting that Kir channel modulation inhibits later stages of the virus lifecycle.

Interestingly, the inhibitory effects of both ruthenium red and haloperidol were less potent when added 3 hpi (Figure 4.6B), suggesting that K_{2P} modulation primarily restricts the early stages of the HRSV ΔSH lifecycle. When these data are compared to the HRSV WT parental virus (Chapter 3), where $BaCl_2$ was inhibitory only when added during the early stages of HRSV WT infection, it is suggestive that the absence of the HRSV-SH protein mediates an additional sensitivity to Kir channel blockade during the replication of HRSV ΔSH. Of the other K^+ modulators assessed when added post-virus entry, no significant changes in the numbers of infected A549 cells were observed. Together these data reveal differences between the dependence of HRSV WT and HRSV ΔSH viruses to the modulation of cellular Kir and K_{2P} channels during the virus lifecycle.

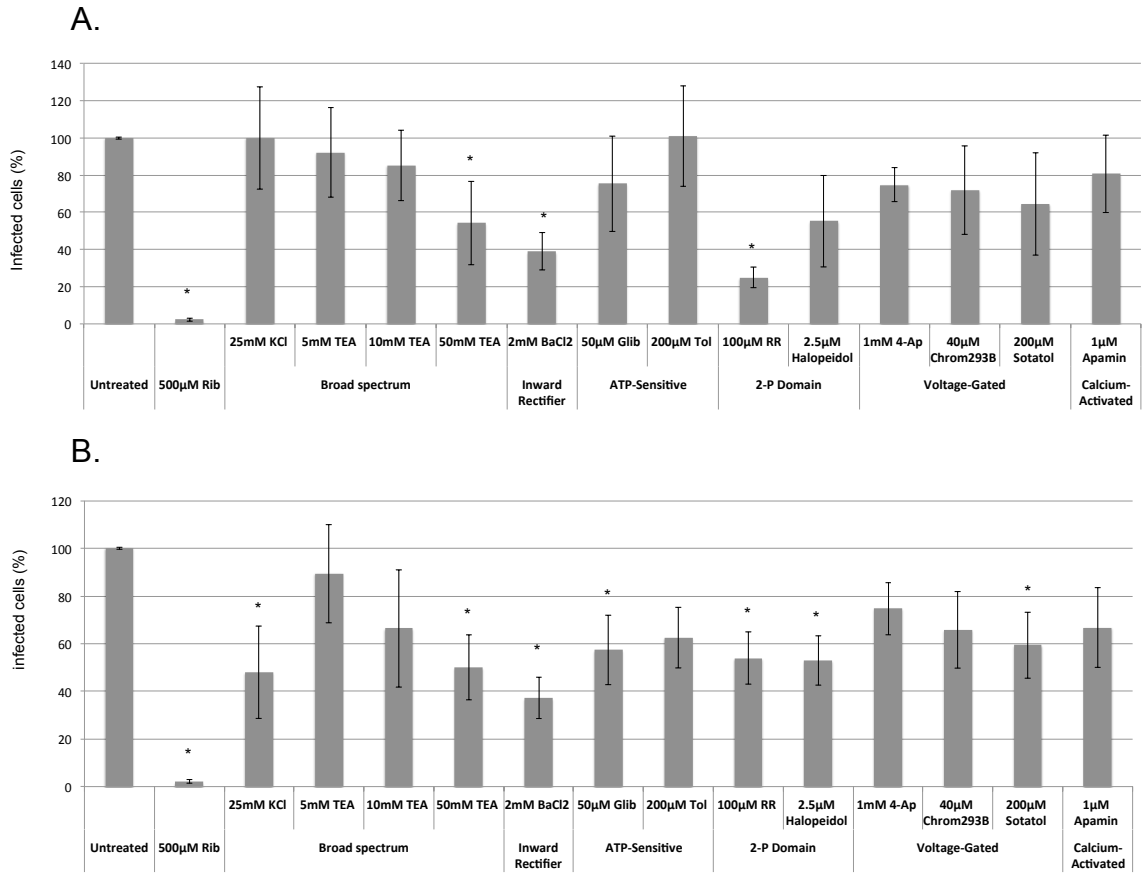

Figure 4. 6. Assessment of the effect of K^+ cellular channel modulation during the pre- or post-entry stages of HRSV rA2 ΔSH infection in A549 cells.

Cells were infected with HRSV rA2 ΔSH at an MOI of 1.0 and treated with the indicated K^+ channel modulators (pre-entry or post-entry treatment). Cells were fixed, permeabilised with 0.5% (v/v) Triton X-100 and labelled with goat anti-HRSV FITC conjugated antibodies. Percentages of infected cells were assessed by FACS analysis and normalized to no-drug infected controls. Cells were treated with 0.5 mM (v/v) ribavirin (Rib; a known inhibitor of HRSV replication) for assay validation. The K^+ channel families targeted included; **A.** Potassium channel blocking drugs, pre-entry treatment. Data points are expressed as mean ± SE (N ≥ 2). *Significant differences from untreated value at the $p<0.05$ levels **B.** K^+ channel blocking drugs, post-entry treatment, following virus attachment and initial entry.

4.3.2 Effects of Ca^{2+}, Na^+ and Cl^- channel modulation during HRSV ΔSH infection

The data from Chapter 3 assessing the effects of Na^+ channel modulation on HRSV WT suggested that the inhibition of specific NaV members, particularly those sensitive to TTX, promotes HRSV infection. When TTX was added during HRSV ΔSH infection, no effects were observed when added either prior to, or post virus infection (Figure 4.7A, 83.7% ± 16% decrease; Figure 4.7B, 81.3% ±18.7% decrease, respectively). In further contrast to the data obtained for HRSV WT, HRSV ΔSH was inhibited by lidocaine (Figure 4.7A &B) addition pre- and post- virus entry (58.7% ± 42.2% inhibition and 63.7% ± 36.3% inhibition, respectively), whilst the parental HRSV WT was unaffected by this compound. These data suggest that the presence of SH can influence the sensitivity of HRSV to cellular NaV modulation. Regarding voltage gated Ca^{2+} channels; Chapter 3 demonstrated that the modulation of this channel family does not impede HRSV WT multiplication. Consistent with this data, HRSV ΔSH infection was not inhibited by pre or post-entry treatment with verapamil (pre-entry treatment, 87.7% ± 12.3% vs. post-entry treatment, 72.4% ± 27.6%) a drug that inhibits T-type and L-type voltage gated Ca^{2+} channels, or nifedipine (pre-entry treatment 85.6 ± 14.4% vs. post-entry treatment 74.8% ± 25.2%) an inhibitor of L-type voltage gated Ca^{2+} channels (Figure 4.7A & B). Surprisingly, Bay K8644 a voltage gated Ca^{2+} channel agonist that activates L-type channels reduced HRSV ΔSH infection when added pre-entry (Bay K = 60.4% ± 39.6% inhibition) and post-entry (Bay K = 51% ± 49% inhibition). These data suggest that the activation of L-type Ca^{2+} channels supresses HRSV infection when SH is absent.

Finally, Cl^- channel modulation was assessed in the presence of the well-characterized Cl^- channel blockers, NPPB, IAA-94 and DIDS. Results presented in Chapter 3 (Figure 3.13) showed these compounds did not significantly inhibit HRSV WT infection when added post-entry, whilst a DIDS sensitive Cl^- channel was identified as being required during HRSV WT attachment/early viral processes. In agreement with this data, DIDS (69.9% ± 30.1% inhibition) and NPPB (69.5% ± 30.5% inhibition) did not inhibit HRSV ΔSH infection when added when added post-entry, whilst DIDS (9.6% ± 90.4% inhibition) when added prior to virus entry, almost completely abolished HRSV ΔSH infection. This confirmed that both WT HRSV and HRSV ΔSH require a DIDS sensitive Cl^- channel during entry/early virus processes.

A.

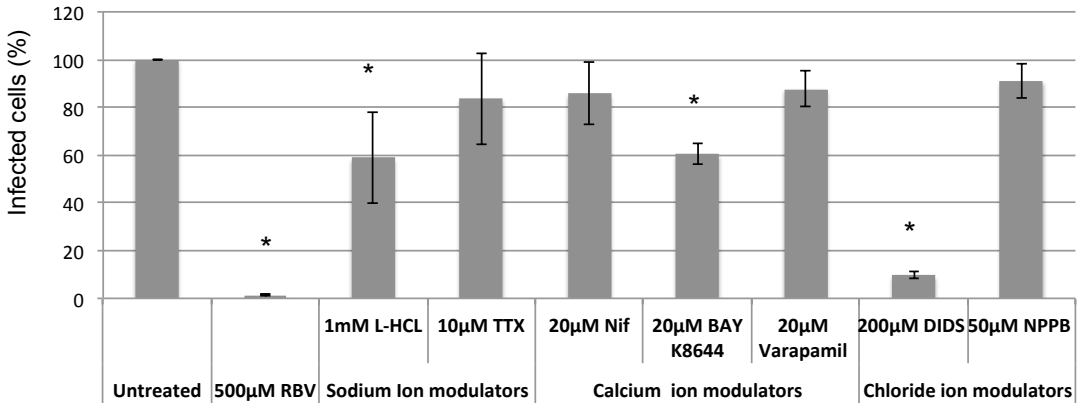

B.

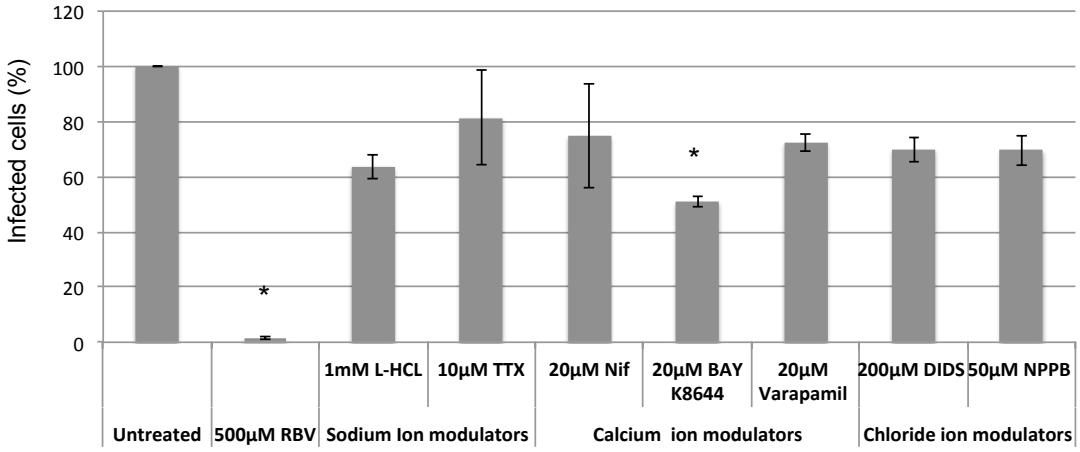

Figure 4. 7. Assessment of the effect of Na^+, Ca^{2+} and Cl^- cellular channel modulation during the pre-entry or post-entry stage of HRSV rA2 ΔSH infection in A549 cells.

Cells were infected with HRSV rA2 WT at an MOI of 1.0 and treated with the indicated K^+ channel modulators (pre- or post-entry treatment). Cells were fixed, permeabilised with 0.5% (v/v) Triton X-100 and labelled with goat anti-HRSV FITC conjugated antibodies. Percentages of infected cells were assessed by FACS analysis and normalized to no-drug infected controls. Cells were treated with 0.5 mM (v/v) ribavirin (RBV; a known inhibitor of HRSV replication) for assay validation. The K^+ channel families targeted included. **A.** Na^+, Ca^{2+} and Cl^- channel modulators, pre-entry drug treatment. **B.** Na^+, Ca^{2+} and Cl^- channel modulators post-entry drug treatment. Data was expressed as mean ± SE (N ≥ 2). *Significant differences from untreated value $p<0.05$ level.

4.3.3 Investigating the effects of $BaCl_2$ and DIDS on HRSV ΔSH entry

The effects of both $BaCl_2$ and DIDS on both HRSV WT and HRSV ΔSH at entry/early viral processes suggests that these viruses utilize similar routes of entry. To assess this, HRSV ΔSH entry was assessed in the presence of DIDS and $BaCl_2$ when added only during the initial 3 hours of the virus lifecycle in assays identical to those described in Chapter 3, section 3.5.1. Cells were washed, and surface attached viruses removed via the addition of 0.5% trypsin, and infection allowed to proceed for 24 hours. As in Figure 4.8, CPZ, amiloride and monensin were included in the HRSV ΔSH chase, as known inhibitors of cellular entry processes.

Figure 4.8 shows that, when cells were HRSV ΔSH infected in the presence of each treatment and infection assessed by IF, HRSV ΔSH entry was inhibited by monensin and CPZ as evidenced by the decrease in HRSV stained cells (Figure 4.8). These findings were confirmed by Western blot analysis whereby both monensin and CPZ reduced viral protein expression when included during HRSV ΔSH entry (Figure 4.9). When cells were treated with amiloride, only a modest reduction in the number of infected cells was observed by IF analysis, with little or no reduction in viral protein expression observed, suggesting that HRSV ΔSH entry is not impeded by amiloride mediated inhibition of macropinocytosis (Figure 4.8 and 4.9). Importantly, when the effects of DIDS and $BaCl_2$ were assessed, both treatments reduced the number of HRSV

infected cells and consistently reduced HRSV ΔSH protein expression as assessed by IF analysis (Figure 4.8 & 4.9). These data confirm that HRSV ΔSH viruses use a similar mechanism of cell entry to HRSV WT that is dependent on DIDS and $BaCl_2$ sensitive cellular ion channels.

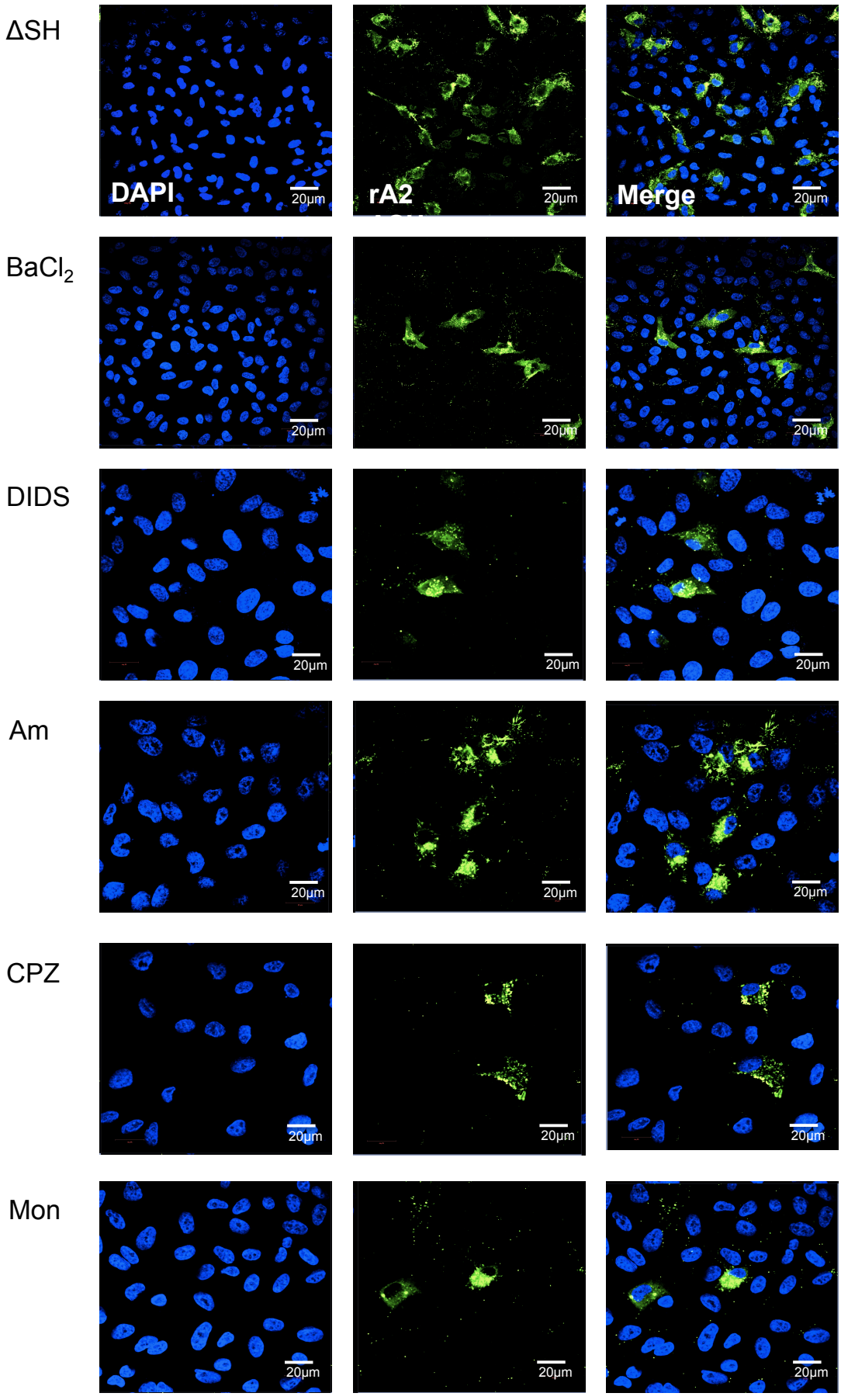
ΔSH
DAPI
rA2
Merge
20μm
BaCl2
DIDS
Am
CPZ
Mon

Figure 4. 8. Representative immunofluorescence images of HRSV rA2 ΔSH entry assay in A549 cells.

Cells were pre-treated with specific concentrations of entry pathway inhibitory drug then infected with virus at an MOI 1.0. Cells were labelled with FITC conjugated anti-HRSV antibodies (green) and the nuclei stained with DAPI. A549 cells were drug treated using the following concentrations, $BaCl_2$, (2 mM); DIDS (200 μM); Am (200 μM); CPZ, (30 μM); Mon (20 μM). Images were taken using upright LSM 510 META Axioplan microscope. Representative images for each time point are shown. Scale bar = 20 μm

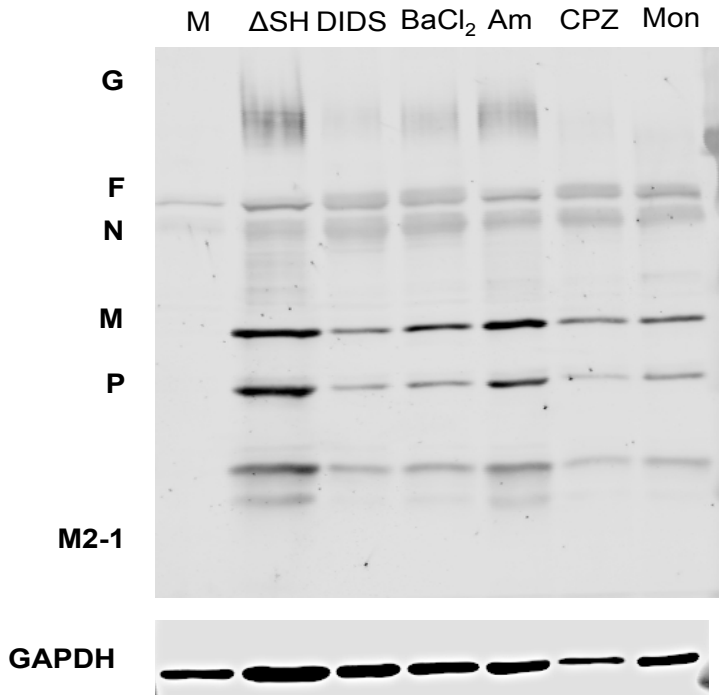

Figure 4. 9. Representative western blots of A549 cells infected with HRSV rA2 ΔSH, and treated at pre-entry stages of virus infection with entry pathway inhibitors.

The effect of pre-treatment with entry pathway inhibitory drugs on HRSV rA2 ΔSH replication was assessed using western blotting using anti-HRSV polyclonal antiserum. Data are expressed as mean ± SE (N ≥ 3). Each lane was loaded with 5 μg of protein content. GAPDH was re-probed as loading control. First lane; Mock neither drug-treated nor virus infected. Second lane; HRSV ΔSH viral protein expression is evident as control. Third lane; cells treated with 200 μM of DIDS. Fourth lane; cells treated with 2 mM of $BaCl_2$. Fifth lane; cells treated with 200 μM Am, macropinocytosis blocker. Sixth lane; cells treated with 30 μM of CPZ, an inhibitor to CME. Seventh lane, cells treated with 20 μM of Mon, also an inhibitor of CME.

4.3.4 Cellular chloride ion homeostasis during early infection of HRSV rA2 ΔSH

In Chapter 3, HRSV was shown to enhance Cl^- influx during the early stages of the virus lifecycle, which is consistent with the finding that DIDS displays anti-HRSV activity. Cl^- homeostasis was compared between HRSV ΔSH infected and mock-infected cells, to investigate if the change in Cl^- influx is also observed during the early stages of HRSV ΔSH infection, and thus is SH independent. A549 cells were treated with MQAE as described in section 3.6 and the cells were assessed by IncuCyte ZOOM live cell to visualise and quantify MQAE fluorescence at 1 hour intervals for up to six hours.

Figure 4.10 displays the changes in intracellular Cl^- flux during HRSV ΔSH infection. In HRSV ΔSH infected cells, MQAE fluorescence was reduced most significantly at 1 hpi, but continued below the threshold of uninfected cells, throughout the 6-hour time course, decreasing rapidly at 6 hpi. These findings suggest that, like HRSV WT, HRSV ΔSH increases Cl^- influx during early virus lifecycle stages in comparison with uninfected cells, leading to the quenching and loss of MQAE staining. These data suggest that the HRSV mediated changes in Cl^- influx are not mediated by HRSV-SH and that HRSV ΔSH modulates Cl^- flux and enters susceptible A549 cells via an identical mechanism to HRSV WT.

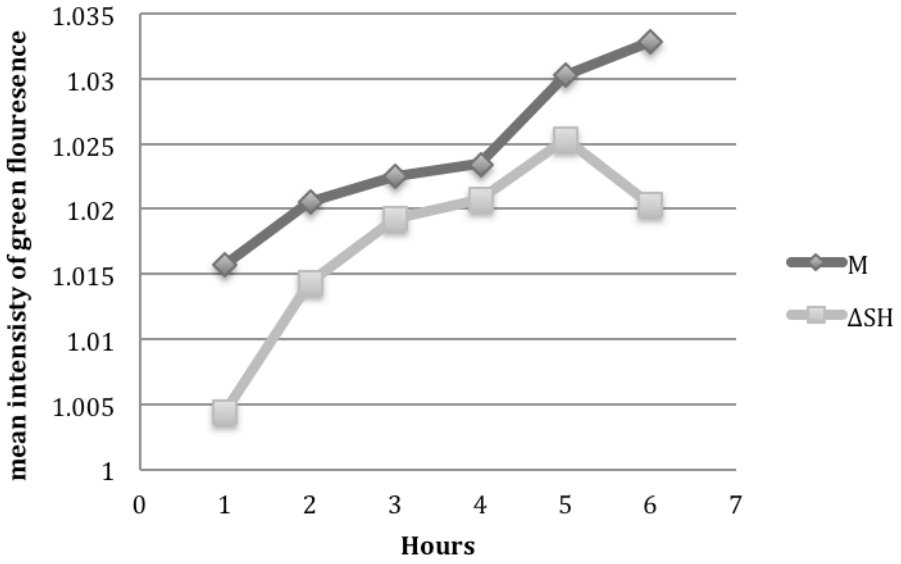

Figure 4. 10. Measuring Cl- influx at the early stage of HRSV rA2 ΔSH infection in A549 cells.

A549 cells were treated with 5 mM of MQAE green fluorescent dye for one hour then infected with MOI 1.0 of HRSV rA2 ΔSH. Mock (M) represents the A549 Cl^- intracellular concentration in uninfected cells. Green fluorescent intensity (average of GCU/well) was measured using the IncuCyte ZOOM live cell imaging system. Values represent 6 hours post infection time point. Experiments were performed a minimum of three times and mean values plotted.

4.4 Global proteomic changes mediated by SH during HRSV infection

Whilst it was identified that the deletion of HRSV-SH can enhance the sensitivity of HRSV to cellular K_{2P} and Kir channel modulation in A549 cells, the key findings from Chapter 3, namely virus entry being dependent on both Cl^- and Kir channels was common between HRSV WT and HRSV ΔSH. In addition, it was revealed that HRSV ΔSH viruses grew as efficiently as HRSV WT in A549 cells suggesting the deletion of HRSV-SH does not disadvantage virus growth. To further investigate any effects mediated by HRSV-SH during the HRSV lifecycle, the changes in the A549 cellular proteome were compared during HRSV rA2 and HRSV ΔSH infection. As no changes in growth kinetics between HRSV rA2 verses HRSV ΔSH were identified earlier in this chapter (figures 4.3 and 4.5), gross proteomic shifts between the viruses were not expected. However, subtle proteomic changes (for example regarding cellular ion channel expression profiles) may reveal the enhanced sensitivity to the ion channel modulators' identified for HRSV ΔSH earlier in this chapter. Proteomic changes induced by HRSV rA2 infection of A549 cells were therefore assessed using label-free relative quantitation by mass spectrometry and compared to cells infected with the HRSV ΔSH viruses.

This methodology involves evaluating the abundance of all proteins, both cellular and viral, in virus-infected cells without the use of stable isotope labelling by amino acids in cell culture (SILAC). Label-free proteomics allows peptide quantification using spectral characteristics such as retention time, m/z ratio (mass-to-charge ratio) and peak intensity by comparing and measuring the direct mass spectrometric signal intensity for any given peptide ions fitting to a specific proteins, or by counting and comparing the number of acquired tandem mass spectra matching a specific peptide as an indicator for their abundance in a given sample (Bantscheff et al., 2007).

Cell lysates destined for label-free protein quantification (LFPQ) to assess the role of HRSV-SH were prepared as follows. (1) Cells were infected with HRSV rA2, HRSV ΔSH and HRSV ΔSH eGFP at an MOI of 1.0 for 24 hours. Cellular

proteome changes resulting from A549 infection with both HRSV ΔSH and ΔSH eGFP viruses were investigated to maintain consistent gene expression (both genomes contain 10 genes). This was important as deletion of the SH gene has been shown to lead to enhanced synthesis of G, F, and M2 mRNAs due to their closer proximity to the promoter in the gene order, and a steeper gradient of polarity of the transcription of genes downstream of the engineered site. By replacing the SH ORF with that for eGFP, the gradient of expression is maintained. A549 cells were lysed, and proteins extracted and subjected to alkylation and digestion to generate short peptides, (2) Samples were analysed by LC-MS/MS (liquid chromatography-tandem mass spectrometry) using the Orbitrap velos platform. This analysis combines the physical separation competences of liquid chromatography with the mass analysis competency of mass spectrometry. (3) The subsequently generated raw data were analysed to derive peptide identities and their corresponding quantities, and allowed the identification of those cellular proteins with dysregulated expression, as a consequence of viral infection. (4) Data were interpreted using previously described protocols including the protein-protein networks (M. Wang et al., 2008). Figure 4.11 provides a flow chart of LFPQ stages.

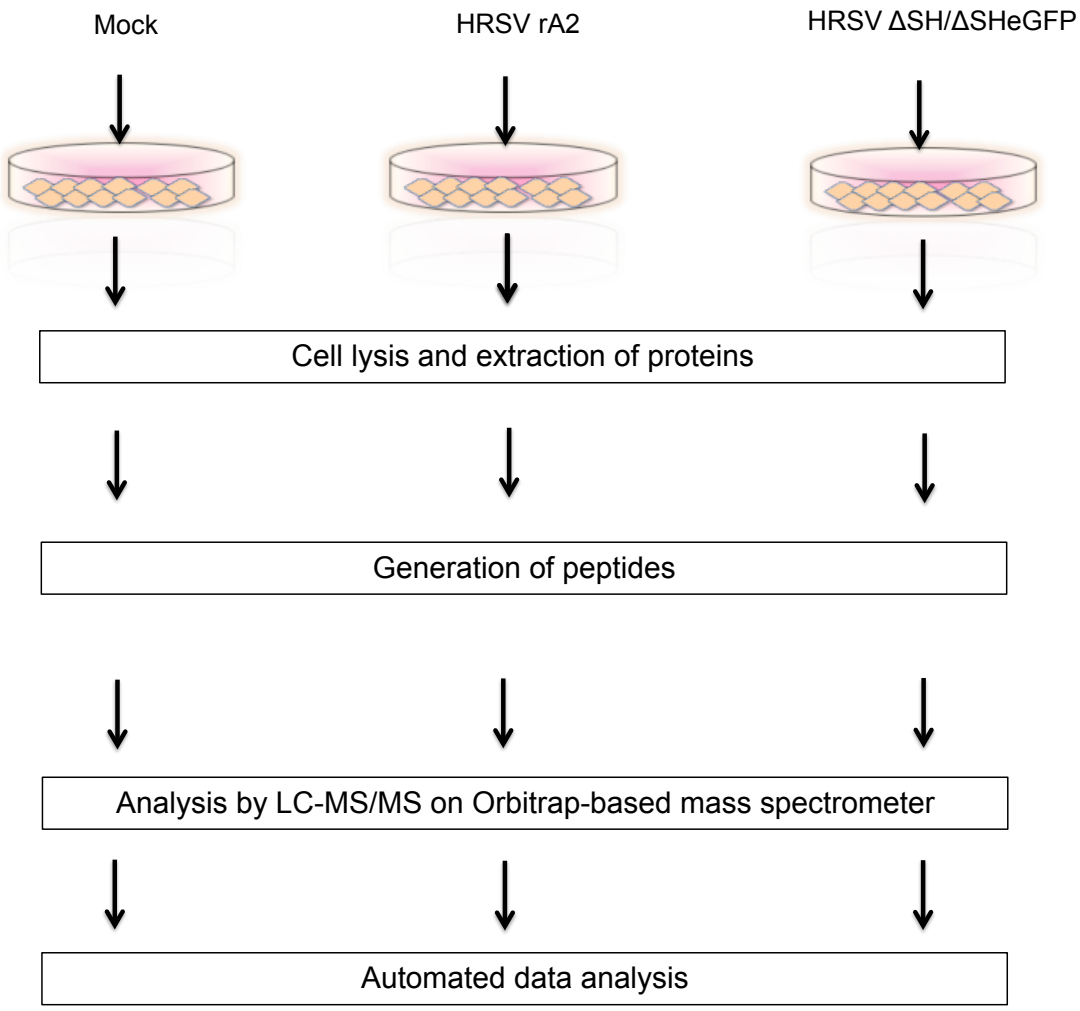

Figure 4. 11. Schematic representation of the label free protein quantification pipeline performed in this study.

A549 cells were either mock infected, or infected with HRSV rA2 WT, HRSV rA2 ΔSH, or HRSV rA2 ΔSH eGFP at an MOI=1.0 for 24 hours. Cells were lysed and label free protein quantification with mass spectrometry performed to assess proteins dysregulated during virus infection.

4.4.1 Sample preparation for label-free protein quantification

A549 cells were infected with purified recombinant HRSV strains at an MOI of 1.0 and incubated for 24 hours at 37°C as described in the methodology Chapter 2, section 2.2.8. The recombinant viruses employed included HRSV rA2, HRSV ΔSH and HRSV ΔSH eGFP. A mock-infected sample was included to assess the proteomic content of untreated A549 cells. All samples were performed in triplicate to provide sufficient data for the identification of statistically significant changes, a key approach in label free quantification. All

samples were lysed in 0.1% RapiGest diluted in 25 mM ammonium bicarbonate. RapiGest solubilisation enhances enzymatic cleavage of cellular proteins without affecting enzymatic activity, and is heat stable during protein digestion (Stover et al., 2003). Details of the cell lysis procedure are explained in detail in Section 2.2.8.1. Briefly, cell lysates were heat-inactivated at 80°C for 10 min and centrifuged at 14000 rpm for 30 minutes. The soluble fraction was transferred to low adhesion tubes and the protein content adjusted by BCA assay (Chapter 2 section 2.2.3.2). A mass of 100 µg of protein was collected for each sample of which 10 µg of sample were run per lane. Western blots were performed to confirm virus infection (Figure 4.12A). In addition cellular proteins were analysed by SDS-PAGE, with proteins detected using Coomassie stain (Figure 4.12B).

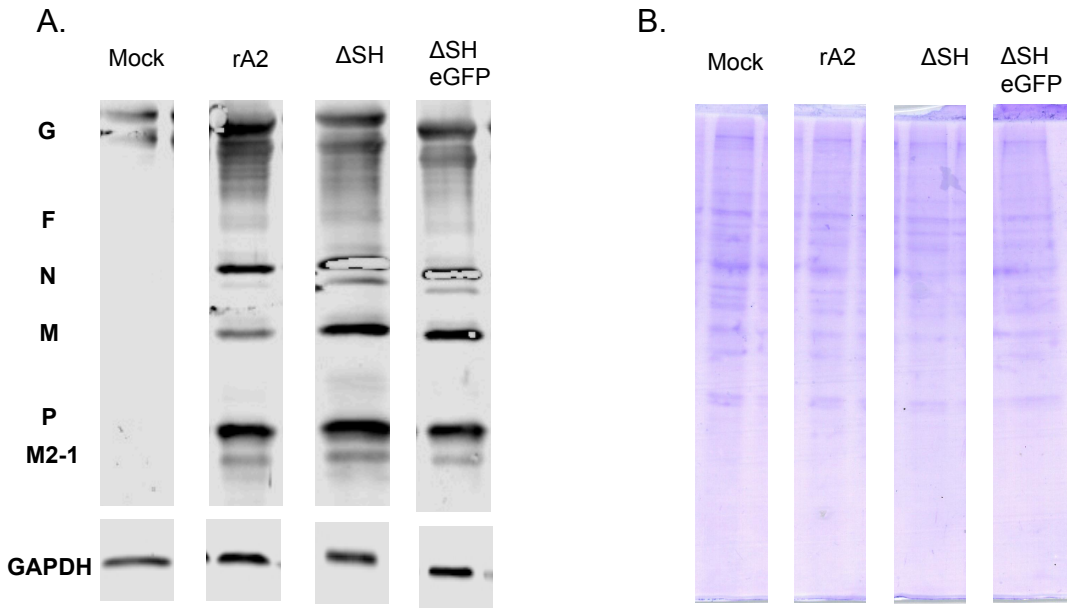

Figure 4. 12. Validation of A549 protein extracts prepared for label free protein quantification.

A. Western blot representing HRSV protein expression from infected A549 lysates. Membranes were probed with primary polyclonal goat anti-HRSV antibodies and donkey anti-goat HRP conjugated secondary antibodies. **B.** Lysates (10 µg per lane) from infected A549 cells were assessed by Coomassie stain prior to analysis by MS.

For protein digestion and peptide generation, the reducing agent DTT was added, and iodoacetamide (IAA), which is an alkylating agent, was added to

free the peptides of cysteine residues in order to form S-caroxyamidomethyl-cysteine that cannot be re-oxidised to form disulphide bonds. This is important to enhance trypsin cleavage at sites without protein sulfhydryl groups. The protein mixture was digested by trypsin overnight. Trifluoroacetic acid (TFA) was used as an ion-pair reagent to separate proteins into peptides and to improve the sensitivity of LC-MS/MS detection. Peptides were analysed in an Orbitrap Velos with standard fmol sensitivity. Statistical analyses were performed to identify significantly up and down- regulated proteins.

4.4.2 Identification and quantification of HRSV proteins in infected A549 cells.

LC-MS/MS was first used to quantify the expression of HRSV-specific proteins from infected A549 cells (Figure 4.13). HRSV ΔSH displayed the highest abundance of viral proteins across all infected samples. Seven HRSV proteins were identified including N (nucleoprotein), M (matrix protein), F (fusion protein), P (phosphoprotein), G (glycoprotein), M2-1 and non-structural-1 (NS1) protein. M2-1 and was the most abundant HRSV protein in all viruses (ΔSH = 8 and ΔSH eGFP = 2.6 fold change, followed by HRSV G (ΔSH = 7.9 and ΔSH eGFP = 2.6 fold change over mock infected samples). HRSV-F displayed the abundancy for recombinant HRSV ΔSH types (ΔSH = 11.3, ΔSH eGFP = 3.9). HRSV-SH was not detected in the proteomics data sets. Therefore, the abundance of these proteins appeared to differ between HRSV strains. Whilst this finding was unexpected, the comparable levels of virus growth identified earlier in this chapter between HRSV rA2 and HRSV ΔSH, suggested that the altered protein abundance did not lead to enhanced levels of HRSV ΔSH growth.

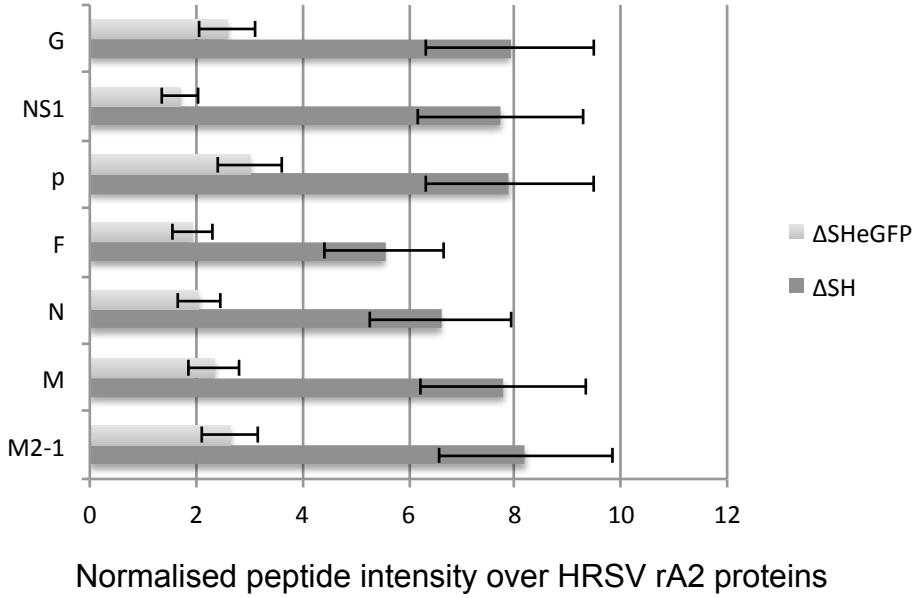

Figure 4. 13. Comparison of the normalised abundance of HRSV proteins in HRSV rA2 ΔSH and HRSV rA2 ΔSH eGFP infected A549 cell lysates over HRSV rA2.

Cells were either mock infected, or infected with HRSV rA2 ΔSH and HRSV rA2 ΔSH eGFP at an MOI of 1.0 for 24 hrs. The abundance of HRSV proteins was assessed by LFPQ and normalised to HRSV rA2 infected samples (n=3).

4.4.3 Data analysis of significant proteins

Data was assessed from the peptide quantification obtained from the chromatographic peak intensities. Each protein identified by fewer than 2 peptides was excluded from the data analysis. In the final dataset, each protein value was represented with an N=3, therefore, each protein value was averaged and divided by the mock-infected averaged value to normalise the protein abundance. The abundance fold change (FC) was then calculated and expressed as a value in Log_2. The significance of all data was described as a $-Log_{10}$ value, calculated as a p-value using a one-way ANOVA that was provided with the proteomics data set. The resulting abundance and protein significance values were displayed using a volcano plot (Figure 4.14), in which the protein significance value (p-value) is shown on the y axis using a $-log_{10}$ scale, and fold changes in abundance are shown on the x-axis, using a log_2 scale. Proteins identified with a significance p-value equal or less than 0.05 are found above the dotted red line (Figure 4.14), at a $-log_{10}$ value of 1.3 or higher. Changes in protein abundance over 2-fold (1 log_2 unit) are considered

significantly up or down regulated, and are potential candidates for further validation studies. From the datasets, 39 proteins were identified as up regulated, and 100 proteins identified as down regulated (Figure 4.14A) that are normalised over mock. Figure 4.14B represents the cellular protein changes from HRSV ΔSH infected cells in comparison to mock infected. A total of 47 proteins were identified as up regulated and 115 down regulated. From HRSV ΔSH eGFP infected cells (Figure 4.14C), 48 proteins were identified as up-regulated and 63 proteins were down regulated in comparison to mock infected.

As described above, the reason for investigating the cellular proteome resulting from infection of cells using both ΔSH eGFP and ΔSH viruses, was firstly because HRSV ΔSH eGFP has an equal number of genes, thus the expression profile of HRSV genes will be unaffected. Secondly, testing HRSV ΔSH eGFP alongside to HRSV ΔSH would reveal if GFP could cause any cellular changes that would cause significant changes to the expression of cellular proteins, a situation that would be expected if eGFP was toxic, for example. Importantly, upon comparison of HRSV ΔSH eGFP and HRSV ΔSH cellular proteomic changes (Figure 4.14D) both viruses produced comparable proteomic changes, thus indicating these changes were not dependent on eGFP expression.

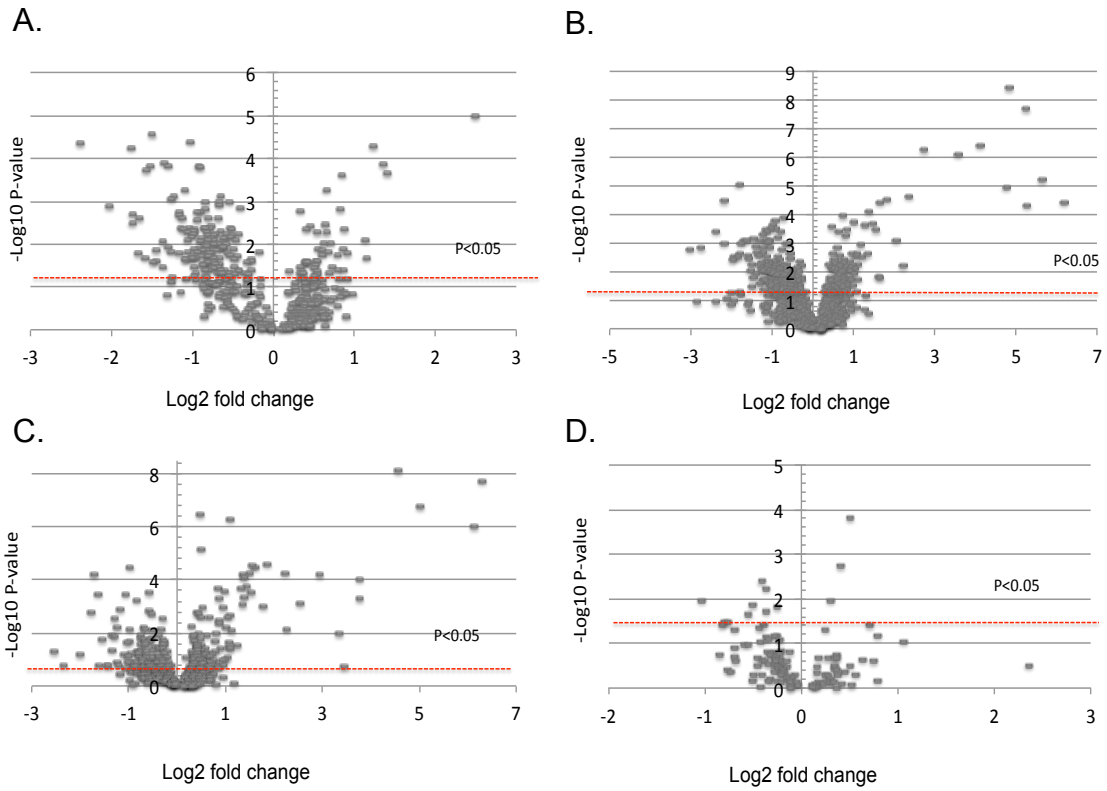

Figure 4. 14. Volcano plots from label free protein quantification of the cellular proteome in HRSV infected A549 cells.

The y-axis shows protein significance, represented as $-\log_{10}$ of the calculated p-value. The x-axis indicates the fold change of each identified cellular protein, represented as $\log_2$ of the fold change (FC). Red dashed lines represent p=0.05 where any value above the line represents a low p-value and so high significance. **A.** Cellular proteins dysregulated in HRSV rA2 infected cells normalised to mock infected cells. **B.** Cellular proteins dysregulated in HRSV ΔSH infected cells normalised to mock infected cells. **C.** Cellular proteins dysregulated during HRSV ΔSH eGFP infection of A549 cells normalised to mock infected cells. **D.** Data analysis of cellular proteins dysregulated in HRSV rA2 ΔSH eGFP infected A549 cells normalised to the proteomic changes detected in cells infected with HRSV ΔSH.

From the datasets, significant changes in protein abundance were confirmed according to a p-value ≤ 0.05 and ≥ ±2 fold change. Therefore, the top 10 proteins with the highest total fold change from HRSV rA2, HRSV ΔSH and HRSV ΔSH eGFP were identified, and proteins were allocated to their biological process (GOBP) using gene Ontology via the Uniprot website (http://www.uniprot.org). Tables 4.1A and B list the unique proteins most highly dysregulated during HRSV rA2 infection, normalised to mock-infected cells. Tables 4.2A and B list the unique proteins dysregulated during infection with

HRSV rA2 ΔSH normalised to mock-infected cells, Finally, Tables 4.3A and B list the unique proteins dysregulated during HRSV ΔSH GFP infection of A549 cells normalised to mock-infected cells. Some identified proteins were previously detected in infected cells with HRSV such as PML (promyelocytic leukmia) bodies (Munday et al., 2010) and STAT2 (signal transducers and activators of transcription protein) (Elliott et al., 2007).

A. Proteins up regulated in expression during HRSV rA2 infection.

Uniprot ID	Gene	Protein name	Log2 FC		−Log10 (P-value)	GOBP
			rA2	ΔSH		
Q9H0P0	5NT3A	Cytosolic 5'-nucleotidase 3A	2.45	2.42	4.9	Dephosphorylation
P42224	STAT1	Signal transducer and activator of transcription 1	1.2	0.9	4.3	Cellular responses to interferons (IFNs)
P19525	E2AK2	Interferon-induced, double-stranded RNA-activated protein kinase	1.3	1.1	3.8	Defence response to virus
P02792	FRIL	Ferritin light chain	1.3	1.0	3.6	Cellular iron homeostasis
P21283	VATC1	V-type proton ATPase subunit C	1.1	0.9	2.1	Ion transmembrane transport
P09601	HMOX 1	Heme oxygenase 1	1.1	0.5	1.6	Cellular iron homeostasis

B. Proteins down regulated during HRSV rA2 infection.

Uniprot ID	Gene	Protein name	Log2 FC		−Log10 (P-value)	GOBP
			rA2	ΔSH		
P09493	TPM1	Tropomyosin alpha-1 chain	-1.5	-1.0	4.5	Cellular response to reactive oxygen species
Q6PUV4	CPLX2	Complexin-2	-2.4	-2.1	4.3	Regulation of exocytosis
Q8N6H7	ARFG2	ADP-ribosylation factor GTPase-activating protein 2	-1.8	-1.5	4.2	Protein transport

Q9Y618	NCOR2	Nuclear receptor corepressor 2	-2.0	-1.8	2.8	Negative regulation of transcription from RNA polymerase II promoter
Q16625	OCLN	Occludin	-1.7	-1.1	2.7	Apoptotic process
Q15154	PCM1	Peri centriolar material 1 protein	-1.7	-1.1	2.5	Cilium assembly
Q9H1E3	NUCKS	Nuclear ubiquitous casein and cyclin-dependent kinase substrate	-1.5	-1.3	1.8	Glucose homeostasis
Q4V328	GRAP1	GRIP1-associated protein	-1.7	-0.9	1.7	Early endosome
Q96IZ0	PAWR	PRKC apoptosis WT1 regulator protein	-1.0	-0.9	1.69	Pro-apoptotic protein capable of selectively inducing apoptosis process

Table 4. 1 The top 10 most significant changes in protein abundance identified in A549 cells infected with HRSV rA2 by label free protein quantification by MS.

Data were analysed from HRSV rA2 infected A549 cell lysates and normalized to mock infected A549 cells. **A**. Top up regulated proteins detected in HRSV rA2 infected A549 cell lysates and normalized to mock infected A549 cells. **B**. Down regulated protein analysed from HRSV rA2 infected A549 cell lysates and normalized to mock infected A549 cells.

A. Proteins up regulated during HRSV rA2 ΔSH infection.

Uniprot ID	Gene	Protein name	Log2 FC		−Log10 (P-value)	GOBP
			ΔSH	rA2		
P09913	IFIT2	Interferon-induced protein with tetratricopeptide repeats 2	2.6	2.0	6.2	Apoptotic mitochondrial changes
O95786	DDX58	Probable ATP-dependent RNA	5.5	5.2	5.2	Cytoplasmic pattern recognition receptor

		helicase				signalling pathway in response to virus
P17301	ITA2	Integrin alpha-2	2.3	1.7	4.6	Collagen-activated signalling pathway
P10909	CLUS	Clusterin	1.7	0.9	4.5	Chaperone-mediated protein complex assembly
Q9Y624	JAM1	Junctional adhesion molecule A	1.5	0.7	4.4	Cell-cell junction organization
O00194	RB27B	Ras-related protein Rab-27B	1.3	1.2	4.0	Intracellular protein transport
P24941	CDK2	Cyclin-dependent kinase 2	1.2	1.0	3.6	Anaphase-promoting complex-dependent proteasomal ubiquitin-dependent protein catabolic process
Q9NQ88	TIGAR	Fructose-2,6-bisphosphatase TIGAR	1.47	1.46	3.4	apoptotic process
P08648	ITA5	Integrin alpha-5	1.9	0.7	3.1	Virus receptor activity
Q7Z2W4	ZCCHV	Zinc finger CCCH-type antiviral protein1	1.0	0.7	2.9	Innate immune response

B. Proteins down-regulated during HRSV rA2 ΔSH infection.

Uniprot ID	Gene	Protein name	Log2 FC		−Log10 (P-value)	GOBP
			ΔSH	rA2		
Q9ULD2	MTUS1	Microtubule-associated tumour suppressor	-3.0	-2.5	2.7	Delays the progression of mitosis by prolonging metaphase and reduces tumour

						growth
P56211	ARP19	cAMP-regulated phosphoprotein	-2.8	-2.0	2.8	Cell division
Q9P013	CWC15	Spliceosome-associated protein CWC15 homolog	-2.4	-1.6	3.4	Gene expression
Q92823	NRCAM	Neuronal cell adhesion molecule	-2.2	-1.6	4.4	Clustering of voltage-gated sodium channels
Q16527	CSRP2	Cysteine and glycine-rich protein 2	-2.0	-1.6	2.4	Cell differentiation
Q8IVM0	CCD50	Coiled-coil domain-containing protein 50	-2.0	-1.4	2.5	Involved in EGFR (epidermal growth factor receptor) signalling.
P10109	ADX	Adrenodoxin, mitochondrial	-1.9	-1.4	2.5	C21-steroid hormone biosynthetic process
Q9ULW0	TPX2	Targeting protein for Xklp2	-1.8	-1.5	2.6	activation of protein kinase activity
Q8IWX8	CHERP	Calcium homeostasis endoplasmic reticulum protein	-1.6	-0.2	2.0	Cellular calcium ion homeostasis
P62158	CALM	Calmodulin	-1.1	-1.0	2.0	Control of a large number of enzymes, ion channels, aquaporins and other proteins by Ca^{2+}.

Table 4. 2 The top 10 most significant changes in protein abundance identified in A549 cells infected with HRSV rA2 ΔSH by label free protein quantification by MS.

Data were analysed from HRSV rA2 ΔSH infected A549 cell lysates and normalized to mock infected A549 cells. **A**. Top up regulated protein analysed from HRSV rA2 ΔSH infected A549 cell lysates and normalized to mock infected A549 cells. **B**. Down

regulated protein analysed from HRSV rA2 ΔSH infected A549 cell lysates and normalized to mock infected A549 cells.

A. Proteins up regulated during HRSV ΔSH eGFP infection.

Uniprot ID	Gene	Protein name	Log2 FC		−Log10 (P-value)	GOBP
			ΔSH eGFP	rA2		
P20592	MX1	Interferon-induced GTP-binding protein	6.2	5.9	7.7	Cytokine mediated signalling pathway
P05161	ISG15	Ubiquitin-like protein	6.0	5.6	6.0	Cytokine-mediated signalling pathway
GFP	AEQV		4.9	0.0	6.7	
O14879	IFIT3	Interferon-induced protein with tetratricopeptide repeats 3	4.4	4.2	8.1	Cellular response to interferon-alpha
P09914	IFIT1	Interferon-induced protein with tetratricopeptide repeats 1	3.7	2.8	3.3	Cellular response to exogenous dsRNA
Q460N5	PAR14	Poly [ADP-ribose] polymerase 14	3.7	3.5	4.0	Regulation of cellular transcription, DNA-dependent
Q00169	PIPNA	Phosphatidylinositol transfer protein	3.2	0.4	1.9	Sensory visual

		alpha isoform				perception
P05452	TETN	Tetranectin	2.8	2.3	4.2	Cellular response to organic substance
Q9Y6K5	OAS3	2'-5'-oligoadenylate synthase 3	2.477	2.472	3.1	Cytokine mediated signalling pathway

B. Proteins down-regulated during HRSV ΔSH eGFP infection

Uniprot ID	**Gene**	**Protein name**	**Log2 FC**		**−Log10 (P-value)**	**GOBP**
			ΔSH eGFP	**rA2**		
P20645	MPRD	Cation-dependent mannose-6-phosphate receptor	-1.0	-0.8	1.6	Endosome to lysosome transport
P61457	PHS	Pterin-4-alpha-carbinolamine dehydratase	-1.3	-0.6	2.1	Cellular nitrogen compound metabolic process
P62861	RS30	40S ribosomal protein S30	-1.3	-1.0	2.5	Innate immune response in mucosa
O75506	HSBP1	Heat shock factor-binding protein 1	-1.3	-1.1	1.8	Cellular response to heat stress
P18084	ITB5	Integrin beta-5	-1.4	-0.6	1.3	Epithelial cell-

						proliferation
Q7L9L4	MOB1B	MOB kinase activator	-1.5	0.0	2.9	Positive regulation of phosphorylation
P35237	SPB6	Serpin B6	-1.7	-0.8	3.4	Cellular response to osmotic stress
O43294	TGFI1	Transforming growth factor beta-1-induced transcript 1 protein	1.7	-1.3	4.1	Androgen receptor binding
Q5SSJ5	HP1B3	Heterochromatin protein 1-binding protein 3	-1.8	-0.8	2.7	Cellular response to hypoxia

Table 4. 3 The top 10 most significant changes in protein abundance of infected HRSV rA2 ΔSH eGFP identified by Label free protein quantification by MS.

Data were analysed from HRSV rA2 ΔSH eGFP infected A549 cell lysates and normalized to mock infected A549 cells. **A**. Top up regulated protein analysed from HRSV rA2 ΔSH infected A549 cell lysates and normalized to mock infected A549 cells. **B**. Down regulated protein analysed from HRSV rA2 ΔSH infected A549 cell lysates and normalized to mock infected A549 cells.

4.4.4 Validation of cellular proteins dysregulated during HRSV infection

Assessment of the cellular proteomic data sets did not reveal any significant changes in cellular ion channel expression induced by HRSV rA2, HRSV ΔSH or HRSV ΔSH eGFP compared to mock infected cells, or between HRSV rA2 or the ΔSH viruses. Given this lack of an effect, the proteomic data sets were re-examined for the dysregulation of cellular proteins that may exhibit altered expression levels as the downstream targets of an altered ionic conductance. Few cellular proteins matched this criterion. However, in the quantitative proteomics analysis of A549 cells infected with HRSV rA2, HRSV

ΔSH and HRSV ΔSH eGFP viruses, the cellular protein calmodulin was consistently identified as being down regulated during virus infection compared to mock infected cells (shown in Figure 4.15).

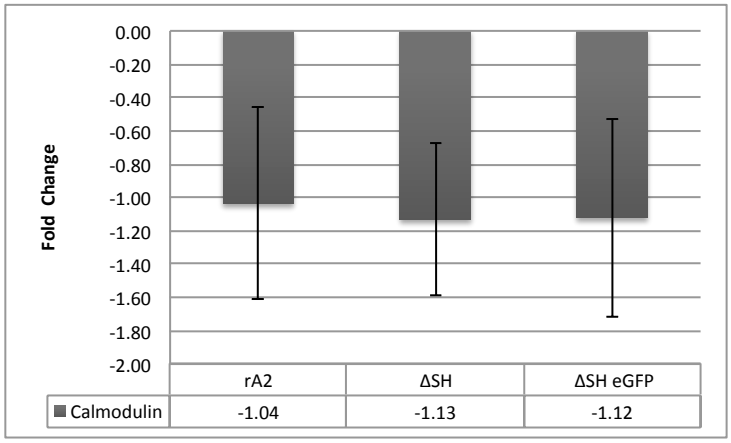

Figure 4. 15. LC-MS/MS quantification of calmodulin (CaM) protein of label-free samples.

Log_2 fold change of CaM protein of each sample of label free infected A549 (rA2, ΔSH, ΔSH eGFP). Each value of normalized abundance were averaged and normalised by mock and calculated as a log_2 fold change. All 3 samples are significantly down regulated compared to mock, (n=3).

Calmodulin (CaM; calcium-modulated protein) is a multifunctional intermediate Ca^{2+} binding messenger protein that is part of the calcium signal transduction pathway (Stevens, 1983). CaM regulates key cellular functions known to be modulated during HRSV infection, including apoptosis, inflammation and cell metabolism (Zhou et al., 2009). In addition, CaM has been demonstrated to be modulated by several viruses including rubella virus (RUBV), HIV-1, Simian immunodeficiency virus (SIV) (Zhou et al., 2007; Radding et al., 2000; Yuan et al., 1995). Despite CaM expression being down regulated in response to infection with all three viruses, CaM was selected as a protein of interest due to this consistent trend, and suitable to validate the proteomic data sets.

CaM expression was first assessed by Western blot analysis from A549 infected cell and mock-infected lysates. CaM expression was quantified using the LiCor Odyssey Infrared imaging system (LiCor) and normalised to GAPDH expression. Figure 14.16A shows that CaM expression decreased during HRSV, ΔSH and ΔSH eGFP infection and this was confirmed by quantification of the blot (Figure 4.16B). This outcome was consistent with the proteomic data,

and thus we conclude that while HRSV rA2, ΔSH and ΔSH eGFP were all capable of down regulating CaM expression, confirming this effect to be virus specific, this down regulation was not influenced by the expression the HRSV-SH protein.

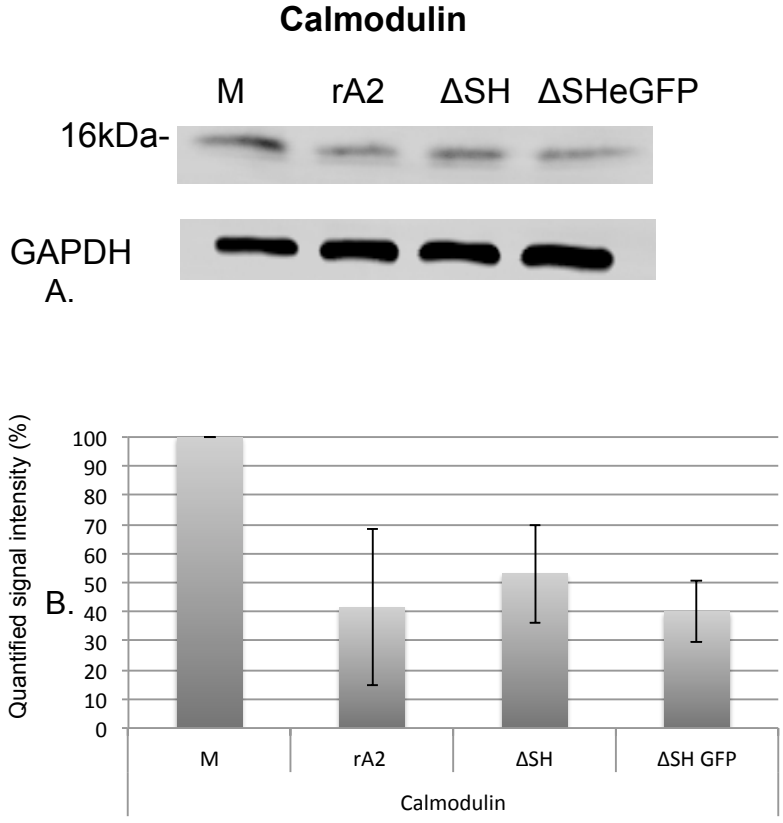

Figure 4. 16. Validation of calmodulin expression during HRSV infection by western blot analysis.

A549 lysates from cells infected with recombinant HRSV (rA2, ΔSH, and ΔSH eGFP) at an MOI of 1.0 for 24 hours. Lysates were resolved by SDS-PAGE and calmodulin expression was assessed using rabbit anti-calmodulin primary antibodies. GAPDH was probed as a loading control. **A**. WB of identified calmodulin protein in each HRSV recombinant type (rA2, ΔSH and ΔSH eGFP). **B.** For each cell lysate, the identified calmodulin protein band was quantified using the LiCor Odyssey Infrared imaging system (LiCor). Plotted values represent a mean calculated from n=5.

4.4.5. Comparison between HRSV rA2 vs HRSV ΔSH cellular proteins of proteomic analysis

Further examination of the proteomics data was performed to reveal differences in cellular protein expression levels between the HRSV rA2 and HRSV ΔSH infected cells. To simplify the analysis, this comparison was done between HRSV rA2 and HRSV ΔSH only, and not between HRSV rA2 and ΔSH eGFP, because the two SH-deleted viruses exhibited very similar cellular proteome changes to each other. All cellular proteins with fold changes of ± 2 and significance levels of $p < 0.05$ were examined and these are plotted as up- or down-regulated proteins normalized in each case to the protein abundance detected in mock infected cells (Figures 4.17 and 4.18). These histograms shows several cellular proteins were detected that showed some variances in fold change in A549 cells infected with both virus types, HRSV rA2 and HRSV ΔSH. However it was notable that no cellular proteins showed fold changes that were above 4 fold, and the majority of fold changes were slight. Several of these possibly dysregulated proteins are known to be highly abundant cell components that are frequently identified in similar proteomics studies, and it has been suggested that their frequent identification as being dysregulated may be due to their high abundance, and subsequent errors in protein quantification. One such protein is integrin alpha-5, and on this basis, it was discounted from further validation analysis. Additional cellular proteins such as ribosome maturation protein SBDS were also detected as being dysregulated, but where the known function of the identified protein did not correlate or align with the known requirements or effects of the HRSV life cycle, these proteins were also discounted from further validation studies.

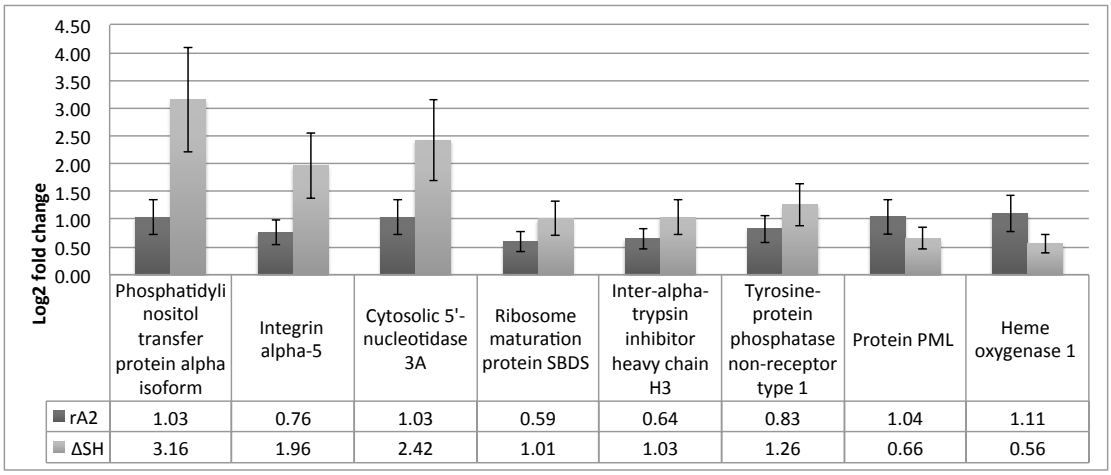

	Phosphatidylinositol transfer protein alpha isoform	Integrin alpha-5	Cytosolic 5'-nucleotidase 3A	Ribosome maturation protein SBDS	Inter-alpha-trypsin inhibitor heavy chain H3	Tyrosine-protein phosphatase non-receptor type 1	Protein PML	Heme oxygenase 1
rA2	1.03	0.76	1.03	0.59	0.64	0.83	1.04	1.11
ΔSH	3.16	1.96	2.42	1.01	1.03	1.26	0.66	0.56

Figure 4. 17. Up regulated proteins of cellular changes between infected HRSV rA2 and HRSV ΔSH.

Data were obtained from proteomics data and each protein abundance was averaged from n=3 and normalized to protein abundance in mock infected cells.

In order to focus subsequent validation experiments to independently confirm changes in protein abundances that were likely to be relevant, cellular proteins with known associations with cellular functions influenced by changes in ionic flux were selected. These included calcium homeostasis endoplasmic reticulum protein (CHERP), which showed considerably reduced expression in HRSV ΔSH infected cells compared to HRSV rA2 (Figure 4.18). CHERP is a regulator of agonist-evoked Ca^{2+} signalling, and is involved in cell proliferation and growth as it has in impact on the Ca^{2+} mobilization in the cell. Reduction or inhibition of CHERP expression could decrease cell proliferation (Laplante et al., 2000). Attempts were made to validate CHERP expression levels in HRSV rA2 and HRSV ΔSH infected cells by western blotting, however, these were unsuccessful most likely due to poor performance of the CHERP antibodies obtained from multiple sources.

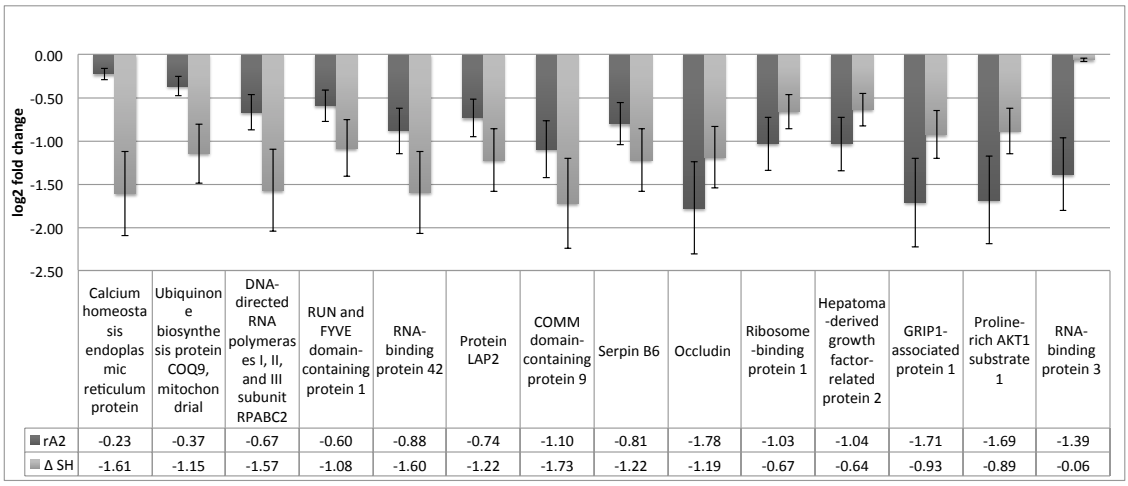

	Calcium homeostasis endoplasmic reticulum protein	Ubiquinone biosynthesis protein COQ9, mitochondrial	DNA-directed RNA polymerases I, II, and III subunit RPABC2	RUN and FYVE domain-containing protein 1	RNA-binding protein 42	Protein LAP2	COMM domain-containing protein 9	Serpin B6	Occludin	Ribosome-binding protein 1	Hepatoma-derived growth factor-related protein 2	GRIP1-associated protein 1	Proline-rich AKT1 substrate 1	RNA-binding protein 3
rA2	-0.23	-0.37	-0.67	-0.60	-0.88	-0.74	-1.10	-0.81	-1.78	-1.03	-1.04	-1.71	-1.69	-1.39
Δ SH	-1.61	-1.15	-1.57	-1.08	-1.60	-1.22	-1.73	-1.22	-1.19	-0.67	-0.64	-0.93	-0.89	-0.06

Figure 4. 18. Down regulated proteins of cellular changed between infected HRSV rA2 and HRSV ΔSH.

Data were obtained from proteomics data and each protein abundance was averaged from n=3 and normalized to protein abundance in mock infected cells.

An additional protein that exhibited dysregulation in A549 cells infected with HRSV rA2 compared to HRSV ΔSH, and has known functions that are linked to altered ion flux, is heme oxygenase 1 (HO-1) (4.17). This protein is induced by oxidative stress (Choi and Alam, 1996), as well as the CaM-dependent protein kinase II (Kim et al., 2010). HO-1 expression was increased in the HRSV rA2 infected cells (log_2[1.1] = 2.1 fold) and also increased, but to a lesser extent in HRSV ΔSH infected cells (log_2[0.56] = 1.5 fold). Because of these small differential abundance changes that did not suggest a dramatic influence on cellular processes, HO-1 expression was not validated further. In addition, the other cellular proteins shown in Figures 4.17 and 4.18 were similarly judged to not represent attractive targets for further validation experiments due to either lack of functional significance or low differential fold changes.

4.6. Summary and discussion

4.6.1. The influence of ion channel modulation on HRSV lacking (SH) in A549 cells

Ion channels regulate a range of important cellular activities and emerging work has linked ion channel modulation as a virus-host interaction, important for virus entry (Dimitrov, 2004; Tsai, 2007; Grove and Marsh, 2011), viral release and replication (Sze and Tan, 2015; Van Kuppeveld et al., 1997). The importance of these interactions is highlighted by the fact that specific ion channel modulating compounds can impede virus infection (Hover et al., 2015; Igloi et al., 2015). In this regard, the data presented in Chapter 3 revealed for the first time that HRSV infection could be inhibited by specific ion channel modulating drugs including DIDS and $BaCl_2$. HRSV-SH has been classified as a viroporin, reported to alter membrane permeability and display the properties of a cation-selective ion channel (Gan et al., 2008). In this Chapter, the effects of deletion of HRSV-SH (reported not to influence viral replication *in vitro*) were investigated to see if its deletion during HRSV infection altered the HRSV sensitivity to cellular ion channel modulation.

The data revealed that $BaCl_2$ (a Kir modulator), ruthenium red (a K_{2P} modulator), high concentrations of TEA (a broad spectrum K^+ channel inhibitor) and Haloperidol (known to inhibit a range of K^+ channels including Kv, calcium-activated, and K_{2P} channels) could significantly inhibit HRSV viruses that lacked the SH protein when added at the time of virus entry. Of the other drugs assessed, 5mM TEA, ruthenium red, glibenclamide (an ATP-sensitive K^+ channel blocker) and sotalol (a Kv blocker) also were found to influence HRSV ΔSH when added at the post entry stages. Upon comparison of this data set to rA2 HRSV, a common cluster of K^+ channels that could influence HRSV ΔSH but not rA2 HRSV were not definitively identified. However, haloperidol and ruthenium red when added pre- and post-entry did impede HRSV ΔSH but not rA2 HRSV implicating that HRSV replication is inhibited by these compounds only when SH is deleted. Haloperidol and ruthenium red (whilst not completely selective for this channel family) are known modulators of K_{2P} channels. Studies

by Hover et al 2015 found that the functionality of K_{2P} channels is required to regulate the early entry processes of bunyamwera virus (BUNV) infection (a negative sense RNA virus that apparently lacks a viroporin). Given the effects of K_{2P} modulation only when SH is absent, it is interesting to speculate that HRSV-SH by some process, mediates K^+ fluxes that can substitute K_{2P} functionality and allow HRSV WT to be K_{2P} channel independent. Since BUNV appears to lack viroporin activity, asensitivity to this channel family (although at a different stage to that observed for HRSV) remains. Why K_{2P} channels would influence HRSV-ΔSH replication specifically is as yet unidentified, but this data is suggestive that HRSV-SH performs a cellular role shared by specific K_{2P} channel members. In this regard, a key feature of the 15 identified K_{2P} channels is their ability to be regulated by intracellular/organelle pH, also previously demonstrated for HRSV-SH (D O'Connell et al., 2002). Future studies investigating the cellular role of the haloperidol and ruthenium red sensitive K_{2P} channel family members (including the ability to leak K^+ across intracellular membranes) may reveal new insights into potential new roles of both HRSV-SH and ionic homeostasis mediated by viroporins may emerge.

Of the other channel families investigated, lidocaine, an inhibitor of voltage gated Na^+ channels significantly lowered virus infection when included either early or 3 hpi. However TTX showed no effect of the HRSV-ΔSH lifecycle. Activating voltage gated Ca^{2+} notably reduced HRSV-ΔSH infection following treatment either pre or post virus infection suggesting that increasing cell surface Ca^{2+} influx impedes the growth of HRSV-ΔSH. Most importantly, DIDS, as reported for HRSV WT, was inhibitory to HRSV-ΔSH entry, whilst other broad spectrum inhibitors including NPPB had no effects. Moreover, DIDS did not affect HRSV-ΔSH when added post entry confirming its ability to impede HRSV at this stage of the virus lifecycle, regardless of the presence of HRSV-SH.

4.6.2 Global proteins mediated by the viroporin SH during HRSV infection

Whilst differences in the growth kinetics between HRSV rA2 and mutant HRSV ΔSH were not observed in A549 cells, the global proteomic changes observed during infection of these viruses was assessed to reveal if deletion of HRSV-SH was able to influence the induction or repression of specific cellular pathways. This analysis was performed using label-free MS, in triplicate to allow for statistical significance to be assigned to the resulting data sets. Unsurprisingly, given the comparable growth kinetics of all viruses assessed, recombinant HRSV and the two ΔSH-deleted viruses induced comparable proteomic changes, and clear or large-scale dysregulation of any specific cellular proteins by one or other of these virus types was not observed.

Given our previous findings that the HRSV SH protein alters ion channel modulator sensitivity, the identification of CaM within the dysregulated cellular proteins following HRSV infection was interesting, although it was significantly down-regulated in both WT and ΔSH virus types, When CaM expression was assessed by western blot analysis the outcome showed reduced CaM expression across all virus strains, thus coinciding with the quantification of CaM by proteomic analysis, and validating the dataset. Whilst this suggests HRSV-SH does not mediate CaM down-regulation, it is interesting that HRSV would down-regulate CaM expression, since both rotavirus and HIV require CaM functionality to complete their virus lifecycles (Micoli et al., 2000). Given this finding it would be interesting to speculate that HRSV infection could be promoted by CaM inhibition (for example through treating cells with the CaM inhibitor (W-7) resulting in increased viral titres. If this was the case, the recovery of CaM functionality would be expected to be inhibitory to HRSV, never previously reported for any virus infection. Thus, CaM functionality represents a new anti-HRSV target worth further assessment in future studies.

Taken together, these data show that both rA2 and HRSV ΔSH display similar growth kinetics in A549 cells, suggesting that HRSV-SH does not heavily influence HRSV infection in this cultured cell line. HRSV lacking HRSV-SH was identical to HRSV WT to some cellular ion channel modulators including DIDS,

but additionally enhanced HRSV sensitivity to K_{2P} channel modulation, suggesting that HRSV-SH may impart some protection from K_{2P} channel inhibition during HRSV replication.

As expected, and consistent with a minimal role of HRSV-SH during HRSV growth in A549 cells, the proteomic data sets revealed only modest proteomic changes specifically mediated by HRSV-SH, but did identify CaM as cellular factor targeted for HRSV down-regulation regardless of the presence or absence of HRSV-SH. This may infer that CaM down-regulation promotes HRSV infection but this requires further confirmation. Taken together, these findings, coupled to the knowledge that HRSV-SH is required for efficient virus propagation *in vivo* but not *in vitro* suggests that A549 cells may not represent an ideal cell line to assess HRSV-SH functionality during virus infection. More representative models of HRSV infection in airway primary cells may be more reflective of HRSV infection, and thus required to reveal the functionality of HRSV-SH during the virus lifecycle.

Proteomics data also reveals broad increases or decrease in abundance in the a protein known to involve in antiviral response including interferons stimulated genes found in the infected rA2 and deleted SH HRSV, the flowing table 4.4 shows the most significant interferons.

Uniprot ID	Gene	Protein name	Log2 FC		−Log10 (P-value)
			rA2	ΔSH	
P20591	MX1	Interferon-induced GTP-binding protein	5.9	5.7	7.7
O14879	IFIT3	Interferon-induced protein with tetratricopeptide repeats 3	4.2	4.3	8.1
P09914	IFIT1	Interferon-induced protein	2.9	3.2	3.3

		with tetratricopeptide repeats 1			
Q9Y6K5	OAS3	2'-5'-oligoadenylate synthase 3	2.5	2.0	3.1
P09913	IFIT2	Interferon-induced protein with tetratricopeptide repeats 2	2	2.6	6.3
P19525	E2AK2	Interferon-induced, double-stranded RNA-activated protein kinase	1.3	1.1	3.9
Q7Z5L9	I2BP2	Interferon regulatory factor 2-binding protein 2	1.3	-1.0	2.1

Table 4. 1 Stimulated interferons found in the proteomics data in the infected A549 cell with HRSV rA2 and HRSV rA2 ΔSH.

Chapter 5: investigating the role of HRSV-SH during virus infection in human bronchial epithelial primary cells

Chapter 5: Investigating the role of HRSV-SH during virus infection in Human bronchial epithelial primary cells

5.1. Introduction

From previous chapters, data was obtained from HRSV infection in A549 cells, the cell line of choice for numerous HRSV studies (Fiedler et al., 1995; Martinez et al., 2007; Munday et al., 2010). Cell lines such as A549s are often used as models for primary cells, as they were derived from a type II pneumocyte lung tumour by Giard et al. in 1972 and have since been used for many studies of virus-host interactions. A549s are easier to culture than primary cells, have a higher proliferation rate, and are able to maintain their phenotype under cell culture conditions (Swain et al., 2010). However, a weakness of A549s is that these properties mean they are not consistent with the true phenotype of their primary counterparts. HBEpCs are advantageous when compared to A549s as these primary cells are obtained from the bronchial epithelium surface of healthy human adults (Bernacki et al., 1999). These cells therefore reflect the surface epithelium of human bronchi more accurately, and HRSV-mediated cellular changes in these cells are more likely to closely reflect key virus-host interactions that occur during *in vivo* HRSV infection.

In this chapter, the results obtained in Chapters 3 and 4 were reassessed during HRSV growth in primary HBEpC cells. Firstly, the role of cellular ion channels during HRSV infection was assessed to observe if the phenotypes of ion channel dependence were conserved in HBEpCs. Secondly, this chapter repeated the proteomic analysis during HRSV infection in the presence and absence of the SH protein by comparing the cellular proteome of cells infected with either recombinant HRSV or ΔSH viruses. This was again performed using the label free proteomic approaches described for A549s in Chapter 4. Where appropriate, the identified up/down-regulated proteins were confirmed by

western blot analysis to validate these proteomic changes. This chapter reveals critical information regarding differences between HRSV-host interactions between A549 cells and HBEpCs. It is concluded that the HBEpCs provide information that is likely to be more applicable to *in vivo* HRSV infection.

5.2. Optimisation of HRSV infection in HBEpCs

5.2.1. Assessment of HRSV infection in HBEpCs

HBEpCs were obtained from the European collection of cell culture (ECACC) that operates through Public Health England (PHE). HBEpCs were grown in bronchia/trachea epithelial growth media (serum free) for 4-5 passages. Consistent with previous reports (Wu et al., 2011), HBEpCs displayed reduced proliferation when compared to A549 cells.

HBEpCs were infected with HRSV (MOI=1) for 3, 6, 12, 24, 48 or 72 hours to assess both their permissiveness to HRSV infection and to establish whether the timeline of infection was comparable to that seen in A549 cells. HBEpCs were infected with HRSV A2 WT, HRSV rA2, HRSV rA2 ΔSH and HRSV rA2 ΔSH eGFP to ensure all virus strains displayed comparable growth kinetics. HRSV infection was assessed by IF analysis as described in Chapter 3 section 3.2.2.

Figure 5.1 shows that both wild type (left panel) and recombinant (right panel) HRSV rA2 display similar levels of infection which was evident as early as 3 hpi when viral proteins were detectable. As expected, the levels of HRSV staining increased 6-12 hpi, corresponding to increased virus gene expression during this timeframe. At 24 hpi, the number of infected cells and fluorescent intensity of HRSV proteins increased, and continued to increase 48-72 hpi consistent with further increases in gene expression, and then spread of HRSV to infect new cells within the culture. Infected cells were enlarged, and displayed the characteristic fusion phenotype associated with HRSV induced syncytia formation from 24 hpi as previously described (Kotelkin et al., 2003) (Figure 5.1). Importantly, HRSV ΔSH (Figure 5.2 left panel) and HRSV ΔSH eGFP (Figure 5.2 right panel) displayed no reduction in infection kinetics when

compared to WT HRSV in HBEpCs, as evidenced by the comparable levels of HRSV staining throughout the time course of infection. Figure 5.3 shows the total number of A549 and HBEpC cells infected with HRSV WT following infection with an MOI of 1. After 24 hpi, 19% of A549 cells were infected in comparison with mock-infected A549 cells, whereas 16.7% of HBEpCs were HRSV positive in comparison with mock-infected HBEpCs. Taken together these data indicated that the growth kinetics of all HRSV strains used in this study exhibited comparable growth kinetics in both A549s and HBEpCs.

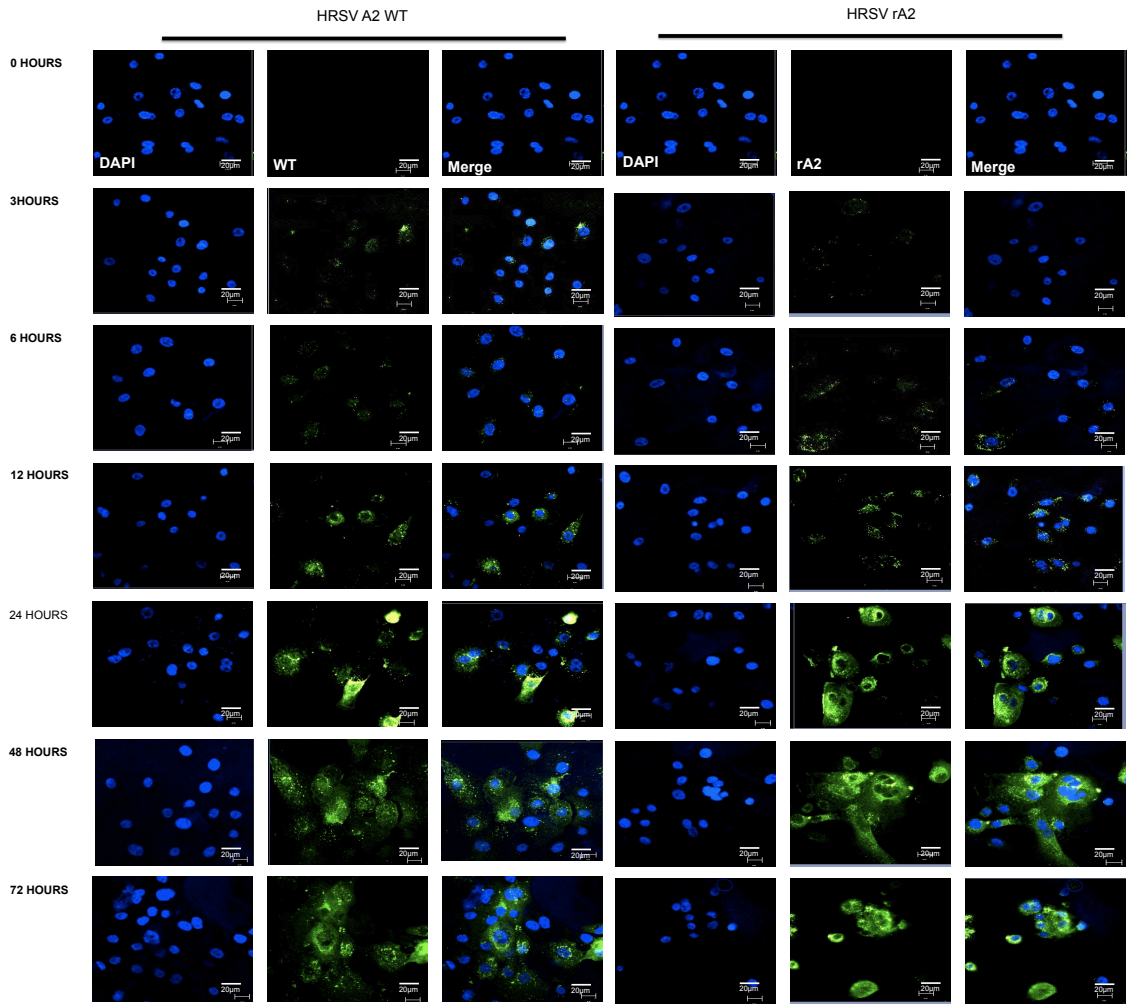

Figure 5. 1. Representative IF images of HBEpCs infected with HRSV WT and recombinant HRSV strains.

Cells were fixed and imaged 3, 6, 12, 24, 48 and 72 hpi at an MOI 1.0. Cells were labelled with FITC conjugated anti-RSV antibodies (green) and the nucleus stained with DAPI. Images were taken using the Zeiss upright LSM 510 META Axioplan microscope. Representative images for each time point are shown. Scale bar = 20μm.

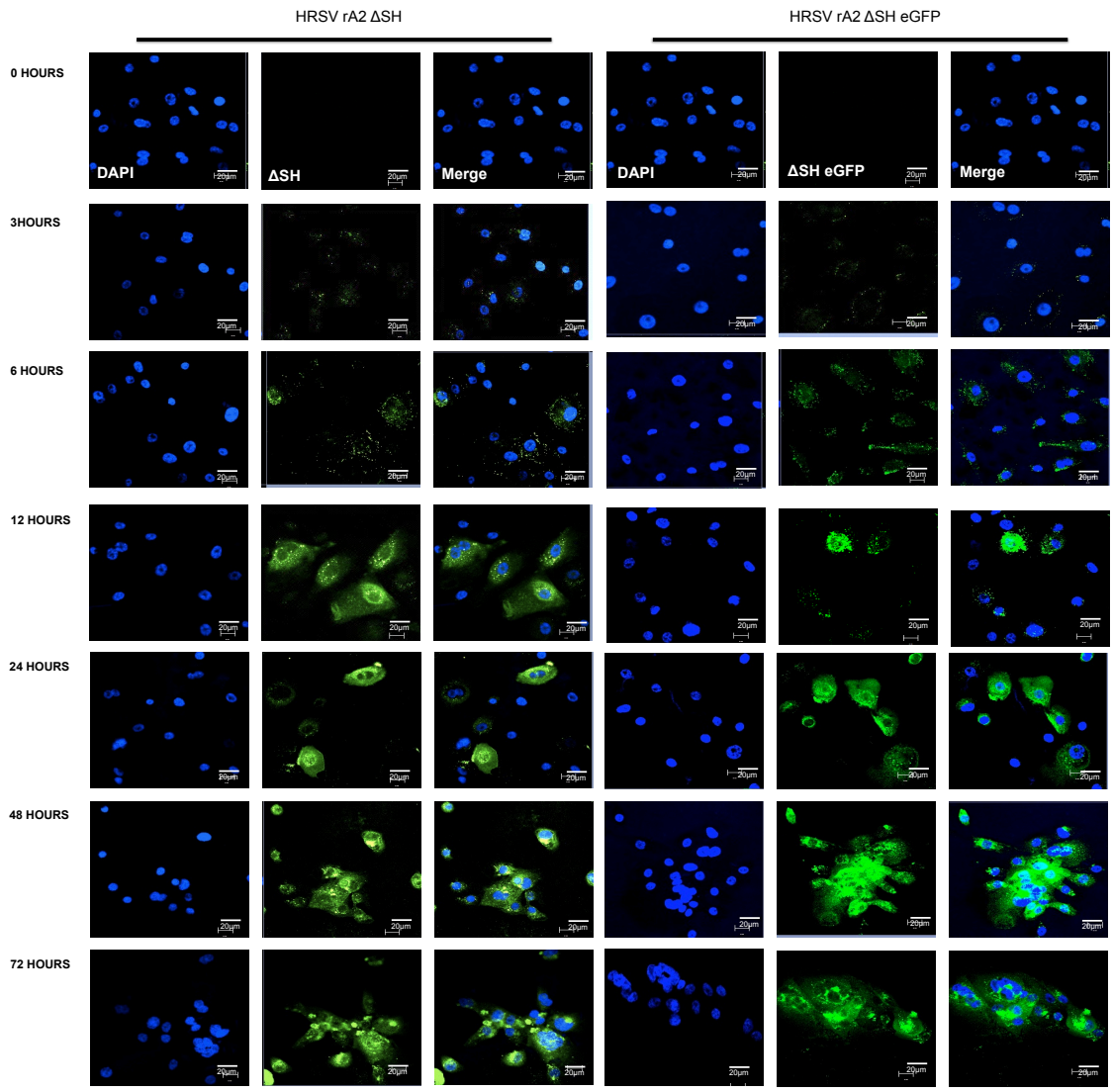

Figure 5. 2. Representative IF images of HBEpCs infected with HRSV ΔSH and HRSV ΔSH eGFP strains.

Cells were fixed and imaged 3, 6, 12, 24, 48 and 72 hpi at an MOI 1.0. Cells were labelled with FITC conjugated anti-RSV antibodies (green) and the nucleus stained with DAPI. Images were taken using upright LSM 510 META Axioplan microscope. Representative images for each time point are shown. Scale bar = 20μm.

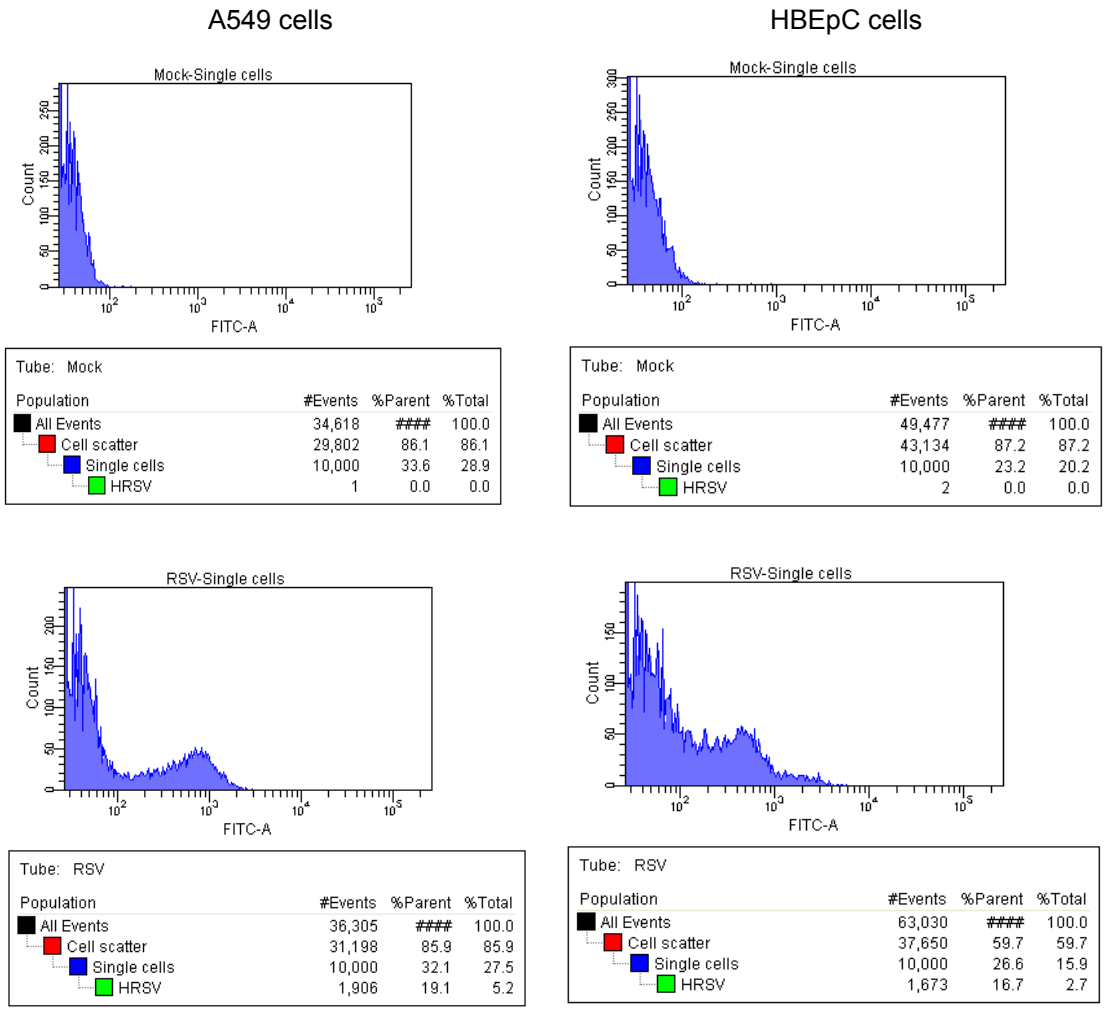

Figure 5. 3. Comparison of the HRSV infection levels between HBEpCs **and A549s.**

Representative FACS plots from HRSV WT infected cells (MOI = 1, 24 hpi). Top left panel represents Mock infected A549 cells. Bottom left panel represents HRSV infected A549 cells. Top right panel represents Mock infected HBEpCs. Bottom left panel represents HRSV HBEpCs. Infected cells showed a rightward shift (shown in bottom graphs) indicating fluorescently labelled cells.

5.3. Analysis of HBEpC cell viability treated with cellular ion channel modulating drugs

HBEpCs express an array of ion channels and transporters (Hollenhorst et al., 2011) that perform many crucial physiological functions including the regulation of ion transport and mucus fluidity. Cancer cell lines such as A549 cells are known to express ion channels that may not be present in their primary counterparts. Examples include the overexpression of NaV channels in breast cancer lines (Roger et al., 2015). It was therefore important to assess if the effects of the ion channel modulator panel assessed in Chapter 3 displayed comparable effects in HBEpCs.

Since modulation of channels in primary tissue can imbalance ionic homeostasis, the effects of the ion channel modulator panel on cell viability was reassessed as described in Chapter 3. To select concentrations of ion channel modulators that would be applicable for their assessment on HRSV infection in HBEpCs, MTT assays were performed following treatment of cells for 24 hours with each of the K^+, Ca^{2+}, Na^+ and Cl^- modulators described in Chapter 3 (section 3.3) where non-toxic cell represent equal or more than 80% of cell proliferation. Figure 5.4 shows the corresponding non-toxic concentrations of K^+ channel modulators in A549 cells, most notably 50μM glibenclamide (Glib = 47.6% ± 52.4% decrease), 200 μM tolbutamide (Tol = 70% ± 30% decrease), 5 μM haloperidol (Halo = 70.4% ± 29.6% decrease) and were highly toxic to HBEpCs. Table 5.1 shows a comparison of the highest concentration of K^+ channel drugs treated in A549 and HBEpC cells.

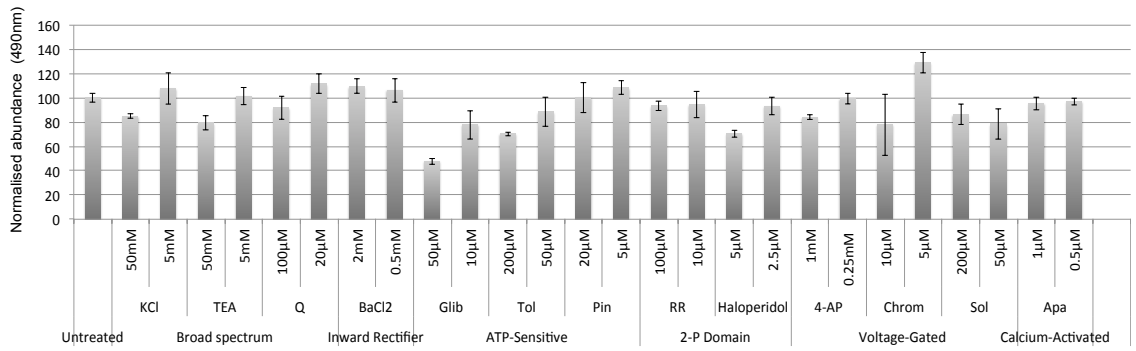

Figure 5. 4. Assessment of cell viability in the presence of K^+ channel modulators in HBEpC cells.

HBEpC cells were treated with the indicated concentrations of K^+ ion channel modulators for 24 hours and the cell viability assessed by MTT assays. Cells were treated with modulators of all the major K^+ channel families. Each drug concentration was assessed in triplicate (n=3).

Ion channel modulator	Prefix	Non- toxic drug concentration in A549s	Non- toxic drug concentration in HBEpCS
Potassium chloride	KCl	25mM	50mM
Tetraethylammonium	TEA	50mM-10mM-5mM	50mM-5mM
Quinine	Q	100µM	100µM
Barium Chloride	$BaCl_2$	2mM	2mM
Glibenclamide	Glib	50µM	10µM
Tolbutamide	Tol	200µM	50µM
Pinacidil	Pin	20µM	20µM
Ruthenium red	RR	100µM	100µM

Halothane	Hal	5μM	2.5μM
4- Aminopyridine	4-AP	1mM	1mM
Chromanol 293B	Chrom	40μM	5μM
Sotalol	Sot	200μM	200μM
Apamin	Apa	1μM	1μM

Table 5. 1. Comparison of the highest non-toxic concentrations of K^+ channel modulators in A549 vs. HBEpCs.

When the Na^+ channel modulators were assessed, similar toxicity profiles were observed between A549 and HBEpCs (Figure 5.5). Table 5.2 shows the highest non-toxic concentrations of Na^+ channel modulators in HBEpCs and A549s.

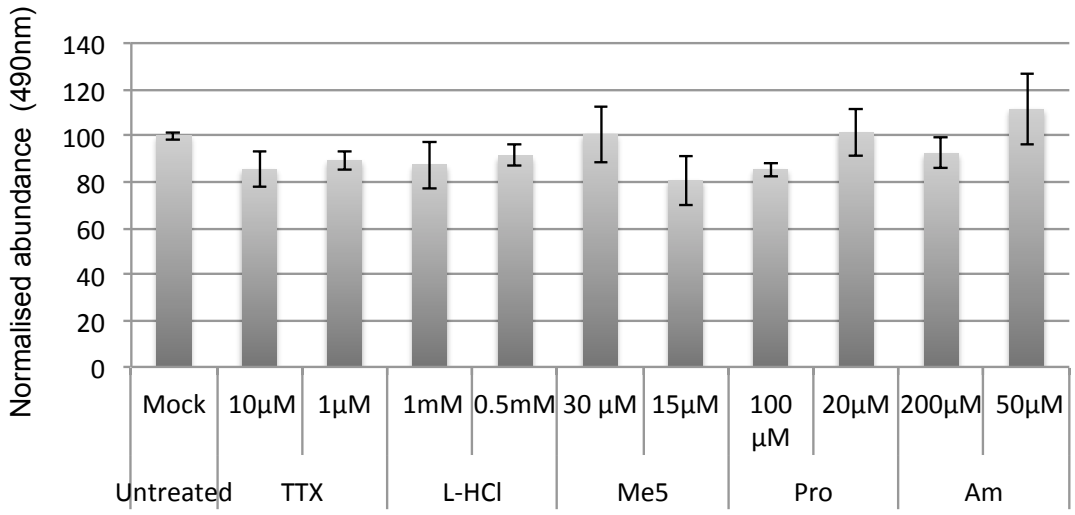

Figure 5. 5. Cellular toxicity of Na^+ ion channel modulators in HBEpC cells.

HBEpC cells were treated with the indicated concentrations of several ion channel modulators for 24 hours and the cell viability assessed by MTT assay. Each drug concentration was assessed in triplicate (n=3).

Name of the ion channel modulator	Prefix	Drug concentration used A549	Drug concentration used HBEpC
Tetrodotoxin	TTX	10µM	10µM
Lidocaine *N*-ethyl bromide	L-HCl	1mM	1mM
R(-) Me5	Me5	30µM	30µM

Hydriodide			
Procainamide hydrochloride	Pro	100µM	100µM
Amiloride HCL	Am	200µM	200µM

Table 5. 2. Comparison of highest non-toxic Na^+ ion channel modulators concentrations in A549 and HBEpC cells.

Of the Ca^{2+} channel modulators assessed, most were toxic to HBEpCs at concentrations that were non-toxic to A549 cells, namely 100 µM 2APB (47.4% ± 52.2% decrease), 10 µM Nitrendipine (61.6% ± 38.4% decrease), 20 µM Nifedipine (42.1% ± 57.9% decrease), 20 µM Nimodipine (63.3% ± 36.7% decrease) and 20 µM Bay K8644 (41.7% ± 58.3% decrease) (see Figure 5.6). Only Verapamil (an inhibitor of L-type (long-lasting and T (transient) - Ca^{2+} channel) was non-toxic to HBEpCs at comparable concentrations to A549s (see Table 5.3).

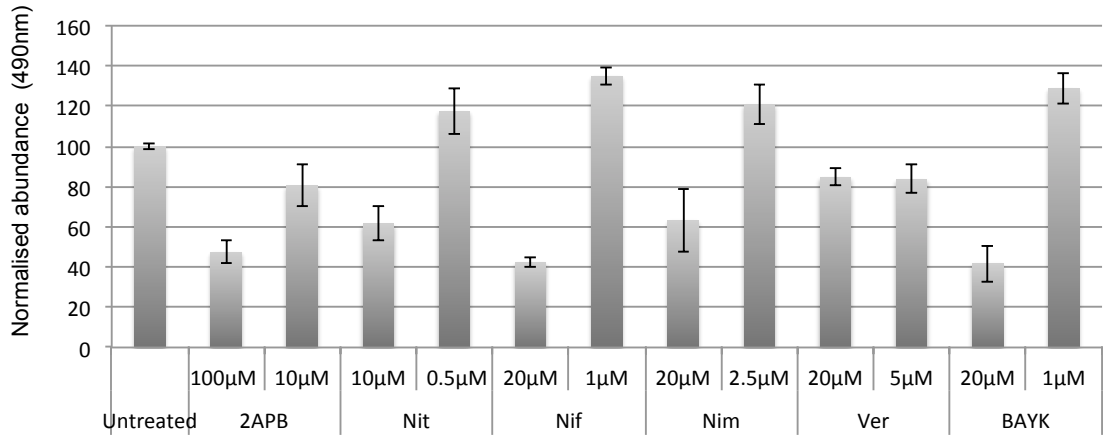

Figure 5. 6. Cellular toxicity of Ca^{2+} ion channel modulators in HBEpCs.

HBEpCs were treated with the indicated concentrations of Ca^{2+} channel modulators for 24 hours and the cell viability assessed by MTT assay. Each drug concentration was assessed in triplicate (n=3).

Name of the ion channel modulator	Prefix	Drug concentration used A549	Drug concentration used HBEpC
2-Aminoethoxydiphenylborane	2APB	100μM	10μM
Nitrendipine	Nit	10μM	0.5μM
Nifedipine	Nif	20μM	1μM
Nimodipine	Nim	20μM	1.5μM
Verapamil	Ver	20μM	20μM
Bay K8644	Bay K	20μM	1μM

Table 5. 3. Comparison of highest non-toxic Ca^{2+} ion channel modulators concentrations in A549 and HBEpC cells.

Of the Cl^- modulators assessed, the concentrations of DIDS, RIAA and NPPB (Figure 5.7) that displayed no toxicity in A549 cells, were highly toxic to HBEpCs (200μM DIDS = 38.3% ± 61.7% decrease; 100μM RIAA = 42.2% ± 5 7.8% decrease; 50μM NPPB = 38% ± 62% decrease) illustrated in Figure 5.7). These drugs were assessed at lower concentrations until a non-toxic

concentration was obtained. Table 5.4 shows the highest non-toxic concentrations of the Cl^- channel modulators used in HBEpCs and A549s.

As confirmation, RBV toxicity was assessed in HBEpCs at the concentrations described as inhibitory to HRSV in A549 cells. Treatment of HBEpCs with 500μM and 250μM RBV displayed no loss in viability compared to no-drug controls (Figure 5.8).

Taken together the altered toxicity profiles of the channel modulators were suggestive that HBEpCs display differences in their ion channel expression profiles when compared to A549s. Non-toxic concentrations of each modulator were taken forward for their analysis on HRSV infection in HBEpCs.

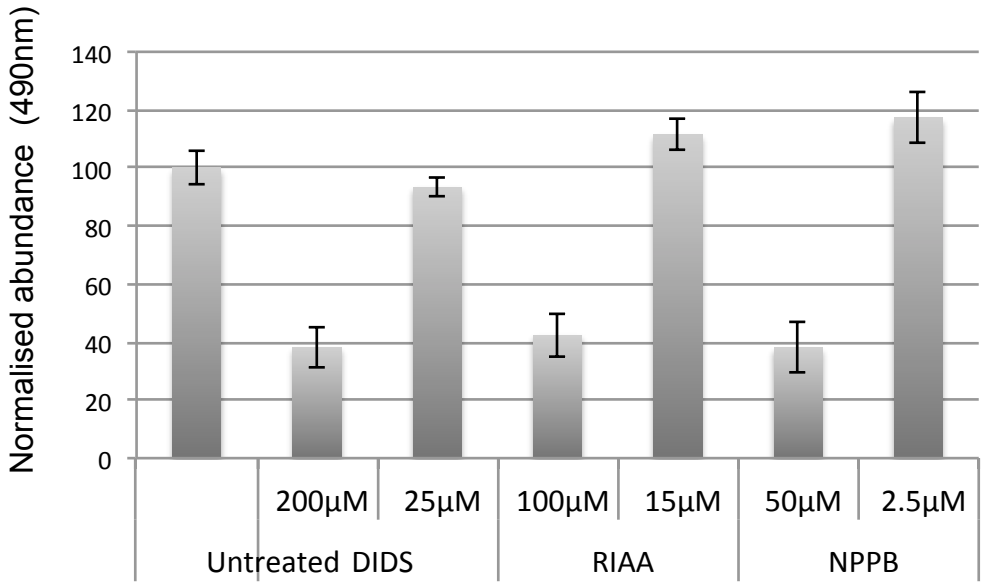

Figure 5. 7. Cellular toxicity of Cl^- channel modulators in HBEpCs.

HBEpCs were treated with the indicated concentrations of Cl^- channel modulators for 24 hours and cell viability assessed by MTT assay. Each drug concentration was assessed in triplicate (n=3).

Name of the ion channel modulator	Prefix	Drug concentration used A549	Drug concentration used HBEpC
4,4'-diisothiocyanatostilbene-2,2'-disulfonic acid disodium salt hydrate	DIDS	200μM	25μM
R(+)IAA-94	RIAA	100μM	15μM
5-Nitro-2-(3-phenylpropylamino) benzoic acid	NPPB	50μM	2.5μM

Table 5. 4. Comparison of highest non-toxic Cl^- ion channel modulators concentrations that used and treated in A549 and HBEpC cells

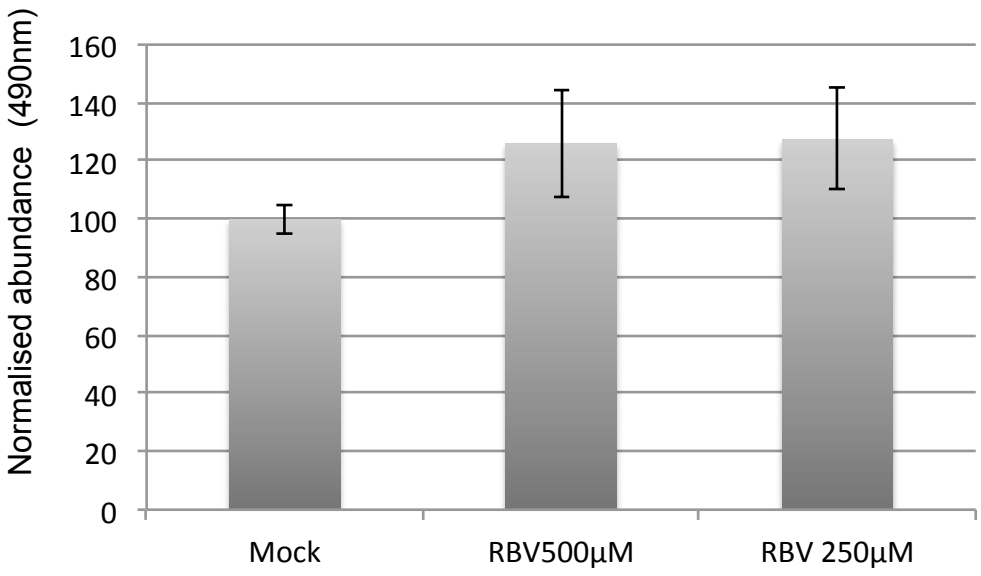

Figure 5. 8. Assessment of cell viability in response to RBV treatment of HBEpCs.

Cells were treated with 500μM and 250μM RBV for 24 hours then cell viability was assessed by MTT assay (n=3).

5.4. Assessment of cellular ion channel modulation on HRSV in HBEpCs

The results of Chapter 3, in which the effects of cellular ion channel modulation during HRSV infection in A549 cells were tested, indicated a role for DIDS sensitive Cl^- channels, and to a lesser degree Kir channels during the very early stages of HRSV infection. The ion channel modulator screen was re-assessed in primary HBEpCs to confirm that HRSV infection was similarly sensitive to Cl^- channel modulation, and insensitive to the channel modulators of other families described in Chapter 3.

HRSV infection of cells in culture was assessed in the presence of non-toxic concentrations of each individual ion channel modulator. The effect of cellular ion channels was screened at two time points during HRSV infection. For assessment of the effects following virus attachment/entry and during HRSV WT replication/later stages of infection, ion channel modulators were added 3 hpi, and the percentage of HRSV infected cells assessed 24 hpi. For pre-drug treatments, ion channel modulators were added 45-60 minutes prior to infection, and the percentage of HRSV infected cells assessed 24 hpi. HRSV infection levels were assessed by FACS analysis as described in Chapter 2 (section 2.2.5).

5.4.1. Effects of K^+ modulation on HRSV infection in HBEpCs

HRSV WT infection was first assessed in the presence of K^+ channel modulators in HBEpCs. When the K^+ channel drugs were added at the 3 hpi time point, which would avoid the very early stages of virus entry, KCl (50mM) and $BaCl_2$ (2mM) reduced the number of HRSV infected cells to 38.8% and 42.8%, respectively (Figure 5.9A). This data was suggestive that HRSV is sensitive to changes in K^+ gradients in HBEpCs, an inhibitory effect of $BaCl_2$ further implicating Kir channels in this process. In contrast, inhibition of Kv channels through 4AP (78.7% ± 21.3), chromanol 293B (86.8% ± 13.2,) and Sotalol (77.7% ± 22.3%), K_{ATP} channels using glibenclamide (82.1% ± 17.9%), tolbutamide (94.8% ± 5.2%), pinacidil (79.5% ± 20.5%), K_{Ca} channels using

apamin (85.5% ±14.5) and K_{2P} channels using Ruthenium red (81.8% ±18.2), and haloperidol (80.7% ±19.3%), all showed no significant changes to HRSV infection levels when added 3 hpi (Figure 5.9A), suggesting these channel families are not required for HRSV replication in HBEpCs.

To assess the role of K^+ channels during early HRSV processes, the K^+ modulating drugs were next assessed when added prior to HRSV infection (Figure 5.9B). K^+ gradients were found to be similarly important since KCl treatment reduced HRSV infection levels to 47.5%. Since the effect was more potent when added during the early stages of virus infection (52.5% inhibition, when added at 0 hpi, compared to 38.8% inhibition when added 3 hpi), a secondary dependence on K^+ channel gradients during HRSV attachment/entry processes was likely. Using more selective inhibitors of the K^+ channel families (Figure 5.9B), modulation of Kv channels through TEA (5mM) and quinidine (100μM), surprisingly enhanced HRSV infection (TEA 5mM 138.6% ± 38.6% compared to mock; quinidine (Q) 156% ± 56% increase, compared to mock treated cells). An additional surprising result was that $BaCl_2$ appeared to lose its inhibitory effects on HRSV when added early during the HRSV HBEpC infection cycle (102%, Figure 5.9B compared to 57.2% 3hpi, Figure 5.9A). Further analysis revealed no effects of K_{ATP} channel modulation using glibenclamide (Glib = 118.4% ± ,18.4%) tolbutamide (Tol = 141.6% ± 41.6%), pinacidil (Pin = 133.6% ± 33.6%), or K_{Ca} channels using Apamin (137.7% ± 37.7%). Interestingly, when the K_{2P} channel modulators Ruthenium Red and Haloperidol (which showed no significant changes to HRSV infection was added 3hpi), reduced the number of HRSV infected cells to 31.4% and 24.5%. This suggests that, whilst K_{2P} modulation does not affect HRSV in HBEpCs once virus infection has been established, their modulation during HRSV entry processes can restrict virus infection in HBEpCs.

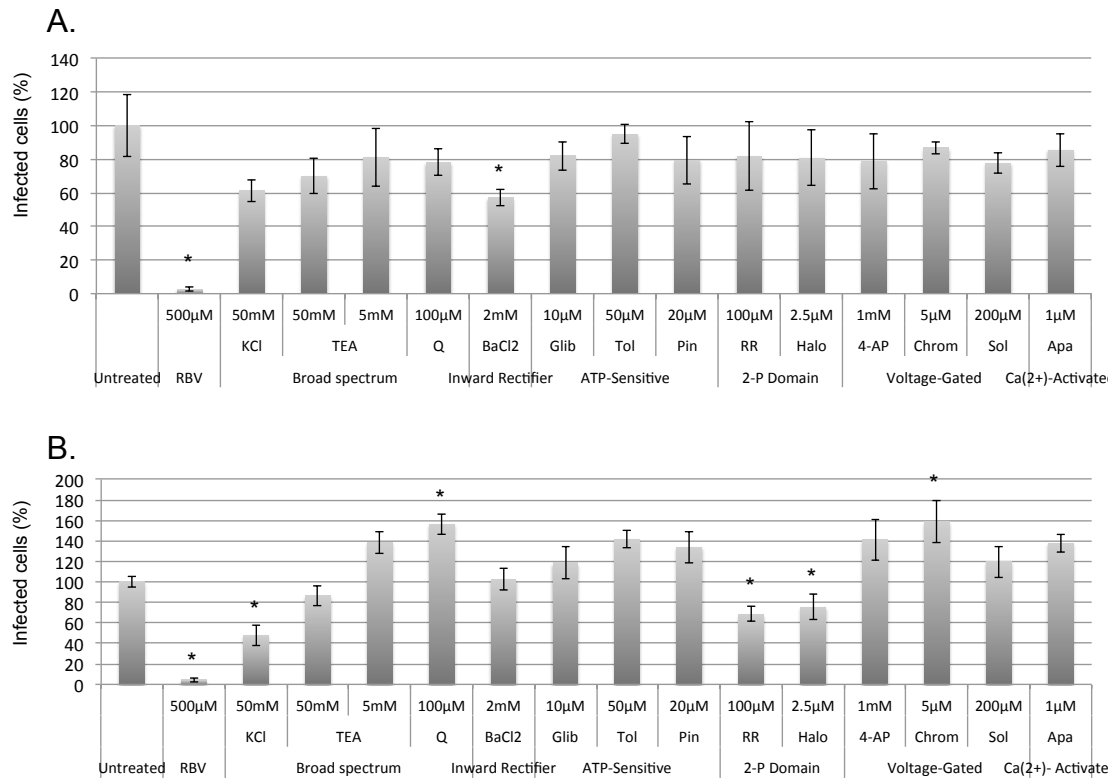

Figure 5. 9. Assessment of the effects of K^+ cellular channel modulation during the post/pre-entry stage of HRSV WT infection of HBEpC cells.

Cells were infected with HRSV WT at an MOI of 1.0 and treated with the indicated K^+ channel modulators (pre or post treatment). Cells were fixed, permeabilised with 0.5% (v/v) Triton X-100 and labelled with goat anti-HRSV FITC conjugated antibodies. Percentages of infected cells were assessed by FACS analysis and normalized to no-drug infected controls. Cells were treated with 0.5mM RBV for assay validation. **A.** K^+ channel drugs, post-entry treatment. **B.** K^+ channel drugs pre-entry treatment. Data is expressed as mean ± SE (N ≥ 2). *Significant differences from untreated value P<0.05 level.

5.4.2. Effects of Na^+ modulation on HRSV infection in HBEpCs

HBEpCs were treated with a range of Na^+ channel modulators to investigate the role of Na^+ channels in the HRSV life cycle. Na^+ channel modulators showed no influence on HRSV replication whether applied to cells at early or post infection stages of the HRSV life cycle (Figure 5.10A and B). HRSV replication in HBEpCs was firstly monitored with post entry treatment using the broad spectrum NaV blockers (Figure 5.10A) TTX (105.1% ± 5.1%),

R(-) Me5 Hydriodide (104.8% ± 4.8%), Lidocaine *N*-ethyl bromide (80.7% ± 19.3%) and *Procainamide (80.5%* ± 19.5%), none of which showed a significant effect on virus replication following post entry treatment. Similarly, the use of the ENaC blocker, amiloride (78.3% ± 21.75) showed no effect on HRSV growth at post entry phases in these cells (Figure 5.10A). Following this, lidocaine was assessed for its effects prior to infection, but no significant impact of HRSV was observed (109.3% ± 9.3% ; Figure 5.10B). This indicates that Na^+ channel blockade did not influence HRSV infection, and consequently these results suggest that cellular Na^+ channels are not required for the HRSV life cycle in HBEpCs.

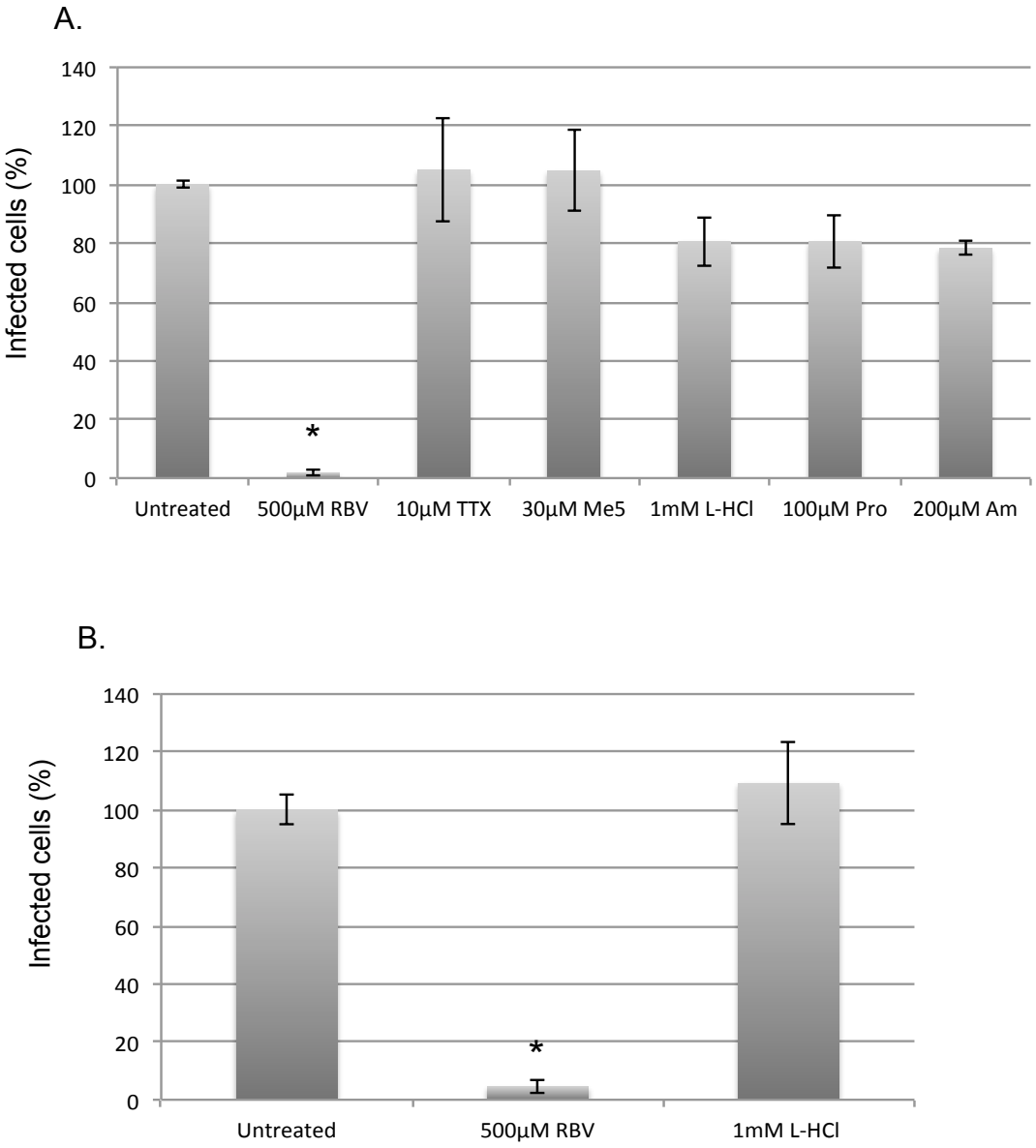

Figure 5. 10. Assessment of the effect of Na^+ channel modulation during the post/pre-entry stage of HRSV WT replication in HBEpCs.

Cells were infected with HRSV WT at an MOI of 1.0 and treated with the indicated Na^+ channel modulators, pre or post entry treatment. Cells were fixed, permeabilised and labelled with goat anti-HRSV FITC conjugated antibodies. Percentages of infected cells were assessed by FACS analysis and normalized to no-drug infected controls. Cells were treated with 0.5mM RBV for assay validation. **A.** Na^+ channel modulating drugs added to cells at the post-entry stage. **B.** Na^+ channel modulating drugs added to cells

at the pre-entry stage .Data is expressed as mean ± SE (N = 2). *Significant differences from untreated value P<0.05 level.

5.4.3. Effects of Ca^{2+} modulation on HRSV infection in HBEpCs

The role of cellular Ca^{2+} channels in the HRSV life cycle was tested by adding Ca^{2+} channel modulators to infected HBEpCs at both pre- and post-entry phases of the virus life cycle. All Ca^{2+} channel modulators showed no significant effects on HRSV replication at post entry stage (Figure 5.11A) including the use of the broad spectrum Ca^{2+} channel modulator verapamil (72.5% ± 27.5%), the TRP- channel inhibitor 2APB(93.4% ± 6.6%), and the dihydropyridine Ca^{2+} channel blockers comprising nitrendipine (84% ±16%), nifedipine (62.6% ± 37.6%), nimodipine (73.8% ± 26.2%) as well as Bay K(72.7% ± 27.3%) a Ca^{2+} channel activator. Taken together, these drugs showed no significant effects on HRSV in HBEpCs when supplied during the post entry life cycle phase.

In contrast, inhibiting Ca^{2+} channels at an early stage of the infection cycle significantly affected HRSV infection in HBEpCs (Figure 5.11B). Treatment during entry or early infection with Verapamil (157.4% ± 57.4%) and Nifedipine (159.1% ± 59.1%) significantly increased the number of infected cells, suggesting that disrupting Ca^{2+} homeostasis in HBEpCs stimulates HRSV replication, which consequently enhances HRSV in the host cell.

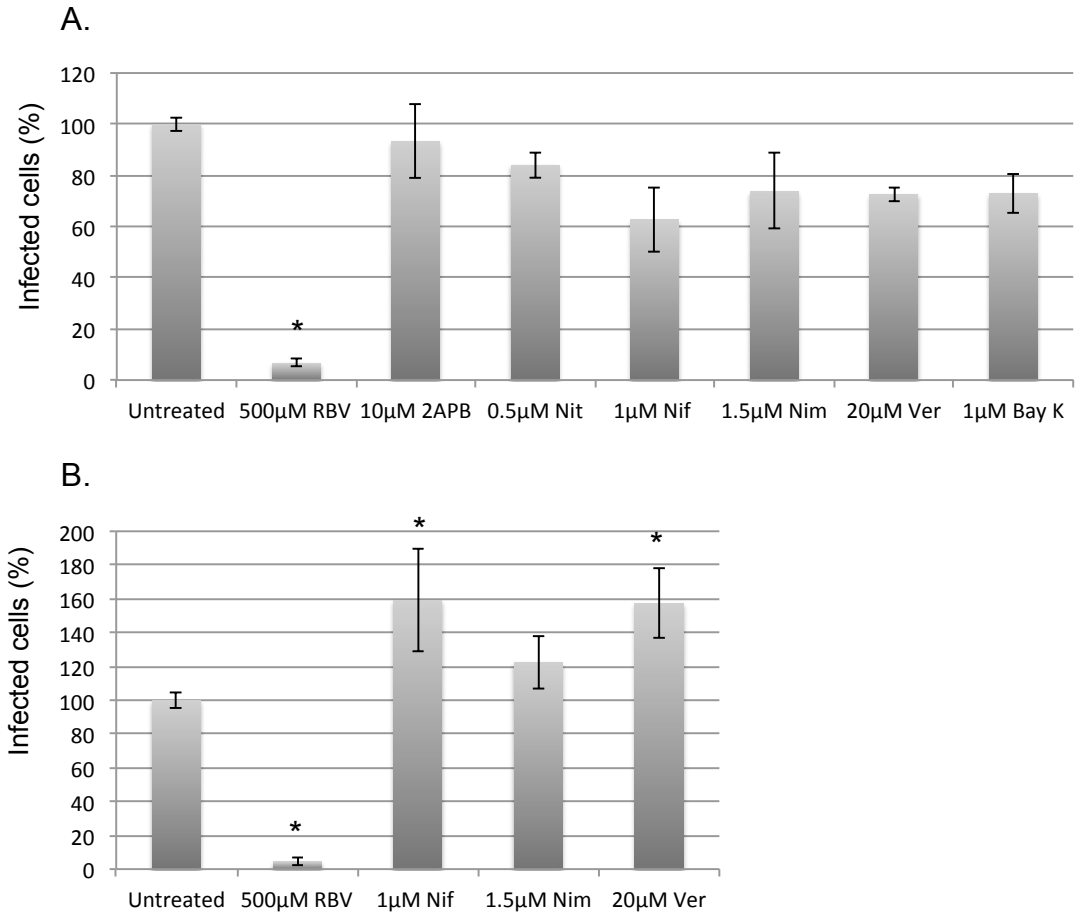

Figure 5. 11. Assessment of the effects of Ca^{2+} cellular channel modulation during the post/pre entry stage of HRSV HBEpCs.

Cells were infected with HRSV at an MOI of 1.0 and treated with the indicated Ca^{+} channel modulators (pre- or post-entry treatment). Cells were fixed, permeabilised with 0.5% (v/v) Triton X-100 and labelled with goat anti-HRSV FITC conjugated antibodies. Percentages of infected cells were assessed by FACS analysis and normalized to no-drug infected controls. Cells were treated with RBV for assay validation. **A.** Ca^{2+} channel blocking drugs, post-entry treatment. **B.** Ca^{2+} channel blocking drugs pre-entry treatment. Data is expressed as mean ± SE (N =2). *Significant differences from untreated value $P<0.05$ level.

5.4.4. Effects of Cl^{-} modulation on HRSV infection in HBEpCs

Finally, the role of cellular Cl^{-} channels in the replication of HRSV in HBEpCs was assessed by treating infected cells with Cl^{-} channel modulators at both pre-entry and post-entry stages of the virus life cycle. The use of the broad

spectrum Cl^- drugs R(+)IAA-94 (66.7% ± 33.3%) and 5-Nitro-2-3-phenylpropylamino benzoic acid (NPPB = 63.3% ± 36.7%) showed no significant effects at the post-entry stages of the replication cycle, in comparison with untreated infected HBEpCs (Figure 5.12A). However, the post-entry treatment of HBEpCs with DIDS was the only Cl^- channel drug that significantly affected HRSV and resulted in a significant drop in number of infected cells (30.5% ± 61.8% inhibition; $p \leq 0.05$). Interestingly, pre-entry DIDS treatment of infected HBEpCs also resulted in a significant drop in the number of HRSV infected cells (Figure 5.12B, DIDS = 30.5% ± 69.5% inhibition $p \leq 0.5$). These results suggested a secondary effect on DIDS during late viral process that is not observed in A549 cells. Pre-entry treatment with both RIAA and NPPB resulted in a consistent increase in viral infection (130.9% ± 30.9% increase and 147.3% ± 47.3% increase, respectively), although neither increase was deemed significant. Taken together, these results confirm that DIDs sensitive Cl^- ion channels are required for HRSV entry and infection in both HBEpCs and A549 cells.

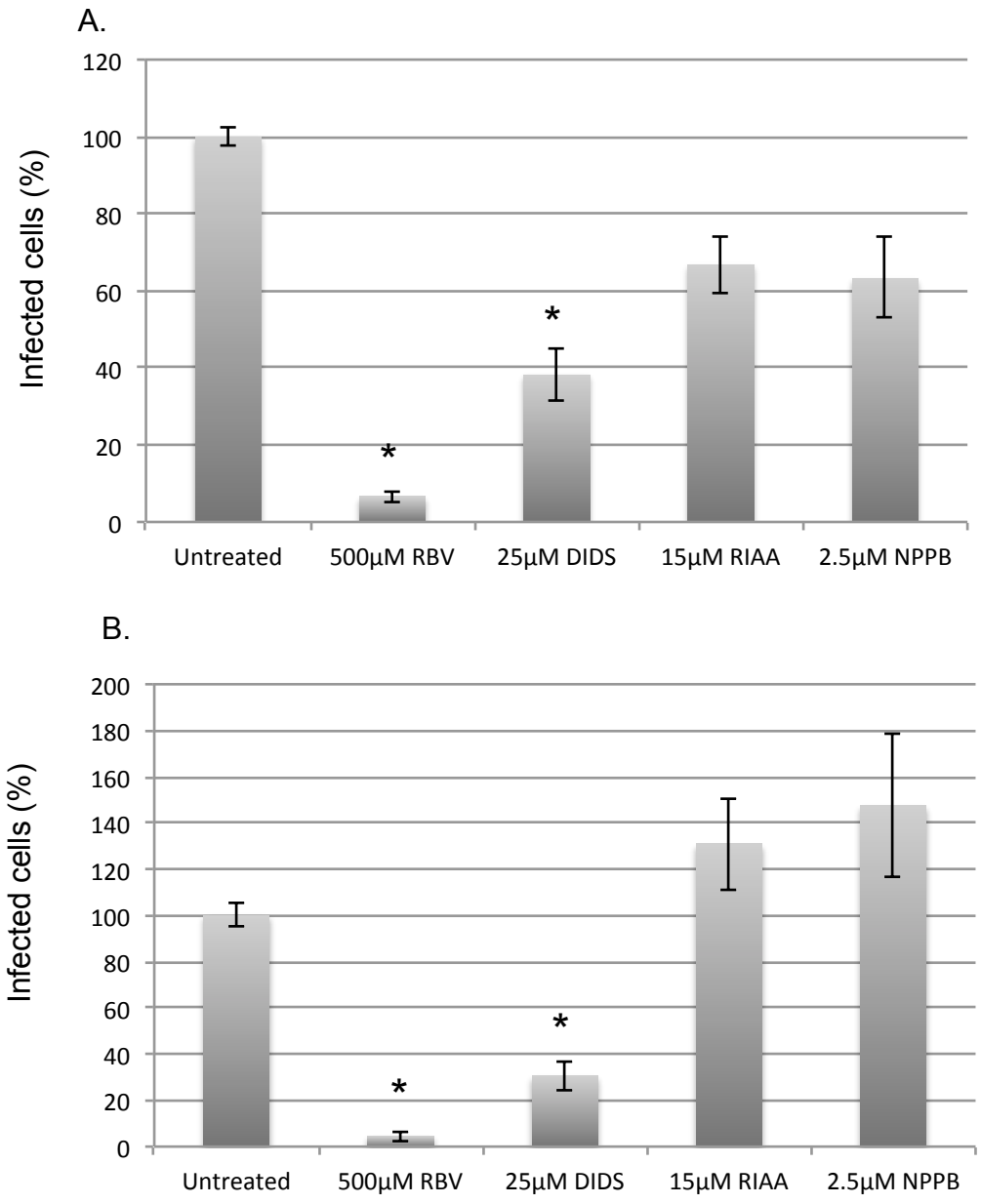

Figure 5. 12. Assessment of the effect of Cl^- cellular channel modulation during the post/pre entry stage of HRSV in HBEpCs.

Cells were infected with HRSV WT at an MOI of 1.0 and treated with the indicated Cl^- channel modulators (pre- or post-entry treatment). Cells were fixed, permeabilised with 0.5% (v/v) Triton X-100 and labelled with goat anti-HRSV FITC conjugated antibodies. Percentages of infected cells were assessed by FACS analysis and normalized to no-drug infected controls. Cells were treated with 0.5mM (v/v) RBV for assay validation. The Cl^- channel families targeted included. **A.** Cl^- channel blocking drugs, post-entry treatment. **B.** Chloride ion channel blocking drugs, pre-entry treatment. Data is expressed as mean ± SE (N ≥ 2). *Significant differences from untreated value $P<0.05$ level.

5.5. Global proteomic changes in HBEpCs mediated by HRSV-SH

In the previous Chapter, whole cell proteomic changes that occur during HRSV infection were investigated in A549 cells. In addition, the cellular role of the HRSV SH protein was investigated through comparison of the A549 cellular proteomes following infection with recombinant HRSV and ΔSH HRSV viruses. The resulting data set revealed that few cellular proteins were significantly up or down regulated, suggesting that the SH protein had little influence over the cellular proteome in these cells. Calmodulin expression was identified as down-regulated and its abundance validated by western blot analysis.

Previous work suggests the role of the SH protein in the HRSV life cycle may not be evident in certain continuous cells lines such as the A549 cells used here. Therefore, to examine the role of SH in a more relevant cellular environment, the influence of HRSV-SH on global cellular proteomic changes during virus infection was tested using HBEpCs. To perform this investigation, label free whole cell proteomics was performed for HBEpCs infected with recombinant HRSV (rA2) and HRSV ΔSH viruses, and the key up or down regulated proteins were grouped and validated in similar procedures as described in chapter 4 (section 4.4). Datasets were compared to identify key proteins or pathways that differed between HBEpCs infected with either recombinant HRSV or ΔSH viruses.

5.5.1. Sample preparation for HBEpC label free proteomics

HBEpC whole cell lysates derived from either mock, or cells infected with HRSV rA2, HRSV ΔSH and HRSV ΔSH eGFP were prepared. Each sample was processed in the mass spectrometry pipeline in triplicate for reproducibility and to identify statistically significantly changes. HRSV rA2 HRSV ΔSH eGFP was tested alongside HRSV ΔSH to ensure any SH mediated differences were not due to the differing number of genes in these recombinant viruses.

Cells were infected at an MOI of 1.0 and 24 hpi, cells were lysed using RapiGest buffer as described in Chapter 2 (section 2.2.8) and the protein concentration of each sample was determined by BCA. All sample protein concentrations were adjusted to 10µg/10µl, and equivalent aliquots were analysed by SDS-PAGE followed by western blotting to assure the presence of protein bands corresponding to cellular and viral proteins (Figure 5.13 A and B). Staining of the SDS-PAGE gel showed whole cell lysate protein bands (Figure 5.13B). Western blot analysis using polyclonal anti-HRSV antisera detected bands corresponding to the expected HRSV viral proteins indicating successful infection. A total protein mass of 100µg from each triplicate samples was then subjected to label-free protein quantification (LFPQ) and identification procedures.

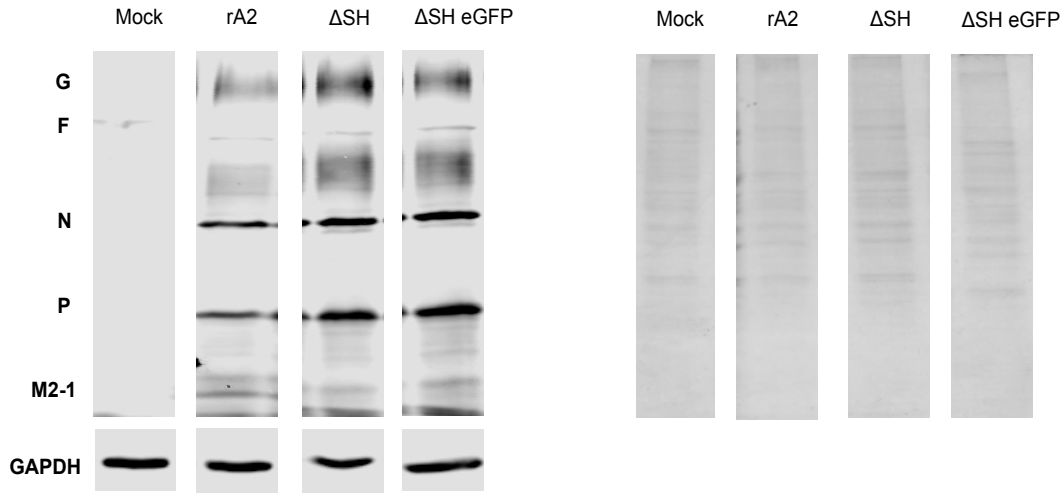

Figure 5. 13. Validation of protein extracts for label free protein quantification.

HBEpCs were infected with the various strains of HRSV (MOI = 1) for 24 hours. Cells were lysed with 0.1% RapiGest in 25mM ammonium bicarbonate and 10µg of each sample run on SDS page gels. Samples were assessed for HRSV infection by **A.** Western blot analysis or **B** coomassie staining.

5.5.2. Identification and quantification of viral proteins expressed in HBEpC

To verify that the proteomic datasets could detect HRSV proteins within infected samples, HRSV protein abundance was initially analysed from the LC-MS/MS data. Figure 5.14, demonstrates that six HRSV proteins were detected namely N (nucleoprotein), M (matrix protein), F (fusion protein), P (phosphoprotein), G (glycoprotein) and M2-1. Interestingly the relative fold abundance of these proteins like in A549 cells appeared to differ between HRSV strains. The fold abundance of HRSV-F was 2.6 fold in HRSVΔSH and HRSVΔSH GFP (1.7 fold change) in comparison with wild type recombinant infected cells. The fold abundance of HRSV-N and HRSV-M2-1 follow similar pattern of abundance (ΔSH = 2.1, ΔSH GFP= 1.4 and ΔSH = 1.9, ΔSH GFP= 1.2, fold change respectively) and showed higher fold change in contrast with HRSV rA2 proteins. HRSV-P and HRSV-G displayed a lower variation of protein abundance between SH deleted viruses, showing 0.62 and 0.73 fold respectively in HRSV ΔSH and in HRSV ΔSH GFP in infected cells compared to HRSV rA2.

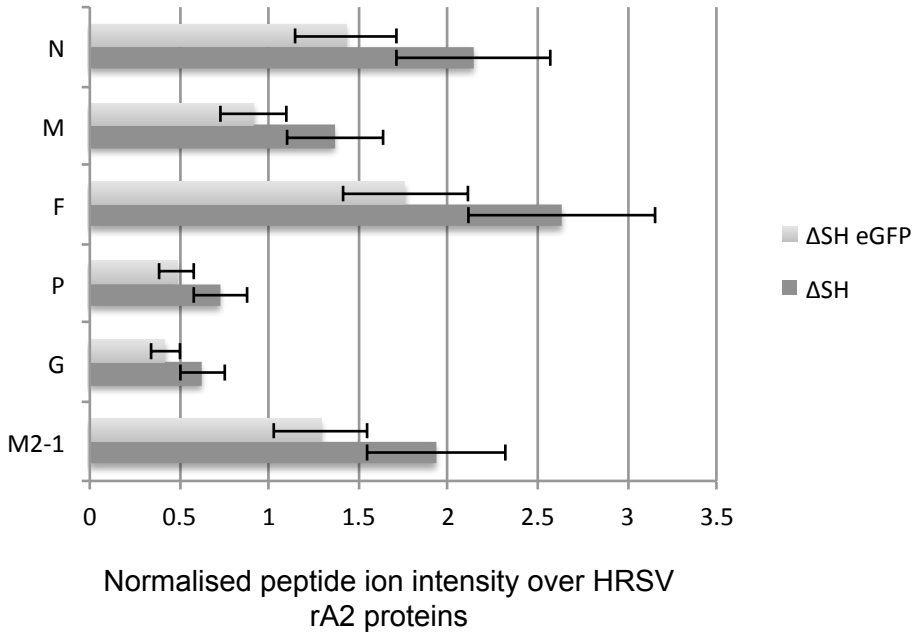

Figure 5. 14. Relative abundances of HRSV proteins expressed by HRSV rA2, HRSV ΔSH and HRSV ΔSH eGFP.

HRSV proteins were detected and quantified by mass spectrometry and proteomics data analysis prepared from HBEpCs infected with all three HRSV strains at an MOI of 1.0. Cells were incubated for 24 hours and HRSV abundancy assessed by LFPQ. Normalised proteins abundance were averaged and normalised to mock. N=3.

5.5.3. Data analysis to identify significant protein abundance changes

Significant proteome changes were derived from a statistical analysis of the data obtained from the MS data, which is the mass-to-charge ratio (m/z ratio) of the peak intensity of ionized peptides derived from specific proteins. Individual peak intensities (n=3) for each identified protein were averaged, and then normalised to the mock-infected value, and then converted to a fold change value. Previous work by others suggests that a ≥ 2 fold change in up or down regulation of protein expression may represent a significant change (2 fold protein abundance change = $\log_2$ fold change of 1.0). The significance value was calculated using statistical analysis (one-way ANOVA) to derive a $-\log_{10}$ (p-value) used as a measure to identify statistically significant values among up or down regulated proteins (where P=0.5 is equivalent to –Log10 (0.05) = 1.3). By representing the fold-change in protein abundance on the x-axis, and the significance (p-value) on the y-axis, volcano plots of the proteomics data can be generated, and are shown in Figure 5.15.

Figure 5.15A shows the total cellular proteomic changes in HBEpCs following infection with recombinant HRSV, in comparison to mock-infected cells. Proteins that are 2-fold or more increased in abundance are depicted in the top right hand corner of the plot, which indicates a total of 44 potentially up-regulated proteins. The top left corner side of the graph shows the proteins that are reduced in abundance by 2-fold or more, and in this section there are 2 potentially down-regulated proteins.

Figure 5.15B represents the proteome changes that occurred in HBEpCs infected with HRSV ΔSH, in comparison to mock-infected cells. This plot indicates no cellular proteins were up regulated in their expression compared to mock infected HBEpCs , however, a total of 18 proteins were present with a 2-fold or more reduced abundance in comparison to mock infected cells.. The fact

that the volcano plots depicting proteome changes following HRSV rA2 and HRSV ΔSH infections compared to mock infected cells (figures 5.15A and B) are different, suggests that expression of HRSV-SH during infection influences the total cellular proteome.

Figure 5.15C shows the proteome changes that were detected between HBEpCs infected with HRSV ΔSH eGFP compared to uninfected cells. The plot shows infection with HRSV ΔSH eGFP resulted in 35 up-regulated proteins and 38 down-regulated proteins. A comparison of proteome changes in HBEpCs infected with HRSV ΔSH and HRSV ΔSH eGFP (Figure 5.15D) suggested that inclusion of the GFP expressing gene within the HRSV ΔSH eGFP genome had no major effect on the cellular proteome, which further suggested the HRSV-SH mediated effects observed and plotted in Figure 5.15B were due to the loss of HRSV-SH protein expression, and not due to general effects of HRSV gene deletion. However, some up/down regulated cellular proteins were noted in cells infected with HRSV ΔSH that are not significantly changed in cells infected with HRSV ΔSH eGFP or vice versa, but the changing magnitude was very low and not significant between them (ΔSH vs ΔSH eGFP) as an example, IF4G2 protein (Eukaryotic translation initiation factor 4 gamma 2, [Uniprot= P78344, shown in the appendix]) shows -0.88 log_2 fold change in ΔSH while gives -1.0 log_2 fold change which is the significant cut off of 2-fold change in comparison with the control (mock). Therefore, the changes in protein fold change between HRSV ΔSH eGFP and HRSV ΔSH is minor and not deemed to be significant.

All the indicated proteins were not unique to a particular HRSV strain used in this analysis, and could be indicated as significantly up/down regulated . The following section describes the dysregulated proteins identified when HBEpCs were infected with each virus type that are represented as the highest and lowest mean protein fold change.

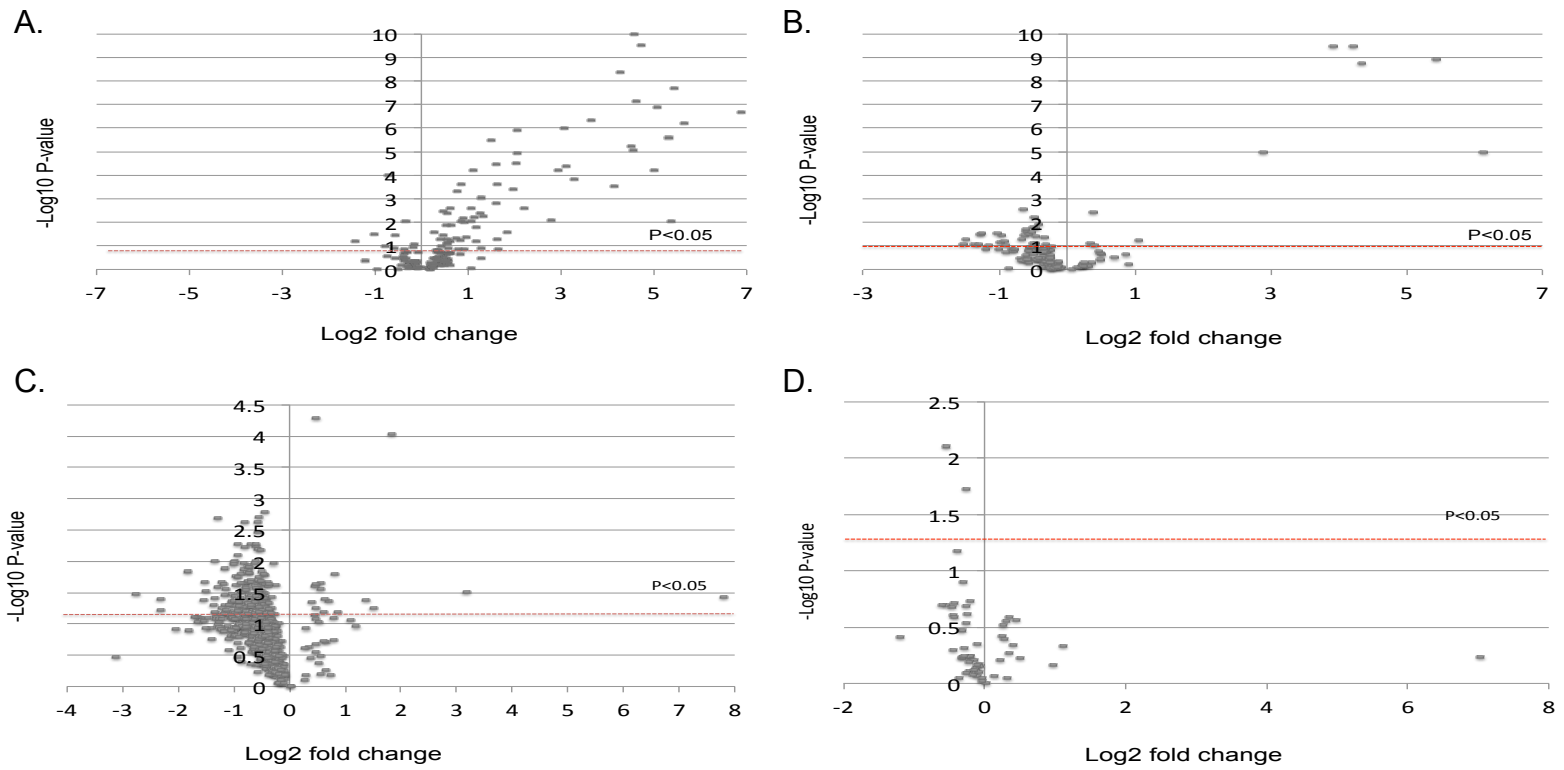

Figure 5. 1. Volcano plots showing global HBEpC proteomic changes during HRSV (rA2, ΔSH and ΔSH eGFP) infection.

The Y-axis represents significance of $-\log_{10}$ of p-value and the x-axis represents the fold change of proteins. Red-lines represent p=0.05. Data points that are above the red line represent p <0.05, which are displaying the significance of $-\log_{10}$(p-value)**. A**. Cellular proteome changes resulting from HRSV rA2 infection normalised to uninfected cells. **B.** Cellular proteome changes resulting from infection with HRSV ΔSH, normalised to uninfected cells. **C.** Cellular proteome changes resulting from infection with HRSV ΔSH eGFP normalised to uninfected cells. **D.** Comparison of proteome changes in HBEpCs infected with HRSV ΔSH eGFP normalized to HRSV ΔSH.

Table 5.5 lists the unique cellular proteins judged to be either significantly up- or down-regulated following infection of HBEpCs with HRSV rA2 compared to mock infected cells. A total of 10 proteins were identified as being significantly up regulated, whereas only one unique protein was judged to be significantly down regulated. As described in Chapter 2, the mean protein abundance was calculated from three separate mass spectrometry analyses, and the protein fold change was derived by comparing these mean protein abundances between the relevant virus-infected and mock-infected data sets.

Table 5.6 lists the cellular proteins up or down regulated following HRSV ΔSH infection of HBEpCs compared to mock infected cells, which reveals only 5 unique significantly down-regulated proteins . In addition, no unique proteins were judged to have been significantly up regulated, indicating that all HRSV ΔSH significantly upregulated proteins are not unique to the deletion virus and are similarly upregulated during WT HRSV rA2 infection.

Table 5.7 lists the cellular proteins most highly up or down regulated following HRSV ΔSH eGFP infection of HBEpCs compared to mock infected cells. The table represents the most significant top 10 unique up-regulated proteins and only 3 unique down-regulated proteins.

Up/Down regulated proteins in HRSV rA2 infected cells

Uniprot ID	Gene	Protein name	Log_2 FC		$-Log_{10}$ (P-value)	GOBP
			rA2	ΔSH		
P29728	OAS2	2'-5'-oligoadenylate synthase 2	6.8	5.9	6.65	Cytokine-mediated signalling pathway
Q9BYX4	IFIH1	Interferon-induced helicase C domain-	5.5	4.0	6.21	Cytoplasmic pattern recognition receptor signalling pathway in

		containing protein 1				response to virus
P05161	ISG15	Ubiquitin-like protein	5.3	4.1	7.69	Cytokine-mediated signalling pathway
Q8IY21	DDX60	Probable ATP-dependent RNA helicase	5.3	2.3	2.05	Defence response to virus
Q460N5	PAR14	Poly [ADP-ribose] polymerase 14	5.2	4.5	5.60	Regulation of transcription, DNA-template
P09914	IFIT1	Interferon-induced protein with tetratricopeptide repeats 1	5.0	3.7	6.89	Cellular response to exogenous dsRNA
Q8WXG1	RSAD2	Radical S-adenosyl methionine domain-containing protein 2	4.9	3.4	4.19	CD4-positive, alpha-beta T cell activation
P20591	MX1	Interferon-induced GTP-binding protein	4.6	3.6	9.53	Apoptotic process
P00973	OAS1	2'-5'-oligoadenylate synthase 1	4.5	4.0	7.13	Cellular response to interferon-alpha

O95786	DDX58	Probable ATP-dependent RNA helicase	4.52	3.9	9.98	Cytoplasmic caspase-recruiting domain (CARD) helicase signalling pathway
P16402	H13	Histone H1.3	-1.09	-0.7	1.48	Negative regulation of transcription from RNA polymerase II promoter

Table 5. 5. Identities of cellular proteins detected within HBEpCs infected with HRSV rA2 that exhibit the most increased and decreased abundance over mock infected cells using label free protein MS protein quantification.

Proteins listed are those that exhibited an over ±2 fold change (1 = $\log_2$ fold change) and significance values of $p<0.05$ which is equal as 1.3 in $-\log_{10}$. Proteins were identified and allocated to their biological process (GOBP) by gene ontology via the Uniprot website, which is http://www.uniprot.org.

Down regulated cellular proteins of infected HRSV ΔSH

Uniprot ID	Gene	Protein name	Log2 FC		−Log 10 (P-value)	GOBP
			ΔSH	rA2		
Q08209	PP2A	Serine/threonine-protein phosphatase 2B catalytic subunit alpha isoform	-1.0	-0.2	1.47	Calcineurin-NFAT signalling cascade Ontology

Q01130	SRSF 2	Serine/arginine -rich splicing factor 2	-1.3	-0.03	1.55	mRNA 3'-end processing
P82909	RT36	28S ribosomal protein S36	-1.3	-0.04	1.54	2-oxoglutarate metabolic process
P78344	IF4G2	Eukaryotic translation initiation factor 4 gamma 2	-1.0	-0.6	1.50	Cell cycle arrest
Q08209	PP2B A	Serine/threoni ne-protein phosphatase 2B catalytic subunit alpha isoform	-1.0	-0.2	1.47	Calcineurin-NFAT signaling cascade

Table 5. 6. Identities of cellular proteins detected within HBEpCs infected with HRSV ΔSH that show the most increased and decreased abundance over mock infected cells using label free protein MS protein quantification.

Proteins listed are those that exhibited an over ±2 fold change (1 = $\log_2$ fold change) and significance values of $p<0.05$ which is equal as 1.3 in $-\log_{10}$. Proteins were identified and allocated to their biological process (GOBP) by gene ontology via the Uniprot website, which is http://www.uniprot.org.

Up/Down regulated proteins in HRSV ΔSH eGFP infected cells

Uniprot ID	Gene	Protein name	Log2 FC		−Log10 (P-value)	GOBP
			ΔSH GFP	rA2		
P37198	NUP62	Nuclear pore glycoprotein p62	3.1	0.1	1.52	Cell surface receptor signaling

						pathway
Q8IYM9	TRI22	E3 ubiquitin-protein ligase	1.79	1.78	4.02	Cytokine-mediated signaling pathway
P49354	FNTA	Protein farnesyltransferase/geranylgeranyltransferase type-1 subunit alpha	1.32	0.00	1.39	Apoptotic process
Q9H3P7	GCP60	Golgi resident protein	-1.2	-1.4	1.67	Steroid biosynthetic process
Q9H1E3	NUCKS	Nuclear ubiquitous casein and cyclin-dependent kinase substrate 1	-1.3	-0.5	2.70	Glucose homeostasis
Q8N8S7	ENAH	Protein enabled homolog	-1.3	-0.2	1.60	Actin polymerization or depolymerization
O14896	IRF6	Interferon regulatory factor 6	-1.4	-0.09	1.99	Cell cycle arrest
Q9Y3C6	PPIL1	Peptidyl-prolyl cis-trans isomerase-like 1	-1.5	-0.1	1.52	mRNA splicing, via spliceosome

Q9Y2S6	TMA7	Translation machinery-associated protein 7	-1.6	-0.3	1.67	Apoptosis process
O60271	JIP4	C-Jun-amino-terminal kinase-interacting protein 4	-1.6	0.0	1.38	Activation of JUN kinase activity
Q13428	TCOF	Treacle protein	-1.8	-0.6	1.84	Skeletal system development
Q9UBV8	PEF1	Peflin	-2.3	-0.4	1.40	Response to calcium ion
Q16527	CSRP 2	Cysteine and glycine-rich protein 2	-2.8	-1.0	1.47	Cell differentiation

Table 5. 1. Identities of cellular proteins detected within HBEpCs infected with HRSV ΔSH eGFP that show the most increased and decreased abundance over mock infected cells using label free protein MS protein quantification.

Proteins listed are those that exhibited an over ±2 fold change (1 = $\log_2$ fold change) and significance values of $p<0.05$ which is equal as 1.3 in $-\log_{10}$. Proteins were identified and allocated to their biological process (GOBP) by gene ontology via the Uniprot website, which is http://www.uniprot.org.

1.11.4 Comparison of the major proteomic changes during HRSV rA2 and HRSV ΔSH infection in HBEpCs

It has previously been shown that the HRSV-SH protein plays a critical role during HRSV infection, with its roles in cell culture systems including the modulation of apoptosis induction, inhibition of TNF-signalling (S Fuentes et al., 2007) as well as influencing the activation of the inflammasome (Triantafilou et al., 2013c). Furthermore, during *in vivo* studies, HRSV-SH has been implicated

in suppressing IL-1β responses (Russell et al., 2015). Taken together, the available evidence suggests SH has immunomodulatory roles that may contribute towards viral pathogenesis.

To further characterize SH function during the HRSV infectious cycle, we compared our proteome data sets derived from HBEpCs infected with either recombinant HRSV or HRSV ΔSH viruses. This provided an unbiased and global view of the cellular changes induced by HRSV infection with and without HRSV-SH protein expression. Figures 5.16 and 5.17 show all cellular proteins displaying statistically significant abundance changes (± 1 Log_2 fold change; $p<0.05$) resulting from infection of HBEpCs with recombinant HRSV ΔSH compared to HRSV rA2. Figure 5.16 lists those cellular proteins that were down regulated by HRSV ΔSH compared to HRSV rA2. Of these proteins, the family of signal transducers and activators of transcription (STATs) were represented, with STAT-3 in particular showing the most decreased abundance in HRSV-ΔSH vs HRSV rA2 viruses. STAT-3 is a cytoplasmic transcription factor that facilitates important biological responses such as cell differentiation, proliferation, survival and apoptosis (Akira, 1999). Further analysis identified that caspase-1, a known regulator of the production of pro-inflammatory cytokines including IL-1 β and IL-18 (Shim et al., 2014) was down regulated in HRSV ΔSH compared to recombinant HRSV, implicating a role for the HRSV-SH protein during the regulation of these pathways. These proteins displaying the most significant changes in abundance and also matching pathways known to be induced by HRSV were selected for validation.

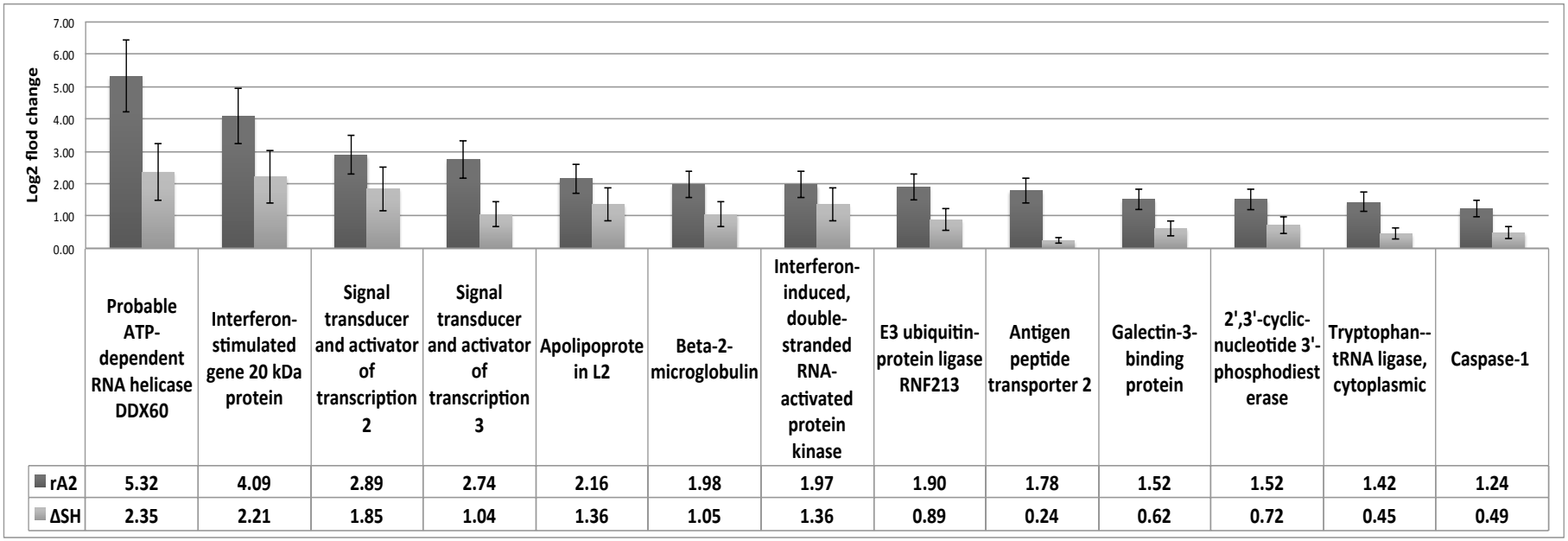

	Probable ATP-dependent RNA helicase DDX60	Interferon-stimulated gene 20 kDa protein	Signal transducer and activator of transcription 2	Signal transducer and activator of transcription 3	Apolipoprotein L2	Beta-2-microglobulin	Interferon-induced, double-stranded RNA-activated protein kinase	E3 ubiquitin-protein ligase RNF213	Antigen peptide transporter 2	Galectin-3-binding protein	2',3'-cyclic-nucleotide 3'-phosphodiesterase	Tryptophan--tRNA ligase, cytoplasmic	Caspase-1
rA2	5.32	4.09	2.89	2.74	2.16	1.98	1.97	1.90	1.78	1.52	1.52	1.42	1.24
ΔSH	2.35	2.21	1.85	1.04	1.36	1.05	1.36	0.89	0.24	0.62	0.72	0.45	0.49

Figure 5. 1. Cellular proteins with lower abundance in HBEpCs infected with HRSV ΔSH compared to HRSV rA2.

Protein abundance was calculated by comparing fold changes between virus infected and mock infected cells. The fold change was averaged over three independent mass spectrometry analyses (N=3).

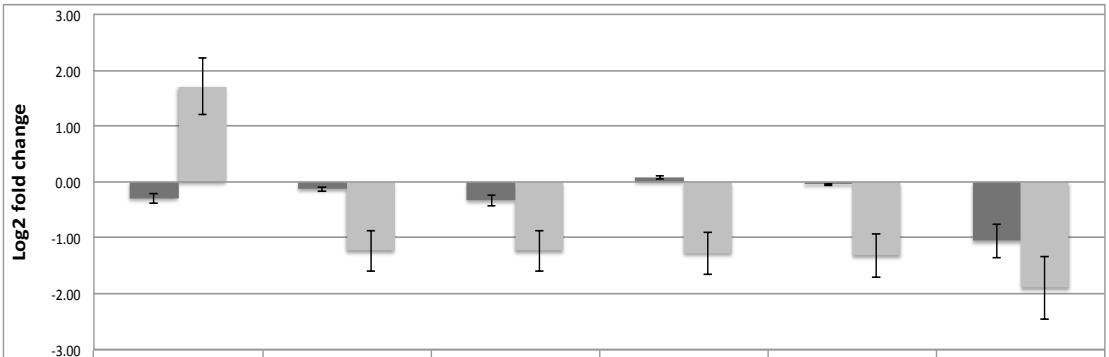

	AP-1 complex subunit mu-2	Peptidyl-prolyl cis-trans isomerase-like 1	Translation machinery-associated protein 7	Transmembrane emp24 domain-containing protein 2 11	28S ribosomal protein S36, mitochondrial	Cysteine and glycine-rich protein 2
rA2	-0.29	-0.13	-0.33	0.08	-0.05	-1.05
ΔSH	1.71	-1.23	-1.23	-1.27	-1.31	-1.89

Figure 5. 17. Cellular proteins that were expressed with higher abundance in HBEpCs infected with HRSV ΔSH compared to HRSV rA2.

Abundance values were calculated by comparing fold changes between virus infected and mock infected cells. The fold change was averaged over three independent mass spectrometry analyses (N=3).

5.5.5. Validation of significant cellular protein resulted from label free proteomics

STAT-3, a member of the family of STAT proteins was shown to display a significant increase in abundance in infected HRSV rA2 cells in comparison with mock-infected cells (6.67 fold change). Interestingly, when the increase of protein abundance was assessed in the HRSV ΔSH viruses, the increase was found to be significantly less substantial (2.06 fold change), implicating a role for the HRSV-SH in the up-regulation of expression of this protein/pathway (Figure 5.18). As described above, STAT-3 is a transcription factor that facilitates expression of multiple genes (Akira, 1999). STAT3 is phosphorylated by receptor-associated Janus kinases (JAK), to form homo- or heterodimers that translocate to the cell nucleus and act as transcriptional activators (Rane and Reddy, 2000).

Of the other proteins identified from the proteomic screen, caspase-1 was up regulated in cells infected with recombinant HRSV (2.36 fold), but displayed non-significant up-regulation in HRSV ΔSH/ ΔSH eGFP infected cells (1.4 and

1.3 fold change, respectively). This was consistent with previous studies that demonstrated that the HRSV-SH protein enhances pro-inflammatory cytokine production (IL-1b & IL-18) through SH-mediated inflammasome activation. These proteins were selected for further validation in HBEpCs

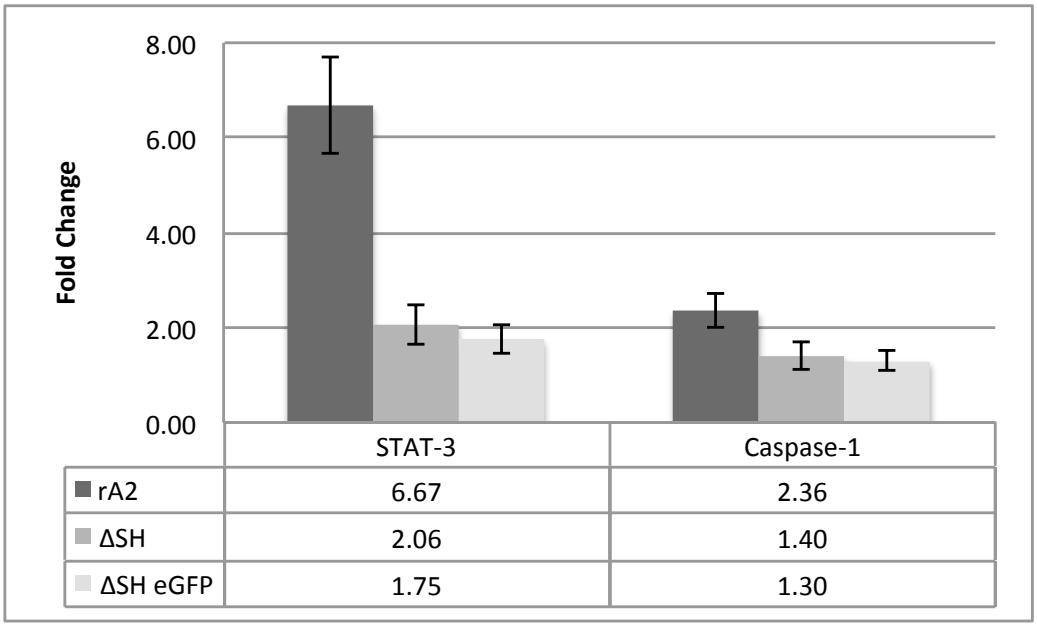

	STAT-3	Caspase-1
rA2	6.67	2.36
ΔSH	2.06	1.40
ΔSH eGFP	1.75	1.30

Figure 5. 18. LC-MS/MS quantification of STAT-3 and caspase-1 in label-free whole cell proteomic samples.

The log_2 fold change between the expression levels of STAT-3 and caspase-1 in virus infected cells compared to mock infected cells was determined by label free proteomics analysis using HBEpCs infected with all three recombinant viruses. Values from three independent mass spectrometry analyses were averaged and normalised to mock infected samples and are listed here. Expression of both STAT-3 and caspase-1 in the HRSV rA2 sample is significantly up-regulated compared to the other ΔSH virus strains.

For independent validation of the proteomics findings, STAT-3 and caspase-1 abundance in infected cell lysates were first assessed by western blot analysis (5.19A). Cells were infected with an MOI of 1 for 24 hours with all HRSV recombinant types (Figure 5.19A). The abundance of both proteins was quantified and normalised to GAPDH. Caspase-1 showed low levels of expression in mock-infected HBEpCs consistent with the proteomic data, whereas caspase-1 levels were reproducibly up regulated in HBEpCs when

infected with HRSV rA2 (compare lanes 1 and 2 in the western blot, 2.2 fold up-regulation (n=3). However, HBEpCs infected with HRSV ΔSH and HRSV ΔSH eGFP viruses displayed low levels of up-regulation (1.0 fold change and 1.12 fold change, respectively), displaying comparable levels of Caspase-1 to uninfected cells, suggesting that HRSV does not activate caspase-1 when HRSV-SH is not present.

When the levels of STAT-3 were assessed (Figure 5.19B), low level expression was evident in mock-infected cells, which was considerably up regulated following infection with recombinant HRSV rA2. No such up-regulation was evident in ΔSH/ eGFP infected cells. This independently confirmed that HRSV infection up regulates both STAT-3 and caspase -1, and suggests these two cellular proteins are up-regulated during HRSV infection in an SH dependent manner.

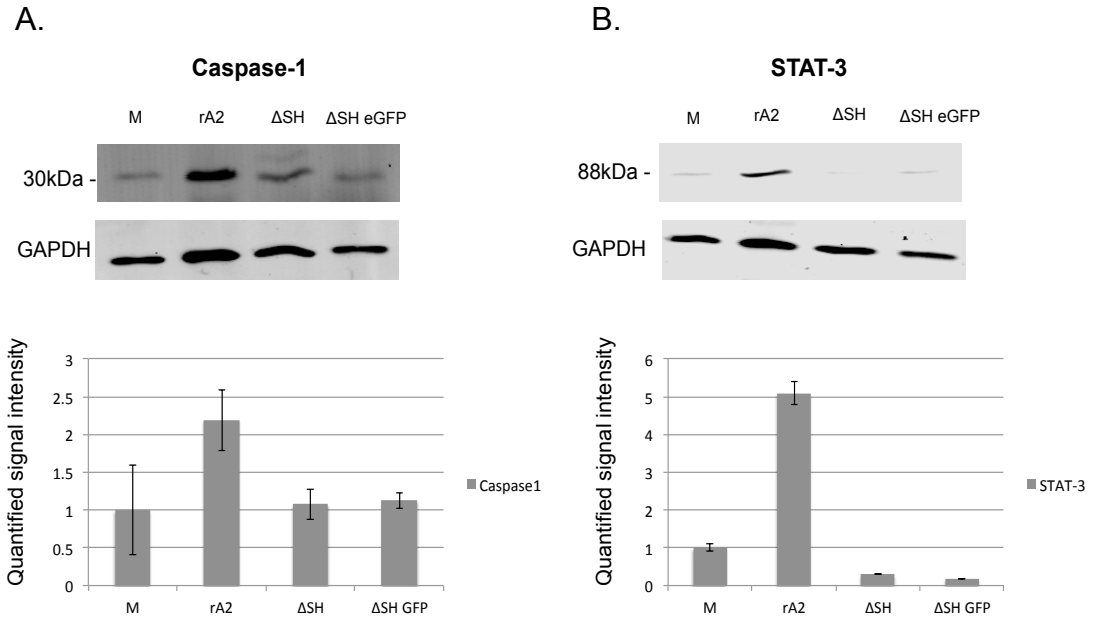

Figure 5. 19. Validation of abundance changes of selected cellular proteins in HBEpCs infected with HRSV rA2, HRSV-ΔSH, and HRSV-ΔSH eGFP.

Cells were infected with different recombinant HRSV strains (rA2, ΔSH, and ΔSH eGFP) at an MOI of 1 for 24 hours. Infected cells were lysed and 10µg samples of each were analysed by SDS-PAGE and western blotting. Proteins identified by specific antibodies were quantified using the LiCor Odyssey Infrared imaging system (LiCor). Protein abundances were calculated from signal intensity value then divided

by GAPDH intensity of each lane to derive net protein quantities. Abundances of protein bands were expressed as a mean value from three independent experiments and then normalised to mock infected cells. **A.** Western blot of caspase-1 using a rabbit anti-caspase-1, and bottom, shows quantified caspaae-1 in cells infected with each HRSV recombinant type. **B.** Western blot of STAT-3 assessed by western blot analysis and quantification of STAT-3 protein levels in cells infected with each HRSV recombinant type.

5.5.6. Cellular pathways of significant proteins

Cellular pathway networks were obtained from ingenuity pathway analysis (IPA) software. Each protein identified to be regulated by HRSV-SH functional networks using IPA software was assessed. Caspase-1 networks (Figure 5.20) illustrated several direct and indirect connections with specific cytokines such as IL1 (shown in grey). The interleukin-1 family of cytokines contains 11 members that are responsible for inflammatory responses, which are also indicated in grey circle with pro-inflammatory cytokines. A previous study showed that HRSV-SH activates the NLRP3 inflammasome that triggers the secretion of pro-inflammatory cytokines such as IL-1β and IL-18, which then trigger caspase-1 expression, that leads to cell death (Triantafilou and Triantafilou, 2014; Miao et al., 2011). On the basis of this work, the role of HRSV-SH in the induction of pyroptosis was examined.

STAT-3 network shows a direct connection with the cysteine-aspartic proteases family that are protease enzymes responsible for programmed cell death (Pyroptosis, apoptosis, autophagy and necrosis) such as caspase-5 and caspase-7 (Figure 5.21A). Caspase-5 is subcategorised as inflammatory as is involved in the activation of caspase-1 to induce IL- 1β and IL-18 cytokines that lead to pyroptosis (Galluzzi et al., 2016). Caspase-8 is categorized as an executioner enzyme that induces host cell apoptosis (Sollberger et al., 2014). STAT-3 also showed a predicted activation of caspase-1 (Figure 5.21B).

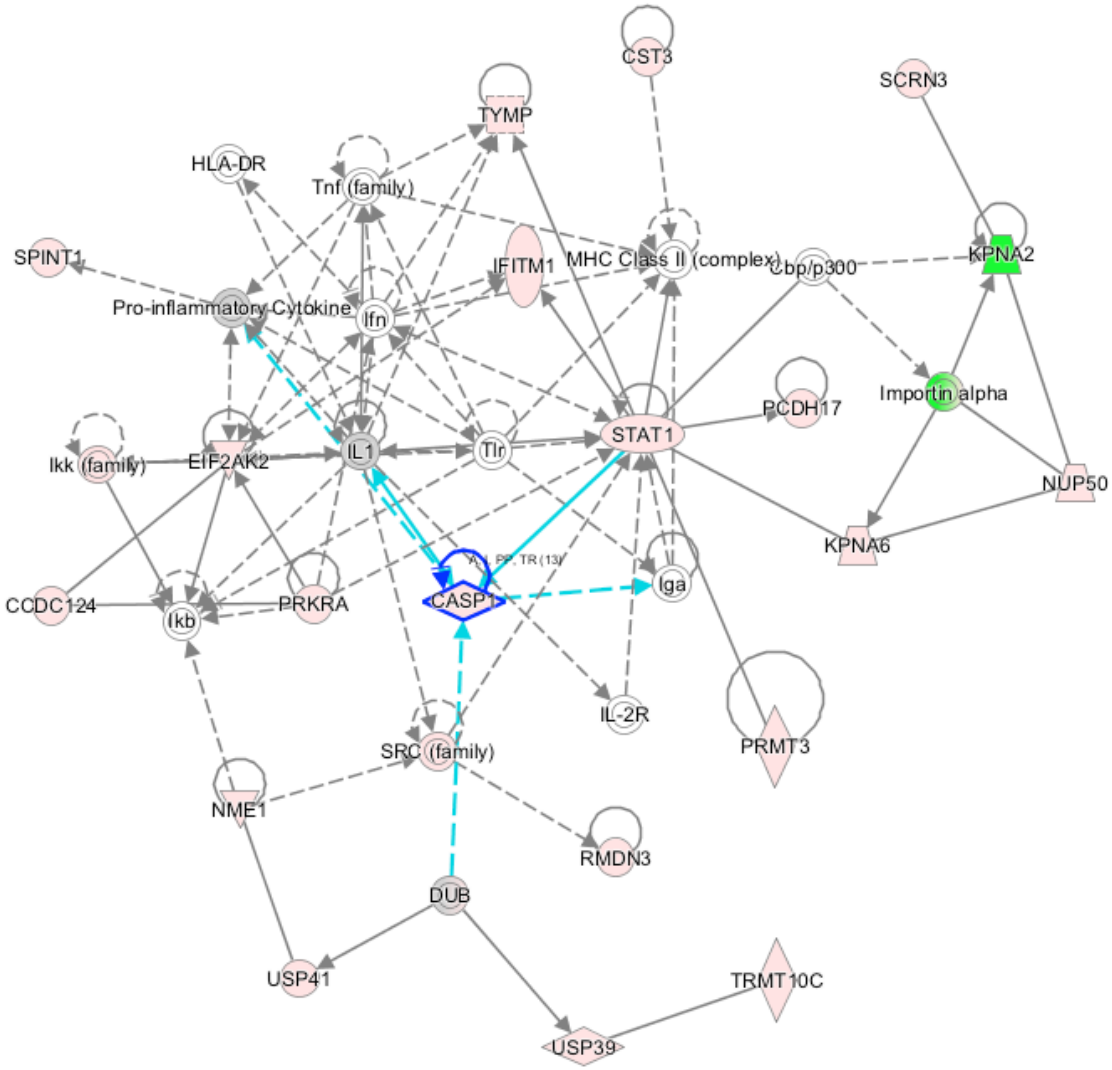

Figure 5. 20. Network analysis of up-regulated Caspase-1 interacting proteins overlapped with the well-characterized pathways using IPA.

Red shaded proteins indicate a minimum 2-fold increase and green shaded proteins correspond to a greater than -2-fold down-regulation. The intensity of the coloured protein indicates the relative abundancy. Grey coloured proteins represent non-significant proteins that mapped within the proteomics results. White shaded proteins were identified based on the IPA knowledge.

A.

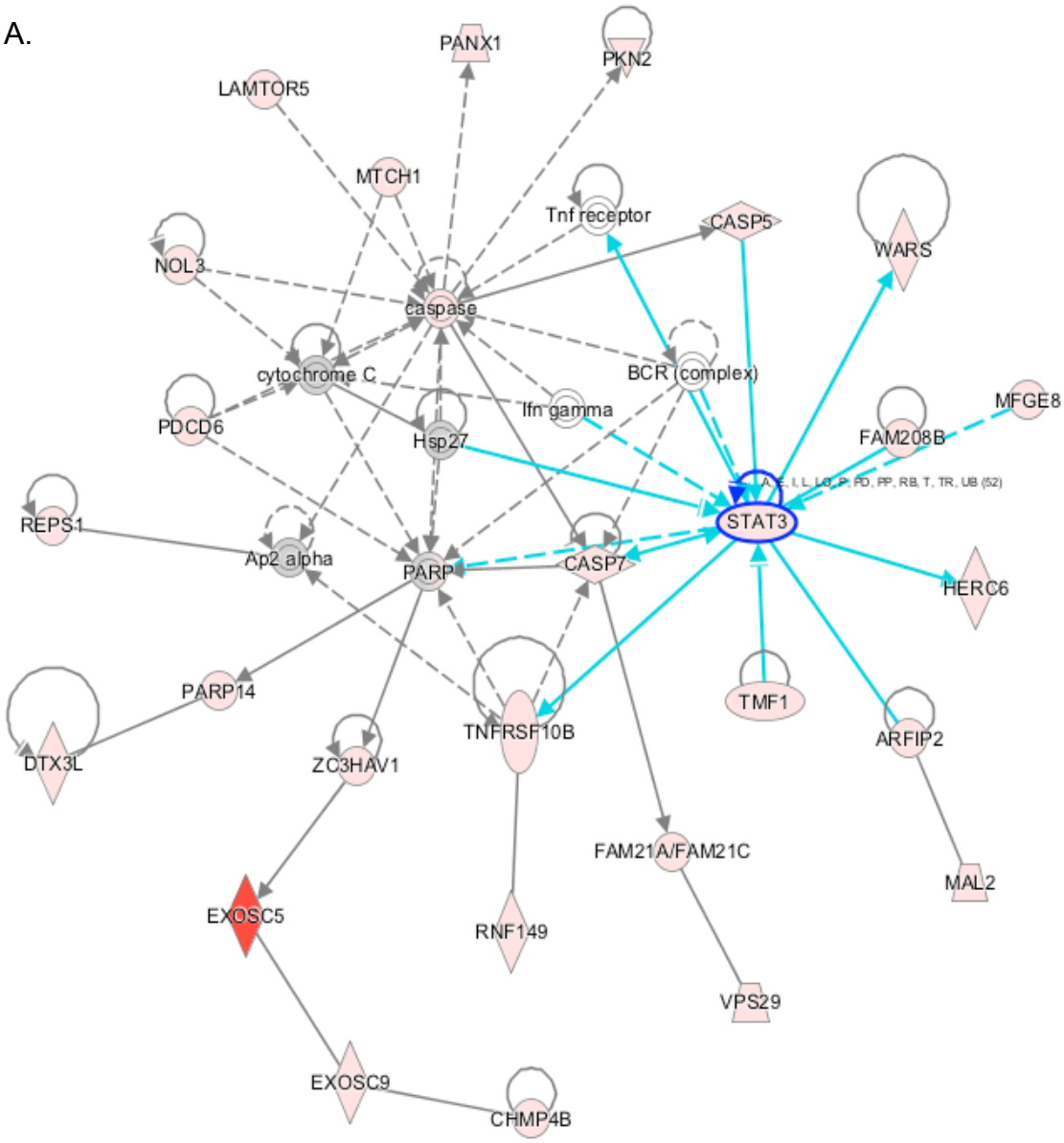
PANX1
PKN2
LAMTOR5
MTCH1
Tnf receptor
CASP5
WARS
NOL3
caspase
cytochrome C
BCR (complex)
MFGE8
PDCD6
Ifn gamma
FAM208B
Hsp27
STAT3
REPS1
Ap2 alpha
PARP
CASP7
HERC6
PARP14
TMF1
DTX3L
TNFRSF10B
ARFIP2
ZC3HAV1
FAM21A/FAM21C
MAL2
EXOSC5
RNF149
VPS29
EXOSC9
CHMP4B

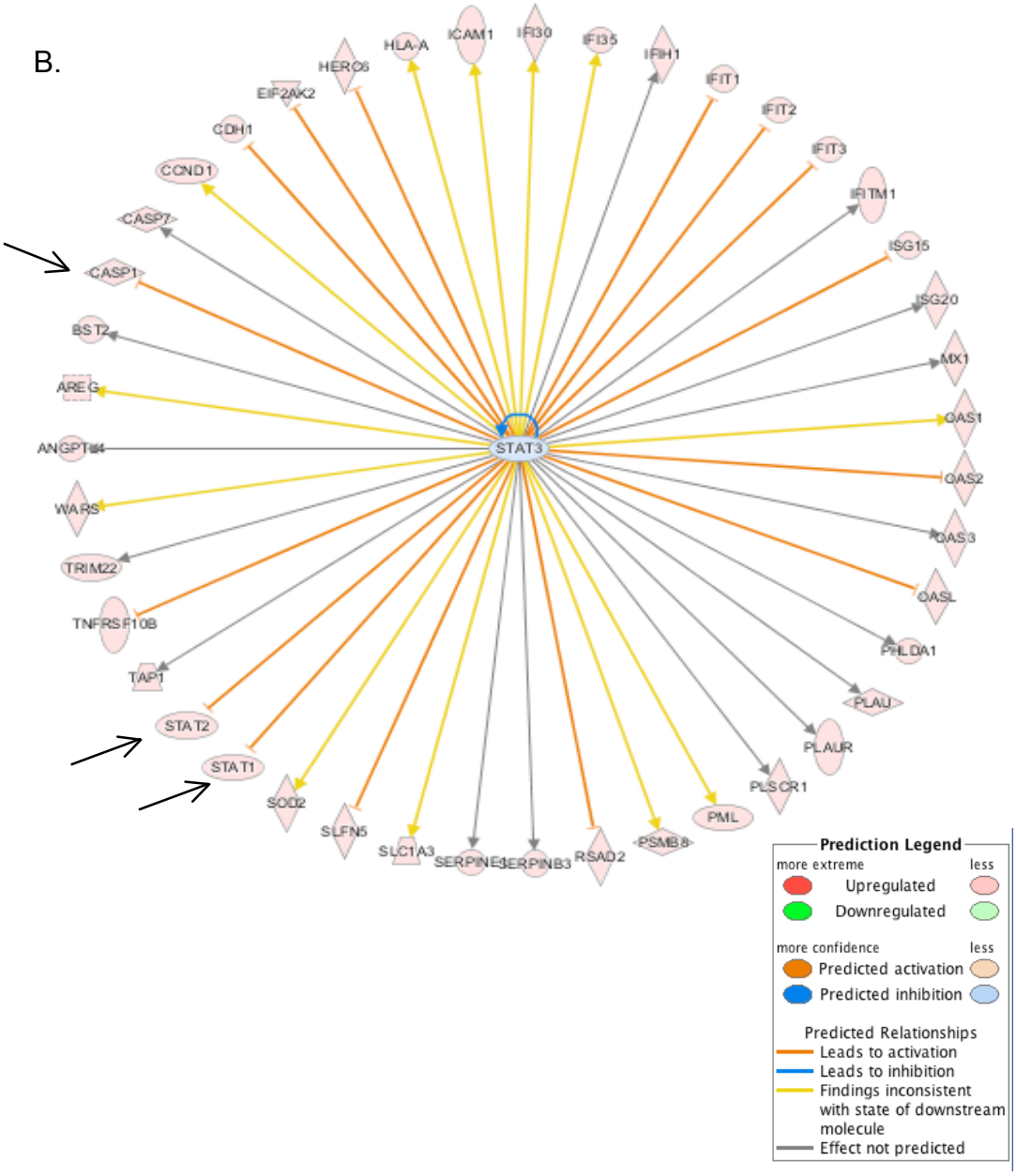

Figure 5. 21. Network analysis of STAT-3 interacting proteins overlapped with the well-characterized pathways using IPA.

Cellular activity of HBEpCs infected with HRSV rA2. Red shaded proteins indicate a minimum 2-fold up-regulation and green shaded proteins correspond to a greater than -2-fold down-regulation. The intensity of the coloured protein indicates its abundancy. Grey coloured proteins represent non-significant proteins that were mapped from within the proteomic datasets. White shaded proteins were identified based on the IPA knowledge. The shapes offered the molecular class of the protein.

A. STAT-3 pathway map obtained from proteomics data and IPA programme knowledge. B. General direct relationship of STAT-3 towards other cellular molecules shown in proteomics data.

5.5.7. Detection of pyroptosis in HBEpCs infected cells

Pyroptosis is a highly inflammatory form of programmed cell death that, in contrast to apoptosis, requires the activity of caspase-1. Unlike apoptosis, cell death by pyroptosis results in plasma-membrane rupture characterised by the release of lactate dehydrogenase (LDH). LDH is an enzyme that is associated with the plasma membrane and is secreted in response to injury or inflammation (Click, 1969). In cell culture, it has been well characterised that an enhancement of LDH secretion is indicative of necrosis and/or pyroptosis. Given the ability of HRSV to enhance caspase-1 activation the levels of LDH secretion was assessed in HRSV infected cells.

LDH assays were performed from supernatants of HBEpCs infected with HRSV rA2 and HRSV ΔSH stains at an MOI of 1 for 24 hrs. LDH concentrations in the cell supernatants were quantified by colorimetric assays described in materials and methods (Section 2.2.6.2). The result of the LDH assay (Figure 5.22) shows an increase in LDH release within the supernatants of HBEpCs infected with HRSV rA2 in comparison with mock-infected cells. HRSV ΔSH infected cells also showed also an increase in LDH levels but to a lesser degree than when compared to HRSV rA2.

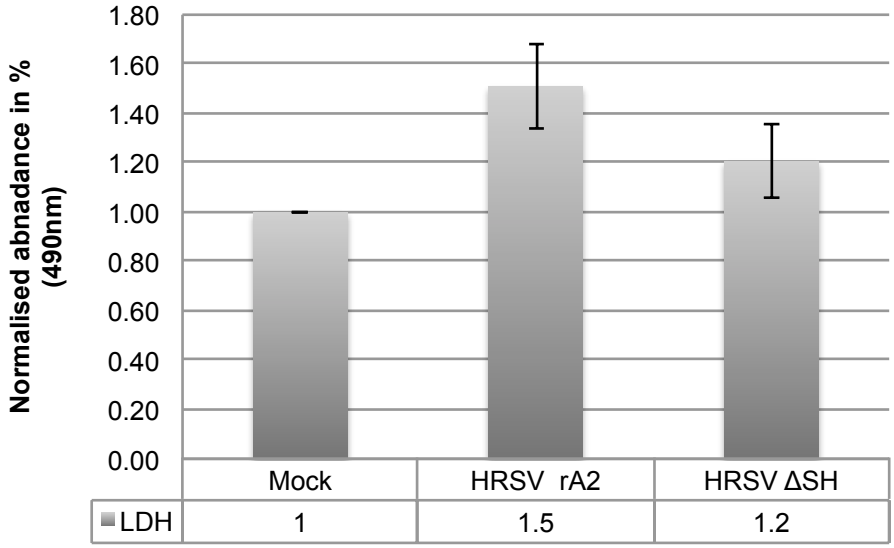

Figure 5. 22. Measurement of LDH levels in HBEpCs infected with HRSV rA2/ ΔSH.

Cells were grown in 12-well plates and infected with HRSV rA2 and HRSV rA2 ΔSH for 48 hours. Cell supernatants were transferred to a 96-well plate and incubated with LDH reaction buffer for 30 min at room temperature. LDH concentrations were measured by assessment of the absorbance at 490nm referenced to 690nm. Each sample were averaged and normalised to mock values. Each test was repeated in triplicate.

5.6. Discussion and summary

In this chapter focussed on two main areas (1) The effects of cellular ion channel modulation on the HRSV life cycle in primary cell cultures, (2) The effects of HRSV-SH on the global proteomic changes that occur during virus infection of primary cells. The unique feature of this chapter is the use of HBEpCs, that more physiologically reflect the cell physiology of human lung cells *in vivo*. Using these cells, it was deemed interesting to investigate whether the modulation of HBEpC ion channels and the effect of that modulation on HRSV infection, was similar or differed to A549 cells. Similarly, the influence of HRSV-SH on the cellular proteome and its comparison to A549 cells would reveal the importance of using these cell lines in future HRSV studies.

An issue of this procedure was that dealing with primary cells enhanced the experiment limitations, as they are very fragile, have a short lifespan, and easy detach during experimentation. Moreover, these cells require a longer time period to reach confluency (70% cells confluency), and specialist growth media is required for their maintenance. These challenges were overcome through the preparation of frozen stocks, which were routinely thawed and grown to confluency when required for experimental analysis. The infection conditions were determined by IF analysis to ensure cells maintained their health and could be infected. MTT assays were performed to determine the highest non-toxic concentration of each channel modulator for the experiments FACS analysis was performed to screen the effects of ion channel modulation on the HRSV lifecycle, while the global cellular proteomic changes induced by HRSV-SH was performed using label-free quantification by mass spectrometry.

5.6.1 The effect of HRSV lifecycle in modulation ion channels in HBEpC cells

HBEpCs were infected and the effects of ion channel modulation assessed . Each ion channel modulator was added either at the post entry stage of infection, or 3hpi as described in Chapter 3.

When the effects of K^+ channels were assessed, through the use of $BaCl_2$, Glibenclamide , Tolbutamide , Ruthenium red Chromanol 293B , Haloperidol , Apamin , 4-AP and broad spectrum K^+ channel inhibitors; TEA, Quinine and KCl, the results were variable (Figure 5.9) depending on the time of drug addition. KCl treatment showed a 53% reduction in HRSV infected cells (47% HRSV positive) when added during virus entry while a 39% reduction in infected cells (61% HRSV positive) was observed when added 3hpi. This indicates that KCl affects virus infection at the early stages of virus life cycle but exerts no significant changes when HRSV infection is established 3hpi in the primary cells. Quinine significantly enhanced viral infection when added

during virus entry, but had no significant effects when added at the post entry stage of HRSV infection. Similar results were observed with Chromanol 293B, a voltage-gated K^+ channel inhibitor. In contrast to the A549 cell data the Kir modulator $BaCl_2$ did not impact HRSV early infection/entry but caused the number of HRSV infected cells to decrease to 57% of the no-drug infected cells. Therefore, multiple K^+ families may influence HRSV infection in primary cell cultures, dependent on the time of drug addition. These data differed to that obtained in A549 cells where only Kir channel families impacted HRSV, specifically during HRSV entry.

When the Na^+ channel modulators were assessed, no impact on the HRSV life cycle regardless of the time of drug addition was observed (Figure 5.10). This ruled out a role for cellular Na^+ channels during primary cell infection.

When the effects of Ca^{2+} channel modulation were assessed (Figure 5.11), Nifedipine increased HRSV infection when added at entry and post-entry stages, but these values were not statically significant. Verapamil that inhibits T-type and L- Ca^{2+} channels did significantly increase HRSV infection when added at early stages, but had no significant effects when added post-entry. Nimodipine that modulates L-type Ca^{2+} channels did not affect HRSV infection regardless of the time of drug addition. From these data it appears that the specific modulation of both L and T type Ca^{2+} channels can enhance HRSV entry processes. This differs from the effects of Ca^{2+} channel inhibition of Ebola virus were that the inhibition of two pore Ca^{2+} channels is detrimental to HRSV infection (Sakurai et al., 2015a).

Regarding the Cl^- channel data (Figure 5.12), R (+) IAA-94 and NPPB increased the levels of infection by 31% and 47% respectively and caused a non- significant reduction in HRSV infected cell numbers (reduced to 66% and 63% respectively) compared to no-drug cells. On the other hand, DIDS as observed in A549 cells, decreased HRSV infection by 70% (30% HRSV positive cells) when added during entry and led to a 38% reduction of HRSV positive cells when added 3hpi Thus as in A549 cells, DIDs sensitive Cl^- channels are required for HRSV entry in primary cell cultures. These data

combined with Chapter 3 indicate that DIDS is a potent inhibitor of HRSV entry across cell types. The future challenge will be to identify the Cl^- channel(s) that mediate this effect so they can be targeted with more specific Cl^- modulators to inhibit HRSV infection, if such compounds become available.

5.6.2 SH viroporin mediated pyroptosis during HRSV infection in HBEpC cells

Label-free proteomics was able to identify proteins that were affected directly or indirectly by HRSV-SH in HBEpCs. Capsape-1 was detected as up-regulated by HRSV rA2 but not HRSV ΔSH which was validated by western blot analysis (Figure 5.19A). Caspase-1 can trigger the secretion of pro-inflammatory cytokines (IL-18, IL-1β) (Miao et al., 2011) and activate the NLRP3 inflammasome (Triantafilou et al., 2013c). Caspase-1 activation is also known to trigger pyroptosis, a form of cell lysis. The ability of HRSV rA2 to induce pyroptosis was confirmed (Figure 5.22) and this was more pronounced that of HRSV ΔSH despite the comparable levels of virus infection. This implicated HRSV-SH in mediating pyroptosis induction which may contribute to the reduced infectivity of HRSV ΔSH in vivo, for example if pyroptosis induction contributes to HRSV spread in these systems.

STAT-3 was also up regulated during HRSV rA2 infection in HBEpC cells. This validated previous findings (Kong, San Juan, Kumar, Aruna K Behera, et al., 2003) that identified STAT-3 and STAT-1α induction during HRSV infection. An unreported finding was that HRSV ΔSH infection did not influence STAT-3 levels implicating HRSV-SH in this process (Figure 5.19B). Taken together these findings validated the proteomic data sets and revealed new roles of HRSV-SH in pathogenic functions during the infection of primary cell cultures.

Chapter 6: Discussion

Discussion

HRSV is one of the major causes of severe lower respiratory tract infection in infants and young children (Woensel et al., 2003). Globally, all children under the age of 2 are likely to have been infected with HRSV. Since there are no effective vaccines or treatments currently available to treat HRSV infections, this study focused on identifying new HRSV-host interactions (Rivera et al., 2015). It was hoped that increased knowledge in this area would provide new avenues to impede HRSV-host interactions, thus opening new potential angles of anti-HRSV treatment.

The study focused on two key areas. (1) The dependence of HRSV on host cell ion channel function, through investigating whether ion channel modulating compounds could inhibit HRSV infection. (2) The role of HRSV-SH in the HRSV lifecycle. HRSV-SH is a viroporin that is known to be required for HRSV infection *in vivo* (Gan et al., 2012), however its precise contribution to the HRSV lifecycle has remained largely undefined.

Two cell types were used in this study. A549 cells formed the basis of the data obtained in Chapters 3 and 4, whereas HBEpCs were used in Chapter 5 as they are thought to represent a more physiologically-relevant cell for HRSV studies. A549 cells are an adenocarcinoma continuous cell line that are derived from an explanted tumor of an adult Caucasian male and are frequently used as a model for alveolar type II (ATII) cells (Don J Giard et al., 1973). The disadvantage of these cells is that they do not maintain a phenotype characteristic of primary cell cultures but they are robust for use for in *in vitro* analysis (Swain et al., 2010). HBEpCs are human bronchial epithelial primary cells that are obtained from the airway epithelium surface of normal adult lungs. Primary cells such as HBEpCs are the gold standard for *in vitro* human lung cell analysis, and adhere to many of the characteristics of the original cells. However, these cells have disadvantages for their regular use in cell culture, including slow growth kinetics and their differential growth behavior after continual passages. Thus, although HBEpCs are an excellent model to study HRSV infection, they do come with experimental limitations. For this reason, in this study, both ion channel and

proteomic analyses were performed in A549 cells and the findings further verified in HBEpCs.

6.1. The effects of cellular ion channel modulation on the HRSV lifecycle

6.1.1. Cellular K^+ channels

The role of host cell K^+ channel function during HRSV infection is not restricted to a specific type of K^+ channel. In A549 cells, all K^+ channel modulators tested did not influence HRSV when added 3hpi (Figure 3.10). When added at the early stages, Kir channels were implicated in HRSV entry, as $BaCl_2$, KCl and TEA decreased HRSV infection (Figure 3.16). Interestingly, inhibiting K^+ channels in A549 cells infected with HRSV ΔSH was inhibitory at both entry and post entry stages of viral life cycle (Figure 4.6). At the early stages of virus adsorption, $BaCl_2$, ruthenium red and haloperidol significantly reduced HRSVΔSH infection. Moreover, KCl, $BaCl_2$, glibenclamide, haloperidol and Sotalol were able to inhibit HRSV when added during the post entry stages of HRSV ΔSH infection. These finding suggested that blocking K^+ channel activity can efficiently impede the growth of HRSV lacking its SH protein. This may implicate some role of the HRSV-SH viroporin in the conductance and/or regulation of K^+ fluxes during the HRSV infectious cycle.

When these experiments were repeated in HBEpCs, the response of HRSV to ion channel modulation differed from the A549 cell data (Figure 5.9). KCl lowered the levels of HRSV infection only when added during HRSV entry. Quinine and Chromanol 293B increased the levels of HRSV infection at the viral attachment stage but not post-infection. $BaCl_2$ was able to impede HRSV regardless of its time of addition.

Taken together these data demonstrate that K^+ channels can influence the HRSV lifecycle, however the specific K^+ channel of the 70 K^+ channels expressed per cell, remains to be defined. The ability of KCl and $BaCl_2$ to impede virus growth in both cell types implicates Kir channels as the key K^+ channel family member, but why Kir modulation would impede HRSV infection requires further characterisation. As Kir channels vary in their contribution to

cellular physiology across cell types, it will crucial to confirm the sensitivity to Kir modulation across all HRSV permissive cells. As many cancer cell lines display up/downregulated ion channel expression (Pardo and Stuhmer, 2014) they are thought to contribute to the metastatic processes of many cancers (Storm et al., 2013), studies in primary cell lines represent the ideal model system to further such studies.

6.1.2. Cellular Na^+ ion channel

In A549 cells, blocking Na^+ channels with NaV modulators such as TTX enhanced HRSV infection when the Na^+ channel drugs were added post-virus entry (Figure 3.12). The amiloride-sensitive, Na^+-absorptive ENaC has been characterised in human airway epithelium as critical for many lung cell functions (Bennett et al., 2016), but surprisingly the addition of amiloride (that blocks these channels) did not affect HRSV infection. For HRSV ΔSH, NaV channel modulation with lidocaine significantly inhibited virus infection, highlighting further differences between HRSV sensitivity to ion channel modulation when SH is absent (Figure 4.7). However, in HBEpCs, Na^+ channel modulation had no influence on HRSV during both viral attachment and post infection treatment (Figure 5.10). From this data, it can be suggested that Na^+ channel modulation imparts effects on HRSV only in cancer cell lines. In this regard, many NaV channels are known to be overexpressed in metastatic cells from a number of cancers (Brackenbury, 2012). NaV overexpression enhances Na^+ currents that increase migration, invasion and metastasis (Roger et al., 2015). It is likely that HRSV has adapted to these differential NaV expression patterns in the A549 cell line.

6.1.3. Cellular Ca^{2+} channels

Rises in cytosolic Ca^{2+} are sufficient to initiate many signaling processes, including those related to host cell defence mechanisms in endothelial cells. For this reason, many viruses including Coxsakievirus, CMV, HCV and HIV have become adept at utilizing Ca^{2+} signaling to create an optimal cellular environment that suits their demands (Bozym et al., 2010; Manninen and Saksela, 2002; Li et al., 2007; Sharon-Friling et al., 2006; Zhou et al., 2009). Ca^{2+} influx can be controlled by plasma membrane Ca^{2+} channels, most notably

voltage gated Ca^{2+} channels. In this study, blockers of these channels including nitrendipine, an L-type Ca^{2+} channel inhibitor, which reduced HRSV infection in A549 cells but this data could not be recapitulated by other modulators of this channel family including Bay K, Nifedipine and nimodipine (Figure 3.13). It was therefore somewhat surprisingly concluded that the HRSV lifecycle is not affected by Ca^{2+} channel modulation in A549 cells and the inhibitory effects of nitrendipine were likely due to off-target effects of this compound. For HRSV ΔSH infection, activating Ca^{2+} influx through Bay K treatment reduced the levels of HRSV infection whilst other Ca^{2+} channel modulators had no effects (Figure 4.7). Thus, it appears that the presence of HRSV-SH can dictate the sensitivity to both nitrendipine and BayK but whether this is mediated through Ca^{2+} channels remains to be determined.

In primary HBEpCs, the HRSV sensitivity to Ca^{2+} channel modulation differed from A549 cells. Nifedipine (an inhibitor of L-type Ca^{2+} channels) and verapamil (an inhibitor of T-type and L- type Ca^{2+} channels) both significantly increased virus infection when added during HRSV entry (Figure 5.11). Thus, HRSV infection was enhanced in HBEpCs when Ca^{2+} influxes were inhibited. This may be explained by the fact that an alteration of Ca^{2+} homeostasis is known to prevent apoptosis or induce apoptosis typically elicited as an innate defence mechanism to counteract virus infection and control virus production (Pinton et al., 2001; Pinton et al., 2008). HRSV may thus target these apoptotic checkpoints, preventing Ca^{2+} influx that would induce host immune responses, ultimately promoting HRSV growth in HBEpCs.

6.1.4. Cellular Cl^- channels

Perhaps the most striking effects on HRSV were observed in the face of Cl^- channel modulation. HRSV entry was strongly inhibited by the addition of the broad-spectrum anion channel inhibitor DIDS (Figure 3.17C and 4.7A) regardless of the presence of SH (HRSV ΔSH was similarly inhibited) or cell type (the inhibitory effects of DIDS were conserved in A549 and HBEpCs). NPPB, a broad spectrum anion channel blocker (particularly large-conductance Cl^- channels) and R(+)IAA-94 that blocks medium-conductance, voltage-sensitive Ca^{2+} channels such as CLC-2 and CLC-3, had no effects on HRSV

infection in either A549 or HBEpCs. Interestingly for HCV, an opposite effect was observed, namely HCV replication was inhibited by R(+)IAA-94 and NPPB but not DIDS (Igloi et al., 2015). DIDS was also shown to inhibit the release of BK polyomavirius (Evans et al., 2015). DIDS has been shown to block a range of Cl^- channels including ClC-Kb, ClC-Ka, ClC-6, ClC-7, ClC-2, Ca^{2+}-activated Cl^- channels, volume regulated Cl^- channels and maxi- Cl^- channels, but does not inhibit ClC-3, ClC-4 or ClC-5 (Evans et al., 2015). Similarly many Cl^- channels are NPPB/IAA-94 insensitive. This information may guide future studies that narrow down the HRSV dependency to single or cooperative Cl^- channel family members. This will important since, to date, nearly 40 different genes have been shown to mediate Cl^- conductances.

The effects of DIDS were restricted to HRSV entry suggesting Cl^- channels are involved in viral attachment or an early HRSV infection stage. To confirm this, Cl^- homeostasis was examined during the early stages of HRSV infection (1-6 hpi) using well-established MQAE assays. HRSV was found to enhance Cl^- influx early in the infection cycle in the presence and absence of HRSV-SH, confirming the importance of Cl^- channels during HRSV entry and the lack of effect of SH in this process (Figure 3.22 and Figure 4.10). Further experiments also confirmed that DIDS did not globally inhibit cellular endocytic processes such as EGF internalisation, which occurred in the face of DIDS treatment (Figure 3.21), although a clearly altered distribution of EGF positive puncta was observed. In this regard, previous studies have shown that Cl^-/H^+ antiporters that are sensitive to DIDS localise to late endosomes and control endosomal pH (Graves et al., 2008; Igloi et al., 2015). Thus, based on our results, DIDS did not inhibit endocytosis but may alter the post internalization fate of both cellular receptors and invading viruses (such as HRSV) through alterations of endosomal pH gradients. The precise mechanism of how DIDS inhibits HRSV entry processes now requires further analysis.

6.2. The role of the HRSV-SH during HRSV infection

Label-free mass spectrometry was used to identify globular proteomic changes of recombinant HRSV and HRSV lacking its SH protein in both A549 and HBEpCs. The ultimate aim of these experiments was to identify significant

cellular changes that are dependent on HRSV-SH expression during HRSV infection. In A549 cells, when focus was placed upon the cellular proteins related to ionic homeostasis, it was found that CaM was significantly down regulated in both HRSV rA2 and HRSV ΔSH infected cells. This was an interesting finding since CaM plays a major role in Ca^{2+} mediated signaling, and typically when inhibited, decreases virus infection as demonstrated for both RV and HIV (Chattopadhyay et al., 2013). CHERP was also found to be significantly down regulated particularly during HRSV ΔSH infection, but due to the limitations discussed in Chapter 4, this result was not confirmed in biochemical assays.

The proteomic analysis of HBEpCs revealed more significant changes that were dependent on HRSV-SH. Caspase-1 as previously identified (Miao et al., 2011) was activated in response to HRSV infection in an SH dependent manner (Segovia et al., 2012). A novel aspect of the experiments performed in this study revealed that this caspase-1 activation triggers pyroptosis in HRSV infected HBEpCs (Figure 5.22). Viruses lacking HRSV-SH could be dependent on mediating pyroptosis confirming the importance of HRSV-SH protein. Other viruses containing viroporins including HIV have been shown to similarly induce pyroptosis in infected cells though this effect has never been linked to HIV viroporin activity (Doitsh et al., 2014; Lupfer et al., 2015). Future studies assessing the effects of caspase-1 inhibition in animal models of HRSV infection may reveal if SH mediated caspase-1 induction and pyroptosis contribute to HRSV pathogenesis *in vivo*. Of the other proteins identified, STAT-3 and STAT-1 were significantly upregulated during HRSV infection, and STAT-3 was validated to be up regulated in a HRSV-SH dependent manner (HRSV-ΔSH viruses did not up-regulate STAT 3) (Kong, San Juan, Kumar, Aruna K. Behera, et al., 2003). This identified new cellular targets regulated through HRSV-SH during HRSV infection. Further investigation is needed to investigate the relation of STAT-3 and HRSV-SH protein.

In conclusion, the identification of key virus-host cell interactions required during the HRSV lifecycle, such as those reported in this study, may pave the way for the development of novel anti-HRSV drugs. Cellular ion channels were found to play a key role in many aspects of the HRSV lifecycle most notably the

dependence on Cl^- channel functionality during HRSV entry. New cellular targets mediated by HRSV-SH were identified, including the dependence of HRSV-SH to induce caspase 1 activity and trigger pyroptosis. These studies add to our current knowledge of HRSV-host interactions and the role of HRSV-SH during virus infection.

References

Abdallah, A, Rowland, K.E., Schepetiuk, S.K., To, L.B. and Bardy, P. 2003. An outbreak of respiratory syncytial virus infection in a bone marrow transplant unit: effect on engraftment and outcome of pneumonia without specific antiviral treatment. *Bone marrow transplantation*. **32**(2),pp.195–203.

Åkerström, S., Mirazimi, A. and Tan, Y.J. 2007. Inhibition of SARS-CoV replication cycle by small interference RNAs silencing specific SARS proteins, 7a/7b, 3a/3b and S. *Antiviral Research*. **73**(3),pp.219–227.

Akira, S. 1999. Functional roles of STAT family proteins: lessons from knockout mice. *Stem cells*. **17**(3),pp.138–146.

Andrejeva, J., Childs, K.S., Young, D.F., Carlos, T.S., Stock, N., Goodbourn, S. and Randall, R.E. 2004. The V proteins of paramyxoviruses bind the IFN-inducible RNA helicase, mda-5, and inhibit its activation of the IFN-β promoter. *Proceedings of the National Academy of Sciences of the United States of America*. **101**(49),pp.17264–17269.

Arnott, A., Vong, S., Mardy, S., Chu, S., Naughtin, M., Sovann, L., Buecher, C., Beauté, J., Rith, S., Borand, L., Asgari, N., Frutos, R., Guillard, B., Touch, S., Deubel, V. and Buchy, P. 2011. A study of the genetic variability of human respiratory syncytial virus (HRSV) in Cambodia reveals the existence of a new HRSV group B genotype. *Journal of Clinical Microbiology*. **49**(10),pp.3504–3513.

Bantscheff, M., Schirle, M., Sweetman, G., Rick, J. and Kuster, B. 2007. Quantitative mass spectrometry in proteomics: a critical review. *Analytical and bioanalytical chemistry*. **389**(4),pp.1017–1031.

Bardou, O., Trinh, N.T.N. and Brochiero, E. 2009a. Molecular diversity and function of K+ channels in airway and alveolar epithelial cells. *Am.J.Physiol Lung Cell Mol.Physiol*. **296** (1040-0605) pp.L145–L155..

Bardou, O., Trinh, N.T.N. and Brochiero, E. 2009b. Molecular diversity and function of K+ channels in airway and alveolar epithelial cells. *American*

journal of physiology. Lung cellular and molecular physiology. [Online]. **296**(1040-0605) p. L145–L155.

Barends, M., De Rond, L.G.H., Dormans, J., Van Oosten, M., Boelen, A., Neijens, H.J., Osterhaus, A. and Kimman, T.G. 2004. Respiratory syncytial virus, pneumonia virus of mice, and influenza A virus differently affect respiratory allergy in mice. *Clinical & Experimental Allergy*. **34**(3),pp.488–496.

Barik, S. 1992. Transcription of human respiratory syncytial virus genome RNA in vitro: requirement of cellular factor(s). *Journal of virology*. **66**(11),pp.6813–6818.

Beigelman, A. and Bacharier, L.B. 2013. The role of early life viral bronchiolitis in the inception of asthma. *Current opinion in allergy and clinical immunology*. **13**(2),pp.211–6.

Bembridge, G.P., Lopez, J.A., Cook, R., Melero, J.A. and Taylor, G. 1998. Recombinant Vaccinia Virus Coexpressing the F Protein of Respiratory Syncytial Virus (RSV) and Interleukin-4 (IL-4) Does Not Inhibit the Development of RSV-Specific Memory Cytotoxic T Lymphocytes, whereas Priming Is Diminished in the Presence of High Leve. *J. Virol.* **72**(5),pp.4080–4087.

Bennett, B., Fong, D., Fiorino, M., Zhang, X., Edson, K., Johnston, J.A. and Phillips, J.E. 2016. Characterization Of An Inhaled Epithelial Sodium Channel (ENaC) Blocker In Mice To Improve Mucociliary Clearance *In*: *C60. ALL ABOUT CYSTIC FIBROSIS*. Am Thoracic Soc, pp. A5564–A5564.

Berger, J., Richter, K., Clauss, W.G. and Fronius, M. 2011. Evidence for basolateral Cl- channels as modulators of apical Cl- secretion in pulmonary epithelia of Xenopus laevis. *American journal of physiology. Regulatory, integrative and comparative physiology*. **300**,pp.R616–R623.

Bermingham, A. and Collins, P.L. 1999. The M2-2 protein of human respiratory syncytial virus is a regulatory factor involved in the balance between RNA

replication and transcription. *Proceedings of the National Academy of Sciences*. **96**(20),pp.11259–11264.

Bernacki, S.H., Nelson, a L., Abdullah, L., Sheehan, J.K., Harris, a, Davis, C.W. and Randell, S.H. 1999. Mucin gene expression during differentiation of human airway epithelia in vitro. Muc4 and muc5b are strongly induced. *American journal of respiratory cell and molecular biology*. **20**(4),pp.595–604.

Bernard, K., Bogliolo, S., Soriani, O. and Ehrenfeld, J. 2003. Modulation of Calcium-dependent Chloride Secretion by Basolateral SK4-like Channels in a Human Bronchial Cell Line. *Journal of Membrane Biology*. **196**(1),pp.15–31.

Biacchesi, S., Skiadopoulos, M.H., Yang, L., Lamirande, E.W., Tran, K.C., Murphy, B.R., Collins, P.L. and Buchholz, U.J. 2004. Recombinant human Metapneumovirus lacking the small hydrophobic SH and/or attachment G glycoprotein: deletion of G yields a promising vaccine candidate. *Journal of virology*. [Online]. **78**(23),pp.12877–87.

Bitko, V., Shulyayeva, O., Mazumder, B., Musiyenko, A., Ramaswamy, M., Look, D.C. and Barik, S. 2007. Nonstructural proteins of respiratory syncytial virus suppress premature apoptosis by an NF-kappaB-dependent, interferon-independent mechanism and facilitate virus growth. *J Virol*. [Online]. **81**(4),pp.1786–1795.

Boucher, R.C. 2002. An overview of the pathogenesis of cystic fibrosis lung disease. *Advanced Drug Delivery Reviews*. **54**(11),pp.1359–1371.

Boucher, R.C. 2004. Relationship of Airway Epithelial Ion Transport to Chronic Bronchitis. *Proc Am Thprac Soc*. **1**,p.pp 66–70.

Bozym, R.A., Morosky, S.A., Kim, K.S., Cherry, S. and Coyne, C.B. 2010. Release of intracellular calcium stores facilitates coxsackievirus entry into polarized endothelial cells. *PLoS Pathogens*. **6**(10).

Brackenbury, W.J. 2012. Voltage-gated sodium channels and metastatic

disease. *Channels (Austin, Tex.)*. [Online]. **6**(5),pp.352–61.

Breckenridge, D.G., Nguyen, M., Kuppig, S., Reth, M. and Shore, G.C. 2002. The procaspase-8 isoform, procaspase-8L, recruited to the BAP31 complex at the endoplasmic reticulum. *Proceedings of the National Academy of Sciences of the United States of America*. **99**(7),pp.4331–6.

Breckenridge, D.G., Stojanovic, M., Marcellus, R.C. and Shore, G.C. 2003. Caspase cleavage product of BAP31 induces mitochondrial fission through endoplasmic reticulum calcium signals, enhancing cytochrome c release to the cytosol. *The Journal of cell biology*. **160**(7),pp.1115–27.

Brochiero, E., Dagenais, A., Privé, A., Berthiaume, Y. and Grygorczyk, R. 2004. Evidence of a functional CFTR Cl(-) channel in adult alveolar epithelial cells. *American journal of physiology. Lung cellular and molecular physiology*. [Online]. **287**(2),pp.L382–92.

Brock, S.C., Goldenring, J.R. and Crowe, J.E. 2003. Apical recycling systems regulate directional budding of respiratory syncytial virus from polarized epithelial cells. *Proceedings of the National Academy of Sciences* . [Online]. **100** (25),pp.15143–15148.

Brown, G., Rixon, H.W. and Sugrue, R.J. 2002. Respiratory syncytial virus assembly occurs in GM1-rich regions of the host-cell membrane and alters the cellular distribution of tyrosine phosphorylated caveolin-1. *J Gen Virol*. **83**.

Bukreyev, a, Whitehead, S.S., Murphy, B.R. and Collins, P.L. 1997. Recombinant respiratory syncytial virus from which the entire SH gene has been deleted grows efficiently in cell culture and exhibits site-specific attenuation in the respiratory tract of the mouse. *Journal of virology*. **71**(12),pp.8973–8982.

Bukreyev, A., Yang, L. and Collins, P.L. 2012. The Secreted G Protein of Human Respiratory Syncytial Virus Antagonizes Antibody-Mediated Restriction of Replication Involving Macrophages and Complement. *Journal of Virology*. **86**(19),pp.10880–10884.

Bullough, P.A., Hughson, F.M., Skehel, J.J. and Wiley, D.C. 1994. Structure of influenza haemagglutinin at the pH of membrane fusion. *Nature*. **371**(6492),pp.37–43.

Burch, L.H., Talbot, C.R., Knowles, M.R., Canessa, C.M., Rossier, B.C. and Boucher, R.C. 1995. Relative expression of the human epithelial Na+ channel subunits in normal and cystic fibrosis airways. *Am J Physiol*. **269**(2 Pt 1),pp.C511–518.

Burke, P., Schooler, K. and Wiley, H.S. 2001. Regulation of epidermal growth factor receptor signaling by endocytosis and intracellular trafficking. *Molecular biology of the cell*. **12**(6),pp.1897–910.

Cantero-Recasens, G., Fandos, C., Rubio-Moscardo, F., Valverde, M.A. and Vicente, R. 2009. The asthma-associated ORMDL3 gene product regulates endoplasmic reticulum-mediated calcium signaling and cellular stress. *Human Molecular Genetics*. **19**(1),pp.111–121.

Carter, S.D., Dent, K.C., Atkins, E., Foster, T.L., Verow, M. and Gorny, P. 2010. Direct visualization of the small hydrophobic protein of human respiratory syncytial virus reveals the structural basis for membrane permeability. *FEBS Lett*. **584**.

Castagné, N., Barbier, A., Bernard, J., Rezaei, H., Huet, J.C., Henry, C., Da Costa, B. and Eléouët, J.F. 2004. Biochemical characterization of the respiratory syncytial virus P-P and P-N protein complexes and localization of the P protein oligomerization domain. *Journal of General Virology*. **85**(6),pp.1643–1653.

Chanock, R., Rolizman, B. and Myers, R. 1957. Recovery from infants with respiratory illness of a virus related to chimpanzee coryza agent (CCA). I. Isolation, properties and characterization. *American journal of hygiene*. [Online]. **66**(3),pp.281–90.

Chattopadhyay, S., Basak, T., Nayak, M.K., Bhardwaj, G., Mukherjee, A., Bhowmick, R., Sengupta, S., Chakrabarti, O., Chatterjee, N.S. and Chawla-Sarkar, M. 2013. Identification of cellular calcium binding protein calmodulin

as a regulator of rotavirus A infection during comparative proteomic study. *PloS one*. [Online]. **8**(2),p.e56655.

Cheng, X., Park, H., Zhou, H. and Jin, H. 2005. Overexpression of the M2-2 Protein of Respiratory Syncytial Virus Inhibits Viral Replication. *Journal of Virology*. [Online]. **79**(22),pp.13943–13952.

Chirkova, T., Boyoglu-Barnum, S., Gaston, K. a, Malik, F.M., Trau, S.P., Oomens, A.G.P. and Anderson, L.J. 2013. Respiratory Syncytial Virus G Protein CX3C Motif Impairs Human Airway Epithelial and Immune Cell Responses. *Journal of Virology*. **87**(24),pp.13466–79.

Choi, A.M.K. and Alam, J. 1996. Heme Oxygenase-1: Function, Regulation, and Implication of a Novel Stress-inducible Protein in Oxidant-induced Lung Injury. *American Journal of Respiratory Cell and Molecular Biology*. **15**(1),pp.9–19.

Choi, J., Chang, J.S., Song, M.S., Ahn, B.Y., Park, Y.I., Lim, D.S. and Han, Y.S. 2003. Association of hepatitis B virus polymerase with promyelocytic leukemia nuclear bodies mediated by the S100 family protein p11. *Biochemical and Biophysical Research Communications*. **305**(4),pp.1049–1056.

Ciampor, F. 2003. The ion channels coded by viruses. *Acta microbiologica et immunologica Hungarica*. **50**(4),pp.433–442.

Click, J.H. 1969. Serum Lactate Dehydrogenase Isoenzyme and Total Lactate Dehydrogenase Values in Health and Disease, and Clinical Evaluation of These Tests by Means of Discriminant Analysis. *American Journal of Clinical Pathology*. **52**(3),pp.320–328.

Collins, P.. 2007. *Respiratory Syncytial Virus and Metapneumovirus* (E. 2007 D.M. Knipe, ed.). New York: Lippincott & Wilkins.

Collins, P.L. and Graham, B.S. 2008. Viral and host factors in human respiratory syncytial virus pathogenesis. *Journal of virology*. **82**(5),pp.2040–55.

Collins, P.L., Hill, M.G., Camargo, E., Grosfeld, H., Chanock, R.M. and Murphy, B.R. 1995. Production of infectious human respiratory syncytial virus from cloned cDNA confirms an essential role for the transcription elongation factor from the 5'proximal open reading frame of the M2 mRNA in gene expression and provides a capability for vaccine development. *Proceedings of the National Academy of Sciences*. **92**(25),pp.11563–11567.

Collins, P.L., Hill, M.G., Cristina, J. and Grosfeld, H. 1996. Transcription elongation factor of respiratory syncytial virus, a nonsegmented negative-strand RNA virus. *Proceedings of the National Academy of Sciences of the United States of America*. **93**(1) pp.81–5.

Collins, P.L. and Melero, J.A. 2011. Progress in understanding and controlling respiratory syncytial virus: still crazy after all these years. *Virus research*. [Online]. **162**(1-2),pp.80–99.

Collins, P.L. and Mottet, G. 1993. Membrane orientation and oligomerization of the small hydrophobic protein of human respiratory syncytial virus. *Journal of General Virology*. **74**(7),pp.1445–1450.

Collins, P.L., Olmsted, R.A. and Johnson, P.R. 1990. The small hydrophobic protein of human respiratory syncytial virus: Comparison between antigenic subgroups A and B. *Journal of General Virology*. **71**(7),pp.1571–1576.

Cook, G.A. and Opella, S.J. 2010. NMR studies of p7 protein from hepatitis C virus. *Eur Biophys J*. [Online]. **39**(7),pp.1097–1104.

Cordey, S. and Roux, L. 2007. Further characterization of a paramyxovirus transcription initiation signal: search for required nucleotides upstream and importance of the N phase context. *The Journal of general virology*. [Online]. **88**(Pt 5),pp.1555–64. Crump, R.G., Askew, G.R., Wert, S.E., Lingrel, J.B. and Joiner, C.H. 1995. In situ localization of sodium-potassium ATPase mRNA in developing mouse lung epithelium. *Am J Physiol*. **269**(3 Pt 1) ,pp.L299–308.

D O'Connell, A., Morton, M.J. and Hunter, M. 2002. Two-pore domain K+ channels—molecular sensors. *Biochimica et Biophysica Acta (BBA)-*

Biomembranes. **1566**(1),pp.152–161.

Dakhama, A., Park, J.W., Taube, C., Joetham, A., Balhorn, A., Miyahara, N., Takeda, K. and Gelfand, E.W. 2005. The enhancement or prevention of airway hyperresponsiveness during reinfection with respiratory syncytial virus is critically dependent on the age at first infection and IL-13 production. *Journal of Immunology*. **175**(3),pp.1876–1883.

DeDiego, M.L., Alvarez, E., Almazan, F., Rejas, M.T., Lamirande, E., Roberts, A., Shieh, W.J., Zaki, S.R., Subbarao, K. and Enjuanes, L. 2007. A severe acute respiratory syndrome coronavirus that lacks the E gene is attenuated in vitro and in vivo. *J Virol*. **81**(4),pp.1701–1713.

Diciccio, J.E. and Steinberg, B.E. 2011. Lysosomal pH and analysis of the counter ion pathways that support acidification. (2009),pp.385–390.

Dickens, L.E., Collins, P.L. and Wertz, G.W. 1984. Transcriptional mapping of human respiratory syncytial virus. *J Virol*. **52**(2),pp.364–369.

Dikic, I. 2003. Mechanisms controlling EGF receptor endocytosis and degradation. *Biochemical Society transactions*. **31**(Pt 6),pp.1178–1181.

Dimitrov, D.S. 2004. Virus entry: molecular mechanisms and biomedical applications. *Nature reviews. Microbiology*. **2**(2),pp.109–122.

Dnb, N., Theodoratou, E., Rudan, I., Campbell, H., Nokes, D.J., Hnd, N., Munywoki, P.K., Dherani, M., Phd, B., Nair, H., Nokes, J., Gessner, B.D., Dherani, M., Madhi, S.A., Singleton, R.J., O ’brien, K.L., Roca, A., Wright, P.F., Bruce, N., Chandran, A., Theodoratou, E., Sutanto, A., Sedyaningsih, E.R., Ngama, M., Munywoki, P.K., Kartasasmita, C., Simões, E.A.F., Rudan, I., Weber, M.W. and Campbell, H. 2010. Global burden of acute lower respiratory infections due to respiratory syncytial virus in young children: a systematic review and meta-analysis. *The Lancet*. **375**,pp.1545–1555.

Dodrill, M.W. and Fedan, J.S. 2010. Lipopolysaccharide hyperpolarizes guinea pig airway epithelium by increasing the activities of the epithelial Na(+)

channel and the Na(+)-K(+) pump. *American journal of physiology. Lung cellular and molecular physiology*. **299**(4),pp.L550–8.

Doitsh, G., Galloway, N.L.K., Geng, X., Yang, Z., Monroe, K.M., Zepeda, O., Hunt, P.W., Hatano, H., Sowinski, S. and Muñoz-Arias, I. 2014. Cell death by pyroptosis drives CD4 T-cell depletion in HIV-1 infection. *Nature*. **505**(7484),pp.509–514.

Douglas, J.L., Panis, M.L., Ho, E., Lin, K.-Y., Krawczyk, S.H., Grant, D.M., Cai, R., Swaminathan, S. and Cihlar, T. 2003. Inhibition of respiratory syncytial virus fusion by the small molecule VP-14637 via specific interactions with F protein. *J Virol.* **77**(9),pp.5054–64.

Dowall, S.D., Findlay-Wilson, S., Rayner, E., Pearson, G., Pickersgill, J., Rule, A., Merredew, N., Smith, H., Chamberlain, J. and Hewson, R. 2012. Hazara virus infection is lethal for adult type I interferon receptor-knockout mice and may act as a surrogate for infection with the human-pathogenic Crimean-Congo hemorrhagic fever virus. *Journal of General Virology*. **93**(3),pp.560–564.

Draft, C., Mortality, G.B.D., Collaborators, D., Burden, T.G., Gbd, T., Goal-related, M.D., Africa, S., Kingdom, U., States, U., Goals, M.D., Commission, T.L. and Convergence, G. 2015. Global, regional and national levels of age-specific mortality and 240 causes of death , 1990-2013 : A systematic analysis for the Global Burden of Disease Study 2013. *The Lancet*. **385** (9963),pp.1990–2013.

Dubyak, G.R. 2004. Ion homeostasis, channels, and transporters: an update on cellular mechanisms. *Advances in physiology education*. **28**,pp.143–154.

Ducharme, F.M., Tse, S.M. and Chauhan, B. 2014. Diagnosis, management, and prognosis of preschool wheeze. *The Lancet*. **383** (9928),pp.1593–1604.

Empey, K.M., Peebles, R.S. and Kolls, J.K. 2010. Pharmacologic advances in the treatment and prevention of respiratory syncytial virus. *Clinical infectious diseases : an official publication of the Infectious Diseases*

Society of America. **50**(9),pp.1258–1267.

Escobar, G.J., Masaquel, A.S., Li, S.X., Walsh, E.M. and Kipnis, P. 2013. Persistent recurring wheezing in the fifth year of life after laboratory-confirmed, medically attended respiratory syncytial virus infection in infancy. *BMC pediatrics*. **13**(1),p.97.

Evans, G.L., Caller, L.G., Foster, V. and Crump, C.M. 2015. Anion homeostasis is important for non-lytic release of BK polyomavirus from infected cells. *Open Biology*. **5**(8).

Ewart, G.D., Mills, K., Cox, G.B. and Gage, P.W. 2002. Amiloride derivatives block ion channel activity and enhancement of virus-like particle budding caused by HIV-1 protein Vpu *In*: *European Biophysics Journal*., pp. 26–35.

Falsey, A.R., Hennessey, P.A., Formica, M.A., Cox, C. and Walsh, E.E. 2005. Respiratory syncytial virus infection in elderly and high-risk adults. *The New England journal of medicine*. **352**(17),pp.1749–59.

Fang, X., Song, Y., Hirsch, J., Galietta, L.J. V, Pedemonte, N., Zemans, R.L., Dolganov, G., Verkman, a S. and Matthay, M. a 2006. Contribution of CFTR to apical-basolateral fluid transport in cultured human alveolar epithelial type II cells. *American Journal of Physiology. Lung Cellular and Molecular Physiology*. **290**(2),pp.242–9.

Fearns, R. and Collins, P.L. 1999. Model for polymerase access to the overlapped L gene of respiratory syncytial virus. *Journal of virology*. **73**(1),pp.388–97.

Feldman, A.S., He, Y., Moore, M.L., Hershenson, M.B. and Hartert, T. V. 2015. Toward primary prevention of asthma: Reviewing the evidence for early-life respiratory viral infections as modifiable risk factors to prevent childhood asthma. *American Journal of Respiratory and Critical Care Medicine*. **191**(1),pp.34–44.

Feske, S., Wulff, H. and Skolnik, E.Y. 2015. *Ion channels in innate and adaptive immunity.*

Fiedler, M.A., Wernke-Dollries, K. and Stark, J.M. 1995. Respiratory syncytial virus increases IL-8 gene expression and protein release in A549 cells. *American Journal of Physiology-Lung Cellular and Molecular Physiology*. **269**(6),pp.L865–L872.

Fischer, H., Illek, B., Finkbeiner, W.E. and Widdicombe, J.H. 2007. Basolateral Cl channels in primary airway epithelial cultures. *American journal of physiology. Lung cellular and molecular physiology*. **292** pp.L1432–L1443.

Förster, A., Maertens, G.N., Farrell, P.J. and Bajorek, M. 2015. Dimerization of matrix protein is required for budding of respiratory syncytial virus. *Journal of virology*. **89**(8),pp.4624–35.

Foster, T.L., Thompson, G.S., Kalverda, A.P., Kankanala, J., Bentham, M., Wetherill, L.F., Thompson, J., Barker, A.M., Clarke, D., Noerenberg, M., Pearson, A.R., Rowlands, D.J., Homans, S.W., Harris, M., Foster, R. and Griffin, S. 2014. Structure-guided design affirms inhibitors of hepatitis C virus p7 as a viable class of antivirals targeting virion release. *Hepatology*. **59**(2),pp.408–422.

Foster, T.L., Verow, M., Wozniak, A.L., Bentham, M.J., Thompson, J., Atkins, E., Weinman, S.A., Fishwick, C., Foster, R., Harris, M. and Griffin, S. 2011. Resistance mutations define specific antiviral effects for inhibitors of the hepatitis C virus p7 ion channel. *Hepatology*. **54**(1),pp.79–90.

Freundt, E.C., Yu, L., Goldsmith, C.S., Welsh, S., Cheng, A., Yount, B., Liu, W., Frieman, M.B., Buchholz, U.J., Screaton, G.R., Lippincott-Schwartz, J., Zaki, S.R., Xu, X.-N.N., Baric, R.S., Subbarao, K. and Lenardo, M.J. 2010. The open reading frame 3a protein of severe acute respiratory syndrome-associated coronavirus promotes membrane rearrangement and cell death. *J Virol*. **84**(2),pp.1097–1109.

Fuentes, S., Tran, K.C., Luthra, P., Teng, M.N. and He, B. 2007. Function of the respiratory syncytial virus small hydrophobic protein. *J Virol*. **81**.

Fuentes, S., Tran, K.C., Luthra, P., Teng, M.N. and He, B. 2007. Function of the Respiratory Syncytial Virus Small Hydrophobic Protein **81**(15),pp.8361–

8366.

Fung, T.S., Torres, J. and Liu, D.X. 2015. The emerging roles of viroporins in ER stress response and autophagy induction during virus infection. *Viruses*. **7**(6),pp.2834–2857.

Galluzzi, L., López-Soto, A., Kumar, S. and Kroemer, G. 2016. Caspases Connect Cell-Death Signaling to Organismal Homeostasis. *Immunity*.. **44**(2),pp.221–231.

Gan, S.-W., Tan, E., Lin, X., Yu, D., Wang, J., Tan, G.M.-Y., Vararattanavech, A., Yeo, C.Y., Soon, C.H., Soong, T.W., Pervushin, K. and Torres, J. 2012. The small hydrophobic protein of the human respiratory syncytial virus forms pentameric ion channels. *The Journal of biological chemistry*.. **287**(29),pp.24671–89.

Gan, S.W., Ng, L., Lin, X., Gong, X. and Torres, J. 2008. Structure and ion channel activity of the human respiratory syncytial virus (hRSV) small hydrophobic protein transmembrane domain. *Protein science : a publication of the Protein Society*. **17**,pp.813–820.

Ghildyal, R., Baulch-Brown, C., Mills, J. and Meanger, J. 2003. The matrix protein of Human respiratory syncytial virus localises to the nucleus of infected cells and inhibits transcription. *Archives of virology*. **148**,pp.1419–1429.

Ghildyal, R., Mills, J., Murray, M., Vardaxis, N. and Meanger, J. 2002. Respiratory syncytial virus matrix protein associates with nucleocapsids in infected cells. *The Journal of general virology*. **83**(2002),pp.753–757.

Giard, D.J., Aaronson, S.A., Todaro, G.J., Arnstein, P., Kersey, J.H., Dosik, H. and Parks, W.P. 1973. In vitro cultivation of human tumors: establishment of cell lines derived from a series of solid tumors. *Journal of the National Cancer Institute*. **51**(5),pp.1417–23.

Giard, D.J., Aaronson, S.A., Todaro, G.J., Arnstein, P., Kersey, J.H. and Parks, W.P. 1973. In Vitro Cultivation of Human Tumors : Establishment of Cell

Lines Derived From. *Journal of the National Cancer Institute*. **51**(5),pp.1417–1423.

Gladue, D.P., Holinka, L.G., Largo, E., Fernandez Sainz, I., Carrillo, C., O'Donnell, V., Baker-Branstetter, R., Lu, Z., Ambroggio, X., Risatti, G.R., Nieva, J.L. and Borca, M. V 2012. Classical swine fever virus p7 protein is a viroporin involved in virulence in swine. *Journal of virology*. **86**(12),pp.6778–91.

Gonzalez, M.E. and Carrasco, L. 2003. Viroporins *In*: *FEBS Letters*., pp. 28–34.

Graham, B.S. 2016. Vaccines against respiratory syncytial virus: The time has finally come. *Vaccine*, In press

Graham, B.S., Modjarrad, K. and McLellan, J.S. 2015. Novel antigens for RSV vaccines. *Current opinion in immunology*. **35**,pp.30–8.

Graves, A.R., Curran, P.K., Smith, C.L. and Mindell, J.A. 2008. The Cl-/H+ antiporter ClC-7 is the primary chloride permeation pathway in lysosomes. *Nature*. **453**(7196),pp.788–792.

Griffin, S., StGelais, C., Owsianka, A.M., Patel, A.H., Rowlands, D. and Harris, M. 2008. Genotype-dependent sensitivity of hepatitis C virus to inhibitors of the p7 ion channel. *Hepatology*. **48**(6),pp.1779–1790.

Griffin, S.D.C., Beales, L.P., Clarke, D.S., Worsfold, O., Evans, S.D., Jaeger, J., Harris, M.P.G., Rowlands, D.J. and Klenk, H.D. 2003. The p7 protein of hepatitis C virus forms an ion channel that is blocked by the antiviral drug, Amantadine *In*: *FEBS Letters*., pp. 34–38.

Grove, J. and Marsh, M. 2011. The cell biology of receptor-mediated virus entry. *Journal of Cell Biology*. **195**(7),pp.1071–1082.

Hall, C.B., Hall, W.J., Gala, C.L., MaGill, F.B. and Leddy, J.P. 1984. Long-term prospective study in children after respiratory syncytial virus infection. *The Journal of pediatrics*. **105**(3),p.358.

Hall, C.B., Weinberg, G.A., Iwane, M.K., Blumkin, A.K., Edwards, K.M., Staat,

M.A., Auinger, P., Griffin, M.R., Poehling, K.A., Erdman, D., Grijalva, C.G., Zhu, Y. and Szilagyi, P. 2009. The burden of respiratory syncytial virus infection in young children. *The New England journal of medicine*. **360**(6),pp.588–98.

Hallak, L.K., Collins, P.L., Knudson, W. and Peeples, M.E. 2000. Iduronic acid-containing glycosaminoglycans on target cells are required for efficient respiratory syncytial virus infection. *Virology*. **271**(2),pp.264–275.

Hart, R.J.C. 1984. An outbreak of respiratory syncytial virus infection in an old people's home. *Journal of Infection*. **8**(3),pp.259–261.

Hay, a J., Zambon, M.C., Wolstenholme, a J., Skehel, J.J. and Smith, M.H. 1986. Molecular basis of resistance of influenza A viruses to amantadine. *The Journal of antimicrobial chemotherapy*. **18 Suppl B**,pp.19–29.

Hayashi, N., Matsubara, M., Jinbo, Y., Titani, K., Izumi, Y. and Matsushima, N. 2002. Nef of HIV-1 interacts directly with calcium-bound calmodulin. *Protein science : a publication of the Protein Society*. **11**(3),pp.529–537.

Haynes, L.M., Moore, D.D., Kurt-Jones, E.A., Finberg, R.W., Anderson, L.J. and Tripp, R.A. 2001. Involvement of toll-like receptor 4 in innate immunity to respiratory syncytial virus. *J Virol*. **75**.

Henderson, G., Murray, J. and Yeo, R.P. 2002. Sorting of the Respiratory Syncytial Virus Matrix Protein into Detergent-Resistant Structures Is Dependent on Cell-Surface Expression of the Glycoproteins. *Virology*. **300**(2),pp.244–254.

Holgate, S.T., Roberts, G., Arshad, H.S., Howarth, P.H. and Davies, D.E. 2009. The role of the airway epithelium and its interaction with environmental factors in asthma pathogenesis. *Proceedings of the American Thoracic Society*. **6**(8),pp.655–659.

Hollenhorst, M.I., Richter, K. and Fronius, M. 2011. Ion transport by pulmonary epithelia. *Journal of Biomedicine and Biotechnology*. **2011**.

Holman, R.C., Shay, D.K., Curns, A.T., Lingappa, J.R. and Anderson, L.J. 2003.

Risk factors for bronchiolitis-associated deaths among infants in the United States. *The Pediatric infectious disease journal*. **22**(6),pp.483–490.

Horisberger, J.D. and Chraïbi, A. 2004. Epithelial sodium channel: A ligand-gated channel? *Nephron - Physiology*. **96**(2).

Hover, S., King, B., Hall, B., Loundras, E.-A., Taqi, H., Daly, J., Dallas, M., Peers, C., Schnettler, E., McKimmie, C., Kohl, A., Barr, J.N. and Mankouri, J. 2015. Modulation of potassium channels inhibits bunyavirus infection. *Journal of Biological Chemistry*. doi/10.1074/jbc.M115.692673.

Howard, T.D., Koppelman, G.H., Xu, J., Zheng, S.L., Postma, D.S., Meyers, D.A. and Bleecker, E.R. 2002. Gene-gene interaction in asthma: IL4RA and IL13 in a Dutch population with asthma. *The American Journal of Human Genetics*. **70**(1),pp.230–236.

Hsieh, P.-K., Chang, S.C., Huang, C.-C., Lee, T.-T., Hsiao, C.-W., Kou, Y.-H., Chen, I.-Y., Chang, C.-K., Huang, T.-H. and Chang, M.-F. 2005. Assembly of severe acute respiratory syndrome coronavirus RNA packaging signal into virus-like particles is nucleocapsid dependent. *Journal of virology*. **79**(22),pp.13848–13855.

Hsu, K., Seharaseyon, J., Dong, P., Bour, S. and Marba, E. 2004. Mutual Functional Destruction of HIV-1 Vpu and Host TASK-1 Channel. . **14**,pp.259–267.

Huang, Y.T., Collins, P.L. and Wertz, G.W. 1985. Characterization of the 10 proteins of human respiratory syncytial virus: Identification of a fourth envelope-associated protein. *Virus Research*. **2**(2),pp.157–173.

Hummler, E., Barker, P. and Gatzy, J. 1996. Early death due to defective neonatal lung liquid clearance in αENaC-deficient mice. *Nature Genetics*. **12**(3),pp.325–328.

Ichinohe, T., Pang, I.K. and Iwasaki, A. 2010. Influenza virus activates inflammasomes via its intracellular M2 ion channel. *Nature immunology*. **11**(5),pp.404–10.

Igloi, Z., Mohl, B.-P., Lippiat, J.D., Harris, M. and Mankouri, J. 2015. Requirement for Chloride Channel Function during the Hepatitis C Virus Lifecycle. *Journal of Virology*. **44** (January) doi/10.1128/JVI.02946-14.

Irvine, E., Keblesh, J., Liu, J. and Xiong, H. 2007. Voltage-gated Potassium Channel Modulation of Neurotoxic Activity in Human Immunodeficiency Virus Type-1(HIV-1)-Infected Macrophages. *Journal of Neuroimmune Pharmacology*. (3),pp.265–269.

Ito, M., Yanagi, Y. and Ichinohe, T. 2012. Encephalomyocarditis Virus Viroporin 2B Activates NLRP3 Inflammasome. *PLoS Pathogens*. **8**(8).

Iwasawa, R., Mahul-Mellier, A.-L., Datler, C., Pazarentzos, E. and Grimm, S. 2011. Fis1 and Bap31 bridge the mitochondria-ER interface to establish a platform for apoptosis induction. *The EMBO journal*. [Online]. **30**(3),pp.556–568.

Jack, P.J.M., Boyle, D.B., Eaton, B.T. and Wang, L.-F. 2005. The complete genome sequence of J virus reveals a unique genome structure in the family Paramyxoviridae. *Journal of virology*. **79**(16),pp.10690–700.

Jiang, X., Ingbar, D.H. and O'Grady, S.M. 1998. Adrenergic stimulation of Na+ transport across alveolar epithelial cells involves activation of apical Cl- channels. *The American journal of physiology*. **275**(6 Pt 1),pp.C1610–20.

Jin, H., Clarke, D., Zhou, H.Z., Cheng, X., Coelingh, K., Bryant, M. and Li, S. 1998. Recombinant human respiratory syncytial virus (RSV) from cDNA and construction of subgroup A and B chimeric RSV. *Virology*. **251**(1),pp.206–14.

Jin, H., Zhou, H., Cheng, X., Tang, R., Munoz, M. and Nguyen, N. 2000. Recombinant Respiratory Syncytial Viruses with Deletions in the NS1, NS2, SH, and M2-2 Genes Are Attenuated in Vitro and in Vivo. *Virology*. **273**(1),pp.210–218.

Jin, N., Kolliputi, N., Gou, D., Weng, T. and Liu, L. 2006. A novel function of ionotropic γ-aminobutyric acid receptors involving alveolar fluid

homeostasis. *Journal of Biological Chemistry*. **281**(47),pp.36012–36020.

Johnson, J.E., Gonzales, R. a, Olson, S.J., Wright, P.F. and Graham, B.S. 2007. The histopathology of fatal untreated human respiratory syncytial virus infection. *Modern pathology : an official journal of the United States and Canadian Academy of Pathology, Inc*. **20**(1),pp.108–19.

Johnson, M., Allen, L. and Dobbs, L. 2009. Characteristics of Cl- uptake in rat alveolar type I cells. *American journal of physiology. Lung cellular and molecular physiology*. **297**(5),pp.L816–27.

Johnson, M.D., Widdicombe, J.H., Allen, L., Barbry, P. and Dobbs, L.G. 2002. Alveolar Epithelial Type I Cells Contain Transport Proteins and Transport Sodium, Supporting an Active Role for Type I Cells in Regulation of Lung Liquid Homeostasis. *Proceedings of the National Academy of Sciences of the United States of America*. **99**(4),pp.1966–1971.

Johnson, P.R., Spriggs, M.K., Olmsted, R.A. and Collins, P.L. 1987. The G glycoprotein of human respiratory syncytial viruses of subgroups A and B: extensive sequence divergence between antigenically related proteins. *Proceedings of the National Academy of Sciences of the United States of America*. **84**(16),pp.5625–9.

Johnson, S.M., McNally, B.A., Ioannidis, I., Flano, E., Teng, M.N., Oomens, A.G., Walsh, E.E. and Peeples, M.E. 2015. Respiratory Syncytial Virus Uses CX3CR1 as a Receptor on Primary Human Airway Epithelial Cultures. *PLoS Pathogens*. **11**(12).

de Jong, A.S., de Mattia, F., Van Dommelen, M.M., Lanke, K., Melchers, W.J.G., Willems, P.H.G.M. and van Kuppeveld, F.J.M. 2008. Functional analysis of picornavirus 2B proteins: effects on calcium homeostasis and intracellular protein trafficking. *Journal of virology*. **82**(7),pp.3782–90.

Jovanović, S., Crawford, R.M., Ranki, H.J. and Jovanović, A. 2003. Large conductance Ca2+-activated K+ channels sense acute changes in oxygen tension in alveolar epithelial cells. *American journal of respiratory cell and molecular biology*. **28**(3),pp.363–72.

Karron, R.A., Buonagurio, D.A., Georgiu, A.F., Whitehead, S.S., Adamus, J.E., Clements-Mann, M. Lou, Harris, D.O., Randolph, V.B., Udem, S.A., Murphy, B.R. and Sidhu, M.S. 1997. Respiratory syncytial virus (RSV) SH and G proteins are not essential for viral replication in vitro: Clinical evaluation and molecular characterization of a cold-passaged, attenuated RSV subgroup B mutant. *Proceedings of the National Academy of Sciences.* **94** (25) pp.13961–13966.

Kemp, P.J. and Peers, C. 2007. Oxygen sensing by ion channels. *Essays in biochemistry*. **43**,pp.77–90.

Kim, A.N., Jeon, W.-K., Lee, J.J. and Kim, B.-C. 2010. Up-regulation of heme oxygenase-1 expression through CaMKII-ERK1/2-Nrf2 signaling mediates the anti-inflammatory effect of bisdemethoxycurcumin in LPS-stimulated macrophages. *Free Radical Biology and Medicine*. **49**(3),pp.323–331.

Kipper, S., Hamad, S., Caly, L., Avrahami, D., Bacharach, E., Jans, D.A., Gerber, D. and Bajorek, M. 2015. New host factors important for respiratory syncytial virus (RSV) replication revealed by a novel microfluidics screen for interactors of matrix (M) protein. *Molecular & cellular proteomics :* **14**(3),pp.532–43.

Kiss, G., Holl, J.M., Williams, G.M., Alonas, E., Vanover, D., Lifland, A.W., Gudheti, M., Guerrero-Ferreira, R.C., Nair, V. and Yi, H. 2014. Structural analysis of respiratory syncytial virus reveals the position of M2-1 between the matrix protein and the ribonucleoprotein complex. *Journal of virology*. **88**(13),pp.7602–7617.

Knudson, C.J. and Varga, S.M. 2015. The relationship between respiratory syncytial virus and asthma. *Veterinary pathology*. **52**(1),pp.97–106.

Kolakofsky, D., Pelet, T., Garcin, D., Hausmann, S., Curran, J. and Roux, L. 1998. Paramyxovirus RNA synthesis and the requirement for hexamer genome length: the rule of six revisited. *Journal of virology*. **72**(2),pp.891–899.

Kolokoltsov, A.A., Deniger, D., Fleming, E.H., Roberts, N.J., Karpilow, J.M. and

Davey, R.A. 2007a. Small Interfering RNA Profiling Reveals Key Role of Clathrin-Mediated Endocytosis and Early Endosome Formation for Infection by Respiratory Syncytial Virus **81**(14),pp.7786–7800.

Kolokoltsov, A.A., Deniger, D., Fleming, E.H., Roberts, N.J., Karpilow, J.M. and Davey, R.A. 2007b. Small interfering RNA profiling reveals key role of clathrin-mediated endocytosis and early endosome formation for infection by respiratory syncytial virus. *Journal of virology*. **81**(14),pp.7786–800.

Kong, X., San Juan, H., Kumar, M., Behera, A.K., Mohapatra, A., Hellermann, G.R., Mane, S., Lockey, R.F. and Mohapatra, S.S. 2003. Respiratory syncytial virus infection activates STAT signaling in human epithelial cells. *Biochemical and Biophysical Research Communications*. **306**(2),pp.616–622.

Kong, X., San Juan, H., Kumar, M., Behera, A.K., Mohapatra, A., Hellermann, G.R., Mane, S., Lockey, R.F. and Mohapatra, S.S. 2003. Respiratory syncytial virus infection activates STAT signaling in human epithelial cells. *Biochemical and Biophysical Research Communications*. **306**(2),pp.616–622.

Kotelkin, A., Prikhod'ko, E.A., Cohen, J.I., Collins, P.L. and Bukreyev, A. 2003. Respiratory syncytial virus infection sensitizes cells to apoptosis mediated by tumor necrosis factor-related apoptosis-inducing ligand. *Journal of virology*. **77**(17),pp.9156–72.

Krishnamoorthy, N., Khare, A., Oriss, T.B., Raundhal, M., Morse, C., Yarlagadda, M., Wenzel, S.E., Moore, M.L., Peebles Jr., R.S., Ray, A. and Ray, P. 2012. Early infection with respiratory syncytial virus impairs regulatory T cell function and increases susceptibility to allergic asthma. *Nat Med*. **18**(10),pp.1525–1530.

Kristjansson, S., Bjarnarson, S.P., Wennergren, G., Palsdottir, A.H., Arnadottir, T., Haraldsson, A. and Jonsdottir, I. 2005. Respiratory syncytial virus and other respiratory viruses during the first 3 months of life promote a local TH2-like response. *Journal of Allergy and Clinical Immunology*.

116(4),pp.805–811.

Krogh, A., Larsson, B., von Heijne, G. and Sonnhammer, E.L.L. 2001. Predicting transmembrane protein topology with a hidden Markov model: Application to complete genomes. *Journal of molecular biology*. **305**(3),pp.567–580.

Krug, R.M., Angelo, C.S., Broni, B. and Shapiro, G. 1987. Transcription and replication of influenza virion RNA in the nucleus of infected cells *In*: *Cold Spring Harbor symposia on quantitative biology*. Cold Spring Harbor Laboratory Press, pp. 353–358.

Krzyzaniak, M.A., Zumstein, M.T., Gerez, J.A., Picotti, P. and Helenius, A. 2013. Host Cell Entry of Respiratory Syncytial Virus Involves Macropinocytosis Followed by Proteolytic Activation of the F Protein. *PLoS Pathogens*. **9**(4).

Kunzelmann, K., Sun, J., Meanger, J., King, N.J. and Cook, D.I. 2007. Inhibition of airway Na+ transport by respiratory syncytial virus. *Journal of virology*. **81**(8),pp.3714–20.

Kuo, L., Fearns, R. and Collins, P.L. 1997. Analysis of the gene start and gene end signals of human respiratory syncytial virus: quasi-templated initiation at position 1 of the encoded mRNA. *Journal of virology*. **71**(7),pp.4944–4953.

Kuo, L. and Masters, P.S. 2003. The small envelope protein E is not essential for murine coronavirus replication. *Journal of virology*. **77**(8),pp.4597–608.

Van Kuppeveld, F.J.M., Hoenderop, J.G.J., Smeets, R.L.L., Willems, P.H.G.M., Dijkman, H.B.P.M., Galama, J.M.D. and Melchers, W.J.G. 1997. Coxsackievirus protein 2B modifies endoplasmic reticulum membrane and plasma membrane permeability and facilitates virus release. *EMBO Journal*. **16**(12),pp.3519–3532.

Kurtz, S., Luo, G., Hahnenberger, K.M., Brooks, C., Gecha, O., Ingalls, K., Numata -, K.I. and Krystal, M. 1995. Growth impairment resulting from

expression of influenza virus M2 protein in Saccharomyces cerevisiae: Identification of a novel inhibitor of influenza virus. *Antimicrobial Agents and Chemotherapy*. **39**(10),pp.2204–2209.

Kwilas, S., Liesman, R.M., Zhang, L., Walsh, E., Pickles, R.J. and Peeples, M.E. 2009. Respiratory syncytial virus grown in Vero cells contains a truncated attachment protein that alters its infectivity and dependence on glycosaminoglycans. *Journal of virology*. **83**(20),pp.10710–10718.

Lang, F., Föller, M., Lang, K., Lang, P., Ritter, M., Vereninov, A., Szabo, I., M. Huber, S. and Gulbins, E. 2007. Cell Volume Regulatory Ion Channels in Cell Proliferation and Cell Death. *Methods in Enzymology*. **428**,pp.209–225.

Lang, F., Föller, M., Lang, K.S., Lang, P.A., Ritter, M., Gulbins, E., Vereninov, A. and Huber, S.M. 2005. Ion channels in cell proliferation and apoptotic cell death. *Journal of Membrane Biology*. **205**(3),pp.147–157.

Laplante, J.M., O'rourke, F., Xinghua, L.U., Alan, F., OLSEN, A. and FEINSTEIN, M.B. 2000. Cloning of human Ca2+ homoeostasis endoplasmic reticulum protein (CHERP): regulated expression of antisense cDNA depletes CHERP, inhibits intracellular Ca2+ mobilization and decreases cell proliferation. *Biochemical Journal*. **348**(1),pp.189–199.

Leroy, C., Privé, A., Bourret, J.-C., Berthiaume, Y., Ferraro, P. and Brochiero, E. 2006. Regulation of ENaC and CFTR expression with K+ channel modulators and effect on fluid absorption across alveolar epithelial cells. *American journal of physiology. Lung cellular and molecular physiology*. **291**,pp.L1207–L1219.

Li, D., Jans, D. a, Bardin, P.G., Meanger, J., Mills, J. and Ghildyal, R. 2008. Association of respiratory syncytial virus M protein with viral nucleocapsids is mediated by the M2-1 protein. *Journal of virology*. **82**(17),pp.8863–70.

Li, Y., Boehning, D.F., Qian, T., Popov, V.L. and Weinman, S. a 2007. Hepatitis C virus core protein increases mitochondrial ROS production by stimulation of Ca2+ uniporter activity. *FASEB journal : official publication of the*

Federation of American Societies for Experimental Biology. **21**(10),pp.2474–85.

Li, Y., Jain, N., Limpanawat, S., To, J., Quistgaard, E.M., Nordlund, P., Thanabalu, T. and Torres, J. 2015. Interaction between human BAP31 and respiratory syncytial virus small hydrophobic (SH) protein. *Virology*. **482**,pp.105–10.

Li, Y., To, J., Dossena, S., Surya, W., Huang, M., Paulmichl, M., Liu, D.X., Aguilella, V.M. and Torres, J. 2014. Inhibition of the Human Respiratory Syncytial Virus Small Hydrophobic Protein and Structural Variations in a Bicelle. **88**(20),pp.11899–11914.

Li, Z., Xu, J., Patel, J., Fuentes, S., Lin, Y., Anderson, D., Sakamoto, K., Wang, L.-F. and He, B. 2011. Function of the small hydrophobic protein of J paramyxovirus. *Journal of virology*. **85**(1),pp.32–42.

Liljeroos, L., Krzyzaniak, M.A., Helenius, A. and Butcher, S.J. 2013. Architecture of respiratory syncytial virus revealed by electron cryotomography. *Proceedings of the National Academy of Sciences of the United States of America*. **110**(27),pp.11133–11138.

Liuzzi, M., Mason, S.W., Cartier, M., Lawetz, C., McCollum, R.S., Dansereau, N., Bolger, G., Lapeyre, N., Gaudette, Y., Lagacé, L., Massariol, M.-J., Dô, F., Whitehead, P., Lamarre, L., Scouten, E., Bordeleau, J., Landry, S., Rancourt, J., Fazal, G. and Simoneau, B. 2005. Inhibitors of respiratory syncytial virus replication target cotranscriptional mRNA guanylylation by viral RNA-dependent RNA polymerase. *Journal of virology*. **79**(20),pp.13105–15.

López-Barneo, J., del Toro, R., Levitsky, K.L., Chiara, M.D. and Ortega-Sáenz, P. 2004. Regulation of oxygen sensing by ion channels. *Journal of applied physiology* **96**(3),pp.1187–1195

Lupfer, C., Malik, A. and Kanneganti, T.-D. 2015. Inflammasome control of viral infection. *Current opinion in virology*. **12**,pp.38–46.

Luscombe, C.A., Huang, Z., Murray, M.G., Miller, M., Wilkinson, J. and Ewart, G.D. 2010. A novel Hepatitis C virus p7 ion channel inhibitor, BIT225, inhibits bovine viral diarrhea virus in vitro and shows synergism with recombinant interferon-2b and nucleoside analogues. *Antiviral Research*. **86**(2),pp.144–153.

Mall, M., Bleich, M., Greger, R., Schreiber, R. and Kunzelmann, K. 1998. The amiloride-inhibitable Na+ conductance is reduced by the cystic fibrosis transmembrane conductance regulator in normal but not in cystic fibrosis airways. *Journal of Clinical Investigation*. **102**(1),pp.15–21.

Mall, M., Wissner, A., Schreiber, R., Kuehr, J., Seydewitz, H.H., Brandis, M., Greger, R. and Kunzelmann, K. 2000. Role of K(v)LQT1 in cyclic adenosine monophosphate-mediated Cl- secretion in human airway epithelia. *American Journal of Respiratory Cell and Molecular Biology*. **23**(3),pp.283–289.

Manninen, A. and Saksela, K. 2002. HIV-1 Nef interacts with inositol trisphosphate receptor to activate calcium signaling in T cells. *The Journal of experimental medicine*. **195**(8),pp.1023–1032.

Manzanares, D., Gonzalez, C., Ivonnet, P., Chen, R.-S., Valencia-Gattas, M., Conner, G.E., Larsson, H.P. and Salathe, M. 2011. Functional apical large conductance, Ca2+-activated, and voltage-dependent K+ channels are required for maintenance of airway surface liquid volume. *The Journal of biological chemistry*. **286**(22),pp.19830–9.

Martinez, I., Lombardia, L., Garcia-Barreno, B., Dominguez, O. and Melero, J.A. 2007. Distinct gene subsets are induced at different time points after human respiratory syncytial virus infection of A549 cells. *Journal of General Virology*. **88**,pp.570–581.

Marty, A., Meanger, J., Mills, J., Shields, B. and Ghildyal, R. 2003. Association of matrix protein of respiratory syncytial virus with the host cell membrane of infected cells. *Archives of Virology*. **149**(1),pp.199–210.

Matthay, M.A. and Zemans, R.L. 2011. The acute respiratory distress

syndrome: pathogenesis and treatment. *Annual review of pathology*. **6**,pp.147–63.

Mazur, N.I., Martinón-Torres, F., Baraldi, E., Fauroux, B., Greenough, A., Heikkinen, T., Manzoni, P., Mejias, A., Nair, H., Papadopoulos, N.G., Polack, F.P., Ramilo, O., Sharland, M., Stein, R., Madhi, S.A. and Bont, L. 2015. Lower respiratory tract infection caused by respiratory syncytial virus: current management and new therapeutics. *The Lancet. Respiratory medicine*. **3**(11),pp.888–900.

Mbiguino, A. and Menezes, J. 1991. Purification of human respiratory syncytial virus: superiority of sucrose gradient over percoll, renografin, and metrizamide gradients. *Journal of Virological Methods*. **31**(2-3),pp.161–170.

McKimm-Breschkin, J.L. 2004. A simplified plaque assay for respiratory syncytial virus - Direct visualization of plaques without immunostaining. *Journal of Virological Methods*. **120**(1),pp.113–117.

McLellan, J.S., Chen, M., Joyce, M.G., Sastry, M., Stewart-Jones, G.B.E., Yang, Y., Zhang, B., Chen, L., Srivatsan, S., Zheng, A., Zhou, T., Graepel, K.W., Kumar, A., Moin, S., Boyington, J.C., Chuang, G.-Y., Soto, C., Baxa, U., Bakker, A.Q., Spits, H., Beaumont, T., Zheng, Z., Xia, N., Ko, S.-Y., Todd, J.-P., Rao, S., Graham, B.S. and Kwong, P.D. 2013. Structure-based design of a fusion glycoprotein vaccine for respiratory syncytial virus. *Science (New York, N.Y.)*. **342**(6158),pp.592–8.

McLellan, J.S., Chen, M., Kim, A., Yang, Y., Graham, B.S. and Kwong, P.D. 2010. Structural basis of respiratory syncytial virus neutralization by motavizumab. *Nature structural & molecular biology*. **17**(2),pp.248–250.

McLellan, J.S., Ray, W.C. and Peeples, M.E. 2013. Structure and function of respiratory syncytial virus surface glycoproteins. *Current Topics in Microbiology and Immunology*. **372**,pp.83–104.

Miao, E.A., Rajan, J. V and Aderem, A. 2011. Caspase-1-induced pyroptotic cell death. *Immunological reviews*. **243**(1),pp.206–14.

Michelangeli, F., Liprandi, F., Chemello, M.E., Ciarlet, M. and Ruiz, M.C. 1995. Selective depletion of stored calcium by thapsigargin blocks rotavirus maturation but not the cytopathic effect. *Journal of virology*. **69**(6),pp.3838–3847.

Micoli, K.J., Pan, G., Wu, Y., Williams, J.P., Cook, W.J. and McDonald, J.M. 2000. Requirement of calmodulin binding by HIV-1 gp160 for enhanced FAS-mediated apoptosis. *Journal of Biological Chemistry*. **275**(2),pp.1233–1240.

Minakshi, R., Padhan, K., Rehman, S., Hassan, M.I. and Ahmad, F. 2014. The SARS Coronavirus 3a protein binds calcium in its cytoplasmic domain. *Virus Research*. **191**(1),pp.180–183.

Minor, N.T., Sha, Q., Nichols, C.G. and Mercer, R.W. 1998. The gamma subunit of the Na,K-ATPase induces cation channel activity. *Proceedings of the National Academy of Sciences of the United States of America*. **95**(11),pp.6521–5.

Monaghan, A.S., Baines, D.L., Kemp, P.J. and Olver, R.E. 1996. Inwardly rectifying K+ currents of alveolar type II cells isolated from fetal guinea-pig lung: regulation by G protein-and Mg2+-dependent pathways. *Pflügers Archiv*. **433**(3),pp.294–303.

Money, V.A., McPhee, H.K., Mosely, J.A., Sanderson, J.M. and Yeo, R.P. 2009. Surface features of a Mononegavirales matrix protein indicate sites of membrane interaction. *Proceedings of the National Academy of Sciences*. **106**(11),pp.4441–4446.

Moore, E.C., Barber, J. and Tripp, R.A. 2008. Respiratory syncytial virus (RSV) attachment and nonstructural proteins modify the type I interferon response associated with suppressor of cytokine signaling (SOCS) proteins and IFN-stimulated gene-15 (ISG15). *Virology Journal*. **5**(1),pp.1–11.

Morris, J.A., Blount, R.E. and Savage, R.E. 1956. Recovery of Cytopathogenic Agent from Chimpanzees with Goryza. *Experimental Biology and Medicine*. **92**(3),pp.544–549.

Moyes, J., Cohen, C., Pretorius, M., Groome, M., Von Gottberg, A., Wolter, N., Walaza, S., Haffejee, S., Chhagan, M., Naby, F., Cohen, A.L., Tempia, S., Kahn, K., Dawood, H., Venter, M. and Madhi, S.A. 2013. Epidemiology of respiratory syncytial virus-associated acute lower respiratory tract infection hospitalizations among HIV-infected and HIV-uninfected South African children, 2010-2011. *Journal of Infectious Diseases*. **208** (SUPPL. 3).

Mufson, M.A., Orvell, C., Rafnar, B. and Norrby, E. 1985. Two distinct subtypes of human respiratory syncytial virus. *The Journal of general virology*. **66 Pt 10**,pp.2111–2124.

Munday, D.C., Emmott, E., Surtees, R., Lardeau, C.-H., Wu, W., Duprex, W.P., Dove, B.K., Barr, J.N. and Hiscox, J.A. 2010. Quantitative proteomic analysis of A549 cells infected with human respiratory syncytial virus. *Molecular & Cellular Proteomics*. **9**(11),pp.2438–2459.

Muñoz-Planillo, R., Kuffa, P., Martínez-Colón, G., Smith, B.L., Rajendiran, T.M. and Núñez, G. 2013. K^+ efflux is the common trigger of NLRP3 inflammasome activation by bacterial toxins and particulate matter. *Immunity*. **38**(6),pp.1142–53.

Murakami, T., Ockinger, J., Yu, J., Byles, V., McColl, A., Hofer, A.M. and Horng, T. 2012. Critical role for calcium mobilization in activation of the NLRP3 inflammasome. *Proc Natl Acad Sci U S A*. **109**(28),pp.11282–11287.

Murphy, B.R., Prince, G.A. and Walsh, E.E. 1986. Dissociation betwen serum neutralizing and glycoprotein antibody responses of infants and children who received inactivated respiratory syncytial virus vaccine. *Journal of Clinical Microbiology*. **24**(2),pp.197–202.

Nair, H., Nokes, D.J., Gessner, B.D., Dherani, M., Madhi, S.A., Singleton, R.J., O'Brien, K.L., Roca, A., Wright, P.F., Bruce, N., Chandran, A., Theodoratou, E., Sutanto, A., Sedyaningsih, E.R., Ngama, M., Munywoki, P.K., Kartasasmita, C., Simões, E.A.F., Rudan, I., Weber, M.W. and Campbell, H. 2010. Global burden of acute lower respiratory infections due to respiratory syncytial virus in young children: a systematic review and

meta-analysis. *Lancet (London, England)*. **375**(9725),pp.1545–55.

Nakamura, N., Tanaka, S., Teko, Y., Mitsui, K. and Kanazawa, H. 2005. Four Na+/H+ exchanger isoforms are distributed to Golgi and post-Golgi compartments and are involved in organelle pH regulation. *The Journal of biological chemistry*. **280**(2),pp.1561–72.

Nichols, C.G. 2006. KATP channels as molecular sensors of cellular metabolism. *Nature*. **440**(7083),pp.470–476.

Nieto-Torres, J.L., DeDiego, M.L., Verdi??-B??guena, C., Jimenez-Guarde??o, J.M., Regla-Nava, J.A., Fernandez-Delgado, R., Casta??o-Rodriguez, C., Alcaraz, A., Torres, J., Aguilella, V.M. and Enjuanes, L. 2014. Severe Acute Respiratory Syndrome Coronavirus Envelope Protein Ion Channel Activity Promotes Virus Fitness and Pathogenesis. *PLoS Pathogens*. **10**(5).

Nieto-Torres, J.L., Verdiá-Báguena, C., Castaño-Rodriguez, C., Aguilella, V.M. and Enjuanes, L. 2015. Relevance of Viroporin Ion Channel Activity on Viral Replication and Pathogenesis. *Viruses*. **7**(7),pp.3552–73.

Nieva, J.L., Madan, V. and Carrasco, L. 2012. Viroporins: structure and biological functions. *Nat Rev Microbiol*. **10**.

Nizet, V., Kim, K.S., Stins, M., Jonas, M., Chi, E.Y., Nguyen, D. and Rubens, C.E. 1997. Invasion of brain microvascular endothelial cells by group B streptococci. *Infection and immunity*. **65**(12),pp.5074–5081.

O'Brien, K.L., Chandran, A., Weatherholtz, R., Jafri, H.S., Griffin, M.P., Bellamy, T., Millar, E. V., Jensen, K.M., Harris, B.S., Reid, R., Moulton, L.H., Losonsky, G.A., Karron, R.A., Santosham, M., Donaldson, C., Eick-Cost, A., Perilla, M., Campbell, J., VanDeReit, D., Brown, L.B., Gloyd, P.W., Seby, M., Brown, M.A., Candelaria, D., Foti, J.L. and Overturf, G. 2015. Efficacy of motavizumab for the prevention of respiratory syncytial virus disease in healthy Native American infants: A phase 3 randomised double-blind placebo-controlled trial. *The Lancet Infectious Diseases*. **15**(12),pp.1398–1408.

O'Grady, S.M. and Lee, S.Y. 2003. Chloride and potassium channel function in alveolar epithelial cells. *American journal of physiology. Lung cellular and molecular physiology*. **284**(5),pp.L689–L700.

Okada, Y. and Maeno, E. 2001. Apoptosis, cell volume regulation and volume-regulatory chloride channels. *Comparative Biochemistry and Physiology Part A: Molecular & Integrative Physiology*. **130**(3),pp.377–383.

Olmsted, R.A. and Collins, P.L. 1989. The 1A protein of respiratory syncytial virus is an integral membrane protein present as multiple, structurally distinct species. *Journal of virology*. **63**(5),pp.2019–29.

Oomens, a G.P., Megaw, a G. and Wertz, G.W. 2003. Infectivity of a human respiratory syncytial virus lacking the SH, G, and F proteins is efficiently mediated by the vesicular stomatitis virus G protein. *Journal of virology*. **77**(6),pp.3785–3798.

Ortego, J., Ceriani, J.E., Patio, C., Plana, J. and Enjuanes, L. 2007. Absence of E protein arrests transmissible gastroenteritis coronavirus maturation in the secretory pathway. *Virology*. **368**(2),pp.296–308.

Oxford, J.S. and Galbraith, A. 1980. Antiviral activity of amantadine: a review of laboratory and clinical data. *Pharmacology & Therapeutics*. **11**(1),pp.181–262.

Pardo, L.A. and Stuhmer, W. 2014. The roles of K+ channels in cancer. *Nat Rev Cancer*. **14**(1),pp.39–48.

Pavlovic, D., Neville, D.C., Argaud, O., Blumberg, B., Dwek, R.A., Fischer, W.B. and Zitzmann, N. 2003. The hepatitis C virus p7 protein forms an ion channel that is inhibited by long-alkyl-chain iminosugar derivatives. *Proc Natl Acad Sci U S A*. **100**(10),pp.6104–6108.

Pellet, P.E. and Roizmann, B. 2007. Field Virology. 5th edition. *New York: Lippencott-Raven*. **2**,pp.2479–2500.

Pervushin, K., Dan, E., Darthasarathy, K., Din, X., Diang, F.L., Du, D., Dararattanavech, A., Duck, W.S., Ding, X.L. and Dorres, J. 2009. Structure

and inhibition of the SARS coronavirus envelope protein ion channel. *PLoS Pathogens*. **5**(7).

Piccini, L.E., Castilla, V. and Damonte, E.B. 2015. Dengue-3 virus entry into vero cells: Role of clathrin-mediated endocytosis in the outcome of infection. *PLoS ONE*. **10**(10),pp.1–17.

Pielak, R.M. and Chou, J.J. 2010. Flu channel drug resistance: A tale of two sites. *Protein and Cell*. **1**(3),pp.246–258.

Pinton, P., Ferrari, D., Rapizzi, E., Virgilio, F. Di, Pozzan, T. and Rizzuto, R. 2001. The Ca2+ concentration of the endoplasmic reticulum is a key determinant of ceramide-induced apoptosis: significance for the molecular mechanism of Bcl-2 action. *The EMBO Journal*. **20**(11),pp.2690–2701.

Pinton, P., Giorgi, C., Siviero, R., Zecchini, E. and Rizzuto, R. 2008. Calcium and apoptosis: ER-mitochondria Ca2+ transfer in the control of apoptosis. *Oncogene*. **27**(50),pp.6407–6418.

Polack, F.P., Teng, M.N., Collins, P.L., Prince, G.A., Exner, M., Regele, H., Lirman, D.D., Rabold, R., Hoffman, S.J., Karp, C.L., Kleeberger, S.R., Wills-Karp, M. and Karron, R.A. 2002. A role for immune complexes in enhanced respiratory syncytial virus disease. *Journal of Experimental Medicine*. **196**(6),pp.859–865.

Premkumar, A., Horan, C.R. and Gage, P.W. 2005. Dengue virus M protein C-terminal peptide (DVM-C) forms ion channels. *Journal of Membrane Biology*. **204**(1),pp.33–38.

Premkumar, A., Wilson, L., Ewart, G.D. and Gage, P.W. 2004. Cation-selective ion channels formed by p7 of hepatitis C virus are blocked by hexamethylene amiloride. *FEBS Letters*. **557**(1-3),pp.99–103.

Prince, G. a, Hemming, V.G., Horswood, R.L., Baron, P. and Chanock, R.M. 1987. Effectiveness of topically administered neutralizing antibodies in experimental immunotherapy of respiratory syncytial virus infection in cotton rats. *Journal of virology*. **61**(6),pp.1851–4.

Prince, G.A., Jenson, A.B., Hemming, V.G., Murphy, B.R., Walsh, E.E., Horswood, R.L. and Chanock, R.M. 1986. Enhancement of respiratory syncytial virus pulmonary pathology in cotton rats by prior intramuscular inoculation of formalin-inactiva ted virus. *Journal of virology*. **57**(3),pp.721–728.

Pugin, J., Ricou, B., Steinberg, K.P., Suter, P.M. and Martin, T.R. 1996. Proinflammatory activity in bronchoalveolar lavage fluids from patients with ARDS, a prominent role for interleukin-1. *American Journal of Respiratory and Critical Care Medicine*. **153**(6 I),pp.1850–1856.

Radding, W., Williams, J.P., McKenna, M. a, Tummala, R., Hunter, E., Tytler, E.M. and McDonald, J.M. 2000. Calmodulin and HIV type 1: interactions with Gag and Gag products. *AIDS research and human retroviruses*. **16**(15),pp.1519–25.

Ramakrishnan, A.M. and Sankaranarayanan, K. 2016. Understanding autoimmunity: The ion channel perspective. *Autoimmunity Reviews*.

Rane, S.G. and Reddy, E.P. 2000. Janus kinases: components of multiple signaling pathways. *Oncogene*. **19**(49),pp.5662–5679.

Régnier, S.A. and Huels, J. 2013. Association between respiratory syncytial virus hospitalizations in infants and respiratory sequelae: systematic review and meta-analysis. *The Pediatric infectious disease journal*. **32**(8),p.820—826.

Ren, J., Liu, T., Pang, L., Li, K., Garofalo, R.P., Casola, A. and Bao, X. 2011. A novel mechanism for the inhibition of interferon regulatory factor-3-dependent gene expression by human respiratory syncytial virus NS1 protein. *The Journal of general virology*. **92**(Pt 9),pp.2153–9.

Rivera, C.A., Gómez, R.S., Díaz, R.A., Céspedes, P.F., Espinoza, J.A., González, P.A., Riedel, C.A., Bueno, S.M. and Kalergis, A.M. 2015. Novel therapies and vaccines against the human respiratory syncytial virus. *Expert opinion on investigational drugs*. **24**(12),pp.1613–30.

Rixon, H.W.M., Brown, G., Aitken, J., McDonald, T., Graham, S. and Sugrue, R.J. 2004. The small hydrophobic (SH) protein accumulates within lipid-raft structures of the Golgi complex during respiratory syncytial virus infection. *The Journal of general virology*. [Online]. **85**(Pt 5),pp.1153–65.

Rixon, H.W.M., Brown, G., Murray, J.T. and Sugrue, R.J. 2005. The respiratory syncytial virus small hydrophobic protein is phosphorylated via a mitogen-activated protein kinase p38-dependent tyrosine kinase activity during virus infection. *The Journal of general virology*. **86**(Pt 2),pp.375–84.

Rodríguez, L., Cuesta, I., Asenjo, A. and Villanueva, N. 2004. Human respiratory syncytial virus matrix protein is an RNA-binding protein: Binding properties, location and identity of the RNA contact residues. *Journal of General Virology*. **85**(3),pp.709–719.

Rodriguez, R. and Ramilo, O. 2014. Respiratory syncytial virus: how, why and what to do. *The Journal of infection*. **68 Suppl 1**,pp.S115–8.

Roger, S., Gillet, L., Le Guennec, J.Y. and Besson, P. 2015. Voltage-gated sodium channels and cancer: Is excitability their primary role? *Frontiers in Pharmacology*. **6** (July),pp.1–22.

Rosati, E., Sabatini, R., Rampino, G., De Falco, F., Di Ianni, M., Falzetti, F., Fettucciari, K., Bartoli, A., Screpanti, I. and Marconi, P. 2010. Novel targets for endoplasmic reticulum stress-induced apoptosis in B-CLL. *Blood*. **116**(15),pp.2713–2723.

Rossman, J.S., Jing, X., Leser, G.P. and Lamb, R.A. 2010. Influenza Virus M2 Protein Mediates ESCRT-Independent Membrane Scission. *Cell*. **142**(6),pp.902–913.

Ruch, T.R. and Machamer, C.E. 2012. A single polar residue and distinct membrane topologies impact the function of the infectious bronchitis coronavirus E protein. *PLoS Pathogens*. **8**(5).

Ruch, T.R. and Machamer, C.E. 2011. The hydrophobic domain of infectious bronchitis virus E protein alters the host secretory pathway and is important

for release of infectious virus. *Journal of virology*. **85**(2),pp.675–85.

Russell, R.F., McDonald, J.U., Ivanova, M., Zhong, Z., Bukreyev, A. and Tregoning, J.S. 2015. Partial Attenuation of Respiratory Syncytial Virus with a Deletion of a Small Hydrophobic Gene Is Associated with Elevated Interleukin-1β Responses. *Journal of Virology*. **89**(17),pp.8974–8981.

Sakurai, Y., Kolokoltsov, A.A., Chen, C.-C., Tidwell, M.W., Bauta, W.E., Klugbauer, N., Grimm, C., Wahl-Schott, C., Biel, M. and Davey, R.A. 2015a. Ebola virus. Two-pore channels control Ebola virus host cell entry and are drug targets for disease treatment. *Science (New York, N.Y.)*. **347**(6225),pp.995–8.

Sakurai, Y., Kolokoltsov, A.A., Chen, C.-C., Tidwell, M.W., Bauta, W.E., Klugbauer, N., Grimm, C., Wahl-Schott, C., Biel, M. and Davey, R.A. 2015b. Two-pore channels control Ebola virus host cell entry and are drug targets for disease treatment. *Science*. **347**(6225),pp.995–998.

Sambrook, J. and Russell, D.W. 2006. SDS-Polyacrylamide Gel Electrophoresis of Proteins. *CSH protocols*. **2006** (4),pp.1–9.

Santini, F. 2015. Human respiratory syncytial virus and Th1 chemokines. *Clinica Terapeutica*. **166**(3),pp.203–208.

Santos, S. V., Strefezzi, R.F., Pissinatti, A., Takakura, C.F.H., Kanamura, C., Duarte, M.I.S. and Catão-Dias, J.L. 2012. Respiratory syncytial virus (RSV) pneumonia in a southern muriqui (Brachyteles arachnoides). *Journal of Medical Primatology*. **41**(6),pp.403–406.

Schickli, J.H., Dubovsky, F. and Tang, R.S. 2009. Challenges in developing a pediatric RSV vaccine. *Human vaccines*. **5**(9),pp.582–591.

Schnell, J.R. and Chou, J.J. 2008. Structure and mechanism of the M2 proton channel of influenza A virus. *Nature*. **451**(7178),pp.591–5.

Schwarz, S., Wang, K., Yu, W., Sun, B. and Schwarz, W. 2011. Emodin inhibits current through SARS-associated coronavirus 3a protein. *Antiviral Research*. **90**(1),pp.64–69.

Schwarze, J., Cieslewicz, G., Hamelmann, E., Joetham, A., Shultz, L.D., Lamers, M.C. and Gelfand, E.W. 1999. IL-5 and eosinophils are essential for the development of airway hyperresponsiveness following acute respiratory syncytial virus infection. *J Immunol*. **162**(5),pp.2997–3004.

Segovia, J., Sabbah, A., Mgbemena, V., Tsai, S.-Y., Chang, T.-H., Berton, M.T., Morris, I.R., Allen, I.C., Ting, J.P.-Y. and Bose, S. 2012. TLR2/MyD88/NF-κB pathway, reactive oxygen species, potassium efflux activates NLRP3/ASC inflammasome during respiratory syncytial virus infection. *PloS one*. **7**(1),p.e29695.

Shah, A.S., Ben-Shahar, Y., Moninger, T.O., Kline, J.N. and Welsh, M.J. 2009. Motile cilia of human airway epithelia are chemosensory. *Science (New York, N.Y.)*. **325**(5944),pp.1131–4.

Shah, N.R., Sunderland, A. and Grdzelishvili, V.Z. 2010. Cell type mediated resistance of vesicular stomatitis virus and sendai virus to ribavirin. *PLoS ONE*. **5**(6).

Sharon-Friling, R., Goodhouse, J., Colberg-Poley, A.M. and Shenk, T. 2006. Human cytomegalovirus pUL37x1 induces the release of endoplasmic reticulum calcium stores. *Proceedings of the National Academy of Sciences of the United States of America*. **103**,pp.19117–19122.

Sharpe, S., Yau, W.M. and Tycko, R. 2006. Structure and dynamics of the HIV-1 Vpu transmembrane domain revealed by solid-state NMR with magic-angle spinning. *Biochemistry*. **45**(3),pp.918–933.

Shay, D.K., Holman, R.C., Newman, R.D., Liu, L.L., Stout, J.W. and Anderson, L.J. 1999. Bronchiolitis-associated hospitalizations among US children, 1980-1996. *JAMA : the journal of the American Medical Association*. **282**(15),pp.1440–1446.

Sheikh, I.A., Ghosh, P., Hoque, K.M., Division, M.P. and Diseases, E. 2015. Ion channels in obstructive pulmonary disease and their impact on therapy.

Shim, Y.R., Lee, H.K., Kim, T.H., Lee, H.K., Ren, W., Duan, Y., Yang, Y., Ji, Y.

and Chen, F. 2014. Caspase-1 Independent Viral Clearance and Adaptive Immunity Against Mucosal Respiratory Syncytial Virus Infection. *BMB Reports*. **47**(3),pp.297–301.

Shingai, M., Azuma, M., Ebihara, T., Sasai, M., Funami, K., Ayata, M., Ogura, H., Tsutsumi, H., Matsumoto, M. and Seya, T. 2008. Soluble G protein of respiratory syncytial virus inhibits Toll-like receptor 3/4-mediated IFN-beta induction. *International Immunology*. **20**(9),pp.1169–1180.

Siber, G.R., Leombruno, D., Leszczynski, J., Mc Iver, J., Bodkin, D., Gonin, R., Thompson, C.M., Walsh, E.E., Piedra, P.A., Hemming, V.G. and Prince, G.A. 1994. Comparison of antibody concentrations and protective activity of respiratory syncytial virus immune globulin and conventional immune globulin. *Journal of Infectious Diseases*. **169**(6),pp.1368–1373.

Siegl, P.K., Cragoe, E.J., Trumble, M.J. and Kaczorowski, G.J. 1984. Inhibition of Na+/Ca2+ exchange in membrane vesicle and papillary muscle preparations from guinea pig heart by analogs of amiloride. *Proceedings of the National Academy of Sciences*. **81**(10),pp.3238–3242.

Siegle, J.S., Hansbro, N., Herbert, C., Rosenberg, H.F., Domachowske, J.B., Asquith, K.L., Foster, P.S. and Kumar, R.K. 2010. Early-life viral infection and allergen exposure interact to induce an asthmatic phenotype in mice. *Respir Res*. **11**,p.14.

Sigurs, N., Bjarnason, R., Sigurbergsson, F. and Kjellman, B. 2000. Respiratory syncytial virus bronchiolitis in infancy is an important risk factor for asthma and allergy at age 7. *Am J Respir Crit Care Med*. **161**(5),pp.1501–1507.

Sollberger, G., Strittmatter, G.E., Garstkiewicz, M., Sand, J. and Beer, H.-D. 2014. Caspase-1: the inflammasome and beyond. *Innate immunity*. **20**(2),pp.115–25.

Sommer, D., Bogdan, R., Berger, J., Peters, D.M., Morty, R.E., Clauss, W.G. and Fronius, M. 2007. CFTR-dependent Cl- secretion in Xenopus laevis lung epithelium. *Respiratory Physiology and Neurobiology*. **158**(1),pp.97–106.

Song, Y., Namkung, W., Nielson, D.W., Lee, J.-W., Finkbeiner, W.E. and Verkman, a S. 2009. Airway surface liquid depth measured in ex vivo fragments of pig and human trachea: dependence on Na+ and Cl- channel function. *American journal of physiology. Lung cellular and molecular physiology*. **297**(6),pp.L1131–L1140.

Spunk, K.M., Tran, K.C. and Collins, P.L. 2005. Effects of Nonstructural Proteins NS1 and NS2 of Human Respiratory Syncytial Virus on Interferon Regulatory Factor 3 , NF- κ B , and Proinflammatory Cytokines. *Journal of virology*. **79**(9),pp.5353–5362.

Srinivasakumar, N., Ogra, P.L. and Flanagan, T.D. 1991. Characteristics of fusion of respiratory syncytial virus with HEp-2 cells as measured by R18 fluorescence dequenching assay. *Journal of virology*. **65**(8),pp.4063–4069.

Stauffer, S., Feng, Y., Nebioglu, F., Heilig, R., Picotti, P. and Helenius, A. 2014. Stepwise priming by acidic pH and a high K+ concentration is required for efficient uncoating of influenza A virus cores after penetration. *Journal of virology*. **88**(22),pp.13029–46.

Stein, R.T., Sherrill, D., Morgan, W.J., Holberg, C.J., Halonen, M., Taussig, L.M., Wright, A.L. and Martinez, F.D. 1999. Respiratory syncytial virus in early life and risk of wheeze and allergy by age 13 years. *Lancet*. **354**(9178),pp.541–545.

Steinmann, E. and Pietschmann, T. 2010. Hepatitis C virus P7-A viroporin crucial for virus assembly and an emerging target for antiviral therapy. *Viruses*. **2**(9),pp.2078–2095.

Stensballe, L.G., Devasundaram, J.K. and Simoes, E.A.F. 2003. Respiratory syncytial virus epidemics: the ups and downs of a seasonal virus. *The Pediatric Infectious Disease Journal*. **22**(2),pp.S21–S32.

Stevens, F.C. 1983. Calmodulin: an introduction. *Canadian Journal of Biochemistry and Cell Biology*. **61**(8),pp.906–910.

Storm, P., Klausen, T.K., Trulsson, M., Ho C S, J., Dosnon, M., Westergren, T.,

Chao, Y., Rydström, A., Yang, H., Pedersen, S.F. and Svanborg, C. 2013. A unifying mechanism for cancer cell death through ion channel activation by HAMLET. *PloS one*. **8**(3),p.e58578.

Stouffer, A.L., Acharya, R., Salom, D., Levine, A.S., Di Costanzo, L., Soto, C.S., Tereshko, V., Nanda, V., Stayrook, S. and DeGrado, W.F. 2008. Structural basis for the function and inhibition of an influenza virus proton channel. *Nature*. **451**(7178),pp.596–599.

Stover, T., Amari, J. V, Mazsaroff, I., Gilar, M., Yu, Y.Q. and Gebler, J.C. 2003. Novel characterization tool for Mab digestion-Technical note: RapiGest SF denaturant tool for improved trypsin digestion of monoclonal antibodies. *Genetic Engineering News*. **23**(17),pp.48–49.

Strebel, K. 2004. HIV-1 Vpu. *Molecular Cell*. **14**(2),pp.150–152.

Strowig, T., Henao-Mejia, J., Elinav, E. and Flavell, R. 2012. Inflammasomes in health and disease. *Nature*. **481**(7381),pp.278–286.

Sullender, W.M. 2000. Respiratory Syncytial Virus Genetic and Antigenic Diversity. *Clinical Microbiology Reviews*. **13**(1),pp.1–15.

Sun, Z., Pan, Y., Jiang, S. and Lu, L. 2013. Respiratory syncytial virus entry inhibitors targeting the F protein. *Viruses*. **5**(1),pp.211–225.

Swain, R.J., Kemp, S.J., Goldstraw, P., Tetley, T.D. and Stevens, M.M. 2010. Assessment of Cell Line Models of Primary Human Cells by Raman Spectral Phenotyping. *Biophysical Journal*. **98**(8),pp.1703–1711.

Sze, C.W. and Tan, Y.-J. 2015. Viral Membrane Channels: Role and Function in the Virus Life Cycle. *Viruses*. **7**(6),pp.3261–84.

Takeuchi, K. and Lamb, R.A. 1994. Influenza virus M2 protein ion channel activity stabilizes the native form of fowl plague virus hemagglutinin during intracellular transport. *Journal of virology*. **68**(2),pp.911–9.

Tanner, S.J., Ariza, A., Richard, C.-A., Kyle, H.F., Dods, R.L., Blondot, M.-L., Wu, W., Trincão, J., Trinh, C.H., Hiscox, J.A., Carroll, M.W., Silman, N.J.,

Eléouët, J.-F., Edwards, T.A. and Barr, J.N. 2014. Crystal structure of the essential transcription antiterminator M2-1 protein of human respiratory syncytial virus and implications of its phosphorylation. *Proceedings of the National Academy of Sciences of the United States of America*. **111**(4),pp.1580–5.

Tawar, R.G., Duquerroy, S., Vonrhein, C., Varela, P.F., Damier-Piolle, L., Castagné, N., MacLellan, K., Bedouelle, H., Bricogne, G., Bhella, D., Eléouët, J.-F. and Rey, F.A. 2009. Crystal structure of a nucleocapsid-like nucleoprotein-RNA complex of respiratory syncytial virus. *Science (New York, N.Y.)*. **326**(5957),pp.1279–83.

Taylor, G., Wyld, S., Valarcher, J.F., Guzman, E., Thom, M., Widdison, S. and Buchholz, U.J. 2014. Recombinant bovine respiratory syncytial virus with deletion of the SH gene induces increased apoptosis and pro-inflammatory cytokines in vitro, and is attenuated and induces protective immunity in calves. *Journal of General Virology*. **95** (6),pp.1244–1254.

Teng, M.N. and Collins, P.L. 1998. Identification of the Respiratory Syncytial Virus Proteins Required for Formation and Passage of Helper-Dependent Infectious Particles. *J. Virol.* **72**(7),pp.5707–5716.

Tessier, G.J., Traynor, T.R., Kannan, M.S. and O'Grady, S.M. 1990. Mechanisms of sodium and chloride transport across equine tracheal epithelium. *Am J Physiol*. **259**(6 Pt 1),pp.L459–67.

Toms, G.L. and R.S. 1987. No TitleRespiratory syncytial virus and the infant immune response. *Archives of disease in childhood*. **62**(6),pp.544–6.

Toolan, H.W. 1954. Transplantable human neoplasms maintained in cortisone-treated laboratory animals: H.S. No. 1; H.Ep. No. 1; H.Ep. No. 2; H.Ep. No. 3; and H.Emb.Rh. No. 1. *Cancer research*. **14**,pp.660–666.

Torres, J., Surya, W., Li, Y. and Liu, D. 2015. Protein-Protein Interactions of Viroporins in Coronaviruses and Paramyxoviruses: New Targets for Antivirals? *Viruses*. **7**(6),pp.2858–2883.

Triantafilou, K., Kar, S., Vakakis, E., Kotecha, S. and Triantafilou, M. 2013a. Human respiratory syncytial virus viroporin SH: a viral recognition pathway used by the host to signal inflammasome activation. *Thorax*. **68** (1),pp.66–75.

Triantafilou, K., Kar, S., Vakakis, E., Kotecha, S. and Triantafilou, M. 2013b. Human respiratory syncytial virus viroporin SH: a viral recognition pathway used by the host to signal inflammasome activation. *Thorax*. **68**(1),pp.66–75.

Triantafilou, K., Kar, S., Vakakis, E., Kotecha, S. and Triantafilou, M. 2013c. Human respiratory syncytial virus viroporin SH: a viral recognition pathway used by the host to signal inflammasome activation. *Thorax*. **68**(1),pp.66–75.

Triantafilou, K. and Triantafilou, M. 2014. Ion flux in the lung: virus-induced inflammasome activation. *Trends in microbiology*. **22**(10),pp.580–8.

Trinh, N.T.N., Privé, A., Kheir, L., Bourret, J.-C., Hijazi, T., Amraei, M.G., Noël, J. and Brochiero, E. 2007. Involvement of KATP and KvLQT1 K+ channels in EGF-stimulated alveolar epithelial cell repair processes. *American journal of physiology. Lung cellular and molecular physiology*. **293**,pp.L870–L882.

Tripp, R.A., Jones, L.P., Haynes, L.M., Zheng, H., Murphy, P.M. and Anderson, L.J. 2001. CX3C chemokine mimicry by respiratory syncytial virus G glycoprotein. *Nat Immunol*. **2**.

Tsai, B. 2007. Penetration of nonenveloped viruses into the cytoplasm. *Annual review of cell and developmental biology*. **23**,pp.23–43.

Valverde, M.A., Cantero-Recasens, G., Garcia-Elias, A., Jung, C., Carreras-Sureda, A. and Vicente, R. 2011. Ion channels in asthma. *Journal of Biological Chemistry*. **286**(38),pp.32877–32882.

Vieira, A. V., Lamaze, C. and Schmid, S.L. 1996. Control of EGF Receptor Signaling by Clathrin-Mediated Endocytosis. *Science*. **274**(5295),pp.2086–

2089.

Vig, M. and Kinet, J.-P. 2009. Calcium signaling in immune cells. *Nature immunology*. **10**(1),pp.21–27.

Vikerfors, T., M. Grandien, P.O. 1987. Respiratory syncytial virus infections in adults. *The American review of respiratory disease,*. **136**(3),pp.561–4.

Wang, B., Heath-Engel, H., Zhang, D., Nguyen, N., Thomas, D.Y., Hanrahan, J.W. and Shore, G.C. 2008. BAP31 Interacts with Sec61 Translocons and Promotes Retrotranslocation of CFTR??F508 via the Derlin-1 Complex. *Cell*. **133**(6),pp.1080–1092.

Wang, J., Ma, C., Wu, Y., Lamb, R.A., Pinto, L.H. and Degrado, W.F. 2011. Exploring organosilane amines as potent inhibitors and structural probes of influenza a virus M2 proton channel. *Journal of the American Chemical Society*. **133**(35),pp.13844–13847.

Wang, J.J., Wu, Y., Ma, C., Fiorin, G., Pinto, L.H., Lamb, R. a, Klein, M.L. and Degrado, W.F. 2013. Structure and inhibition of the drug-resistant S31N mutant of the M2 ion channel of influenza A virus. *Proc Natl Acad Sci U S A*. **110**(4),pp.1315–1320.

Wang, M., You, J., Bemis, K.G., Tegeler, T.J. and Brown, D.P.G. 2008. Label-free mass spectrometry-based protein quantification technologies in proteomic analysis. *Briefings in functional genomics & proteomics*. **7**(5),pp.329–339.

Weber, M.W., Mulholland, E.K. and Greenwood, B.M. 1998. Respiratory syncytial virus infection in tropical and developing countries. *Tropical medicine & international health : TM & IH*. **3**(4),pp.268–280.

Weir, E.K., Cabrera, J.A., Mahapatra, S., Peterson, D.A. and Hong, Z. 2010. The role of ion channels in hypoxic pulmonary vasoconstriction *In*: *Advances in Experimental Medicine and Biology*., pp. 3–14.

Welliver, R.C. 2003. Review of epidemiology and clinical risk factors for severe respiratory syncytial virus (RSV) infection. *The Journal of Pediatrics*.

[Online]. **143**(5),pp.112–117. [Accessed 16 May 2016]. Available from: http://www.sciencedirect.com/science/article/pii/S0022347603005080.

Wenger, R.H. and Gassmann, M. 1997. Oxygen(es) and the hypoxia-inducible factor-1. *Biological chemistry*. **378**(7),p.609—616.

Wetherill, L.F., Holmes, K.K., Verow, M., Müller, M., Howell, G. and Harris, M. 2012. High-risk human papillomavirus E5 oncoprotein displays channel-forming activity sensitive to small-molecule inhibitors. *J Virol*. **86**.

Wharton, S.A., Belshe, R.B., Skehel, J.J. and Hay, A.J. 1994. Role of virion M2 protein in influenza virus uncoating: Specific reduction in the rate of membrane fusion between virus and liposomes by amantadine. *Journal of General Virology*. **75**(4),pp.945–948.

Whitehead, S.S., Bukreyev, a, Teng, M.N., Firestone, C.Y., St Claire, M., Elkins, W.R., Collins, P.L. and Murphy, B.R. 1999. Recombinant respiratory syncytial virus bearing a deletion of either the NS2 or SH gene is attenuated in chimpanzees. *Journal of virology*. **73**(4),pp.3438–3442.

Wilkinson, W.J., Benjamin, A.R., De Proost, I., Orogo-Wenn, M.C., Yamazaki, Y., Staub, O., Morita, T., Adriaensen, D., Riccardi, D., Walters, D. V. and Kemp, P.J. 2011. Alveolar epithelial CNGA1 channels mediate cGMP-stimulated, amiloride-insensitive, lung liquid absorption. *Pflugers Archiv European Journal of Physiology*. **462**(2),pp.267–279.

Wilson, L., Gage, P. and Ewart, G. 2006. Hexamethylene amiloride blocks E protein ion channels and inhibits coronavirus replication. *Virology*. **353**(2),pp.294–306.

Woensel, J.B.M. van, Aalderen, W.M.C. van and Kimpen, J.L.L. 2003. Viral lower respiratory tract infection in infants and young children. *British Medical Journal (Clinical Research edition)*. **327**(7405),pp.36–40.

Wozniak, A.L., Griffin, S., Rowlands, D., Harris, M., Yi, M., Lemon, S.M. and Weinman, S.A. 2010. Intracellular proton conductance of the hepatitis C virus p7 protein and its contribution to infectious virus production. *PLoS*

Pathogens. **6**(9).

Wu, W., Munday, D.C., Howell, G., Platt, G., Barr, J.N. and Hiscox, J.A. 2011. Characterization of the interaction between human respiratory syncytial virus and the cell cycle in continuous cell culture and primary human airway epithelial cells. *Journal of virology*. **85**(19),pp.10300–9.

Xie, S., Wang, K., Yu, W., Lu, W., Xu, K., Wang, J., Ye, B., Schwarz, W., Jin, Q. and Sun, B. 2011. DIDS blocks a chloride-dependent current that is mediated by the 2B protein of enterovirus 71. *Cell Res*. **21**(8),pp.1271–1275.

Yuan, T., Mietzner, T.A., Montelaro, R.C. and Vogel, H.J. 1995. Characterization of the calmodulin binding domain of SIV transmembrane glycoprotein by NMR and CD spectroscopy. *Biochemistry*. **34**(33),pp.10690–10696.

Zhang, H., Flagg, T.P. and Nichols, C.G. 2010. Cardiac sarcolemmal KATP channels: Latest twists in a questing tale! *Journal of Molecular and Cellular Cardiology*. **48**(1),pp.71–75.

Zhang, L., Peeples, M.E., Boucher, R.C., Collins, P.L. and Pickles, R.J. 2002. Respiratory Syncytial Virus Infection of Human Airway Epithelial Cells Is Polarized, Specific to Ciliated Cells, and without Obvious Cytopathology. *Journal of Virology*. **76**(11),pp.5654–5666.

Zhou, Y., Frey, T.K. and Yang, J.J. 2009. Viral calciomics: Interplays between Ca2+ and virus. *Cell Calcium*. **46**(1),pp.1–17.

Zhou, Y., Tzeng, W.-P., Yang, W., Zhou, Y., Ye, Y., Lee, H., Frey, T.K. and Yang, J. 2007. Identification of a Ca2+-binding domain in the rubella virus nonstructural protease. *Journal of virology*. **81**(14),pp.7517–7528.

Appendix

Significant proteins of infected HBEpC HRSV ΔSH eGFP			
Accession	LOG 2 FC	LOG10 pvalue	Description
1::sp|KRA61_SHEEP|	7.7355636 86	1.4213045 16	; TOPep_Count=3
1::sp|P29728|OAS2_HUMAN	5.8709889 88	6.6501932 63	2'-5'-oligoadenylate synthase 2 OS=Homo sapiens GN=OAS2 PE=1 SV=3; TOPep_Count=38
2::sp|P03423|GLYC_HRSVA	5.1058421 3	5.0015329 49	Major surface glycoprotein G OS=Human respiratory syncytial virus A (strain A2) GN=G PE=1 SV=1
1::sp|Q460N5|PAR14_HUMAN	4.9698440 76	5.5998710 51	Poly [ADP-ribose] polymerase 14 OS=Homo sapiens GN=PARP14 PE=1 SV=3; TOPep_Count=123
2::sp|P03421|PHOSP_HRSVA	4.7906725 86	8.9193090 79	Phosphoprotein OS=Human respiratory syncytial virus A (strain A2) GN=P PE=1 SV=1
1::sp|GFP_AEQVI|	4.5842805 65	7.0807326 53	GFP
1::sp|Q9BYX4|IFIH1_HUMAN	4.4498577 73	6.2130450 9	Interferon-induced helicase C domain-containing protein 1 OS=Homo sapiens GN=IFIH1 PE=1 SV=3; TOPep_Count=57
1::sp|P00973|OAS1_HUMAN	4.1832067 03	7.1265265 1	2'-5'-oligoadenylate synthase 1 OS=Homo sapiens GN=OAS1 PE=1 SV=4; TOPep_Count=18
1::sp|P05161|ISG15_HUMAN	3.9462925 2	7.6902959 63	Ubiquitin-like protein ISG15 OS=Homo sapiens GN=ISG15 PE=1 SV=5; TOPep_Count=10
1::sp|O15162|PLS1_HUMAN	3.9201630 4	5.2553553 08	Phospholipid scramblase 1 OS=Homo sapiens GN=PLSCR1 PE=1 SV=1; TOPep_Count=10
1::sp|O95786|DDX58_HUMAN	3.8503433 79	9.9766609 52	Probable ATP-dependent RNA helicase DDX58 OS=Homo sapiens GN=DDX58 PE=1 SV=2; TOPep_Count=58
2::sp|P03419|MATRX_HRSVA	3.8108930 85	8.7533741 04	Matrix protein OS=Human respiratory syncytial virus A (strain A2) GN=M PE=1 SV=1
1::sp|P20591|MX1_HUMAN (+1)	3.7578783 94	9.5287568 3	Interferon-induced GTP-binding protein Mx1 OS=Homo sapiens GN=MX1 PE=1 SV=4; TOPep_Count=41
1::sp|P09914|IFIT1_HUMAN (+1)	3.7398275 06	6.8910595 81	Interferon-induced protein with tetratricopeptide repeats 1 OS=Homo sapiens GN=IFIT1 PE=1 SV=2; TOPep_Count=33
2::sp|P04545|M21_HRSVA	3.5933263 74	9.4848184	Matrix M2-1 OS=Human respiratory syncytial virus A (strain A2) GN=M2-1 PE=1 SV=1
1::sp|Q8WXG1|RSAD2_HUMAN	3.5455565	4.1898518 6	Radical S-adenosyl methionine domain-containing protein 2 OS=Homo sapiens GN=RSAD2 PE=1 SV=1; TOPep_Count=26
2::sp|P03418|NCAP_HRSVA	3.3465747 89	9.4711405 57	Nucleoprotein OS=Human respiratory syncytial virus A (strain A2) GN=N PE=1 SV=1
1::sp|Q15646|OASL_HUMAN	3.2476674 38	5.0640680 25	2'-5'-oligoadenylate synthase-like protein OS=Homo sapiens GN=OASL PE=1 SV=2; TOPep_Count=29

1::sp|P37198|NUP62_HUMAN	3.123707901	1.515673972	Nuclear pore glycoprotein p62 OS=Homo sapiens GN=NUP62 PE=1 SV=3; TOPep_Count=13
1::sp|O14879|IFIT3_HUMAN	2.888086303	8.353609125	Interferon-induced protein with tetratricopeptide repeats 3 OS=Homo sapiens GN=IFIT3 PE=1 SV=1; TOPep_Count=30
1::sp|P32455|GBP1_HUMAN	2.724733245	6.320400079	Interferon-induced guanylate-binding protein 1 OS=Homo sapiens GN=GBP1 PE=1 SV=2; TOPep_Count=32
1::sp|Q9Y6Q5|AP1M2_HUMAN	2.6131539 7	1.346974993	AP-1 complex subunit mu-2 OS=Homo sapiens GN=AP1M2 PE=1 SV=4; TOPep_Count=29
2::sp|P03420|FUS_HRSVA	2.599454032	4.986456461	Fusion glycoprotein F0 OS=Human respiratory syncytial virus A (strain A2) GN=F PE=1 SV=1
1::sp|O95994|AGR2_HUMAN	2.527034269	3.826821193	Anterior gradient protein 2 homolog OS=Homo sapiens GN=AGR2 PE=1 SV=1; TOPep_Count=11
1::sp|P52630|STAT2_HUMAN	2.352158472	4.217295341	Signal transducer and activator of transcription 2 OS=Homo sapiens GN=STAT2 PE=1 SV=1; TOPep_Count=43
1::sp|P42224|STAT1_HUMAN	2.245523398	4.389611 52	Signal transducer and activator of transcription 1-alpha/beta OS=Homo sapiens GN=STAT1 PE=1 SV=2; TOPep_Count=45
1::sp|Q8IY21|DDX60_HUMAN	2.045286626	2.046 6777	Probable ATP-dependent RNA helicase DDX60 OS=Homo sapiens GN=DDX60 PE=1 SV=3; TOPep_Count=104
1::sp|Q96AZ6|ISG20_HUMAN	1.920212234	3.522151356	Interferon-stimulated gene 20 kDa protein OS=Homo sapiens GN=ISG20 PE=1 SV=2; TOPep_Count=11
1::sp|Q9H0P0|5NT3A_HUMAN	1.913353038	5.890948919	Cytosolic 5'-nucleotidase 3A OS=Homo sapiens GN=NT5C3A PE=1 SV=3; TOPep_Count=23
1::sp|P09913|IFIT2_HUMAN	1.807829356	5.961824304	Interferon-induced protein with tetratricopeptide repeats 2 OS=Homo sapiens GN=IFIT2 PE=1 SV=1; TOPep_Count=33
1::sp|Q8IYM9|TRI22_HUMAN	1.793526222	4.018618156	E3 ubiquitin-protein ligase TRIM22 OS=Homo sapiens GN=TRIM22 PE=1 SV=1; TOPep_Count=31
1::sp|Q63HN8|RN213_HUMAN	1.557290416	3.374773331	E3 ubiquitin-protein ligase RNF213 OS=Homo sapiens GN=RNF213 PE=1 SV=3; TOPep_Count=306
1::sp|Q9BQE5|APOL2_HUMAN	1.380355482	2.599281383	Apolipoprotein L2 OS=Homo sapiens GN=APOL2 PE=1 SV=1; TOPep_Count=18
1::sp|P49354|FNTA_HUMAN	1.317205405	1.386356494	Protein farnesyltransferase/geranylgeranyltransferase type-1 subunit alpha OS=Homo sapiens GN=FNTA PE=1 SV=1; TOPep_Count=18
1::sp|P19525|E2AK2_HUMAN	1.314434154	4.505683184	Interferon-induced, double-stranded RNA-activated protein kinase OS=Homo sapiens GN=EIF2AK2 PE=1 SV=2; TOPep_Count=25
1::sp|P49023|PAXI_HUMAN	-1.001859927	1.752747085	Paxillin OS=Homo sapiens GN=PXN PE=1 SV=3; TOPep_Count=30
1::sp|Q15075|EEA1_HUMAN	-1.016494984	1.769811859	Early endosome antigen 1 OS=Homo sapiens GN=EEA1 PE=1 SV=2; TOPep_Count=108
1::sp|Q9UHX1|PUF60_HUMAN	-1.021	1.617384591	Poly(U)-binding-splicing factor PUF60 OS=Homo sapiens GN=PUF60 PE=1 SV=1; TOPep_Count=28

	94306		
1::sp|P18859|ATP5J_HUMAN	-1.02404299	1.33277538	ATP synthase-coupling factor 6, mitochondrial OS=Homo sapiens GN=ATP5J PE=1 SV=1; TOPep_Count=7
1::sp|Q99729|ROAA_HUMAN	-1.03153354	1.37755115	Heterogeneous nuclear ribonucleoprotein A/B OS=Homo sapiens GN=HNRNPAB PE=1 SV=2; TOPep_Count=14
1::sp|P48506|GSH1_HUMAN	-1.03450743	1.44082853	Glutamate--cysteine ligase catalytic subunit OS=Homo sapiens GN=GCLC PE=1 SV=2; TOPep_Count=35
1::sp|Q15942|ZYX_HUMAN	-1.04013234	1.99881138	Zyxin OS=Homo sapiens GN=ZYX PE=1 SV=1; TOPep_Count=21
1::sp|Q13671|RIN1_HUMAN	-1.06176248	1.97805635	Ras and Rab interactor 1 OS=Homo sapiens GN=RIN1 PE=1 SV=4; TOPep_Count=38
1::sp|Q13509|TBB3_HUMAN	-1.06249682	1.37018993	Tubulin beta-3 chain OS=Homo sapiens GN=TUBB3 PE=1 SV=2; TOPep_Count=21
1::sp|P06703|S10A6_HUMAN	-1.06652674	1.95499395	Protein S100-A6 OS=Homo sapiens GN=S100A6 PE=1 SV=1; TOPep_Count=5
1::sp|Q9UGI8|TES_HUMAN	-1.08034040	1.36086846	Testin OS=Homo sapiens GN=TES PE=1 SV=1; TOPep_Count=27
1::sp|Q9BWD1|THIC_HUMAN	-1.09285517	1.34396236	Acetyl-CoA acetyltransferase, cytosolic OS=Homo sapiens GN=ACAT2 PE=1 SV=2; TOPep_Count=20
1::sp|P52815|RM12_HUMAN	-1.09399282	1.44004998	39S ribosomal protein L12, mitochondrial OS=Homo sapiens GN=MRPL12 PE=1 SV=2; TOPep_Count=10
1::sp|P49841|GSK3B_HUMAN	-1.09446046	1.48377991	Glycogen synthase kinase-3 beta OS=Homo sapiens GN=GSK3B PE=1 SV=2; TOPep_Count=24
1::sp|Q6DKJ4|NXN_HUMAN	-1.15475356	1.30586035	Nucleoredoxin OS=Homo sapiens GN=NXN PE=1 SV=2; TOPep_Count=23
1::sp|Q14240|IF4A2_HUMAN	-1.18771752	1.56905194	Eukaryotic initiation factor 4A-II OS=Homo sapiens GN=EIF4A2 PE=1 SV=2; TOPep_Count=23
1::sp|P06748|NPM_HUMAN	-1.20445470	1.55085320	Nucleophosmin OS=Homo sapiens GN=NPM1 PE=1 SV=2; TOPep_Count=16
1::sp|P02765|FETUA_HUMAN	-1.20662486	1.40039487	Alpha-2-HS-glycoprotein OS=Homo sapiens GN=AHSG PE=1 SV=1; TOPep_Count=17

1::sp|Q9NTZ6|RBM12_HUMAN	-1.21242021111	1.45713087373	RNA-binding protein 12 OS=Homo sapiens GN=RBM12 PE=1 SV=1; TOPep_Count=34
1::sp|P30043|BLVRB_HUMAN	-1.22122970857	1.88030865757	Flavin reductase (NADPH) OS=Homo sapiens GN=BLVRB PE=1 SV=3; TOPep_Count=11
1::sp|Q15363|TMED2_HUMAN	-1.23028307	1.35673796464	Transmembrane emp24 domain-containing protein 2 OS=Homo sapiens GN=TMED2 PE=1 SV=1; TOPep_Count=11
1::sp|Q9BWF3|RBM4_HUMAN	-1.24278939	1.64066889999	RNA-binding protein 4 OS=Homo sapiens GN=RBM4 PE=1 SV=1; TOPep_Count=22
1::sp|Q9H3P7|GCP60_HUMAN	-1.26030514444	1.66798109494	Golgi resident protein GCP60 OS=Homo sapiens GN=ACBD3 PE=1 SV=4; TOPep_Count=21
1::sp|Q01130|SRSF2_HUMAN	-1.26371679595	1.49520822121	Serine/arginine-rich splicing factor 2 OS=Homo sapiens GN=SRSF2 PE=1 SV=4; TOPep_Count=11
1::sp|Q9H1E3|NUCKS_HUMAN	-1.34281793434	2.69816339999	Nuclear ubiquitous casein and cyclin-dependent kinase substrate 1 OS=Homo sapiens GN=NUCKS1 PE=1 SV=1; TOPep_Count=12
1::sp|Q8N8S7|ENAH_HUMAN	-1.36218502121	1.59556003737	Protein enabled homolog OS=Homo sapiens GN=ENAH PE=1 SV=2; TOPep_Count=25
1::sp|Q15041|AR6P1_HUMAN	-1.36432331717	1.67785736161	ADP-ribosylation factor-like protein 6-interacting protein 1 OS=Homo sapiens GN=ARL6IP1 PE=1 SV=2; TOPep_Count=7
1::sp|O14896|IRF6_HUMAN	-1.40581223838	1.98962076161	Interferon regulatory factor 6 OS=Homo sapiens GN=IRF6 PE=1 SV=1; TOPep_Count=23
1::sp|Q9UK76|HN1_HUMAN	-1.41074371919	1.40474200707	Hematological and neurological expressed 1 protein OS=Homo sapiens GN=HN1 PE=1 SV=3; TOPep_Count=8
1::sp|P12277|KCRB_HUMAN	-1.41990649696	1.58171862424	Creatine kinase B-type OS=Homo sapiens GN=CKB PE=1 SV=1; TOPep_Count=21
1::sp|P09417|DHPR_HUMAN	-1.45186586868	1.31121951006	Dihydropteridine reductase OS=Homo sapiens GN=QDPR PE=1 SV=2; TOPep_Count=17
1::sp|Q9Y3C6|PPIL1_HUMAN	-1.55696178787	1.52154348	Peptidyl-prolyl cis-trans isomerase-like 1 OS=Homo sapiens GN=PPIL1 PE=1 SV=1; TOPep_Count=9
1::sp|Q9Y2S6|TMA7_HUMAN	-1.58638714343	1.66685468282	Translation machinery-associated protein 7 OS=Homo sapiens GN=TMA7 PE=1 SV=1; TOPep_Count=2

1::sp|O60271|JIP4_HUMAN	-1.60329080505	1.37937762626	C-Jun-amino-terminal kinase-interacting protein 4 OS=Homo sapiens GN=SPAG9 PE=1 SV=4; TOPep_Count=76
1::sp|Q9Y5Z4|HEBP2_HUMAN	-1.71499513535	1.37500898987	Heme-binding protein 2 OS=Homo sapiens GN=HEBP2 PE=1 SV=1; TOPep_Count=10
1::sp|Q13428|TCOF_HUMAN	-1.88687406161	1.83663146868	Treacle protein OS=Homo sapiens GN=TCOF1 PE=1 SV=3; TOPep_Count=77
1::sp|Q9UBV8|PEF1_HUMAN	-2.37261654	1.39621181818	Peflin OS=Homo sapiens GN=PEF1 PE=1 SV=1; TOPep_Count=9
1::sp|Q16527|CSRP2_HUMAN	-2.80938440707	1.47004521717	Cysteine and glycine-rich protein 2 OS=Homo sapiens GN=CSRP2 PE=1 SV=3; TOPep_Count=13

Significant proteins of infected HBEpC HRSV ΔSH			
Accession	LOG 2 FC	LOG10 P-value	Description
2::sp|P03423|GLYC_HRSVA	6.079805928	5.001532949	Major surface glycoprotein G OS=Human respiratory syncytial virus A (strain A2) GN=G PE=1 SV=1
1::sp|P29728|OAS2_HUMAN	5.596952042	6.650193263	2'-5'-oligoadenylate synthase 2 OS=Homo sapiens GN=OAS2 PE=1 SV=3; TOPep_Count=38
2::sp|P03421|PHOSP_HRSVA	5.395252301	8.919309079	Phosphoprotein OS=Human respiratory syncytial virus A (strain A2) GN=P PE=1 SV=1
1::sp|Q460N5|PAR14_HUMAN	4.553438482	5.599871051	Poly [ADP-ribose] polymerase 14 OS=Homo sapiens GN=PARP14 PE=1 SV=3; TOPep_Count=123
2::sp|P03419|MATRX_HRSVA	4.288014021	8.753374104	Matrix protein OS=Human respiratory syncytial virus A (strain A2) GN=M PE=1 SV=1
2::sp|P04545|M21_HRSVA	4.175198639	9.4848184	Matrix M2-1 OS=Human respiratory syncytial virus A (strain A2) GN=M2-1 PE=1 SV=1
1::sp|P05161|ISG15_HUMAN	4.167667183	7.690295963	Ubiquitin-like protein ISG15 OS=Homo sapiens GN=ISG15 PE=1 SV=5; TOPep_Count=10
1::sp|Q9BYX4|IFIH1_HUMAN	4.036920044	6.21304509	Interferon-induced helicase C domain-containing protein 1 OS=Homo sapiens GN=IFIH1 PE=1 SV=3; TOPep_Count=57
1::sp|P00973|OAS1_HUMAN	4.003626926	7.12652651	2'-5'-oligoadenylate synthase 1 OS=Homo sapiens GN=OAS1 PE=1 SV=4; TOPep_Count=18
1::sp|O95786|DDX58_HUMAN	3.973298353	9.97666095 2	Probable ATP-dependent RNA helicase DDX58 OS=Homo sapiens GN=DDX58 PE=1 SV=2; TOPep_Count=58
2::sp|P03418|NCAP_HRSVA	3.862591424	9.47114055 7	Nucleoprotein OS=Human respiratory syncytial virus A (strain A2) GN=N PE=1 SV=1

1::sp|P09914|IFIT1_HUMAN (+1)	3.794047833	6.89105958 1	Interferon-induced protein with tetratricopeptide repeats 1 OS=Homo sapiens GN=IFIT1 PE=1 SV=2; TOPep_Count=33
1::sp|O15162|PLS1_HUMAN	3.705972345	5.255355308	Phospholipid scramblase 1 OS=Homo sapiens GN=PLSCR1 PE=1 SV=1; TOPep_Count=10
1::sp|P20591|MX1_HUMAN (+1)	3.645031263	9.528 75683	Interferon-induced GTP-binding protein Mx1 OS=Homo sapiens GN=MX1 PE=1 SV=4; TOPep_Count=41
1::sp|Q15646|OASL_HUMAN	3.477085187	5.064068025	2'-5'-oligoadenylate synthase-like protein OS=Homo sapiens GN=OASL PE=1 SV=2; TOPep_Count=29
1::sp|Q8WXG1|RSAD2_HUMAN	3.468451204	4.189 85186	Radical S-adenosyl methionine domain-containing protein 2 OS=Homo sapiens GN=RSAD2 PE=1 SV=1; TOPep_Count=26
1::sp|O95994|AGR2_HUMAN	3.105055078	3.826821193	Anterior gradient protein 2 homolog OS=Homo sapiens GN=AGR2 PE=1 SV=1; TOPep_Count=11
1::sp|P32455|GBP1_HUMAN	2.969032237	6.320400079	Interferon-induced guanylate-binding protein 1 OS=Homo sapiens GN=GBP1 PE=1 SV=2; TOPep_Count=32
2::sp|P03420|FUS_HRSVA	2.831213782	4.986456461	Fusion glycoprotein F0 OS=Human respiratory syncytial virus A (strain A2) GN=F PE=1 SV=1
1::sp|O14879|IFIT3_HUMAN	2.797242197	8.353609125	Interferon-induced protein with tetratricopeptide repeats 3 OS=Homo sapiens GN=IFIT3 PE=1 SV=1; TOPep_Count=30
1::sp|Q8IY21|DDX60_HUMAN	2.349667006	2.046 6777	Probable ATP-dependent RNA helicase DDX60 OS=Homo sapiens GN=DDX60 PE=1 SV=3; TOPep_Count=104
1::sp|Q96AZ6|ISG20_HUMAN	2.211021017	3.522151356	Interferon-stimulated gene 20 kDa protein OS=Homo sapiens GN=ISG20 PE=1 SV=2; TOPep_Count=11
1::sp|P37198|NUP62_HUMAN	2.136661385	1.515673972	Nuclear pore glycoprotein p62 OS=Homo sapiens GN=NUP62 PE=1 SV=3; TOPep_Count=13
1::sp|P42224|STAT1_HUMAN	2.082783533	4.389 61152	Signal transducer and activator of transcription 1-alpha/beta OS=Homo sapiens GN=STAT1 PE=1 SV=2; TOPep_Count=45
1::sp|P52630|STAT2_HUMAN	1.846824268	4.217295341	Signal transducer and activator of transcription 2 OS=Homo sapiens GN=STAT2 PE=1 SV=1; TOPep_Count=43
1::sp|P09913|IFIT2_HUMAN	1.819655222	5.961824304	Interferon-induced protein with tetratricopeptide repeats 2 OS=Homo sapiens GN=IFIT2 PE=1 SV=1; TOPep_Count=33
1::sp|Q9Y6Q5|AP1M2_HUMAN	1.708344536	1.346974993	AP-1 complex subunit mu-2 OS=Homo sapiens GN=AP1M2 PE=1 SV=4; TOPep_Count=29
1::sp|Q8IYM9|TRI22_HUMAN	1.584766843	4.018618156	E3 ubiquitin-protein ligase TRIM22 OS=Homo sapiens GN=TRIM22 PE=1 SV=1; TOPep_Count=31
1::sp|Q9H0P0|5NT3A_HUMAN	1.361275217	5.890948919	Cytosolic 5'-nucleotidase 3A OS=Homo sapiens GN=NT5C3A PE=1 SV=3; TOPep_Count=23
1::sp|Q9BQE5|APOL2_HUMAN	1.355777248	2.599281383	Apolipoprotein L2 OS=Homo sapiens GN=APOL2 PE=1 SV=1; TOPep_Count=18
1::sp|P19525|E2AK2_HUMAN	1.355218 47	4.505683184	Interferon-induced, double-stranded RNA-activated protein kinase OS=Homo sapiens GN=EIF2AK2 PE=1 SV=2; TOPep_Count=25

1::Int_P61769ups|B2MG_HUMAN_UPS	1.052564403	4.93967339 5	Beta-2-microglobulin (Chain 21-119) - Homo sapiens (Human); TOPep_Count=7
1::sp|P40763|STAT3_HUMAN	1.044340538	2.0876265	Signal transducer and activator of transcription 3 OS=Homo sapiens GN=STAT3 PE=1 SV=2; TOPep_Count=45
1::sp|P29590|PML_HUMAN	1.032758987	3.59807121 7	Protein PML OS=Homo sapiens GN=PML PE=1 SV=3; TOPep_Count=49
1::sp|P49354|FNTA_HUMAN	1.031810543	1.38635649 4	Protein farnesyltransferase/geranylgeranyltransferase type-1 subunit alpha OS=Homo sapiens GN=FNTA PE=1 SV=1; TOPep_Count=18
1::sp|O60271|JIP4_HUMAN	-1.002421991	1.37937762 6	C-Jun-amino-terminal kinase-interacting protein 4 OS=Homo sapiens GN=SPAG9 PE=1 SV=4; TOPep_Count=76
1::sp|Q08209|PP2BA_HUMAN	-1.004269101	1.46646136 9	Serine/threonine-protein phosphatase 2B catalytic subunit alpha isoform OS=Homo sapiens GN=PPP3CA PE=1 SV=1; TOPep_Count=27
1::sp|Q99729|ROAA_HUMAN	-1.024642288	1.37755115 9	Heterogeneous nuclear ribonucleoprotein A/B OS=Homo sapiens GN=HNRNPAB PE=1 SV=2; TOPep_Count=14
1::sp|Q15041|AR6P1_HUMAN	-1.054659785	1.67785736 1	ADP-ribosylation factor-like protein 6-interacting protein 1 OS=Homo sapiens GN=ARL6IP1 PE=1 SV=2; TOPep_Count=7
1::sp|Q14240|IF4A2_HUMAN	-1.061396917	1.56905194 5	Eukaryotic initiation factor 4A-II OS=Homo sapiens GN=EIF4A2 PE=1 SV=2; TOPep_Count=23
1::sp|Q9Y5Z4|HEBP2_HUMAN	-1.078108824	1.37500898 7	Heme-binding protein 2 OS=Homo sapiens GN=HEBP2 PE=1 SV=1; TOPep_Count=10
1::sp|P78344|IF4G2_HUMAN	-1.079450381	1.54760752 2	Eukaryotic translation initiation factor 4 gamma 2 OS=Homo sapiens GN=EIF4G2 PE=1 SV=1; TOPep_Count=56
1::sp|Q9UK76|HN1_HUMAN	-1.080227338	1.40474200 7	Hematological and neurological expressed 1 protein OS=Homo sapiens GN=HN1 PE=1 SV=3; TOPep_Count=8
1::sp|Q9Y3C6|PPIL1_HUMAN	-1.227051941	1.52154348	Peptidyl-prolyl cis-trans isomerase-like 1 OS=Homo sapiens GN=PPIL1 PE=1 SV=1; TOPep_Count=9
1::sp|Q9Y2S6|TMA7_HUMAN	-1.229588581	1.66685468 2	Translation machinery-associated protein 7 OS=Homo sapiens GN=TMA7 PE=1 SV=1; TOPep_Count=2
1::sp|Q15363|TMED2_HUMAN	-1.271286934	1.35673796 4	Transmembrane emp24 domain-containing protein 2 OS=Homo sapiens GN=TMED2 PE=1 SV=1; TOPep_Count=11
1::sp|P82909|RT36_HUMAN	-1.310990993	1.53833854 3	28S ribosomal protein S36, mitochondrial OS=Homo sapiens GN=MRPS36 PE=1 SV=2; TOPep_Count=6

1::sp|Q9UBV8|PEF1_HUMAN	-1.318393146	1.396211818	Peflin OS=Homo sapiens GN=PEF1 PE=1 SV=1; TOPep_Count=9
1::sp|Q01130|SRSF2_HUMAN	-1.323051797	1.495208221	Serine/arginine-rich splicing factor 2 OS=Homo sapiens GN=SRSF2 PE=1 SV=4; TOPep_Count=11
1::sp|O14896|IRF6_HUMAN	-1.342930805	1.989620761	Interferon regulatory factor 6 OS=Homo sapiens GN=IRF6 PE=1 SV=1; TOPep_Count=23
1::sp|Q13428|TCOF_HUMAN	-1.377517701	1.836631468	Treacle protein OS=Homo sapiens GN=TCOF1 PE=1 SV=3; TOPep_Count=77
1::sp|P02765|FETUA_HUMAN	-1.413189955	1.400394878	Alpha-2-HS-glycoprotein OS=Homo sapiens GN=AHSG PE=1 SV=1; TOPep_Count=17
1::sp|Q16527|CSRP2_HUMAN	-1.888095057	1.470045217	Cysteine and glycine-rich protein 2 OS=Homo sapiens GN=CSRP2 PE=1 SV=3; TOPep_Count=13

Significant proteins of infected HBEpC HRSV rA2			
Accession	LOG2 FC	LOG10 P-value	Description
1::sp|P29728|OAS2_HUMAN	6.828802793	6.650193263	2'-5'-oligoadenylate synthase 2 OS=Homo sapiens GN=OAS2 PE=1 SV=3; TOPep_Count=38
1::sp|Q9BYX4|IFIH1_HUMAN	5.577046095	6.21304509	Interferon-induced helicase C domain-containing protein 1 OS=Homo sapiens GN=IFIH1 PE=1 SV=3; TOPep_Count=57
1::sp|P05161|ISG15_HUMAN	5.386494894	7.690295963	Ubiquitin-like protein ISG15 OS=Homo sapiens GN=ISG15 PE=1 SV=5; TOPep_Count=10
1::sp|Q8IY21|DDX60_HUMAN	5.324973539	2.0466777	Probable ATP-dependent RNA helicase DDX60 OS=Homo sapiens GN=DDX60 PE=1 SV=3; TOPep_Count=104
1::sp|Q460N5|PAR14_HUMAN	5.262441814	5.599871051	Poly [ADP-ribose] polymerase 14 OS=Homo sapiens GN=PARP14 PE=1 SV=3; TOPep_Count=123
1::sp|P09914|IFIT1_HUMAN (+1)	5.018019082	6.891059581	Interferon-induced protein with tetratricopeptide repeats 1 OS=Homo sapiens GN=IFIT1 PE=1 SV=2; TOPep_Count=33
1::sp|Q8WXG1|RSAD2_HUMAN	4.946115395	4.18985186	Radical S-adenosyl methionine domain-containing protein 2 OS=Homo sapiens GN=RSAD2 PE=1 SV=1; TOPep_Count=26
2::sp|P03423|GLYC_HRSVA	4.847421671	5.001532949	Major surface glycoprotein G OS=Human respiratory syncytial virus A (strain A2) GN=G PE=1 SV=1
1::sp|P20591|MX1_HUMAN (+1)	4.667658899	9.52875683	Interferon-induced GTP-binding protein Mx1 OS=Homo sapiens GN=MX1 PE=1 SV=4; TOPep_Count=41

2::sp|P03421|PHOSP_HRSVA	4.625847644	8.91930907	Phosphoprotein OS=Human respiratory syncytial virus A (strain A2) GN=P PE=1 SV=1
1::sp|P00973|OAS1_HUMAN	4.543280692	7.12652651	2'-5'-oligoadenylate synthase 1 OS=Homo sapiens GN=OAS1 PE=1 SV=4; TOPep_Count=18
1::sp|O95786|DDX58_HUMAN	4.518419438	9.97666095	Probable ATP-dependent RNA helicase DDX58 OS=Homo sapiens GN=DDX58 PE=1 SV=2; TOPep_Count=58
1::sp|Q15646|OASL_HUMAN	4.469455548	5.06406802	2'-5'-oligoadenylate synthase-like protein OS=Homo sapiens GN=OASL PE=1 SV=2; TOPep_Count=29
1::sp|O15162|PLS1_HUMAN	4.450210511	5.25535530	Phospholipid scramblase 1 OS=Homo sapiens GN=PLSCR1 PE=1 SV=1; TOPep_Count=10
1::sp|O14879|IFIT3_HUMAN	4.219694742	8.35360912	Interferon-induced protein with tetratricopeptide repeats 3 OS=Homo sapiens GN=IFIT3 PE=1 SV=1; TOPep_Count=30
1::sp|Q96AZ6|ISG20_HUMAN	4.089889966	3.52215135	Interferon-stimulated gene 20 kDa protein OS=Homo sapiens GN=ISG20 PE=1 SV=2; TOPep_Count=11
2::sp|P03419|MATRX_HRSVA	3.723284308	8.75337410	Matrix protein OS=Human respiratory syncytial virus A (strain A2) GN=M PE=1 SV=1
1::sp|P32455|GBP1_HUMAN	3.602763473	6.32040007	Interferon-induced guanylate-binding protein 1 OS=Homo sapiens GN=GBP1 PE=1 SV=2; TOPep_Count=32
1::sp|O95994|AGR2_HUMAN	3.228704451	3.82682119	Anterior gradient protein 2 homolog OS=Homo sapiens GN=AGR2 PE=1 SV=1; TOPep_Count=11
2::sp|P04545|M21_HRSVA	3.224893314	9.4848184	Matrix M2-1 OS=Human respiratory syncytial virus A (strain A2) GN=M2-1 PE=1 SV=1
2::sp|P03418|NCAP_HRSVA	3.076712671	9.47114055	Nucleoprotein OS=Human respiratory syncytial virus A (strain A2) GN=N PE=1 SV=1
1::sp|P42224|STAT1_HUMAN	3.050778931	4.38961152	Signal transducer and activator of transcription 1-alpha/beta OS=Homo sapiens GN=STAT1 PE=1 SV=2; TOPep_Count=45
1::sp|P09913|IFIT2_HUMAN	3.000201169	5.96182430	Interferon-induced protein with tetratricopeptide repeats 2 OS=Homo sapiens GN=IFIT2 PE=1 SV=1; TOPep_Count=33
1::sp|P52630|STAT2_HUMAN	2.890553795	4.21729534	Signal transducer and activator of transcription 2 OS=Homo sapiens GN=STAT2 PE=1 SV=1; TOPep_Count=43
2::sp|P03420|FUS_HRSVA	2.779107912	4.98645646	Fusion glycoprotein F0 OS=Human respiratory syncytial virus A (strain A2) GN=F PE=1 SV=1
1::sp|P40763|STAT3_HUMAN	2.738172977	2.0876265	Signal transducer and activator of transcription 3 OS=Homo sapiens GN=STAT3 PE=1 SV=2; TOPep_Count=45
1::sp|Q9BQE5|APOL2_HUMAN	2.156606395	2.59928138	Apolipoprotein L2 OS=Homo sapiens GN=APOL2 PE=1 SV=1; TOPep_Count=18
1::sp|Q9H0P0|5NT3A_HUMAN	1.980693534	5.89094891	Cytosolic 5'-nucleotidase 3A OS=Homo sapiens GN=NT5C3A PE=1 SV=3; TOPep_Count=23
1::Int_P61769ups|B2MG_HUMAN_UPS	1.980191445	4.93967339	Beta-2-microglobulin (Chain 21-119) - Homo sapiens (Human); TOPep_Count=7

1::sp|P19525|E2AK2_HUMAN	1.967857929	4.50568318 4	Interferon-induced, double-stranded RNA-activated protein kinase OS=Homo sapiens GN=EIF2AK2 PE=1 SV=2; TOPep_Count=25
1::sp|Q63HN8|RN213_HUMAN	1.900307401	3.37477333 1	E3 ubiquitin-protein ligase RNF213 OS=Homo sapiens GN=RNF213 PE=1 SV=3; TOPep_Count=306
1::sp|Q8IYM9|TRI22_HUMAN	1.783675599	4.01861815 6	E3 ubiquitin-protein ligase TRIM22 OS=Homo sapiens GN=TRIM22 PE=1 SV=1; TOPep_Count=31
1::sp|Q03519|TAP2_HUMAN	1.778589388	1.56714664 6	Antigen peptide transporter 2 OS=Homo sapiens GN=TAP2 PE=1 SV=1; TOPep_Count=29
1::sp|P29590|PML_HUMAN	1.564153601	3.59807121 7	Protein PML OS=Homo sapiens GN=PML PE=1 SV=3; TOPep_Count=49
1::sp|Q08380|LG3BP_HUMAN	1.524028157	2.83811256 3	Galectin-3-binding protein OS=Homo sapiens GN=LGALS3BP PE=1 SV=1; TOPep_Count=29
1::sp|P09543|CN37_HUMAN	1.516772761	4.48173758 3	2',3'-cyclic-nucleotide 3'-phosphodiesterase OS=Homo sapiens GN=CNP PE=1 SV=2; TOPep_Count=32
1::sp|P23381|SYWC_HUMAN	1.424627443	5.52227551 4	Tryptophan--tRNA ligase, cytoplasmic OS=Homo sapiens GN=WARS PE=1 SV=2; TOPep_Count=29
1::sp|P29466|CASP1_HUMAN	1.238907403	2.24913394 6	Caspase-1 OS=Homo sapiens GN=CASP1 PE=1 SV=1; TOPep_Count=21
1::sp|P28062|PSB8_HUMAN	1.232481167	3.02129588 2	Proteasome subunit beta type-8 OS=Homo sapiens GN=PSMB8 PE=1 SV=3; TOPep_Count=17
1::sp|Q6P179|ERAP2_HUMAN	1.204078932	2.37436046 4	Endoplasmic reticulum aminopeptidase 2 OS=Homo sapiens GN=ERAP2 PE=1 SV=2; TOPep_Count=57
1::sp|P21980|TGM2_HUMAN (+1)	1.140159763	1.88678887 1	Protein-glutamine gamma-glutamyltransferase 2 OS=Homo sapiens GN=TGM2 PE=1 SV=2; TOPep_Count=36
1::sp|P19474|RO52_HUMAN	1.114500758	1.81152195 8	E3 ubiquitin-protein ligase TRIM21 OS=Homo sapiens GN=TRIM21 PE=1 SV=1; TOPep_Count=30
1::sp|Q08AF3|SLFN5_HUMAN	1.060846842	2.21322556 7	Schlafen family member 5 OS=Homo sapiens GN=SLFN5 PE=1 SV=1; TOPep_Count=54
1::sp|P19971|TYPH_HUMAN	1.041262595	4.20602005 4	Thymidine phosphorylase OS=Homo sapiens GN=TYMP PE=1 SV=2; TOPep_Count=27
1::sp|Q16527|CSRP2_HUMAN	-1.050568885	1.47004521 7	Cysteine and glycine-rich protein 2 OS=Homo sapiens GN=CSRP2 PE=1 SV=3; TOPep_Count=13
1::sp|P16402|H13_HUMAN (+4)	-1.085079182	1.47909176 1	Histone H1.3 OS=Homo sapiens GN=HIST1H1D PE=1 SV=2; TOPep_Count=13

Significant proteins of infected A549 HRSV rA2

Accession		LOG 2 FC	LOG10 p-value	Description
1::sp|P20591|MX1_HUMAN (+1)		5.906004927	7.736568344	Interferon-induced GTP-binding protein Mx1 OS=Homo sapiens GN=MX1 PE=1 SV=4; TOPep_Count=41
1::sp|P05161|ISG15_HUMAN		5.619281647	6.012055426	Ubiquitin-like protein ISG15 OS=Homo sapiens GN=ISG15 PE=1 SV=5; TOPep_Count=10
1::sp|O95786|DDX58_HUMAN		5.266060206	5.212602809	Probable ATP-dependent RNA helicase DDX58 OS=Homo sapiens GN=DDX58 PE=1 SV=2; TOPep_Count=58
1::sp|O14879|IFIT3_HUMAN		4.249330867	8.108517603	Interferon-induced protein with tetratricopeptide repeats 3 OS=Homo sapiens GN=IFIT3 PE=1 SV=1; TOPep_Count=30
1::sp|Q460N5|PAR14_HUMAN		3.573297163	4.018265965	Poly [ADP-ribose] polymerase 14 OS=Homo sapiens GN=PARP14 PE=1 SV=3; TOPep_Count=123
2::sp|P04544|NS1_HRSVA		3.167283258	4.405507117	Non-structural protein 1 OS=Human respiratory syncytial virus A (strain A2) GN=1C PE=1 SV=1
1::sp|P09914|IFIT1_HUMAN		2.877662764	3.302083002	Interferon-induced protein with tetratricopeptide repeats 1 OS=Homo sapiens GN=IFIT1 PE=1 SV=2; TOPep_Count=33
1::sp|Q9Y6K5|OAS3_HUMAN		2.472001601	3.134644872	2'-5'-oligoadenylate synthase 3 OS=Homo sapiens GN=OAS3 PE=1 SV=3; TOPep_Count=54
1::sp|Q9H0P0|5NT3A_HUMAN		2.458310523	4.986224773	Cytosolic 5'-nucleotidase 3A OS=Homo sapiens GN=NT5C3A PE=1 SV=3; TOPep_Count=23
1::sp|P05452|TETN_HUMAN		2.305417782	4.213586792	Tetranectin OS=Homo sapiens GN=CLEC3B PE=1 SV=3; TOPep_Count=12
2::sp|P03423|GLYC_HRSVA		2.205712716	4.334149423	Major surface glycoprotein G OS=Human respiratory syncytial virus A (strain A2) GN=G PE=1 SV=1
2::sp|P03419|MATRX_HRSVA		2.195356043	7.705297566	Matrix protein OS=Human respiratory syncytial virus A (strain A2) GN=M PE=1 SV=1
1::sp|P09913|IFIT2_HUMAN		2.026787554	6.267843497	Interferon-induced protein with tetratricopeptide repeats 2 OS=Homo sapiens GN=IFIT2 PE=1 SV=1; TOPep_Count=33
1::sp|P0C0L4|CO4A_HUMAN		1.744446696	4.247125021	Complement C4-A OS=Homo sapiens GN=C4A PE=1 SV=2; TOPep_Count=88
1::sp|P17301|ITA2_HUMAN		1.730257899	4.620598277	Integrin alpha-2 OS=Homo sapiens GN=ITGA2 PE=1 SV=1; TOPep_Count=50
1::sp|Q9BQE5|APOL2_HUMAN		1.728934439	2.212818401	Apolipoprotein L2 OS=Homo sapiens GN=APOL2 PE=1 SV=1; TOPep_Count=18
2::sp|P03421|PHOSP_HRSVA		1.711085879	4.976448913	Phosphoprotein OS=Human respiratory syncytial virus A (strain A2) GN=P PE=1 SV=1
2::sp|P04545|M21_HRSVA		1.698998818	8.462873011	Matrix M2-1 OS=Human respiratory syncytial virus A (strain A2) GN=M2-1 PE=1 SV=1

1::sp|Q9NQ88|TIGAR_HUMAN		1.468424934	3.47926817	Fructose-2,6-bisphosphatase TIGAR OS=Homo sapiens GN=TIGAR PE=1 SV=1; TOPep_Count=15
1::sp|P02792|FRIL_HUMAN		1.363723925	3.65104621 9	Ferritin light chain OS=Homo sapiens GN=FTL PE=1 SV=2; TOPep_Count=11
1::sp|O15498|YKT6_HUMAN		1.322083672	1.77476112 4	Synaptobrevin homolog YKT6 OS=Homo sapiens GN=YKT6 PE=1 SV=1; TOPep_Count=14
1::sp|P19525|E2AK2_HUMAN		1.317753469	3.86663207 5	Interferon-induced, double-stranded RNA-activated protein kinase OS=Homo sapiens GN=EIF2AK2 PE=1 SV=2; TOPep_Count=25
2::sp|P03418|NCAP_HRSVA		1.310954587	6.41800827 1	Nucleoprotein OS=Human respiratory syncytial virus A (strain A2) GN=N PE=1 SV=1
1::sp|O00194|RB27B_HUMAN		1.258320943	4.08884201 7	Ras-related protein Rab-27B OS=Homo sapiens GN=RAB27B PE=1 SV=4; TOPep_Count=14
1::sp|P27105|STOM_HUMAN (+1)		1.249635704	1.81793660 7	Erythrocyte band 7 integral membrane protein OS=Homo sapiens GN=STOM PE=1 SV=3; TOPep_Count=18
1::sp|RETBP_HUMAN|		1.240322475	3.00169081 7	; TOPep_Count=10
1::sp|P42224|STAT1_HUMAN		1.205213055	4.29449914	Signal transducer and activator of transcription 1-alpha/beta OS=Homo sapiens GN=STAT1 PE=1 SV=2; TOPep_Count=45
1::sp|P13987|CD59_HUMAN		1.160785375	3.33372763 8	CD59 glycoprotein OS=Homo sapiens GN=CD59 PE=1 SV=1; TOPep_Count=6
1::sp|P01024|CO3_HUMAN		1.145069654	4.46016198 1	Complement C3 OS=Homo sapiens GN=C3 PE=1 SV=2; TOPep_Count=107
1::sp|Q08380|LG3BP_HUMAN		1.124964849	3.07707134	Galectin-3-binding protein OS=Homo sapiens GN=LGALS3BP PE=1 SV=1; TOPep_Count=29
1::sp|P02774|VTDB_HUMAN		1.120694014	4.59683629 6	Vitamin D-binding protein OS=Homo sapiens GN=GC PE=1 SV=1; TOPep_Count=29
1::sp|ANT3_HUMAN|		1.114841312	3.51038065	; TOPep_Count=30
1::sp|P09601|HMOX1_HUMAN		1.106612401	1.66627772	Heme oxygenase 1 OS=Homo sapiens GN=HMOX1 PE=1 SV=1; TOPep_Count=18
1::sp|P21283|VATC1_HUMAN		1.101440084	2.10902859 6	V-type proton ATPase subunit C 1 OS=Homo sapiens GN=ATP6V1C1 PE=1 SV=4; TOPep_Count=28
1::sp|P24941|CDK2_HUMAN		1.093694291	3.63635465 5	Cyclin-dependent kinase 2 OS=Homo sapiens GN=CDK2 PE=1 SV=2; TOPep_Count=21
1::sp|P16190|1A33_HUMAN (+7)		1.089163683	3.68964047 8	HLA class I histocompatibility antigen, A-33 alpha chain OS=Homo sapiens GN=HLA-A PE=1 SV=3; TOPep_Count=21
1::sp|P29590|PML_HUMAN		1.043799213	4.18347662 8	Protein PML OS=Homo sapiens GN=PML PE=1 SV=3; TOPep_Count=49
2::sp|P03420|FUS_HRSVA		1.032889042	6.11456508 8	Fusion glycoprotein F0 OS=Human respiratory syncytial virus A (strain A2) GN=F PE=1 SV=1

1::sp|Q8WZ82|OVCA2_HUMAN		1.032322932	2.13102739 1	Ovarian cancer-associated gene 2 protein OS=Homo sapiens GN=OVCA2 PE=1 SV=1; TOPep_Count=10
1::sp|Q96CP2|FWCH2_HUMAN		-1.000088399	2.05279213 5	FLYWCH family member 2 OS=Homo sapiens GN=FLYWCH2 PE=1 SV=1; TOPep_Count=8
1::sp|Q96IZ0|PAWR_HUMAN		-1.001188185	1.69497360 1	PRKC apoptosis WT1 regulator protein OS=Homo sapiens GN=PAWR PE=1 SV=1; TOPep_Count=14
1::sp|Q9Y6I3|EPN1_HUMAN		-1.004385902	2.35907312 3	Epsin-1 OS=Homo sapiens GN=EPN1 PE=1 SV=2; TOPep_Count=15
1::sp|O60888|CUTA_HUMAN		-1.005797713	1.87905135 1	Protein CutA OS=Homo sapiens GN=CUTA PE=1 SV=2; TOPep_Count=7
1::sp|Q86UP2|KTN1_HUMAN		-1.008838 37	2.33957031 2	Kinectin OS=Homo sapiens GN=KTN1 PE=1 SV=1; TOPep_Count=94
1::sp|O00273|DFFA_HUMAN		-1.014372062	2.33130334 6	DNA fragmentation factor subunit alpha OS=Homo sapiens GN=DFFA PE=1 SV=1; TOPep_Count=20
1::sp|O95359|TACC2_HUMAN		-1.015876472	1.46785655 9	Transforming acidic coiled-coil-containing protein 2 OS=Homo sapiens GN=TACC2 PE=1 SV=3; TOPep_Count=141
1::sp|P40222|TXLNA_HUMAN		-1.022302682	2.52749987 7	Alpha-taxilin OS=Homo sapiens GN=TXLNA PE=1 SV=3; TOPep_Count=32
1::sp|P48960|CD97_HUMAN		-1.030150774	2.04375402 7	CD97 antigen OS=Homo sapiens GN=CD97 PE=1 SV=4; TOPep_Count=35
1::sp|Q9P2E9|RRBP1_HUMAN		-1.032214866	2.31404029 3	Ribosome-binding protein 1 OS=Homo sapiens GN=RRBP1 PE=1 SV=4; TOPep_Count=108
1::sp|Q14257|RCN2_HUMAN		-1.032837849	2.25060302 7	Reticulocalbin-2 OS=Homo sapiens GN=RCN2 PE=1 SV=1; TOPep_Count=15
1::sp|Q13561|DCTN2_HUMAN		-1.034194861	1.73868159 5	Dynactin subunit 2 OS=Homo sapiens GN=DCTN2 PE=1 SV=4; TOPep_Count=26
1::sp|P62158|CALM_HUMAN (+1)		-1.035322438	2.02608575 2	Calmodulin OS=Homo sapiens GN=CALM1 PE=1 SV=2; TOPep_Count=9
1::sp|Q7Z4V5|HDGR2_HUMAN		-1.036224779	1.69215619 1	Hepatoma-derived growth factor-related protein 2 OS=Homo sapiens GN=HDGFRP2 PE=1 SV=1; TOPep_Count=40
1::sp|P20674|COX5A_HUMAN		-1.040	2.32029730 8	Cytochrome c oxidase subunit 5A, mitochondrial OS=Homo sapiens GN=COX5A PE=1 SV=2; TOPep_Count=11

		651981		
1::sp|Q05682|CALD1_HUMAN		-1.044911395	1.6885437844	Caldesmon OS=Homo sapiens GN=CALD1 PE=1 SV=3; TOPep_Count=44
1::sp|Q9GZY8|MFF_HUMAN		-1.046898499	2.5736998699	Mitochondrial fission factor OS=Homo sapiens GN=MFF PE=1 SV=1; TOPep_Count=17
1::sp|O75380|NDUS6_HUMAN		-1.047743447	1.70724616	NADH dehydrogenase [ubiquinone] iron-sulfur protein 6, mitochondrial OS=Homo sapiens GN=NDUFS6 PE=1 SV=1; TOPep_Count=9
1::sp|P67936|TPM4_HUMAN (+1)		-1.049678588	2.1766122284	Tropomyosin alpha-4 chain OS=Homo sapiens GN=TPM4 PE=1 SV=3; TOPep_Count=21
1::sp|Q7Z422|SZRD1_HUMAN		-1.052788727	2.6555013705	SUZ domain-containing protein 1 OS=Homo sapiens GN=SZRD1 PE=1 SV=1; TOPep_Count=8
1::sp|Q16626|MEA1_HUMAN		-1.060213542	1.7175074445	Male-enhanced antigen 1 OS=Homo sapiens GN=MEA1 PE=1 SV=2; TOPep_Count=5
1::sp|Q5M775|CYTSB_HUMAN		-1.062385295	3.0957071444	Cytospin-B OS=Homo sapiens GN=SPECC1 PE=1 SV=1; TOPep_Count=64
1::sp|P35221|CTNA1_HUMAN		-1.064050995	4.4029690599	Catenin alpha-1 OS=Homo sapiens GN=CTNNA1 PE=1 SV=1; TOPep_Count=56
1::sp|P54727|RD23B_HUMAN		-1.069549556	3.48906365	UV excision repair protein RAD23 homolog B OS=Homo sapiens GN=RAD23B PE=1 SV=1; TOPep_Count=15
1::sp|Q14444|CAPR1_HUMAN		-1.075025891	3.5268560744	Caprin-1 OS=Homo sapiens GN=CAPRIN1 PE=1 SV=2; TOPep_Count=23
1::sp|O60828|PQBP1_HUMAN		-1.077306203	1.9370341433	Polyglutamine-binding protein 1 OS=Homo sapiens GN=PQBP1 PE=1 SV=1; TOPep_Count=9
1::sp|Q99622|C10_HUMAN		-1.077409744	2.4016416923	Protein C10 OS=Homo sapiens GN=C12orf57 PE=1 SV=1; TOPep_Count=7
1::sp|P30533|AMRP_HUMAN		-1.080330433	2.3260449981	Alpha-2-macroglobulin receptor-associated protein OS=Homo sapiens GN=LRPAP1 PE=1 SV=1; TOPep_Count=26
1::sp|O00193|SMAP_HUMAN		-1.088090003	1.5861061116	Small acidic protein OS=Homo sapiens GN=SMAP PE=1 SV=1; TOPep_Count=8
1::sp|Q7Z4H7|HAUS6_HUMAN		-1.088729218	2.13557802	HAUS augmin-like complex subunit 6 OS=Homo sapiens GN=HAUS6 PE=1 SV=2; TOPep_Count=59

1::sp|Q9P000|COMD9_HUMAN		-1.09685038	3.0843537937	COMM domain-containing protein 9 OS=Homo sapiens GN=COMMD9 PE=1 SV=2; TOPep_Count=12
1::sp|Q9UK76|HN1_HUMAN		-1.09705429	3.1119423321	Hematological and neurological expressed 1 protein OS=Homo sapiens GN=HN1 PE=1 SV=3; TOPep_Count=8
1::sp|Q16643|DREB_HUMAN		-1.09733173	2.1048366422	Drebrin OS=Homo sapiens GN=DBN1 PE=1 SV=4; TOPep_Count=25
1::sp|P62861|RS30_HUMAN		-1.09796354	2.5472348227	40S ribosomal protein S30 OS=Homo sapiens GN=FAU PE=1 SV=1; TOPep_Count=3
1::sp|Q13442|HAP28_HUMAN		-1.09830384	2.2933139976	28 kDa heat- and acid-stable phosphoprotein OS=Homo sapiens GN=PDAP1 PE=1 SV=1; TOPep_Count=10
1::sp|Q96C90|PP14B_HUMAN		-1.09869159	2.8428721322	Protein phosphatase 1 regulatory subunit 14B OS=Homo sapiens GN=PPP1R14B PE=1 SV=3; TOPep_Count=6
1::sp|P20962|PTMS_HUMAN		-1.104187	1.8036435881	Parathymosin OS=Homo sapiens GN=PTMS PE=1 SV=2; TOPep_Count=3
1::sp|Q96GA3|LTV1_HUMAN		-1.11187406	1.64986007	Protein LTV1 homolog OS=Homo sapiens GN=LTV1 PE=1 SV=1; TOPep_Count=26
1::sp|O94992|HEXI1_HUMAN (+1)		-1.11924671	2.8450112822	Protein HEXIM1 OS=Homo sapiens GN=HEXIM1 PE=1 SV=1; TOPep_Count=14
1::sp|Q15654|TRIP6_HUMAN		-1.12117351	3.1163269447	Thyroid receptor-interacting protein 6 OS=Homo sapiens GN=TRIP6 PE=1 SV=3; TOPep_Count=26
1::sp|P49321|NASP_HUMAN		-1.12407825	2.3019976443	Nuclear autoantigenic sperm protein OS=Homo sapiens GN=NASP PE=1 SV=2; TOPep_Count=42
1::sp|C9JLW8|F195B_HUMAN		-1.12696545	1.6414726233	Protein FAM195B OS=Homo sapiens GN=FAM195B PE=1 SV=1; TOPep_Count=9
1::sp|P33316|DUT_HUMAN		-1.12890199	3.2605107855	Deoxyuridine 5'-triphosphate nucleotidohydrolase, mitochondrial OS=Homo sapiens GN=DUT PE=1 SV=4; TOPep_Count=17
1::sp|P36954|RPB9_HUMAN		-1.14653482	3.4370987411	DNA-directed RNA polymerase II subunit RPB9 OS=Homo sapiens GN=POLR2I PE=1 SV=1; TOPep_Count=9
1::sp|P07951|TPM2_HUMAN		-1.15578486	2.3643786777	Tropomyosin beta chain OS=Homo sapiens GN=TPM2 PE=1 SV=1; TOPep_Count=23
1::sp|Q9Y520|PRC2C_HUMAN (+1)		-1.165	2.6121395526	Protein PRRC2C OS=Homo sapiens GN=PRRC2C PE=1 SV=4; TOPep_Count=122

		716799		
1::sp|Q8N4Q1|MIA40_HUMAN		-1.167715652	2.20849805 7	Mitochondrial intermembrane space import and assembly protein 40 OS=Homo sapiens GN=CHCHD4 PE=1 SV=1; TOPep_Count=7
1::sp|Q14157|UBP2L_HUMAN		-1.1700719 8	3.04187612 4	Ubiquitin-associated protein 2-like OS=Homo sapiens GN=UBAP2L PE=1 SV=2; TOPep_Count=32
1::sp|Q93052|LPP_HUMAN		-1.174143747	2.36733711 6	Lipoma-preferred partner OS=Homo sapiens GN=LPP PE=1 SV=1; TOPep_Count=22
1::sp|O75506|HSBP1_HUMAN		-1.180192345	1.86070519 4	Heat shock factor-binding protein 1 OS=Homo sapiens GN=HSBP1 PE=1 SV=1; TOPep_Count=7
1::sp|Q8WTS6|SETD7_HUMAN		-1.190868238	1.77828808 9	Histone-lysine N-methyltransferase SETD7 OS=Homo sapiens GN=SETD7 PE=1 SV=1; TOPep_Count=16
1::sp|P52943|CRIP2_HUMAN		-1.197974317	2.67301855 4	Cysteine-rich protein 2 OS=Homo sapiens GN=CRIP2 PE=1 SV=1; TOPep_Count=10
1::sp|P61457|PHS_HUMAN		-1.200059945	2.17720944 8	Pterin-4-alpha-carbinolamine dehydratase OS=Homo sapiens GN=PCBD1 PE=1 SV=2; TOPep_Count=8
1::sp|Q9Y2V2|CHSP1_HUMAN		-1.203418307	2.74978425 7	Calcium-regulated heat stable protein 1 OS=Homo sapiens GN=CARHSP1 PE=1 SV=2; TOPep_Count=8
1::sp|P40855|PEX19_HUMAN		-1.208030902	2.10858324	Peroxisomal biogenesis factor 19 OS=Homo sapiens GN=PEX19 PE=1 SV=1; TOPep_Count=18
1::sp|Q9BTT0|AN32E_HUMAN		-1.212463323	2.90723671 6	Acidic leucine-rich nuclear phosphoprotein 32 family member E OS=Homo sapiens GN=ANP32E PE=1 SV=1; TOPep_Count=10
1::sp|P61024|CKS1_HUMAN		-1.2187485 7	2.31318502 8	Cyclin-dependent kinases regulatory subunit 1 OS=Homo sapiens GN=CKS1B PE=1 SV=1; TOPep_Count=5
1::sp|P52758|UK114_HUMAN		-1.245580628	1.94281007 3	Ribonuclease UK114 OS=Homo sapiens GN=HRSP12 PE=1 SV=1; TOPep_Count=10
1::sp|P18615|NELFE_HUMAN		-1.250348353	2.58207515 8	Negative elongation factor E OS=Homo sapiens GN=NELFE PE=1 SV=3; TOPep_Count=20
1::sp|Q9Y6K9|NEMO_HUMAN		-1.252466237	1.33659557 7	NF-kappa-B essential modulator OS=Homo sapiens GN=IKBKG PE=1 SV=2; TOPep_Count=28
1::sp|O95302|FKBP9_HUMAN		-1.257281224	1.77834708 2	Peptidyl-prolyl cis-trans isomerase FKBP9 OS=Homo sapiens GN=FKBP9 PE=1 SV=2; TOPep_Count=25

1::sp|P80303|NUCB2_HUMAN		-1.26413912727	3.1186740276	Nucleobindin-2 OS=Homo sapiens GN=NUCB2 PE=1 SV=2; TOPep_Count=24
1::sp|Q9P0P0|RN181_HUMAN		-1.26878274646	2.6925537764	E3 ubiquitin-protein ligase RNF181 OS=Homo sapiens GN=RNF181 PE=1 SV=1; TOPep_Count=9
1::sp|Q9BRK5|CAB45_HUMAN		-1.28834309494	2.0967350934	45 kDa calcium-binding protein OS=Homo sapiens GN=SDF4 PE=1 SV=1; TOPep_Count=19
1::sp|Q3KQU3|MA7D1_HUMAN		-1.30362016666	1.8346898665	MAP7 domain-containing protein 1 OS=Homo sapiens GN=MAP7D1 PE=1 SV=1; TOPep_Count=45
1::sp|P16949|STMN1_HUMAN (+2)		-1.30902437979	3.0533339885	Stathmin OS=Homo sapiens GN=STMN1 PE=1 SV=3; TOPep_Count=10
1::sp|P67809|YBOX1_HUMAN (+1)		-1.30930681	3.1179266632	Nuclease-sensitive element-binding protein 1 OS=Homo sapiens GN=YBX1 PE=1 SV=3; TOPep_Count=13
1::sp|O43294|TGFI1_HUMAN		-1.31148757474	4.18866216	Transforming growth factor beta-1-induced transcript 1 protein OS=Homo sapiens GN=TGFB1I1 PE=1 SV=2; TOPep_Count=24
1::sp|P23434|GCSH_HUMAN		-1.32771845151	1.9326787588	Glycine cleavage system H protein, mitochondrial OS=Homo sapiens GN=GCSH PE=1 SV=2; TOPep_Count=7
1::sp|Q15276|RABE1_HUMAN		-1.33581231361	3.8245169229	Rab GTPase-binding effector protein 1 OS=Homo sapiens GN=RABEP1 PE=1 SV=2; TOPep_Count=62
1::sp|P98179|RBM3_HUMAN		-1.38873077474	3.9051220122	RNA-binding protein 3 OS=Homo sapiens GN=RBM3 PE=1 SV=1; TOPep_Count=9
1::sp|Q13642|FHL1_HUMAN		-1.39652284848	1.4820696577	Four and a half LIM domains protein 1 OS=Homo sapiens GN=FHL1 PE=1 SV=4; TOPep_Count=24
1::sp|Q9NYJ1|COA4_HUMAN		-1.40089764141	2.0811378336	Cytochrome c oxidase assembly factor 4 homolog, mitochondrial OS=Homo sapiens GN=COA4 PE=1 SV=2; TOPep_Count=7
1::sp|P22692|IBP4_HUMAN		-1.42613925	2.9980456344	Insulin-like growth factor-binding protein 4 OS=Homo sapiens GN=IGFBP4 PE=1 SV=2; TOPep_Count=14
1::sp|Q9UMS0|NFU1_HUMAN		-1.43534153939	3.1716053	NFU1 iron-sulfur cluster scaffold homolog, mitochondrial OS=Homo sapiens GN=NFU1 PE=1 SV=2; TOPep_Count=14
1::sp|KRHB1_HUMAN| (+2)		-1.44539513333	5.0737471	; TOPep_Count=31

1::sp|P10109|ADX_HUMAN		-1.453656909	2.523799632	Adrenodoxin, mitochondrial OS=Homo sapiens GN=FDX1 PE=1 SV=1; TOPep_Count=14
1::sp|Q9UGP4|LIMD1_HUMAN		-1.463046258	2.468204675	LIM domain-containing protein 1 OS=Homo sapiens GN=LIMD1 PE=1 SV=1; TOPep_Count=33
1::sp|Q8IVM0|CCD50_HUMAN		-1.470428232	2.535476396	Coiled-coil domain-containing protein 50 OS=Homo sapiens GN=CCDC50 PE=1 SV=1; TOPep_Count=19
1::sp|P46013|KI67_HUMAN		-1.484970547	3.095705719	Antigen KI-67 OS=Homo sapiens GN=MKI67 PE=1 SV=2; TOPep_Count=205
1::sp|Q9H1E3|NUCKS_HUMAN		-1.494000498	1.858564758	Nuclear ubiquitous casein and cyclin-dependent kinase substrate 1 OS=Homo sapiens GN=NUCKS1 PE=1 SV=1; TOPep_Count=12
1::sp|Q9UFN0|NPS3A_HUMAN		-1.494347256	1.601720803	Protein NipSnap homolog 3A OS=Homo sapiens GN=NIPSNAP3A PE=1 SV=2; TOPep_Count=17
1::sp|Q5T6F2|UBAP2_HUMAN		-1.518041115	1.57420479	Ubiquitin-associated protein 2 OS=Homo sapiens GN=UBAP2 PE=1 SV=1; TOPep_Count=30
1::sp|Q9ULW0|TPX2_HUMAN		-1.530303076	2.632235531	Targeting protein for Xklp2 OS=Homo sapiens GN=TPX2 PE=1 SV=2; TOPep_Count=42
1::sp|P09493|TPM1_HUMAN		-1.537985035	4.572767626	Tropomyosin alpha-1 chain OS=Homo sapiens GN=TPM1 PE=1 SV=2; TOPep_Count=23
1::sp|O15027|SC16A_HUMAN		-1.563544669	3.820762107	Protein transport protein Sec16A OS=Homo sapiens GN=SEC16A PE=1 SV=3; TOPep_Count=77
1::sp|Q8WZA0|LZIC_HUMAN		-1.606405523	3.709805551	Protein LZIC OS=Homo sapiens GN=LZIC PE=1 SV=1; TOPep_Count=14
1::sp|Q92823|NRCAM_HUMAN		-1.612806299	4.489506767	Neuronal cell adhesion molecule OS=Homo sapiens GN=NRCAM PE=1 SV=3; TOPep_Count=59
1::sp|O95721|SNP29_HUMAN		-1.631666681	1.695996229	Synaptosomal-associated protein 29 OS=Homo sapiens GN=SNAP29 PE=1 SV=1; TOPep_Count=17
1::sp|Q16527|CSRP2_HUMAN		-1.633770245	2.402626682	Cysteine and glycine-rich protein 2 OS=Homo sapiens GN=CSRP2 PE=1 SV=3; TOPep_Count=13
1::sp|Q9P013|CWC15_HUMAN		-1.656933639	3.415630622	Spliceosome-associated protein CWC15 homolog OS=Homo sapiens GN=CWC15 PE=1 SV=2; TOPep_Count=10

1::sp|Q96B36|AKTS1_HUMAN		-1.68684545818	2.5995293999	Proline-rich AKT1 substrate 1 OS=Homo sapiens GN=AKT1S1 PE=1 SV=1; TOPep_Count=10
1::sp|Q4V328|GRAP1_HUMAN		-1.71342069191	1.78943774343	GRIP1-associated protein 1 OS=Homo sapiens GN=GRIPAP1 PE=1 SV=1; TOPep_Count=57
1::sp|Q15154|PCM1_HUMAN		-1.76886084343	2.50539411343	Pericentriolar material 1 protein OS=Homo sapiens GN=PCM1 PE=1 SV=4; TOPep_Count=96
1::sp|Q16625|OCLN_HUMAN		-1.78074395959	2.70948487141	Occludin OS=Homo sapiens GN=OCLN PE=1 SV=1; TOPep_Count=18
1::sp|Q8N6H7|ARFG2_HUMAN (+1)		-1.80115597	4.25111425145	ADP-ribosylation factor GTPase-activating protein 2 OS=Homo sapiens GN=ARFGAP2 PE=1 SV=1; TOPep_Count=32
1::sp|Q9Y618|NCOR2_HUMAN		-2.06967356262	2.86812546145	Nuclear receptor corepressor 2 OS=Homo sapiens GN=NCOR2 PE=1 SV=2; TOPep_Count=136
1::sp|P56211|ARP19_HUMAN (+1)		-2.09644764644	2.85783307414	cAMP-regulated phosphoprotein 19 OS=Homo sapiens GN=ARPP19 PE=1 SV=2; TOPep_Count=7
1::sp|Q8IWE2|NXP20_HUMAN		-2.19168518181	3.01706022	Protein NOXP20 OS=Homo sapiens GN=FAM114A1 PE=1 SV=2; TOPep_Count=24
1::sp|Q6PUV4|CPLX2_HUMAN		-2.42818142828	4.34466038626	Complexin-2 OS=Homo sapiens GN=CPLX2 PE=1 SV=2; TOPep_Count=8
1::sp|Q9ULD2|MTUS1_HUMAN		-2.57005402	2.77593188949	Microtubule-associated tumor suppressor 1 OS=Homo sapiens GN=MTUS1 PE=1 SV=2; TOPep_Count=77

Significant proteins of infected A549 HRSV ΔSH

Accession details	LOG2 FC	LOG10 p-value	Description
2::sp|P04544|NS1_HRSVA	6.11940241	4.405507117	Non-structural protein 1 OS=Human respiratory syncytial virus A (strain A2) GN=1C PE=1 SV=1
1::sp|P20591|MX1_HUMAN;1::sp|P20592|MX2_HUMAN	5.765601125	7.736568344	Interferon-induced GTP-binding protein Mx1 OS=Homo sapiens GN=MX1 PE=1 SV=4; TOPep_Count=41
1::sp|P05161|ISG15_HUMAN	5.271437903	6.012055426	Ubiquitin-like protein ISG15 OS=Homo sapiens GN=ISG15

			PE=1 SV=5; TOPep_Count=10
2::sp|P03423|GLYC_HRSVA	5.188327899	4.334149423	Major surface glycoprotein G OS=Human respiratory syncytial virus A (strain A2) GN=G PE=1 SV=1
2::sp|P03419|MATRX_HRSVA	5.15728445	7.705297566	Matrix protein OS=Human respiratory syncytial virus A (strain A2) GN=M PE=1 SV=1
2::sp|P04545|M21_HRSVA	4.734360188	8.462873011	Matrix M2-1 OS=Human respiratory syncytial virus A (strain A2) GN=M2-1 PE=1 SV=1
2::sp|P03421|PHOSP_HRSVA	4.693211449	4.976448913	Phosphoprotein OS=Human respiratory syncytial virus A (strain A2) GN=P PE=1 SV=1
1::sp|O14879|IFIT3_HUMAN	4.343843427	8.108517603	Interferon-induced protein with tetratricopeptide repeats 3 OS=Homo sapiens GN=IFIT3 PE=1 SV=1; TOPep_Count=30
2::sp|P03418|NCAP_HRSVA	4.035238187	6.418008271	Nucleoprotein OS=Human respiratory syncytial virus A (strain A2) GN=N PE=1 SV=1
1::sp|Q460N5|PAR14_HUMAN	3.682471081	4.018265965	Poly [ADP-ribose] polymerase 14 OS=Homo sapiens GN=PARP14 PE=1 SV=3; TOPep_Count=123
2::sp|P03420|FUS_HRSVA	3.504818306	6.114565088	Fusion glycoprotein F0 OS=Human respiratory syncytial virus A (strain A2) GN=F PE=1 SV=1
1::sp|P09914|IFIT1_HUMAN	3.288573955	3.302083002	Interferon-induced protein with tetratricopeptide repeats 1 OS=Homo sapiens GN=IFIT1 PE=1 SV=2; TOPep_Count=33
1::sp|Q00169|PIPNA_HUMAN	3.156128424	1.987677708	Phosphatidylinositol transfer protein alpha isoform OS=Homo sapiens GN=PITPNA PE=1 SV=2; TOPep_Count=25
1::sp|Q9H0P0|5NT3A_HUMAN	2.422045706	4.986224773	Cytosolic 5'-nucleotidase 3A

			OS=Homo sapiens GN=NT5C3A PE=1 SV=3; TOPep_Count=23
1::sp|P05452|TETN_HUMAN	2.367108715	4.213586792	Tetranectin OS=Homo sapiens GN=CLEC3B PE=1 SV=3; TOPep_Count=12
1::sp|Q9BQE5|APOL2_HUMAN	2.134314246	2.212818401	Apolipoprotein L2 OS=Homo sapiens GN=APOL2 PE=1 SV=1; TOPep_Count=18
1::sp|Q8WZ82|OVCA2_HUMAN	2.034969636	2.131027391	Ovarian cancer-associated gene 2 protein OS=Homo sapiens GN=OVCA2 PE=1 SV=1; TOPep_Count=10
1::sp|Q9Y6K5|OAS3_HUMAN	2.012706722	3.134644872	2'-5'-oligoadenylate synthase 3 OS=Homo sapiens GN=OAS3 PE=1 SV=3; TOPep_Count=54
1::sp|P08648|ITA5_HUMAN	1.962956647	3.112926532	Integrin alpha-5 OS=Homo sapiens GN=ITGA5 PE=1 SV=2; TOPep_Count=36
1::sp|P0C0L4|CO4A_HUMAN	1.74998519	4.247125021	Complement C4-A OS=Homo sapiens GN=C4A PE=1 SV=2; TOPep_Count=88
1::sp|O15498|YKT6_HUMAN	1.563331732	1.774761124	Synaptobrevin homolog YKT6 OS=Homo sapiens GN=YKT6 PE=1 SV=1; TOPep_Count=14
1::sp|P27105|STOM_HUMAN;1::sp|Q8TAV4|STML3_HUMAN	1.525402807	1.817936607	Erythrocyte band 7 integral membrane protein OS=Homo sapiens GN=STOM PE=1 SV=3; TOPep_Count=18
1::sp|Q9NQ88|TIGAR_HUMAN	1.477808022	3.47926817	Fructose-2,6-bisphosphatase TIGAR OS=Homo sapiens GN=TIGAR PE=1 SV=1; TOPep_Count=15
1::sp|P16190|1A33_HUMAN;1::sp|P30443|1A01_HUMAN;1::sp|P30457|1A66_HUMAN;1::sp|P30460|1B08_HUMAN;1::sp|P30485|1B47_HUMAN;1::sp|Q09160|1A8	1.400348915	3.689640478	HLA class I histocompatibility antigen, A-33 alpha chain OS=Homo sapiens GN=HLA-A PE=1 SV=3; TOPep_Count=21

0_HUMAN;1::sp|Q29836|1B67_HUMAN;1::sp|Q31612|1B73_HUMAN			
1::sp|RETBP_HUMAN|	1.313685275	3.001690817	; TOPep_Count=10
1::sp|P01024|CO3_HUMAN	1.310810213	4.460161981	Complement C3 OS=Homo sapiens GN=C3 PE=1 SV=2; TOPep_Count=107
1::sp|P02774|VTDB_HUMAN	1.303289662	4.596836296	Vitamin D-binding protein OS=Homo sapiens GN=GC PE=1 SV=1; TOPep_Count=29
1::sp|P13987|CD59_HUMAN	1.297073458	3.333727638	CD59 glycoprotein OS=Homo sapiens GN=CD59 PE=1 SV=1; TOPep_Count=6
1::sp|O00194|RB27B_HUMAN	1.296810887	4.088842017	Ras-related protein Rab-27B OS=Homo sapiens GN=RAB27B PE=1 SV=4; TOPep_Count=14
1::sp|P18031|PTN1_HUMAN	1.25940499	2.645438732	Tyrosine-protein phosphatase non-receptor type 1 OS=Homo sapiens GN=PTPN1 PE=1 SV=1; TOPep_Count=30
1::sp|P24941|CDK2_HUMAN	1.210288986	3.636354655	Cyclin-dependent kinase 2 OS=Homo sapiens GN=CDK2 PE=1 SV=2; TOPep_Count=21
1::sp|P19525|E2AK2_HUMAN	1.16219273	3.866632075	Interferon-induced, double-stranded RNA-activated protein kinase OS=Homo sapiens GN=EIF2AK2 PE=1 SV=2; TOPep_Count=25
1::sp|P84095|RHOG_HUMAN	1.118926735	2.527468737	Rho-related GTP-binding protein RhoG OS=Homo sapiens GN=RHOG PE=1 SV=1; TOPep_Count=12
1::sp|Q7Z2W4|ZCCHV_HUMAN	1.089508753	2.957098815	Zinc finger CCCH-type antiviral protein 1 OS=Homo sapiens GN=ZC3HAV1 PE=1 SV=3; TOPep_Count=64
1::sp|Q08380|LG3BP_HUMAN	1.087525877	3.07707134	Galectin-3-binding protein OS=Homo sapiens GN=LGALS3BP

			PE=1 SV=1; TOPep_Count=29
1::sp|ANT3_HUMAN|	1.054747726	3.51038065	; TOPep_Count=30
1::sp|P02792|FRIL_HUMAN	1.046187888	3.651046219	Ferritin light chain OS=Homo sapiens GN=FTL PE=1 SV=2; TOPep_Count=11
1::sp|P57088|TMM33_HUMAN	1.036587927	1.51171189	Transmembrane protein 33 OS=Homo sapiens GN=TMEM33 PE=1 SV=2; TOPep_Count=11
1::sp|P36955|PEDF_HUMAN	1.035968425	4.271367153	Pigment epithelium-derived factor OS=Homo sapiens GN=SERPINF1 PE=1 SV=4; TOPep_Count=23
1::sp|Q06033|ITIH3_HUMAN	1.03355384	4.08943793	Inter-alpha-trypsin inhibitor heavy chain H3 OS=Homo sapiens GN=ITIH3 PE=1 SV=2; TOPep_Count=43
1::sp|P29317|EPHA2_HUMAN;1::sp|P54753|EPHB3_HUMAN;1::sp|P54760|EPHB4_HUMAN;1::sp|P54764|EPHA4_HUMAN;1::sp|Q9UF33|EPHA6_HUMAN	1.024759493	1.711016781	Ephrin type-A receptor 2 OS=Homo sapiens GN=EPHA2 PE=1 SV=2; TOPep_Count=52
1::Int_P61769ups|B2MG_HUMAN_UPS	1.024586969	6.29782423	Beta-2-microglobulin (Chain 21-119) - Homo sapiens (Human); TOPep_Count=7
1::sp|Q9Y3A5|SBDS_HUMAN	1.01260634	2.234194832	Ribosome maturation protein SBDS OS=Homo sapiens GN=SBDS PE=1 SV=4; TOPep_Count=18
1::sp|Q9Y2X3|NOP58_HUMAN	1.004913724	2.588815299	Nucleolar protein 58 OS=Homo sapiens GN=NOP58 PE=1 SV=1; TOPep_Count=29
1::sp|P19823|ITIH2_HUMAN	1.000302324	3.738965243	Inter-alpha-trypsin inhibitor heavy chain H2 OS=Homo sapiens GN=ITIH2 PE=1 SV=2; TOPep_Count=51
1::sp|Q92882|OSTF1_HUMAN	-1.004779308	3.527073741	Osteoclast-stimulating factor 1 OS=Homo sapiens GN=OSTF1 PE=1 SV=2; TOPep_Count=14

1::sp|Q15942|ZYX_HUMAN	-1.006113979	3.808518047	Zyxin OS=Homo sapiens GN=ZYX PE=1 SV=1; TOPep_Count=21
1::sp|Q7Z5L9|I2BP2_HUMAN;1::sp|Q9H1B7|I2BPL_HUMAN	-1.011631045	2.190618438	Interferon regulatory factor 2-binding protein 2 OS=Homo sapiens GN=IRF2BP2 PE=1 SV=2; TOPep_Count=30
1::sp|P80303|NUCB2_HUMAN	-1.012038421	3.118674026	Nucleobindin-2 OS=Homo sapiens GN=NUCB2 PE=1 SV=2; TOPep_Count=24
1::sp|Q92945|FUBP2_HUMAN	-1.012399654	2.381754452	Far upstream element-binding protein 2 OS=Homo sapiens GN=KHSRP PE=1 SV=4; TOPep_Count=41
1::sp|Q8TD16|BICD2_HUMAN	-1.019402939	1.668503488	Protein bicaudal D homolog 2 OS=Homo sapiens GN=BICD2 PE=1 SV=1; TOPep_Count=60
1::sp|P50238|CRIP1_HUMAN	-1.021593457	1.601810568	Cysteine-rich protein 1 OS=Homo sapiens GN=CRIP1 PE=1 SV=3; TOPep_Count=5
1::sp|Q9Y6I3|EPN1_HUMAN	-1.035333691	2.359073123	Epsin-1 OS=Homo sapiens GN=EPN1 PE=1 SV=2; TOPep_Count=15
1::sp|C9JLW8|F195B_HUMAN	-1.036758256	1.641472623	Protein FAM195B OS=Homo sapiens GN=FAM195B PE=1 SV=1; TOPep_Count=9
1::sp|O15446|RPA34_HUMAN	-1.040166629	2.095348089	DNA-directed RNA polymerase I subunit RPA34 OS=Homo sapiens GN=CD3EAP PE=1 SV=1; TOPep_Count=16
1::sp|Q8NBS9|TXND5_HUMAN	-1.048394672	2.21436491	Thioredoxin domain-containing protein 5 OS=Homo sapiens GN=TXNDC5 PE=1 SV=2; TOPep_Count=25
1::sp|Q9UHD9|UBQL2_HUMAN	-1.04889665	1.635865477	Ubiquilin-2 OS=Homo sapiens GN=UBQLN2 PE=1 SV=2; TOPep_Count=14
1::sp|Q9H098|F107B_HUMAN	-1.054346336	2.108094259	Protein FAM107B OS=Homo sapiens

			GN=FAM107B PE=1 SV=1; TOPep_Count=10
1::sp|Q13442|HAP28_HUMAN	-1.054888095	2.293313976	28 kDa heat- and acid-stable phosphoprotein OS=Homo sapiens GN=PDAP1 PE=1 SV=1; TOPep_Count=10
1::sp|Q9Y520|PRC2C_HUMAN;1::sp|Q5JSZ5|PRC2B_HUMAN	-1.058687746	2.612139526	Protein PRRC2C OS=Homo sapiens GN=PRRC2C PE=1 SV=4; TOPep_Count=122
1::sp|Q01844|EWS_HUMAN	-1.060438449	1.995046819	RNA-binding protein EWS OS=Homo sapiens GN=EWSR1 PE=1 SV=1; TOPep_Count=23
1::sp|P52943|CRIP2_HUMAN	-1.069078005	2.673018554	Cysteine-rich protein 2 OS=Homo sapiens GN=CRIP2 PE=1 SV=1; TOPep_Count=10
1::sp|Q13642|FHL1_HUMAN	-1.070653188	1.482069657	Four and a half LIM domains protein 1 OS=Homo sapiens GN=FHL1 PE=1 SV=4; TOPep_Count=24
1::sp|P60660|MYL6_HUMAN;1::sp|P05976|MYL1_HUMAN;1::sp|P08590|MYL3_HUMAN;1::sp|P14649|MYL6B_HUMAN	-1.071490923	2.143446269	Myosin light polypeptide 6 OS=Homo sapiens GN=MYL6 PE=1 SV=2; TOPep_Count=11
1::sp|P62072|TIM10_HUMAN	-1.074455671	1.935201918	Mitochondrial import inner membrane translocase subunit Tim10 OS=Homo sapiens GN=TIMM10 PE=1 SV=1; TOPep_Count=8
1::sp|P07951|TPM2_HUMAN	-1.078955256	2.364378677	Tropomyosin beta chain OS=Homo sapiens GN=TPM2 PE=1 SV=1; TOPep_Count=23
1::sp|Q96GA3|LTV1_HUMAN	-1.082793799	1.64986007	Protein LTV1 homolog OS=Homo sapiens GN=LTV1 PE=1 SV=1; TOPep_Count=26
1::sp|P28799|GRN_HUMAN	-1.083405332	2.001960348	Granulins OS=Homo sapiens GN=GRN PE=1 SV=2; TOPep_Count=23
1::sp|Q96T51|RUFY1_HUMAN	-1.084317084	1.708465826	RUN and FYVE domain-containing protein 1 OS=Homo sapiens GN=RUFY1

			PE=1 SV=2; TOPep_Count=54
1::sp|P16401|H15_HUMAN	-1.090299512	3.642060768	Histone H1.5 OS=Homo sapiens GN=HIST1H1B PE=1 SV=3; TOPep_Count=13
1::sp|Q13428|TCOF_HUMAN	-1.091653441	2.062265882	Treacle protein OS=Homo sapiens GN=TCOF1 PE=1 SV=3; TOPep_Count=77
1::sp|P62310|LSM3_HUMAN	-1.094675706	1.554245614	U6 snRNA-associated Sm-like protein LSm3 OS=Homo sapiens GN=LSM3 PE=1 SV=2; TOPep_Count=4
1::sp|Q5SSJ5|HP1B3_HUMAN	-1.095530218	2.768309305	Heterochromatin protein 1-binding protein 3 OS=Homo sapiens GN=HP1BP3 PE=1 SV=1; TOPep_Count=32
1::sp|Q99614|TTC1_HUMAN	-1.099302367	1.742016282	Tetratricopeptide repeat protein 1 OS=Homo sapiens GN=TTC1 PE=1 SV=1; TOPep_Count=17
1::sp|P18859|ATP5J_HUMAN	-1.106381809	1.527383649	ATP synthase-coupling factor 6, mitochondrial OS=Homo sapiens GN=ATP5J PE=1 SV=1; TOPep_Count=7
1::sp|Q14444|CAPR1_HUMAN	-1.110021411	3.526856074	Caprin-1 OS=Homo sapiens GN=CAPRIN1 PE=1 SV=2; TOPep_Count=23
1::sp|Q99757|THIOM_HUMAN	-1.110638547	2.116946059	Thioredoxin, mitochondrial OS=Homo sapiens GN=TXN2 PE=1 SV=2; TOPep_Count=9
1::sp|Q13561|DCTN2_HUMAN	-1.128609163	1.738681595	Dynactin subunit 2 OS=Homo sapiens GN=DCTN2 PE=1 SV=4; TOPep_Count=26
1::sp|P62158|CALM_HUMAN;1::sp|P27482|CALL3_HUMAN	-1.130830766	2.026085752	Calmodulin OS=Homo sapiens GN=CALM1 PE=1 SV=2; TOPep_Count=9
1::sp|Q5M775|CYTSB_HUMAN	-1.135312037	3.095707144	Cytospin-B OS=Homo sapiens

			GN=SPECC1 PE=1 SV=1; TOPep_Count=64
1::sp|Q9UPT8|ZC3H4_HUMAN	-1.135810165	2.021429023	Zinc finger CCCH domain-containing protein 4 OS=Homo sapiens GN=ZC3H4 PE=1 SV=3; TOPep_Count=48
1::sp|O75208|COQ9_HUMAN	-1.145912217	1.623228585	Ubiquinone biosynthesis protein COQ9, mitochondrial OS=Homo sapiens GN=COQ9 PE=1 SV=1; TOPep_Count=17
1::sp|P63208|SKP1_HUMAN	-1.153068814	1.615455564	S-phase kinase-associated protein 1 OS=Homo sapiens GN=SKP1 PE=1 SV=2; TOPep_Count=12
1::sp|O94992|HEXI1_HUMAN;1::sp|Q96MH2|HEXI2_HUMAN	-1.155890892	2.845011282	Protein HEXIM1 OS=Homo sapiens GN=HEXIM1 PE=1 SV=1; TOPep_Count=14
1::sp|P30533|AMRP_HUMAN	-1.15697249	2.326044981	Alpha-2-macroglobulin receptor-associated protein OS=Homo sapiens GN=LRPAP1 PE=1 SV=1; TOPep_Count=26
1::sp|Q8N806|UBR7_HUMAN	-1.168986614	2.884619033	Putative E3 ubiquitin-protein ligase UBR7 OS=Homo sapiens GN=UBR7 PE=1 SV=2; TOPep_Count=23
1::sp|Q93052|LPP_HUMAN	-1.170703662	2.367337116	Lipoma-preferred partner OS=Homo sapiens GN=LPP PE=1 SV=1; TOPep_Count=22
1::sp|P49790|NU153_HUMAN	-1.170891498	1.725502304	Nuclear pore complex protein Nup153 OS=Homo sapiens GN=NUP153 PE=1 SV=2; TOPep_Count=61
1::sp|Q3KQU3|MA7D1_HUMAN	-1.171448605	1.834689865	MAP7 domain-containing protein 1 OS=Homo sapiens GN=MAP7D1 PE=1 SV=1; TOPep_Count=45
1::sp|Q5T6F2|UBAP2_HUMAN	-1.171489032	1.57420479	Ubiquitin-associated protein 2 OS=Homo sapiens GN=UBAP2

			PE=1 SV=1; TOPep_Count=30
1::sp|Q14157|UBP2L_HUMAN	-1.178846303	3.041876124	Ubiquitin-associated protein 2-like OS=Homo sapiens GN=UBAP2L PE=1 SV=2; TOPep_Count=32
1::sp|Q16625|OCLN_HUMAN	-1.190052682	2.709484871	Occludin OS=Homo sapiens GN=OCLN PE=1 SV=1; TOPep_Count=18
1::sp|O75391|SPAG7_HUMAN	-1.190279397	2.319615238	Sperm-associated antigen 7 OS=Homo sapiens GN=SPAG7 PE=1 SV=2; TOPep_Count=14
1::sp|Q9UK76|HN1_HUMAN	-1.190959533	3.111942321	Hematological and neurological expressed 1 protein OS=Homo sapiens GN=HN1 PE=1 SV=3; TOPep_Count=8
1::sp|Q8N4Q1|MIA40_HUMAN	-1.197551627	2.208498057	Mitochondrial intermembrane space import and assembly protein 40 OS=Homo sapiens GN=CHCHD4 PE=1 SV=1; TOPep_Count=7
1::sp|P36954|RPB9_HUMAN	-1.19785472	3.437098741	DNA-directed RNA polymerase II subunit RPB9 OS=Homo sapiens GN=POLR2I PE=1 SV=1; TOPep_Count=9
1::sp|P40222|TXLNA_HUMAN	-1.209803556	2.527499877	Alpha-taxilin OS=Homo sapiens GN=TXLNA PE=1 SV=3; TOPep_Count=32
1::sp|P61457|PHS_HUMAN	-1.220229351	2.177209448	Pterin-4-alpha-carbinolamine dehydratase OS=Homo sapiens GN=PCBD1 PE=1 SV=2; TOPep_Count=8
1::sp|P35237|SPB6_HUMAN	-1.222395727	3.460373872	Serpin B6 OS=Homo sapiens GN=SERPINB6 PE=1 SV=3; TOPep_Count=24
1::sp|Q9UMX0|UBQL1_HUMAN	-1.223318174	1.7269561	Ubiquilin-1 OS=Homo sapiens GN=UBQLN1 PE=1 SV=2; TOPep_Count=13
1::sp|Q96RT1|LAP2_HUMAN	-1.223831598	2.359017197	Protein LAP2 OS=Homo sapiens

			GN=ERBB2IP PE=1 SV=2; TOPep_Count=83
1::sp|P52758|UK114_HUMAN	-1.224637999	1.942810073	Ribonuclease UK114 OS=Homo sapiens GN=HRSP12 PE=1 SV=1; TOPep_Count=10
1::sp|P54727|RD23B_HUMAN	-1.226743765	3.48906365	UV excision repair protein RAD23 homolog B OS=Homo sapiens GN=RAD23B PE=1 SV=1; TOPep_Count=15
1::sp|P61024|CKS1_HUMAN	-1.227709156	2.313185028	Cyclin-dependent kinases regulatory subunit 1 OS=Homo sapiens GN=CKS1B PE=1 SV=1; TOPep_Count=5
1::sp|P16949|STMN1_HUMAN;1::sp|Q93045|STMN2_HUMAN;1::sp|Q9H169|STMN4_HUMAN	-1.230384968	3.053333985	Stathmin OS=Homo sapiens GN=STMN1 PE=1 SV=3; TOPep_Count=10
1::sp|P40855|PEX19_HUMAN	-1.237450142	2.10858324	Peroxisomal biogenesis factor 19 OS=Homo sapiens GN=PEX19 PE=1 SV=1; TOPep_Count=18
1::sp|Q15654|TRIP6_HUMAN	-1.244173006	3.116326947	Thyroid receptor-interacting protein 6 OS=Homo sapiens GN=TRIP6 PE=1 SV=3; TOPep_Count=26
1::sp|Q9Y6K9|NEMO_HUMAN	-1.270162895	1.336595577	NF-kappa-B essential modulator OS=Homo sapiens GN=IKBKG PE=1 SV=2; TOPep_Count=28
1::sp|Q96CP2|FWCH2_HUMAN	-1.272905059	2.052792135	FLYWCH family member 2 OS=Homo sapiens GN=FLYWCH2 PE=1 SV=1; TOPep_Count=8
1::sp|Q15276|RABE1_HUMAN	-1.284144134	3.824516929	Rab GTPase-binding effector protein 1 OS=Homo sapiens GN=RABEP1 PE=1 SV=2; TOPep_Count=62
1::sp|P55081|MFAP1_HUMAN	-1.287329907	1.706072537	Microfibrillar-associated protein 1 OS=Homo sapiens GN=MFAP1 PE=1 SV=2; TOPep_Count=22

1::sp|O95721|SNP29_HUMAN	-1.293321978	1.695996229	Synaptosomal-associated protein 29 OS=Homo sapiens GN=SNAP29 PE=1 SV=1; TOPep_Count=17
1::sp|P98179|RBM3_HUMAN	-1.296058992	3.905122012	RNA-binding protein 3 OS=Homo sapiens GN=RBM3 PE=1 SV=1; TOPep_Count=9
1::sp|Q7Z4H7|HAUS6_HUMAN	-1.304202168	2.13557802	HAUS augmin-like complex subunit 6 OS=Homo sapiens GN=HAUS6 PE=1 SV=2; TOPep_Count=59
1::sp|Q96C90|PP14B_HUMAN	-1.30498478	2.842872132	Protein phosphatase 1 regulatory subunit 14B OS=Homo sapiens GN=PPP1R14B PE=1 SV=3; TOPep_Count=6
1::sp|P48960|CD97_HUMAN	-1.308070867	2.043754027	CD97 antigen OS=Homo sapiens GN=CD97 PE=1 SV=4; TOPep_Count=35
1::sp|Q16626|MEA1_HUMAN	-1.308843292	1.717507445	Male-enhanced antigen 1 OS=Homo sapiens GN=MEA1 PE=1 SV=2; TOPep_Count=5
1::sp|P16989|YBOX3_HUMAN	-1.30969138	3.311492384	Y-box-binding protein 3 OS=Homo sapiens GN=YBX3 PE=1 SV=4; TOPep_Count=18
1::sp|Q7Z422|SZRD1_HUMAN	-1.318851548	2.655501375	SUZ domain-containing protein 1 OS=Homo sapiens GN=SZRD1 PE=1 SV=1; TOPep_Count=8
1::sp|P23434|GCSH_HUMAN	-1.326335203	1.932678758	Glycine cleavage system H protein, mitochondrial OS=Homo sapiens GN=GCSH PE=1 SV=2; TOPep_Count=7
1::sp|Q9NYJ1|COA4_HUMAN	-1.327866698	2.081137836	Cytochrome c oxidase assembly factor 4 homolog, mitochondrial OS=Homo sapiens GN=COA4 PE=1 SV=2; TOPep_Count=7
1::sp|Q9BRK5|CAB45_HUMAN	-1.336673378	2.096735094	45 kDa calcium-binding protein

			OS=Homo sapiens GN=SDF4 PE=1 SV=1; TOPep_Count=19
1::sp|O75506|HSBP1_HUMAN	-1.34889005	1.860705194	Heat shock factor-binding protein 1 OS=Homo sapiens GN=HSBP1 PE=1 SV=1; TOPep_Count=7
1::sp|P49321|NASP_HUMAN	-1.355188917	2.301997643	Nuclear autoantigenic sperm protein OS=Homo sapiens GN=NASP PE=1 SV=2; TOPep_Count=42
1::sp|Q9H1E3|NUCKS_HUMAN	-1.365338996	1.858564758	Nuclear ubiquitous casein and cyclin-dependent kinase substrate 1 OS=Homo sapiens GN=NUCKS1 PE=1 SV=1; TOPep_Count=12
1::sp|P67809|YBOX1_HUMAN;1::sp|Q9Y2T7|YBOX2_HUMAN	-1.366978613	3.117926632	Nuclease-sensitive element-binding protein 1 OS=Homo sapiens GN=YBX1 PE=1 SV=3; TOPep_Count=13
1::sp|Q96PD2|DCBD2_HUMAN	-1.369481285	2.252869028	Discoidin, CUB and LCCL domain-containing protein 2 OS=Homo sapiens GN=DCBLD2 PE=1 SV=1; TOPep_Count=37
1::sp|O00193|SMAP_HUMAN	-1.370121414	1.586106116	Small acidic protein OS=Homo sapiens GN=SMAP PE=1 SV=1; TOPep_Count=8
1::sp|Q8WZA0|LZIC_HUMAN	-1.394701437	3.709805551	Protein LZIC OS=Homo sapiens GN=LZIC PE=1 SV=1; TOPep_Count=14
1::sp|Q9GZY8|MFF_HUMAN	-1.400886077	2.573699869	Mitochondrial fission factor OS=Homo sapiens GN=MFF PE=1 SV=1; TOPep_Count=17
1::sp|P09493|TPM1_HUMAN	-1.444553641	4.572767626	Tropomyosin alpha-1 chain OS=Homo sapiens GN=TPM1 PE=1 SV=2; TOPep_Count=23
1::sp|Q9P0P0|RN181_HUMAN	-1.446679586	2.692553764	E3 ubiquitin-protein ligase RNF181 OS=Homo sapiens GN=RNF181 PE=1

			SV=1; TOPep_Count=9
1::sp|Q9UFN0|NPS3A_HUMAN	-1.449034343	1.601720803	Protein NipSnap homolog 3A OS=Homo sapiens GN=NIPSNAP3A PE=1 SV=2; TOPep_Count=17
1::sp|Q9BTT0|AN32E_HUMAN	-1.465603128	2.907236716	Acidic leucine-rich nuclear phosphoprotein 32 family member E OS=Homo sapiens GN=ANP32E PE=1 SV=1; TOPep_Count=10
1::sp|O60828|PQBP1_HUMAN	-1.466243103	1.937034143	Polyglutamine-binding protein 1 OS=Homo sapiens GN=PQBP1 PE=1 SV=1; TOPep_Count=9
1::sp|CATA_HUMAN|	-1.474467478	1.753254716	; TOPep_Count=32
1::sp|O15027|SC16A_HUMAN	-1.482913484	3.820762107	Protein transport protein Sec16A OS=Homo sapiens GN=SEC16A PE=1 SV=3; TOPep_Count=77
1::sp|Q8N6H7|ARFG2_HUMAN;1::sp|Q9NP61|ARFG3_HUMAN	-1.513456504	4.251114255	ADP-ribosylation factor GTPase-activating protein 2 OS=Homo sapiens GN=ARFGAP2 PE=1 SV=1; TOPep_Count=32
1::sp|O43294|TGFI1_HUMAN	-1.516174784	4.18866216	Transforming growth factor beta-1-induced transcript 1 protein OS=Homo sapiens GN=TGFB1I1 PE=1 SV=2; TOPep_Count=24
1::sp|Q9UMS0|NFU1_HUMAN	-1.539352793	3.1716053	NFU1 iron-sulfur cluster scaffold homolog, mitochondrial OS=Homo sapiens GN=NFU1 PE=1 SV=2; TOPep_Count=14
1::sp|O95302|FKBP9_HUMAN	-1.55379323	1.778347082	Peptidyl-prolyl cis-trans isomerase FKBP9 OS=Homo sapiens GN=FKBP9 PE=1 SV=2; TOPep_Count=25
1::sp|P61218|RPAB2_HUMAN	-1.572805547	1.470579923	DNA-directed RNA polymerases I, II, and III subunit RPABC2 OS=Homo

			sapiens GN=POLR2F PE=1 SV=1; TOPep_Count=4
1::sp|Q9BTD8|RBM42_HUMAN	-1.596666088	2.244275789	RNA-binding protein 42 OS=Homo sapiens GN=RBM42 PE=1 SV=1; TOPep_Count=16
1::sp|Q8IWX8|CHERP_HUMAN	-1.612464784	2.029441615	Calcium homeostasis endoplasmic reticulum protein OS=Homo sapiens GN=CHERP PE=1 SV=3; TOPep_Count=35
1::sp|Q9UGP4|LIMD1_HUMAN	-1.646087207	2.468204675	LIM domain-containing protein 1 OS=Homo sapiens GN=LIMD1 PE=1 SV=1; TOPep_Count=33
1::sp|P18615|NELFE_HUMAN	-1.669251031	2.582075158	Negative elongation factor E OS=Homo sapiens GN=NELFE PE=1 SV=3; TOPep_Count=20
1::sp|Q15154|PCM1_HUMAN	-1.699403414	2.505394113	Pericentriolar material 1 protein OS=Homo sapiens GN=PCM1 PE=1 SV=4; TOPep_Count=96
1::sp|Q9P000|COMD9_HUMAN	-1.727363449	3.084353797	COMM domain-containing protein 9 OS=Homo sapiens GN=COMMD9 PE=1 SV=2; TOPep_Count=12
1::sp|P46013|KI67_HUMAN	-1.792443659	3.095705719	Antigen KI-67 OS=Homo sapiens GN=MKI67 PE=1 SV=2; TOPep_Count=205
1::sp|Q9Y618|NCOR2_HUMAN	-1.851690376	2.868125465	Nuclear receptor corepressor 2 OS=Homo sapiens GN=NCOR2 PE=1 SV=2; TOPep_Count=136
1::sp|P22692|IBP4_HUMAN	-1.865790569	2.998045634	Insulin-like growth factor-binding protein 4 OS=Homo sapiens GN=IGFBP4 PE=1 SV=2; TOPep_Count=14
1::sp|Q9ULW0|TPX2_HUMAN	-1.870260187	2.632235531	Targeting protein for Xklp2 OS=Homo sapiens GN=TPX2 PE=1 SV=2; TOPep_Count=42

1::sp|KRHB1_HUMAN|;1::sp|K2M2_SHEEP|;1::sp|KRHB2_HUMAN|	-1.879890478	5.07374714	; TOPep_Count=31
1::sp|P10109|ADX_HUMAN	-1.934766091	2.523799632	Adrenodoxin, mitochondrial OS=Homo sapiens GN=FDX1 PE=1 SV=1; TOPep_Count=14
1::sp|Q8IVM0|CCD50_HUMAN	-2.013052041	2.535476396	Coiled-coil domain-containing protein 50 OS=Homo sapiens GN=CCDC50 PE=1 SV=1; TOPep_Count=19
1::sp|Q16527|CSRP2_HUMAN	-2.041481608	2.402626682	Cysteine and glycine-rich protein 2 OS=Homo sapiens GN=CSRP2 PE=1 SV=3; TOPep_Count=13
1::sp|Q6PUV4|CPLX2_HUMAN	-2.132549175	4.344660386	Complexin-2 OS=Homo sapiens GN=CPLX2 PE=1 SV=2; TOPep_Count=8
1::sp|Q92823|NRCAM_HUMAN	-2.2475307	4.489506767	Neuronal cell adhesion molecule OS=Homo sapiens GN=NRCAM PE=1 SV=3; TOPep_Count=59
1::sp|Q8IWE2|NXP20_HUMAN	-2.247572225	3.01706022	Protein NOXP20 OS=Homo sapiens GN=FAM114A1 PE=1 SV=2; TOPep_Count=24
1::sp|Q9P013|CWC15_HUMAN	-2.454363317	3.415630622	Spliceosome-associated protein CWC15 homolog OS=Homo sapiens GN=CWC15 PE=1 SV=2; TOPep_Count=10
1::sp|P56211|ARP19_HUMAN;1::sp|O43768|ENSA_HUMAN	-2.83215548	2.857833074	cAMP-regulated phosphoprotein 19 OS=Homo sapiens GN=ARPP19 PE=1 SV=2; TOPep_Count=7
1::sp|Q9ULD2|MTUS1_HUMAN	-3.094786821	2.775931889	Microtubule-associated tumor suppressor 1 OS=Homo sapiens GN=MTUS1 PE=1 SV=2; TOPep_Count=77

Significant proteins of infected A549 HRSV ΔSH eGFP

Accession details	LOG2 FC	LOG10 p-value	Description
1::sp|P20591|MX1_HUMAN;1::sp|P20592|MX2_HUMAN	6.2289909	7.7365683	Interferon-induced GTP-binding protein Mx1 OS=Homo sapiens GN=MX1 PE=1 SV=4; TOPep_Count=41
1::sp|P05161|ISG15_HUMAN	6.0575092	6.0120554	Ubiquitin-like protein ISG15 OS=Homo sapiens GN=ISG15 PE=1 SV=5; TOPep_Count=10
1::sp|O95786|DDX58_HUMAN	5.5492572	5.2126028	Probable ATP-dependent RNA helicase DDX58 OS=Homo sapiens GN=DDX58 PE=1 SV=2; TOPep_Count=58
1::sp|GFP_AEQVI|	4.9629692	6.7387988	; TOPep_Count=12
1::sp|O14879|IFIT3_HUMAN	4.48719	8.1085176	Interferon-induced protein with tetratricopeptide repeats 3 OS=Homo sapiens GN=IFIT3 PE=1 SV=1; TOPep_Count=30
2::sp|P04544|NS1_HRSVA	3.9309453	4.4055071	Non-structural protein 1 OS=Human respiratory syncytial virus A (strain A2) GN=1C PE=1 SV=1
1::sp|P09914|IFIT1_HUMAN	3.7163585	3.302083	Interferon-induced protein with tetratricopeptide repeats 1 OS=Homo sapiens GN=IFIT1 PE=1 SV=2; TOPep_Count=33
1::sp|Q460N5|PAR14_HUMAN	3.6951727	4.018266	Poly [ADP-ribose] polymerase 14 OS=Homo sapiens GN=PARP14 PE=1 SV=3; TOPep_Count=123
2::sp|P03423|GLYC_HRSVA	3.5824066	4.3341494	Major surface glycoprotein G OS=Human respiratory syncytial virus A (strain A2) GN=G PE=1 SV=1
2::sp|P03419|MATRX_HRSVA	3.4221229	7.7052976	Matrix protein OS=Human respiratory syncytial virus A

			(strain A2) GN=M PE=1 SV=1
2::sp|P03421|PHOSP_HRSVA	3.3095061	4.9764489	Phosphoprotein OS=Human respiratory syncytial virus A (strain A2) GN=P PE=1 SV=1
1::sp|Q00169|PIPNA_HUMAN	3.2747521	1.9876777	Phosphatidylinositol transfer protein alpha isoform OS=Homo sapiens GN=PITPNA PE=1 SV=2; TOPep_Count=25
2::sp|P04545|M21_HRSVA	3.1028663	8.462873	Matrix M2-1 OS=Human respiratory syncytial virus A (strain A2) GN=M2-1 PE=1 SV=1
1::sp|P05452|TETN_HUMAN	2.8708765	4.2135868	Tetranectin OS=Homo sapiens GN=CLEC3B PE=1 SV=3; TOPep_Count=12
1::sp|Q9Y6K5|OAS3_HUMAN	2.4772023	3.1346449	2'-5'-oligoadenylate synthase 3 OS=Homo sapiens GN=OAS3 PE=1 SV=3; TOPep_Count=54
2::sp|P03418|NCAP_HRSVA	2.343916	6.4180083	Nucleoprotein OS=Human respiratory syncytial virus A (strain A2) GN=N PE=1 SV=1
1::sp|Q9H0P0|5NT3A_HUMAN	2.3361048	4.9862248	Cytosolic 5'-nucleotidase 3A OS=Homo sapiens GN=NT5C3A PE=1 SV=3; TOPep_Count=23
1::sp|P09913|IFIT2_HUMAN	2.2779034	6.2678435	Interferon-induced protein with tetratricopeptide repeats 2 OS=Homo sapiens GN=IFIT2 PE=1 SV=1; TOPep_Count=33
1::sp|Q8WZ82|OVCA2_HUMAN	2.1878935	2.1310274	Ovarian cancer-associated gene 2 protein OS=Homo sapiens GN=OVCA2 PE=1 SV=1; TOPep_Count=10
1::sp|P0C0L4|CO4A_HUMAN	2.1617369	4.247125	Complement C4-A OS=Homo sapiens GN=C4A PE=1 SV=2; TOPep_Count=88
1::sp|Q9BQE5|APOL2_HUMAN	2.1161549	2.2128184	Apolipoprotein L2 OS=Homo sapiens GN=APOL2 PE=1 SV=1; TOPep_Count=18
1::sp|P17301|ITA2_HUMAN	2.0615126	4.6205983	Integrin alpha-2 OS=Homo sapiens

			GN=ITGA2 PE=1 SV=1; TOPep_Count=50
2::sp|P03420|FUS_HRSVA	1.9789375	6.1145651	Fusion glycoprotein F0 OS=Human respiratory syncytial virus A (strain A2) GN=F PE=1 SV=1
1::sp|P02774|VTDB_HUMAN	1.7933536	4.5968363	Vitamin D-binding protein OS=Homo sapiens GN=GC PE=1 SV=1; TOPep_Count=29
1::sp|RETBP_HUMAN|	1.7250186	3.0016908	; TOPep_Count=10
1::sp|P08648|ITA5_HUMAN	1.7004307	3.1129265	Integrin alpha-5 OS=Homo sapiens GN=ITGA5 PE=1 SV=2; TOPep_Count=36
1::sp|P01024|CO3_HUMAN	1.5334133	4.460162	Complement C3 OS=Homo sapiens GN=C3 PE=1 SV=2; TOPep_Count=107
1::sp|ALBU_BOVIN|;1::sp|ALBU_HUMAN|	1.4741509	4.5203978	; TOPep_Count=47
1::sp|O15498|YKT6_HUMAN	1.4698418	1.7747611	Synaptobrevin homolog YKT6 OS=Homo sapiens GN=YKT6 PE=1 SV=1; TOPep_Count=14
1::sp|ANT3_HUMAN|	1.4469336	3.5103807	; TOPep_Count=30
1::sp|P36955|PEDF_HUMAN	1.4212494	4.2713672	Pigment epithelium-derived factor OS=Homo sapiens GN=SERPINF1 PE=1 SV=4; TOPep_Count=23
1::sp|P19823|ITIH2_HUMAN	1.3786303	3.7389652	Inter-alpha-trypsin inhibitor heavy chain H2 OS=Homo sapiens GN=ITIH2 PE=1 SV=2; TOPep_Count=51
1::sp|P16190|1A33_HUMAN;1::sp|P30443|1A01_HUMAN;1::sp|P30457|1A66_HUMAN;1::sp|P30460|1B08_HUMAN;1::sp|P30485|1B47_HUMAN;1::sp|Q09160|1A80_HUMAN;1::sp|Q29836|1B67_HUMAN;1::sp|Q31612|1B73_HUMAN	1.3474834	3.6896405	HLA class I histocompatibility antigen, A-33 alpha chain OS=Homo sapiens GN=HLA-A PE=1 SV=3; TOPep_Count=21
1::sp|P27105|STOM_HUMAN;1::sp|Q8TAV4|STML3_HUMAN	1.3351224	1.8179366	Erythrocyte band 7 integral membrane protein OS=Homo sapiens GN=STOM PE=1 SV=3; TOPep_Count=18

1::sp|P13987|CD59_HUMAN	1.3174666	3.3337276	CD59 glycoprotein OS=Homo sapiens GN=CD59 PE=1 SV=1; TOPep_Count=6
1::sp|Q06033|ITIH3_HUMAN	1.3119746	4.0894379	Inter-alpha-trypsin inhibitor heavy chain H3 OS=Homo sapiens GN=ITIH3 PE=1 SV=2; TOPep_Count=43
1::sp|P29590|PML_HUMAN	1.2933777	4.1834766	Protein PML OS=Homo sapiens GN=PML PE=1 SV=3; TOPep_Count=49
1::sp|Q08380|LG3BP_HUMAN	1.2931872	3.0770713	Galectin-3-binding protein OS=Homo sapiens GN=LGALS3BP PE=1 SV=1; TOPep_Count=29
1::sp|P10909|CLUS_HUMAN	1.2857561	4.5104956	Clusterin OS=Homo sapiens GN=CLU PE=1 SV=1; TOPep_Count=22
1::sp|P01023|A2MG_HUMAN	1.2525209	3.6619793	Alpha-2-macroglobulin OS=Homo sapiens GN=A2M PE=1 SV=3; TOPep_Count=75
1::sp|P42224|STAT1_HUMAN	1.1933455	4.2944991	Signal transducer and activator of transcription 1-alpha/beta OS=Homo sapiens GN=STAT1 PE=1 SV=2; TOPep_Count=45
1::sp|P57088|TMM33_HUMAN	1.1672596	1.5117119	Transmembrane protein 33 OS=Homo sapiens GN=TMEM33 PE=1 SV=2; TOPep_Count=11
1::sp|Q9Y624|JAM1_HUMAN	1.1295027	4.4095915	Junctional adhesion molecule A OS=Homo sapiens GN=F11R PE=1 SV=1; TOPep_Count=17
1::sp|P19525|E2AK2_HUMAN	1.1154492	3.8666321	Interferon-induced, double-stranded RNA-activated protein kinase OS=Homo sapiens GN=EIF2AK2 PE=1 SV=2; TOPep_Count=25
1::sp|P02765|FETUA_HUMAN	1.0699276	2.0945068	Alpha-2-HS-glycoprotein OS=Homo sapiens GN=AHSG PE=1 SV=1; TOPep_Count=17
1::sp|Q9NZM1|MYOF_HUMAN;1::sp|O75923|DYSF_HUMAN	1.0425866	2.6818845	Myoferlin OS=Homo sapiens GN=MYOF

			PE=1 SV=1; TOPep_Count=130
1::Int_P61769ups|B2MG_HUMAN_UPS	1.042165	6.2978242	Beta-2-microglobulin (Chain 21-119) - Homo sapiens (Human); TOPep_Count=7
1::sp|P60510|PP4C_HUMAN	1.0345582	1.4003068	Serine/threonine-protein phosphatase 4 catalytic subunit OS=Homo sapiens GN=PPP4C PE=1 SV=1; TOPep_Count=18
1::sp|P07951|TPM2_HUMAN	-1.0000921	2.3643787	Tropomyosin beta chain OS=Homo sapiens GN=TPM2 PE=1 SV=1; TOPep_Count=23
1::sp|Q15654|TRIP6_HUMAN	-1.0008451	3.1163269	Thyroid receptor-interacting protein 6 OS=Homo sapiens GN=TRIP6 PE=1 SV=3; TOPep_Count=26
1::sp|Q16626|MEA1_HUMAN	-1.0027338	1.7175074	Male-enhanced antigen 1 OS=Homo sapiens GN=MEA1 PE=1 SV=2; TOPep_Count=5
1::sp|Q3KQU3|MA7D1_HUMAN	-1.0070861	1.8346899	MAP7 domain-containing protein 1 OS=Homo sapiens GN=MAP7D1 PE=1 SV=1; TOPep_Count=45
1::sp|P63208|SKP1_HUMAN	-1.0161073	1.6154556	S-phase kinase-associated protein 1 OS=Homo sapiens GN=SKP1 PE=1 SV=2; TOPep_Count=12
1::sp|Q9UGP4|LIMD1_HUMAN	-1.0198052	2.4682047	LIM domain-containing protein 1 OS=Homo sapiens GN=LIMD1 PE=1 SV=1; TOPep_Count=33
1::sp|Q9GZY8|MFF_HUMAN	-1.021711	2.5736999	Mitochondrial fission factor OS=Homo sapiens GN=MFF PE=1 SV=1; TOPep_Count=17
1::sp|P18615|NELFE_HUMAN	-1.0222999	2.5820752	Negative elongation factor E OS=Homo sapiens GN=NELFE PE=1 SV=3; TOPep_Count=20
1::sp|P08195|4F2_HUMAN	-1.0281724	4.4795921	4F2 cell-surface antigen heavy chain OS=Homo sapiens GN=SLC3A2 PE=1

			SV=3; TOPep_Count=33
1::sp|O43570|CAH12_HUMAN	-1.0295599	2.1614455	Carbonic anhydrase 12 OS=Homo sapiens GN=CA12 PE=1 SV=1; TOPep_Count=14
1::sp|O00566|MPP10_HUMAN	-1.0367966	1.6691827	U3 small nucleolar ribonucleoprotein protein MPP10 OS=Homo sapiens GN=MPHOSPH10 PE=1 SV=2; TOPep_Count=37
1::sp|P18859|ATP5J_HUMAN	-1.0377498	1.5273836	ATP synthase-coupling factor 6, mitochondrial OS=Homo sapiens GN=ATP5J PE=1 SV=1; TOPep_Count=7
1::sp|Q9UMS0|NFU1_HUMAN	-1.0542624	3.1716053	NFU1 iron-sulfur cluster scaffold homolog, mitochondrial OS=Homo sapiens GN=NFU1 PE=1 SV=2; TOPep_Count=14
1::sp|Q9P0P0|RN181_HUMAN	-1.0728578	2.6925538	E3 ubiquitin-protein ligase RNF181 OS=Homo sapiens GN=RNF181 PE=1 SV=1; TOPep_Count=9
1::sp|Q16625|OCLN_HUMAN	-1.0745337	2.7094849	Occludin OS=Homo sapiens GN=OCLN PE=1 SV=1; TOPep_Count=18
1::sp|P40222|TXLNA_HUMAN	-1.0860154	2.5274999	Alpha-taxilin OS=Homo sapiens GN=TXLNA PE=1 SV=3; TOPep_Count=32
1::sp|Q5T6F2|UBAP2_HUMAN	-1.0903335	1.5742048	Ubiquitin-associated protein 2 OS=Homo sapiens GN=UBAP2 PE=1 SV=1; TOPep_Count=30
1::sp|P09493|TPM1_HUMAN	-1.0921953	4.5727676	Tropomyosin alpha-1 chain OS=Homo sapiens GN=TPM1 PE=1 SV=2; TOPep_Count=23
1::sp|P20645|MPRD_HUMAN	-1.0964487	1.6335469	Cation-dependent mannose-6-phosphate receptor OS=Homo sapiens GN=M6PR PE=1 SV=1; TOPep_Count=18
1::sp|P67809|YBOX1_HUMAN;1::sp|Q9Y2T7|YBOX2_HUMAN	-1.0992305	3.1179266	Nuclease-sensitive element-binding protein 1 OS=Homo

			sapiens GN=YBX1 PE=1 SV=3; TOPep_Count=13
1::sp|P30533|AMRP_HUMAN	-1.1040025	2.326045	Alpha-2-macroglobulin receptor-associated protein OS=Homo sapiens GN=LRPAP1 PE=1 SV=1; TOPep_Count=26
1::sp|P62158|CALM_HUMAN;1::sp|P27482|CALL3_HUMAN	-1.1213	2.0260858	Calmodulin OS=Homo sapiens GN=CALM1 PE=1 SV=2; TOPep_Count=9
1::sp|Q9Y3B8|ORN_HUMAN	-1.1221608	3.4494519	Oligoribonuclease, mitochondrial OS=Homo sapiens GN=REXO2 PE=1 SV=3; TOPep_Count=14
1::sp|Q9BRK5|CAB45_HUMAN	-1.1652695	2.0967351	45 kDa calcium-binding protein OS=Homo sapiens GN=SDF4 PE=1 SV=1; TOPep_Count=19
1::sp|Q15154|PCM1_HUMAN	-1.1915365	2.5053941	Pericentriolar material 1 protein OS=Homo sapiens GN=PCM1 PE=1 SV=4; TOPep_Count=96
1::sp|P22692|IBP4_HUMAN	-1.1930025	2.9980456	Insulin-like growth factor-binding protein 4 OS=Homo sapiens GN=IGFBP4 PE=1 SV=2; TOPep_Count=14
1::sp|Q9UFN0|NPS3A_HUMAN	-1.195719	1.6017208	Protein NipSnap homolog 3A OS=Homo sapiens GN=NIPSNAP3A PE=1 SV=2; TOPep_Count=17
1::sp|P40855|PEX19_HUMAN	-1.2112824	2.1085832	Peroxisomal biogenesis factor 19 OS=Homo sapiens GN=PEX19 PE=1 SV=1; TOPep_Count=18
1::sp|P98179|RBM3_HUMAN	-1.2139449	3.905122	RNA-binding protein 3 OS=Homo sapiens GN=RBM3 PE=1 SV=1; TOPep_Count=9
1::sp|P55081|MFAP1_HUMAN	-1.2380366	1.7060725	Microfibrillar-associated protein 1 OS=Homo sapiens GN=MFAP1 PE=1 SV=2; TOPep_Count=22
1::sp|Q9P000|COMD9_HUMAN	-1.2430172	3.0843538	COMM domain-containing protein 9 OS=Homo sapiens GN=COMMD9 PE=1

			SV=2; TOPep_Count=12
1::sp|Q96B36|AKTS1_HUMAN	-1.2492327	2.5995294	Proline-rich AKT1 substrate 1 OS=Homo sapiens GN=AKT1S1 PE=1 SV=1; TOPep_Count=10
1::sp|Q8N806|UBR7_HUMAN	-1.2513961	2.884619	Putative E3 ubiquitin-protein ligase UBR7 OS=Homo sapiens GN=UBR7 PE=1 SV=2; TOPep_Count=23
1::sp|Q8WZA0|LZIC_HUMAN	-1.2666991	3.7098056	Protein LZIC OS=Homo sapiens GN=LZIC PE=1 SV=1; TOPep_Count=14
1::sp|Q7Z4H7|HAUS6_HUMAN	-1.2758814	2.135578	HAUS augmin-like complex subunit 6 OS=Homo sapiens GN=HAUS6 PE=1 SV=2; TOPep_Count=59
1::sp|Q9BTT0|AN32E_HUMAN	-1.2839179	2.9072367	Acidic leucine-rich nuclear phosphoprotein 32 family member E OS=Homo sapiens GN=ANP32E PE=1 SV=1; TOPep_Count=10
1::sp|Q8IVM0|CCD50_HUMAN	-1.2866478	2.5354764	Coiled-coil domain-containing protein 50 OS=Homo sapiens GN=CCDC50 PE=1 SV=1; TOPep_Count=19
1::sp|Q16527|CSRP2_HUMAN	-1.2948877	2.4026267	Cysteine and glycine-rich protein 2 OS=Homo sapiens GN=CSRP2 PE=1 SV=3; TOPep_Count=13
1::sp|P61457|PHS_HUMAN	-1.3026165	2.1772094	Pterin-4-alpha-carbinolamine dehydratase OS=Homo sapiens GN=PCBD1 PE=1 SV=2; TOPep_Count=8
1::sp|Q9H1E3|NUCKS_HUMAN	-1.3187359	1.8585648	Nuclear ubiquitous casein and cyclin-dependent kinase substrate 1 OS=Homo sapiens GN=NUCKS1 PE=1 SV=1; TOPep_Count=12
1::sp|P62861|RS30_HUMAN	-1.3443498	2.5472348	40S ribosomal protein S30 OS=Homo sapiens GN=FAU PE=1 SV=1; TOPep_Count=3
1::sp|O75506|HSBP1_HUMAN	-1.3521233	1.8607052	Heat shock factor-binding protein 1

			OS=Homo sapiens GN=HSBP1 PE=1 SV=1; TOPep_Count=7
1::sp|P18084|ITB5_HUMAN	-1.397984	1.3497925	Integrin beta-5 OS=Homo sapiens GN=ITGB5 PE=1 SV=1; TOPep_Count=47
1::sp|P52758|UK114_HUMAN	-1.4196765	1.9428101	Ribonuclease UK114 OS=Homo sapiens GN=HRSP12 PE=1 SV=1; TOPep_Count=10
1::sp|CAS1_BOVIN|	-1.4217229	1.3169516	; TOPep_Count=12
1::sp|Q4V328|GRAP1_HUMAN	-1.4618723	1.7894377	GRIP1-associated protein 1 OS=Homo sapiens GN=GRIPAP1 PE=1 SV=1; TOPep_Count=57
1::sp|O15027|SC16A_HUMAN	-1.4769779	3.8207621	Protein transport protein Sec16A OS=Homo sapiens GN=SEC16A PE=1 SV=3; TOPep_Count=77
1::sp|Q9BTD8|RBM42_HUMAN	-1.560349	2.2442758	RNA-binding protein 42 OS=Homo sapiens GN=RBM42 PE=1 SV=1; TOPep_Count=16
1::sp|Q6PUV4|CPLX2_HUMAN	-1.5773563	4.3446604	Complexin-2 OS=Homo sapiens GN=CPLX2 PE=1 SV=2; TOPep_Count=8
1::sp|Q92823|NRCAM_HUMAN	-1.5791078	4.4895068	Neuronal cell adhesion molecule OS=Homo sapiens GN=NRCAM PE=1 SV=3; TOPep_Count=59
1::sp|Q7L9L4|MOB1B_HUMAN	-1.584387	2.9113971	MOB kinase activator 1B OS=Homo sapiens GN=MOB1B PE=1 SV=3; TOPep_Count=10
1::sp|CATA_HUMAN|	-1.6212353	1.7532547	; TOPep_Count=32
1::sp|P10109|ADX_HUMAN	-1.6544993	2.5237996	Adrenodoxin, mitochondrial OS=Homo sapiens GN=FDX1 PE=1 SV=1; TOPep_Count=14
1::sp|KRHB1_HUMAN|;1::sp|K2M2_SHEEP|;1::sp|KRHB2_HUMAN|	-1.6955407	5.0737471	; TOPep_Count=31
1::sp|P35237|SPB6_HUMAN	-1.7059585	3.4603739	Serpin B6 OS=Homo sapiens GN=SERPINB6 PE=1

			SV=3; TOPep_Count=24
1::sp|Q8N6H7|ARFG2_HUMAN;1::sp|Q9NP61|ARFG3_HUMAN	-1.776667	4.2511143	ADP-ribosylation factor GTPase-activating protein 2 OS=Homo sapiens GN=ARFGAP2 PE=1 SV=1; TOPep_Count=32
1::sp|O43294|TGFI1_HUMAN	-1.7913955	4.1886622	Transforming growth factor beta-1-induced transcript 1 protein OS=Homo sapiens GN=TGFB1I1 PE=1 SV=2; TOPep_Count=24
1::sp|Q5SSJ5|HP1B3_HUMAN	-1.8404281	2.7683093	Heterochromatin protein 1-binding protein 3 OS=Homo sapiens GN=HP1BP3 PE=1 SV=1; TOPep_Count=32
1::sp|Q9Y618|NCOR2_HUMAN	-1.8511309	2.8681255	Nuclear receptor corepressor 2 OS=Homo sapiens GN=NCOR2 PE=1 SV=2; TOPep_Count=136
1::sp|P56211|ARP19_HUMAN;1::sp|O43768|ENSA_HUMAN	-2.0612335	2.8578331	cAMP-regulated phosphoprotein 19 OS=Homo sapiens GN=ARPP19 PE=1 SV=2; TOPep_Count=7
1::sp|Q8IWE2|NXP20_HUMAN	-2.100276	3.0170602	Protein NOXP20 OS=Homo sapiens GN=FAM114A1 PE=1 SV=2; TOPep_Count=24
1::sp|Q9ULD2|MTUS1_HUMAN	-2.3703	2.7759319	Microtubule-associated tumor suppressor 1 OS=Homo sapiens GN=MTUS1 PE=1 SV=2; TOPep_Count=77
1::sp|Q9P013|CWC15_HUMAN	-2.4265407	3.4156306	Spliceosome-associated protein CWC15 homolog OS=Homo sapiens GN=CWC15 PE=1 SV=2; TOPep_Count=10